FLORIDA DEPARTMENT OF TRANSPORTATION

FINAL REPORT

Title: Effects of Coarse Aggregate on the Physical Properties of Florida Concrete Mixes

FDOT Contract Number: BDV-31-977-08

University of Florida, Department of Civil & Coastal Engineering

October 2015

Submitted to:

Research Center
The Florida Department of Transportation
605 Suwannee Street, MS 30 Tallahassee, FL 32399

Dr. Harvey DeFord, Ph.D.
Structures Materials Research Specialist
State Materials Office

Submitted by:

Christopher C. Ferraro, Ph.D., P.E. (ferraro@ce.ufl.edu) (Principal Investigator)

Engineering School of Sustainable Infrastructure and Environment

University of Florida

Gainesville, Florida 32611

DISCLAIMER

The opinions, findings, and conclusions expressed in this publication are those of the authors and not necessarily those of the State of Florida Department of Transportation or the U.S. Department of Transportation.

Prepared in cooperation with the State of Florida Department of Transportation and the U.S. Department of Transportation.

SI (MODERN METRIC) CONVERSION FACTORS (FROM FHWA)

Symbol	When You Know	Multiply By	To Find	Symbol
Length				
in	inches	25.4	millimeters	mm
ft	feet	0.305	meters	m
yd	yards	0.914	meters	m
mi	miles	1.61	kilometers	km
Area				
in^2	square inches	645.2	square millimeters	mm^2
ft^2	square feet	0.093	square meters	m^2
yd^2	square yard	0.836	square meters	m^2
mi^2	square miles	2.59	square kilometers	km^2
Volume				
fl oz	fluid ounces	29.57	milliliters	mL
gal	gallons	3.785	liters	L
ft^3	cubic feet	0.028	cubic meters	m^3
yd^3	cubic yards	0.765	cubic meters	m^3
NOTE: volumes greater than 1000 L shall be shown in m^3				
Mass				
oz	ounces	28.35	grams	g
lb	pounds	0.454	kilograms	kg
Temperature (exact degrees)				
°F	Fahrenheit	5 (F-32)/9 or (F-32)/1.8	Celsius	°C
Illumination				
fc	foot-candles	10.76	lux	lx
fl	foot-Lamberts	3.426	candela/m^2	cd/m^2
Force and Pressure or Stress				
lbf	pound-force	4.45	newtons	N
lbf/in^2	pound-force per square inch	6.89	kilopascals	kPa

TECHNICAL REPORT DOCUMENTATION

1. Report No.	2. Government Accession No.	3. Recipient's Catalog No.
4. Title and Subtitle Effects of Coarse Aggregate on the Physical Properties of Florida Concrete Mixes		5. Report Date October 2015 6. Performing Organization Code
7. Author(s) Christopher C. Ferraro, Caitlin M. Tibbetts, Michael C. Perry, Benjamin E. Watts, Jerry M. Paris		8. Performing Organization Report No. 00114669/00114670
9. Performing Organization Name and Address Department of Civil and Coastal Engineering Engineering School of Sustainable Infrastructure & Environment University of Florida 365 Weil Hall Gainesville, FL 32611-6580		10. Work Unit No. 11. Contract or Grant No. BDV-31-977-08se
12. Sponsoring Agency Name and Address Florida Department of Transportation 605 Suwannee Street, MS 30 Tallahassee, FL 32399		13. Type of Report and Period Covered Final Report June 2013 – October 2015 14. Sponsoring Agency Code
15. Supplementary Notes		

16. Abstract

Portland cement concrete is a heterogeneous, composite material composed of coarse and fine granular material embedded in a matrix of hardened paste. The coarse material is aggregate, which is primarily used as inexpensive filler and comprises the majority of the volume of concrete and can be obtained from a variety of different sources. The physical properties of concrete are heavily influenced by the aggregate properties. Most of the coarse aggregate produced in Florida is a limestone material that is more porous, less dense, and softer than limestone produced from other areas of the U.S. To differentiate between limestone produced in Florida and limestone produced elsewhere, limestone from the geologic formations in Florida is typically referred to as "limerock." The coarse aggregate produced in Florida and used in structural concrete require special consideration with regard to relative strength, thermal, and physical properties. The structural design of concrete is based on service limit states and utilizes modulus of elasticity as a design parameter. However, the modulus of elasticity of concrete used for the design of structures is typically determined by relationships which utilize compressive strength. Due to the assumption that structural concrete made with weaker Florida limerock would have lower strength than concrete made with other aggregates, an aggregate correction factor of 0.9 is used in the calculation of elastic modulus from compressive strength testing for structural design equations. The use of an aggregate correction factor of less than 1.0 requires the use of more concrete to meet structural requirements. The primary goal of the research was to study the effects of different coarse aggregate types on the physical properties and design of portland cement concrete, with the emphasis coarse aggregate from Florida foe use in structural concrete. Concrete specimens were made and tested to acquire the information necessary for use in the design equations used to predict the physical properties of the concrete. A value of 1.0, rather than the currently used value of 0.9, was found to be appropriate for the aggregate correction factor for Florida limerock.

17. Keywords.	18. Distribution Statement
Aggregate, Concrete, Design Equations, Modulus of Elasticity, Compressive Strength	No restrictions.

19. Security Classif. (of this report)	20. Security Classif. (of this page)	21. Pages	22. Price
Unclassified.	Unclassified.	175	

EXECUTIVE SUMMARY

Background and Research Needs

Portland cement concrete is a heterogeneous, composite material composed of coarse granular material embedded in a matrix of hardened paste. The coarse material is aggregate, which is primarily used as inexpensive filler and comprises the majority of the volume of concrete. Aggregate materials can be obtained from a variety of different sources, both natural and manufactured. Typically, the aggregate occupies 60% to 75% of the volume of concrete, and the physical properties of concrete are heavily influenced by the aggregate properties.

Most of the coarse aggregate produced in Florida is a limestone material that is more porous, less dense, and softer than limestone produced from other areas of the U.S. To differentiate between limestone produced in Florida, and limestone produced elsewhere, Florida limestone is typically called Florida "limerock." Due to the assumption that structural concrete made with weaker Florida limerock would have lower strength than concrete made with other aggregates, an aggregate correction factor of 0.9 is used in the calculation of elastic modulus for structural design equations. The use of an aggregate correction factor of less than 1.0 results in the use of more concrete to meet structural requirements.

The main goal of the research was to study the effects of different coarse aggregate types on the physical properties and design of portland cement concrete, with the emphasis on Florida aggregate used for structural concrete. Concrete samples were made and tested to acquire the data needed for use in the design equations used to predict the physical properties of the concrete. A value of 1.0, rather than the currently used value of 0.9, was found to be appropriate for the aggregate correction factor for Florida limerock.

Scope and Research Objectives of the Study

The Florida Department of Transportation (FDOT) Structures Design Guidelines uses equations to calculate the modulus of elasticity of portland cement concrete from physical testing of compressive strength and density. Thus, the design values used for modulus of elasticity are based on empirical equations and are obtained indirectly. In addition to the physical testing data, calculation of modulus of elasticity uses an aggregate correction factor for the calculations. Use of an aggregate correction factor that is too low would result in the use of an unnecessary excess of concrete to meet structural design requirements. The Structural Design Office of the FDOT expressed concern that the factor of 0.9 used for Florida structural concrete containing limerock is too low. The primary goals of this research were to address this concern by evaluating the performance of structural concrete made with Florida limerock, to establish appropriate values for the aggregate corrections factors, and to evaluate the resulting accuracy of the design equations used to calculate modulus of elasticity.

Main Findings

The main findings from this study are summarized as follows:

1. Currently adopted correction factors used for the equations to predict modulus of elasticity from compressive strength within the FDOT Structures Design Manual should be revised as they are overly conservative.

2. The incorporation of Miami oolite as coarse aggregate in portland cement concrete resulted in the highest compressive strength and the best correlation between compressive and splitting tensile strengths, and the moduli of elasticity for those aggregates produced in Florida.

3. Florida limerock had lower density, higher porosity, and rougher surfaces compared to Calera limestone aggregates and granite aggregates. The porosity and surface roughness of Florida limerock produced significantly better aggregate-paste bonding, and this was demonstrated by mostly transgranular fracture surfaces. Higher aggregate strengths combined with weaker aggregate-paste bonding, due to lower porosities and smoother surfaces, resulted in mostly intergranular fracture surfaces for concrete with granite and Calera limestone aggregate.

4. Specimens acquired from 4”x8” cylindrical molds do not accurately represent early age concrete hydration and strength development when compared to cored cylinders obtained from larger specimens.

5. While testing was required to determine if aggregates required correction factors, non-destructive methods did not exhibit usable relationships between concrete of different aggregate types. Rebound hammer testing was not found to be effective in determining aggregate effects on modulus or compressive strength.

Recommendations

The following aggregate correction factors should be adopted and incorporated into the FDOT Structures Design Manual:

Aggregate	Correction Factor
Miami Oolite	1.00
Brooksville	0.97
Perry	1.01
Granite	1.06
Calera	1.21

TABLE OF CONTENTS

LIST OF FIGURES

LIST OF TABLES

1. INTRODUCTION

Portland cement concrete is a composite material in which each constituent material influences the behavior of the resultant hardened product. While portland cement is a manufactured product, the aggregate is obtained from natural sources that vary depending on location and geological history. Coarse aggregate is primarily a filler material and constitutes a substantial volume fraction of a concrete mixture, and its physical properties influence hardened concrete properties.

Concerns with respect to aggregate quality are of particular relevance in the state of Florida. South Florida has permeable oolitic limestone; central and other parts of Florida have permeable rock which includes the Ocala formation (Brooksville and Perry). Most of the geologic formations of the inland areas within Florida are marine formations that have rock with relatively low density and high porosity compared to limestone or granite aggregates mined elsewhere.

A research project was designed to study the effect of course aggregate type on the properties of Florida structural concrete. Three Florida limerock aggregates, a Calera limestone aggregate, and a granite aggregate were tested in two classes of structural concrete mix designs. Concrete mixes were evaluated based on physical properties, and the resulting data were used to determine aggregate correction factors for the aggregates studied. These correction factors are used in structural design equations employed to calculate elastic moduli. These factors are important because they help determine that quantity of concrete needed to meet structural design requirements.

2. LITERATURE REVIEW

2.1 BACKGROUND

This document provides the state of the practice with regard to the use of coarse aggregate in concrete used in FDOT mixes and serves to characterize each aggregate and determine relevant properties. The properties of Florida coarse aggregate differ from aggregate typical to other parts of the country and accordingly, concrete design should incorporate the differences.

2.2 GENERAL

Concrete is a composite material for which the *in-situ* properties are the product of the physical behavior of the individual constituents as well as the placement conditions, curing conditions, and early-age physical and environmental conditions. The behavior of concrete subsequent to placement can be predicted more accurately prior to placement when the constituent materials are thoroughly understood. Concrete by definition is a heterogeneous mixture of a cement binder, aggregate (coarse and fine), water, and admixtures (as necessary). In Figure 2.1, the stress-strain behavior of concrete, aggregate, and cement paste can be seen (Neville, 1996).

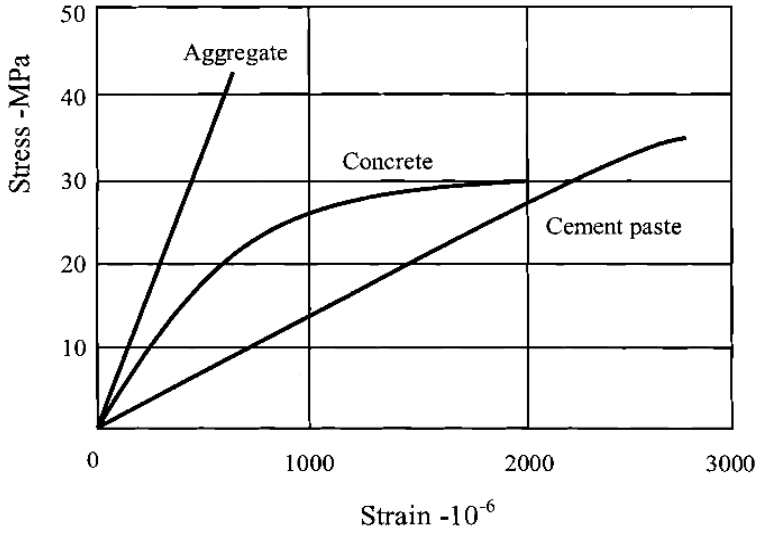

Figure 2.1 Stress vs. Strain on typical concrete ingredient fractions (Neville, 1996)

The modulus of elasticity of concrete, as indicted in Figure 2.1 by the initial slope of the stress-strain curve, lies between the moduli of the aggregate and the hardened cement paste. Thus, the relationship between aggregate modulus and the ultimate concrete strength is dependent upon the properties (strength and modulus) of the aggregate itself. However, mix conditions and aggregate properties affect the relationship between aggregate strength and resultant concrete strength, which includes bonding strength, aggregate gradation, water content, and curing conditions (Iravani, 1996). Studies have shown that the incorporation of stronger aggregates may lead to a lower modulus of elasticity, and concrete composed with weaker aggregates often has higher modulus values than equal mixes made with granite (Aïtcin, 2011). When subjected to ultimate loading conditions, a quasi-brittle material, such as concrete, will fail (crack) first at its weakest

point. The progressive failure of concrete takes place as cracks coalesce throughout the system of different constituent materials that form the concrete matrix. Therefore, being an amalgam of different materials, concrete may have multiple failure modes when subjected to ultimate stresses or loads.

Limestone aggregate is a relatively weak and porous material, and when concrete composed with limestone aggregate is subjected to stress, cracks propagate through the limestone as well as the hardened cement paste matrix (Rich, 1980). However, concrete composed of a stronger aggregate, such as granite, will often experience cracking around the aggregate and through the hardened cement paste matrix (Chen and Su, 2013). Due to the relatively porous nature of limestone, it provides a higher degree of bonding between itself and the cement paste by allowing it to infiltrate the surface pores prior to the hardening of the cement paste (Hussin and Poole, 2011). In addition, the rough surfaces of the aggregates provide higher surface areas available for bonding with the paste. This higher bonding strength that is facilitated from the incorporation of limestone often produces a stiffer mortar near the surfaces of the coarse aggregates in the interfacial transition zone (ITZ). Predicting concrete strength is highly important but can be highly variable. Empirical equations have been determined to fit the strengths of the majority of concrete mixes, and are discussed in the "Modulus Prediction" section (Section 2.3) of this document.

2.2.1 Modulus of Elasticity

Most structures are designed to undergo relatively small in-service deformations; accordingly, it is necessary to quantify the elastic properties of the concrete when subjected to stress. The linear relationship between the stress and the strain of a material is known as Hooke's Law (Beer et al., 2011) and is defined as:

$$\sigma = E\varepsilon \tag{2-1}$$

Where:

σ = stress of the material
E = Young's Modulus
ε = linear strain

However, concrete is a nonlinear inelastic material in both compression and tension; therefore, the elastic modulus does not have a unique value. There are a number of ways to calculate the modulus of elasticity based on the region of the stress-strain curve used for the calculation (Mindess et al. 2003). Figure 2.2 illustrates the various elastic moduli defined for the typical stress-strain curve of concrete (Ferraro, 2009).

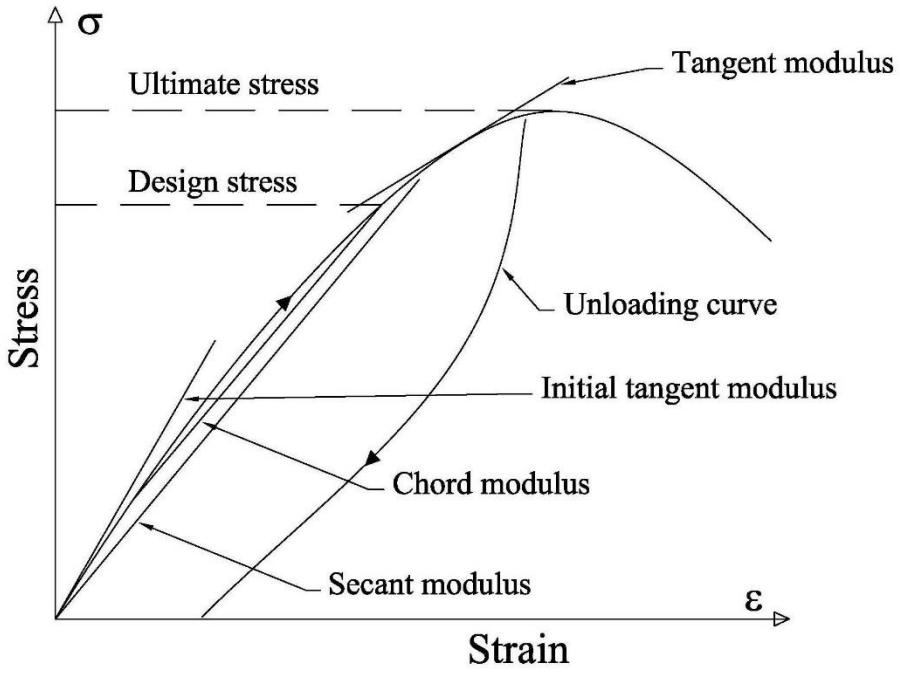

Figure 2.2 Typical stress-strain diagram for concrete, showing the different elastic moduli (Mindess 2003, Ferraro 2009)

2.2.1.1 Tangent Modulus

The tangent modulus is defined as the slope of the stress-strain curve at a given point. It can also be considered the instantaneous rate of change of the stress with respect to strain (Wu et al., 2001). The closest approximation to the modulus of elasticity as described by Hooke's law can be described as the initial tangent modulus, also referred to as the dynamic modulus (Mindess et al., 2003; Mehta, 1986), which is the slope of the tangent to the stress-strain curve at the origin. Both tangent and initial tangent moduli are depicted in Figure 2.2.

2.2.1.2 Secant Modulus

The secant modulus is the slope of the secant between the origin and a given point on the stress-strain curve. It is dependent upon the intersecting point on the stress strain-curve. The secant modulus is considered to be the instantaneous rate of change of the stress with respect to strain (Wu et al., 2001). Typically, the secant modulus is calculated as the secant between the origin and the point on the stress strain curve that corresponds to 40% of the failure stress (Mehta, 1986).

2.2.1.3 Chord Modulus

The chord modulus is the slope of a line drawn between any two points on the stress-strain curve. Research has shown that measurements of the initial tangent and secant moduli can be skewed due to seating effects during initial loading, or due to defects in the specimen which result in non-linearity at the early portions of the stress-strain curve (Mindess et al., 2003, Ferraro, 2009). As such, the Standard Test Method for Static Modulus of Elasticity of Concrete in Compression

(ASTM C469, 2014), specifies that the chord modulus be drawn between points corresponding to 50 microstrain and 40% of the ultimate strength.

2.2.1.4 Factors Affecting Modulus

Despite the fact that the elastic modulus is typically higher for the ITZ in concrete which contains porous and lightweight aggregate, the static modulus of elasticity of the concrete is governed by several properties (Mindess et al., 2003):

- Water-to-cementitious material ratio (w/cm),
- Air content / porosity,
- Degree of saturation during testing, and
- Coarse aggregate and cement modulus and content.

It has been well documented that the strength (and modulus) of concrete is inversely proportional to w/cm and air content. Thus, a lower value of w/cm and air content will result in concrete with a higher strength and modulus (Mindess et al., 2003; Neville, 1996).

The strength and modulus of concrete does not behave in the same manner with respect to the degree of water saturation during the time of testing. The compressive strength of concrete decreases with an increase in degree of saturation at the time of testing. Therefore, concrete that is fully saturated at the time of testing results in a lower strength when compared with concrete that is not fully saturated. However, the modulus of elasticity is higher for concrete that is fully saturated (Yaman et al., 2002). The primary reason for the difference can be attributed to the fracture mechanics of concrete in its saturated state. The strength of saturated concrete is decreased due to moisture forcing the gel particles apart and reducing the Van der Waals forces within the cement matrix (Wittmann, 1973; Ross et al., 1996). Thus, the compressive strength of a saturated concrete specimen is lower than that of an unsaturated specimen (Kesler, 1966). The opposite is true with regard to modulus of elasticity in saturated specimens. The presence of water, an incompressible liquid, in the pore space of the hardened cement matrix provides additional resistance to strain, which contributes to an increase of the overall elastic modulus (Mehta, 1986).

The volume fraction of coarse aggregate and its modulus of elasticity are the biggest contributors (other than w/cm) to the modulus of elasticity of concrete. Thus, the modulus of elasticity of concrete can be increased by using a higher volume of coarse aggregate or by using coarse aggregate with a higher modulus of elasticity, as illustrated in Figure 2.3.

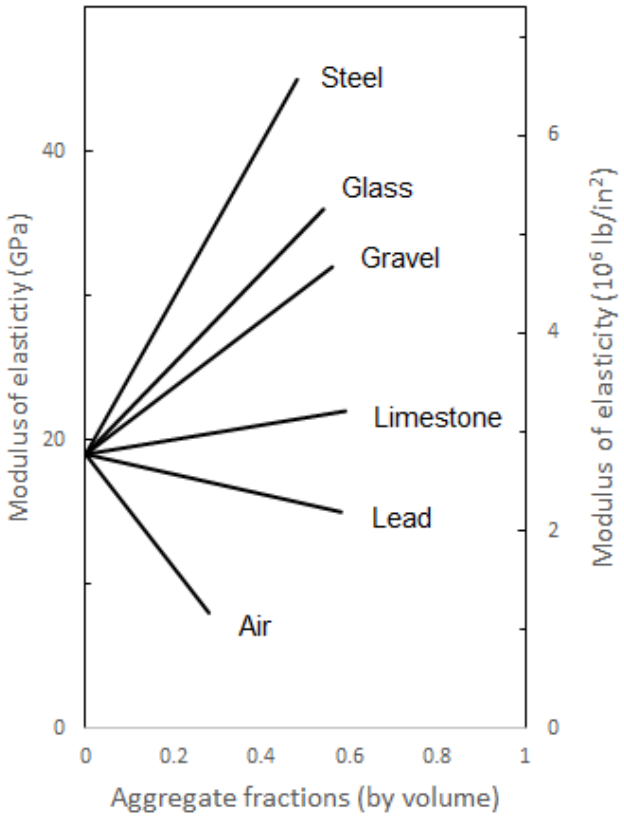

Figure 2.3 The effect of aggregate on the modulus of elasticity of concrete (Mindess et.al, 2003)

Higher strength aggregates with high elastic modulus (such as granite) create a region within the interfacial transition zone where stress concentrations are present due to the differences between elastic moduli of the aggregate and cement paste. These stress concentrations may adversely affect strength by initiating microcracking in the ITZ. The resulting stress concentration effect is less prominent in limestone concretes due to the relatively lower value for the elastic modulus of limestone (Zhang et al., 2009). In addition, the formation of initial defects caused by differential shrinkage and the differences in the moduli of the aggregate particles to the surrounding cement can further weaken the ITZ (Akçaoğlu et al., 2004). Florida limerock can be characterized as lightweight and porous, explaining concrete failure modes similar to those of lightweight and porous materials that utilize Florida materials (Oates, 1998).

2.2.2 Modulus of Elasticity – Florida Materials

The geology of the State of Florida has a soft variety of the limestones known as “limerock”, which is primarily composed of calcium carbonate (Tyner, 1946). A number of different geologic formations are discussed further within Section 2.7 of this report. The use of limerock for coarse aggregate in concrete has been documented in a number of different studies, primarily by the Florida Department of Transportation. Some of the studies are reviewed below.

2.2.2.1 Yazdani and McKinnie 2004:

The research entitled "Time Dependent Compressive Strength and Modulus of Elasticity of Florida Concrete", performed by Yazdani and McKinnie under project FDOT BD-221, investigated a number of properties of concrete containing aggregate from Florida. The research investigated the relationship between compressive strength and modulus of elasticity of concrete, which incorporated several different sources of coarse aggregate from Florida. The research developed several equations used to relate modulus of elasticity and compressive strength of concrete as discussed in Section 2.3 of this report.

2.2.2.2 Tia et al. 2005:

The research entitled, "Modulus of Elasticity, Creep and Shrinkage of Concrete used in Florida", performed by Tia et al., under project FDOT BC-354, evaluated several properties of concrete, primarily the creep of concrete in compression, but included the study of the modulus of elasticity of concrete containing Miami oolite and lightweight aggregate as coarse aggregate. The research established empirical relationships between compressive strength and modulus of elasticity of concrete containing Miami oolite as coarse aggregate, similar to those proposed by ACI 318. Section 2.3 of this report provides information on the relationships as per ACI 318, which is supported by Tia et.al, 2005 although not discussed explicitly.

2.2.2.3 Tia et al. 2009:

The research entitled "Strength, Modulus of Elasticity, Creep and Shrinkage of Concrete used in Florida", performed by Tia et al., under project FDOT BD-545-67, investigated a number of properties of concrete containing coarse aggregate from Florida. The study investigated the differences between a Miami oolite (Florida limerock), a lightweight aggregate, and granite. The results of the study indicated that the modulus of elasticity of concrete created with Florida limerock from the Miami oolite formation is similar to concrete produced with granite. Tia et al. concluded that "compressive strength of concrete with granite aggregate was comparable to or lower than that of Miami oolite limestone aggregate," which is contrary to the consensus of published research with regard to the compressive strength of concrete incorporating granite coarse aggregate as compared to limestone (Mindess et al., 2003; Neville, 1995; FDOT, 2013). Some potential contributing factors to the discrepancy could be attributed to compositional variations, as a number of the concrete mixtures (composed of the same ingredients) produced lower strength and modulus values than comparable mixes with higher w/cm. Another potential reason for the discrepancy could be attributed to the use of procedures to conduct the research that deviated from standard procedures. One example is that the compressive modulus of elasticity testing was not performed in accordance with ASTM C469.

2.2.2.4 Ferraro and Watts 2013:

The research entitled "Development of Design Parameters for Virtual Cement and Concrete Testing", performed by Ferraro and Watts under project BDK75-977-73 investigated the properties of concrete, as simulated by a computer-modeling program, compared to concrete created in the laboratory. The research revealed that concrete made with Miami oolite coarse

aggregate achieved a modulus of elasticity close to what is proposed by ACI 318, as discussed in the next section.

2.3 INTERFACIAL TRANSITION ZONE

The interfacial transition zone is the area within the concrete where the mechanical and chemical connection between aggregate and cement paste takes place, and it is a critical factor in concrete behavior at relatively high stress (Ioannides and Mills, 2006). The ITZ can form a "wall effect," which is caused by the accumulation of anhydrous cement particles against the surfaces of larger aggregate particles. The presence of free water on the surface of coarse aggregate creates a relatively large w/cm at the ITZ, which influences the porosity and strength of the ITZ. The porosity of the ITZ and its influence on transport properties of the concrete vary considerably with the types of microstructure that form during hydration of the cement particles near or adjacent to aggregate particles (Scrivener et al., 2004). The combined effects of aggregate porosity, interfacial transition zone thickness, and density of the cementitious microstructure have been shown to influence concrete strength (Noguchi and Nemati, 1995). Concrete containing porous aggregate usually exhibits the formation of a denser and more homogenous interfacial transition zone, which increases bond strength due to improved mechanical interlocking between the aggregate and cement paste (Wu et al., 2001). In addition, water contained within the aggregate can result in internal curing, which can densify the ITZ at later ages. The "wall effect" is not observed on the surface of porous lightweight aggregate (Lo and Cui, 2004). The combined effect of a dense interfacial transition zone and higher bonding strength produces a concrete with a higher compressive strength near the ITZ (Lo and Cui, 2004; Perry and Gillott, 1977).

The typical order of failure / fracture for concrete in compression is attributed to the stress distribution within the cement paste around the stiffer coarse aggregate particles. The apparent order of failure is (Mindess, 1996):

(1) Tensile bond failure
(2) Shear bond failure
(3) Shear and tensile matrix failure
(4) Occasional aggregate failure

The typical failure / fracture mechanism of concrete in compression occurs when microcracks initiate at the ITZ and propagate through the hardened cement paste (as described by mechanisms 1-3) and around the coarse aggregate particles. This fracture through the cement matrix and around the aggregate is referred to as intergranular fracture (Maso, 1996). However, concrete containing Florida limerock, more specifically Miami oolite, has exhibited transgranular failure, where the fracture planes in the cement matrix propagate through the coarse aggregate particles (Ferraro and Watts, 2013).

The interfacial transition zone within portland cement-based materials is perhaps the largest source of uncertainty with regard to the quantification of physical parameters, especially modulus and strength. The variability and relative uncertainty of the quantifiable physical characteristics of hardened cement paste at the ITZ are ultimately responsible for the uncertainty

in the relationships between the strength and modulus properties of the concrete. The heterogeneous nature of concrete and the relative differences of the nature or behavior of the hardened cement paste, with respect to the coarse aggregate and the resultant ITZ, are not easily described or quantified.

2.4 MODULUS OF ELASTICITY PREDICTION

The modulus of elasticity of concrete is typically predicted through the determination of compressive strength and unit weight of concrete. As discussed in Section 2 of this document, considerable research involving the prediction of strength and modulus of elasticity of concrete has been done. Many models exist for predicting elastic modulus of concrete which offer different equations depending on concrete type, e.g., high strength concrete or lightweight concrete. Other than the research discussed in Section 2.2, little research has been done to develop empirical relationships between the elastic modulus and strength of concrete containing Florida limerock. However, there are a number of relationships that have been developed for predicting the modulus of elasticity of concrete based on compressive strength testing. One of the primary factors that limit the accurate prediction of compressive strength and modulus of concrete is the nature of fracture and ultimate failure of concrete.

2.4.1 American Concrete Institute 318

The equations developed for prediction of the modulus of elasticity of concrete in ACI 318 are given in Chapter 8, and are also presented here as Equations 2-2 and 2-3:

$$E_c = 33 w_c^{\,1.5} \sqrt{f'c} \qquad (2\text{-}2)$$

$$E_c = 57000 \sqrt{f'c} \qquad (2\text{-}3)$$

Where:

E_c = modulus of elasticity (lb/in^2, psi)
w_c = unit weight (density) of concrete (lb/ft^3, pcf)
f'_c = compressive strength (lb/in^2, psi)

Equation 2-2 is equal to Equation 2-3 for normal weight concrete with a unit weight (density) of 145 lb/ft^3 (Mindess et al., 2003). The research conducted by Tia et al. (2005) and Ferraro and Watts (2013) confirmed the relative accuracy of the equations for concrete incorporating Miami oolite.

2.4.2 American Concrete Institute 363

The American Concrete Institute (ACI) Committee 363 report on High-Strength Concrete incorporates a number of parameters with regard to concrete including structural design. Accordingly, there are a number of different compressive strength - modulus of elasticity relationships presented for the design of concrete structures. The report compares different relationships, between modulus of elasticity and compressive strength of concrete, that are based on a number of different variables. Figure 2.4 shows the relationships between modulus of

elasticity and the square root of compressive strength based on a number of best-fit relationships provided by Equations 2-4 through 2-8 (ACI Committee 363, 2010).

$$E_c = 40000\sqrt{f'c} + 10^6 \quad (2\text{-}4)$$
$$E_c = {w_c}^{2.55}(f'c)^{0.315} \quad (2\text{-}5)$$
$$E_c = {w_c}^{2.5}(f'c)^{0.325} \quad (2\text{-}6)$$
$$E_c = 303{,}500(f'c)^{0.3} \quad (2\text{-}7)$$
$$E_c = 2{,}101{,}775 + 26{,}200(f'c)^{0.5} \quad (2\text{-}8)$$

Where:

E_c = concrete secant elastic modulus (psi)
f'_c = specified compressive strength of concrete (psi)

The ACI 363 report on high strength concrete also presents several other strength-modulus relationships that account for variables other than density and strength, such as concrete age, use of pozzolans (silica fume), and aggregate type. Despite the fact that the ACI 363 report presents a number of predictive equations relating the modulus of elasticity of concrete to strength, physical properties, and other variables, the report ultimately concludes that the design engineer should verify the modulus of elasticity by performing field trials (ACI Committee 363, 2010).

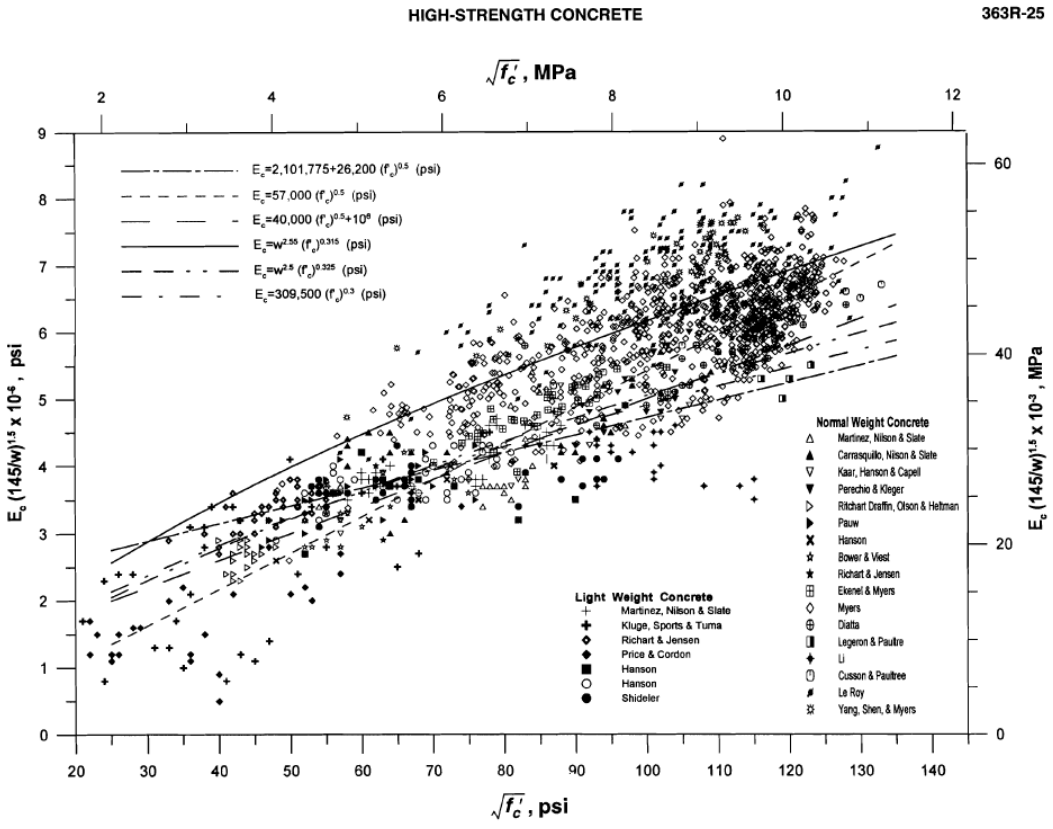

Figure 2.4 Modulus of elasticity equations, with lower and higher-strength concrete data (ACI Committee 363, 2010)

2.4.3 Yazdani and McKinnie (2004)

Yazdani and McKinnie reported that the equations used to relate the compressive strength and modulus of elasticity of concrete in Florida, prior to their research in 2004, underestimated the modulus of elasticity based on Equation 2-9. Their research focused on developing relationships for concrete that contained coarse aggregates from the Brooksville and Chatahoochee formations in Florida, and from Calera, AL. Based on regression analysis of the data obtained from their research, Yazdani and McKinnie developed two relationships, shown below as Equations 2-9 and 2-10, to relate modulus of elasticity to measured compressive strength of concrete (Yazdani and McKinnie, 2004):

$$E_c = 1.45 \cdot 10^{-7} w_c{}^{5.8} (f'c)^{0.28} \quad (2\text{-}9)$$

$$E_c = w_c{}^{2.64} (f'c)^{0.28} \quad (2\text{-}10)$$

Where:

E_c = concrete elastic modulus (psi, where 1 psi =0.00689 MPa)
f'_c = specified compressive strength of concrete (psi)
w_c = unit weight of concrete (in lb/ft^3 (pcf), where 1 pcf = 16.02 kg/m^3)

This first equation, "Option 1," was found to be most accurate for the range of compressive strengths used in the Yazdani study. The second equation is the "next best" model, and is provided because it is of simpler form and similar to the current FDOT and ACI models. Option 2 was found to be less sensitive to variation in unit weight. Both equations are valid for compressive strengths in the range of 859 psi to 8,432 psi and unit weights in the range of 140.8 to 150.3 lbs/ft^3.

2.4.4 Ferraro and Watts (2013)

Ferraro and Watts performed research involving the modeling of the microstructure of cementitious materials using the Virtual Cement and Concrete Testing Laboratory (VCCTL) modeling software created by the National Institute of Standards and Technology (NIST). As part of their research, they investigated the accuracy of the VCCTL software with regard to modeling compressive strength and the modulus of elasticity of concrete. Ferraro and Watts utilized concrete incorporating Miami oolite as coarse aggregate to investigate the accuracy and validity of the VCCTL software for the prediction of modulus of elasticity and compressive strength. The testing revealed that the VCCTL software simulated the modulus of elasticity of concrete with a good degree of accuracy. The research confirmed the relative accuracy of Equation 2-2, as provided by ACI 318 for the prediction of the modulus of elasticity of concrete, using concrete composed with Miami oolite (Ferraro and Watts 2013).

2.5 CORRECTION FACTORS

Several empirical relationships have been proposed that use unit weight and compressive strength to relate modulus of elasticity to compressive strength for normal-density concrete. Other equations, based on the measured density and compressive strength, are considered better suited to relate modulus of elasticity to compressive strength (ACI Committee 363, 2010).

Elastic modulus has been shown to be a function other parameters, such as content and type of coarse aggregate (Mindess et.al, 2003; Neville 1996; Myers and Carrasquillo, 1998), water-to-cementitious material ratio, admixture correction factor, and of particular importance, aggregate correction factor (Tomosawa and Noguchi, 1993; Yazdani et al., 2005). The efforts of various organizations and committees to incorporate factors to account for the effects of aggregate in the calculation of modulus of concrete are presented in sections 2.5.1-2.5.4.

2.5.1 Tomosawa and Noguchi (1993)

Tomosawa and Noguchi proposed the following elastic modulus equation to account for the effects of aggregate type and supplemental cementitious material (SCM) addition (Tomosawa and Noguchi, 1993).

$$E_c = 1486 K_1 K_2 w_c^2 f_c'^{1/3} \quad (2\text{-}11)$$

Where:

E_c = elastic modulus of concrete (MPa)
K_1 = correction factor for the specified coarse aggregate
K_2 = correction factor for the specified supplemental cementitious material
f'_c = compressive strength of concrete (MPa)
w_c = unit weight of concrete (kg/l = g/cm^3)

Calculated values for the K_1 and K_2 correction factors for some typical aggregates are given in Table 2.1.

Table 2.1 K_1 and K_2 correction factors for various aggregate types (Values compiled from Tomosawa and Noguchi, 1993)

		K_2 Correction Factors						
		Supplemental Cementitious Materials						
K_1 Correction Factors		Silica Fume			Slag		UFFA	Fly Ash
Aggregate Type	K_1	<10%	10-20%	20-30%	<30%	>30%		
River Gravel	1.005	1.045	0.995	0.818	1.047	1.118		1.110
Crushed Greywacke	1.002	0.961	0.949	0.923	0.949	0.942	0.927	
Crushed Quartzitic Aggregate	0.931	0.957	0.956		0.942	0.961		
Crushed Limestone	1.207	0.968	0.913					
Crushed Andesite	0.902		1.072	0.959				
Crushed Basalt	0.922							1.087
Crushed Clay Slate	0.928							
Crushed Cobble Stone	0.955							
Blast Furnace Slag	0.987							
Calcined Bauxite	1.163		0.942					
Lightweight Coarse Aggregate	1.035	1.026						

2.5.2 The Comité Euro-International du Beton-Fédération Internationale de la Précontrainte

This organization used an empirical coefficient to account for the effect of aggregate type in its modulus equations, as presented in Equations 2-12 and 2-13 (CEB-FIP, 1993).

$$E_c = 3100\alpha_E \left(\frac{f_{cm}}{1.44}\right)^{1/3} \text{(ksi)} \quad (2\text{-}12)$$

$$E_c = 21500\alpha_E \left(\frac{f_{cm}}{10}\right)^{1/3} \text{(MPa)} \quad (2\text{-}13)$$

Where:

E_c = tangent modulus of elasticity at zero stress and at a concrete age of 28 days
f_{cm} = mean compressive strength of concrete
α_E = empirical coefficient of value 1.2 for basalt and dense limestone, 1.0 for quartz, 0.9 for limestone, and 0.7 for sandstone

The values of the CEB-FIP coefficient are influenced by the elastic modulus of the aggregates, with basalt and dense limestone increasing the predicted strength, and (assumed regular density) limestone and sandstone decreasing the predicted values. This model does not address any other contributing factors such as porosity or density. The studies that were used to develop the values of the adjustment coefficient were not identified.

2.5.3 ACI 318 and Parrott (1969)

Other modifications have also been proposed that pertain to the types of coarse aggregate used, including a coarse aggregate correction coefficient, C_{ca} that is a proposed modification to the ACI 318 modulus equation (ACI 318, 2011). Parrott suggested an equation which predicts modulus based on aggregate strength and type using the factor K_0. It is important to note that the specified equations (Equations 2-14 and 2-15) lack sufficient detail to provide accurate predictions (Parrott, 1969).

$$E_c = 4700 C_{ca} \sqrt{f_c'} \; 55\ MPa < f_c' < 125\ MPa \quad (2\text{-}14)$$

$$E_c = K_0 + 0.2 f_c' \quad (2\text{-}15)$$

2.5.4 LRFD Correction Factors

The American Association of State Highway and Transportation Officials (AASHTO) *LRFD Bridge Design Specifications* formula for modulus of elasticity, as presented in Equation 2-16 below, or Equation 5.4.2.4-1 per the LRFD specifications, is dependent upon compressive strength, unit weight of concrete, and the variable K_1.

$$E_c = 33{,}000 K_1 {w_c}^{1.5} \sqrt{f_c'} \quad (2\text{-}16)$$

K_1 is a correction factor for the source of aggregate and is assumed to be 1.0 unless determined by physical test, and as approved by the authority of jurisdiction (AASHTO, 2011).

The correction factor K_2, in the proposed equation shown in Figure 2.5, is determined by an upper or lower bound on the modulus, which is used to incorporate crack control (upper bound) or prestress losses (lower bound). This factor is apparently different than the K_2 proposed by Tomosawa and Noguchi (1993). It is important to note that the inclusion of aggregate adjustment factors coincides with the use of admixture adjustment factors as well, and is a recent addition to the AASHTO LRFD specification. These bounds were determined statistically with trial data (Tadros et.al, 2003).

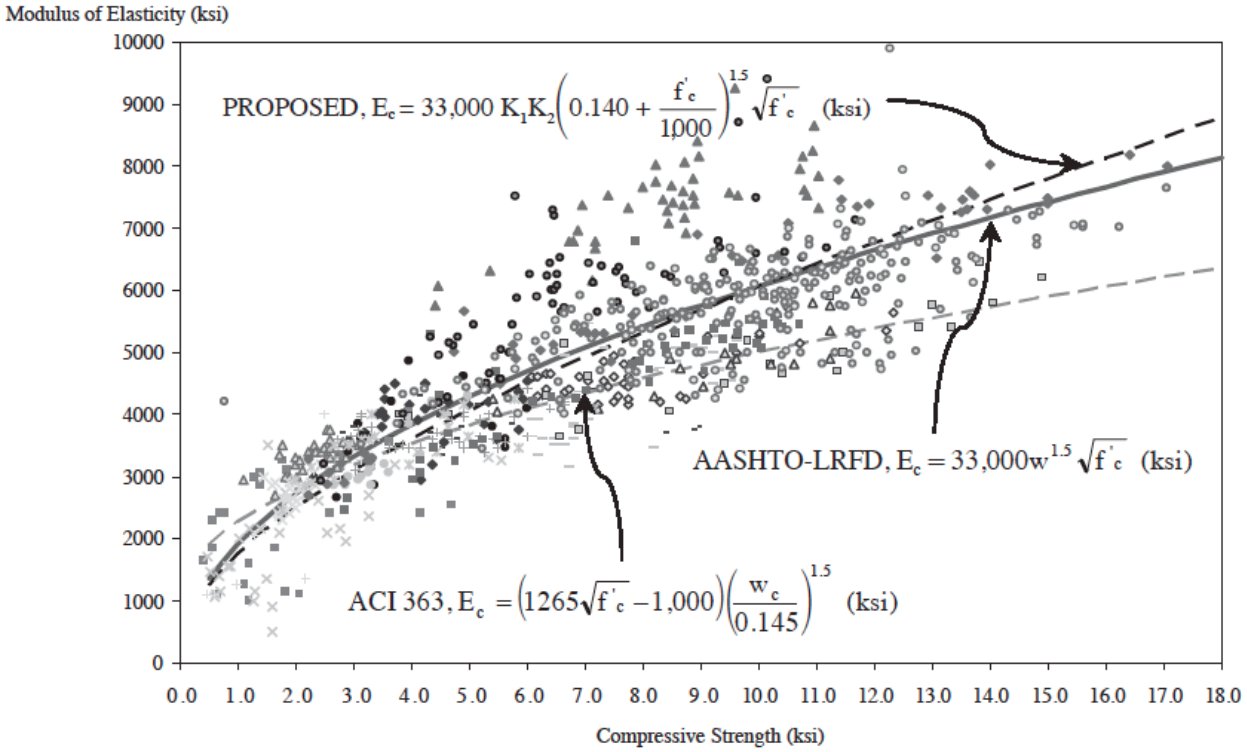

Figure 2.5 Modulus of elasticity equations, with lower- and higher-strength concrete data (Tadros et.al, 2003).

The K_1 aggregate adjustment factor first appeared in a specification in October 2006 as part of the Federal Highway Administrations Proposed Revisions to the AASHTO LRFD Bridge Design Specifications, Appendix D dated October 2006. This proposed revision cites the NCHRP report 496 "Prestress Losses in Pretensioned High-Strength Bridge Girders". NCHRP Project 18-07 found that the accuracy of the existing equations, presented in Figure 2.5, for predicting modulus of elasticity can be improved by the proposed modifications. The AASHTO-LRFD, as used by the FDOT structures design guidelines LRFD 5.4.2.4, equation adopted includes the K_1 aggregate correction presented in equation 2-16, which is not present in figure 2.5 (FDOT, 2015a) A more accurate prediction of modulus of elasticity is needed in calculating prestress losses and camber of high-strength concrete girders, as the values are larger than for conventional strength concrete girders (Tadros et.al, 2003). Based on this background information, these aggregate correction factors are primarily used for prestressed members. There is currently no information that relates these adjustment factors to specific mines, locations, or chemical properties of aggregate.

Correction factors equal to 1 indicate that the uncorrected, predicted values of elastic modulus are essentially equal to the measured values of modulus. Values other than unity are needed to account for the differences in the predicted values of modulus due to the effects of the particular aggregates and SCMs used . The aggregate correction factor has to be calculated for each aggregate type and location, and is only valid for that specific location.

Current LRFD specifications followed by FDOT call for the use of a K_1 value of 0.9 for structural concrete containing Florida limerock as coarse aggregate. While previous papers have proposed K_1 values for limestone, none have supported the use of a K_1 value of 0.9, and there is currently no evidence for the justification of usage of 0.9 for Florida limestone. The choice of 0.9 apparently stems from the perception that, since Florida limerock is more porous and softer than typical limestone, it reduces the concrete strength compared to concrete made with other typical aggregates. The proposed K_1 correction factors by LRFD equation 5.4.2.4 do not consider Florida limerock aggregate and there is inadequate research to establish appropriate K_1 values for Florida limerock.

2.6 AGGREGATE SOURCES

FDOT-approved mines produce a number of different products for varying uses in concrete, asphalt, building, and base construction. The current FDOT certification process consists of four primary means of evaluating aggregate: bulk specific gravity, absorption, sodium sulfate soundness, and the Los Angeles abrasion test. Each test is meant to quantify the material's durability either mechanically, chemically, or a combination of both. The tests are performed on aggregate collected from each quarry. Quarries which produce aggregate which has met specifications on a consistent basis are certified on a regular basis as FDOT-approved sources for aggregate. Quarries with less consistent aggregate may be approved on a conditional basis. Aggregate not meeting specifications is rejected.

Mined aggregates are available in different gradations and densities, and mine variability, even within the same pit, can be high. In order to maintain a consistent product, a series of tests are conducted at the mine to determine where pits will be excavated and the amount of material that will be processed. The result is a product that incorporates many aggregates from different sources geographically and lithographically. The end effect is that mines craft their final aggregate product from many sources in order to meet required FDOT specifications but may not record the specific sources of the constituent materials. This complicates the characterization of aggregate used in concrete mixes. Variability can exist chemically and mechanically at the microscopic scale, but the aggregate may appear homogenous at the macroscopic scale. The FDOT in particular does not have a standard method of evaluating field performance, or other means of comparing actual durability with certification data. Many researchers have recognized a need to find more effective ways of predicting the performance of these construction materials. There is no single test that can accurately evaluate aggregate performance as a function of its service conditions; therefore, the methods of evaluating aggregate quality have evolved into a combination of both chemical and mechanical tests. Various tests may be required to further improve aggregate quality control in order to properly analyze the interactions between aggregate and concrete.

2.7 AGGREGATE GEOLOGY/LITHOLOGY

The term "limestone" can be applied to any rock formed mostly of calcium carbonate ($CaCO_3$), but to geologists, limestone is only one of several types of "carbonate rocks" (Oates, 1998). These carbonate rocks are composed of more than 50% carbonate minerals; generally calcite (pure $CaCO_3$) or dolomite (calcium-magnesium carbonate, $CaMg[CO_3]_2$) or both (Boynton,

1980). Mineralogically, limestone is composed of four minerals: calcite - $CaCO_3$, aragonite (a less stable form of calcite) - $CaCO_3$, dolomite - $CaMg(CO_3)_2$, and magnesium carbonate - $MgCO_3$ (Oates, 1998). These minerals are all present in different quantities depending on the limestone formation; classification of limestone can be complicated due to the numerous varieties, forms, and impurities.

Florida is a unique state where many marine formations have taken place over multiple geological eras. Primary sources of limestone aggregate come from formations deposited from the Eocene, Miocene, Oligocene, and Pleistocene era (Sellards, 1919). Each of these eras contain different characteristics organically, chemically, and lithologically. Analysis of aggregate based on the relationship of chemical properties and the geologic era they come from is not well documented. Marine limestone forms when seawater has high concentrations of two key dissolved chemicals – calcium (C^{++}) and bicarbonate ions. Some limestones have been changed by the introduction of magnesium in ground water. Magnesium in ground water may convert some or all of the calcite in the limestone to dolomite (Sellards, 1919).

The Miami oolite, named by Sanford (1909) for the "oolitic limestone of Pleistocene age which covers a large part of the southern tip of Florida, has been found to consist of two separate units—an upper unit, herein designated the oolitic facies, and a lower unit, called here the bryozoan facies," (Hoffmeister et al., 1967). The difference in these layers is based on the time scale they were formed and it is not clear what effect their formation has on their mechanical or chemical properties, specifically for use in concrete. In this paper the two units are combined as the Miami limestone, a formational name which now seems more appropriate than the Miami oolite. The bryozoan facies accounts for the majority of Dade County and expands into surrounding areas spanning a total area of about 2,000 square miles. These limestone formations, like most formations in Florida, are all marine in origin and have been built up over thousands of years to the aggregate product we use today.

Marine limestone formation consisting of shells and skeletons of plants and animals are accumulated through deposition. Deposition can be the naturally occurring dissolution of these fossils over time and precipitation to form layers of calcium carbonate through the solvent action of carbon dioxide, forming calcium bicarbonate. Direct precipitation of the carbonate through solution is caused by temperature increase or through evaporation (Boynton, 1980). Porosity is of particular importance due to the diagenetic formation of sedimentary rocks. Diagenesis is the change of sediments into rock, during or after lithification, without the pressure or temperature required to form metamorphic rock. This diagenesis process is chemical, physical, or biological but cannot contain metamorphosis and is therefore subject to a greater amount of impurities. Microporosity can vary greatly ranging from hard, well-indurated limestone, to soft, chalky limestone (Maliva et al., 2009).

2.8 SUMMARY

"Concrete can aptly be considered a composite of composites, heterogeneous at both the microscopic and macroscopic levels" (Popovics 2001), thus the determination of a relationship between any two parameters within concrete must incorporate the physical properties of each of the composites.

The accurate determination of the modulus of elasticity and the correction factors for given aggregates requires establishing the physical properties of the aggregates. Additionally, it is imperative that concrete mixtures be understood on both the macroscopic and microscopic levels.

3. COARSE AGGREGATE SELECTION

3.1 BACKGROUND

The selection of aggregate used for this project was to provide a representative sample of different coarse aggregates produced in Florida and used in structural concrete to provide a comparative relationship with granite. Most of the coarse aggregate produced in Florida is a limestone material, which is more porous, less dense, and softer than the aggregates produced from other areas of the U.S. One of the primary goals of this research was to determine the relationship between the physical properties of granite and the variety of limestone aggregates produced in Florida.

The different types of coarse aggregate chosen for this research have a variety of physical properties commonly used to create concrete mixtures for FDOT owned structures. The process of aggregate selection included several different types of limestone from different geological formations throughout Florida. The methodology for aggregate selection for this research focused on the acquisition of representative samples of each aggregate type based on prevalence, use, and class of concrete used by FDOT. Geographic, lithographic and geologic properties were considered, as they often affect the chemistry and physical properties of the aggregate. The potential for deleterious reactions between the aggregate and the portland cement are dependent upon aggregate chemistry as well at the chemistry of the cement. The physical properties such as hardness, absorption, and specific gravity were considered. The primary focus for the aggregate selection itself was based on the use of aggregates used for structural concrete. This included aggregates that are typically used in class II and class VI concrete. The five aggregates selected for physical testing, each exhibit unique characteristics, such as surface roughness and absorption, but additionally may share some properties such as classification (limestone), density (granite and Calera limestone). Ultimately, the selection of aggregate used for this project provides a comparative relationship with granite and a representative sample of different coarse aggregates produced in Florida.

3.2 AGGREGATE AVAILABILITY

The aggregate selection was performed concurrently with the task of mix design and selection as the research is contingent upon the ability to produce consistent concrete mixtures in the laboratory while minimizing variables within each concrete mixture as well as variables within the aggregate itself. The process of aggregate selection involves searching the database of the FDOT approved mining sources with approved mixes and determining potential aggregate sources for research based on frequency of use, location, and composition. Coarse aggregate sources which were prevalent and were currently being mined for use in concrete mixes for FDOT were prioritized. Limestone aggregates that provided major geological differences from the most common aggregates, such as oolite and granite were selected to provide variety within the coarse aggregate sources themselves.

To determine the current status of aggregate use in Florida, approved FDOT mixes were compiled and analyzed for selection. The approval process for concrete mixes is prescribed by the FDOT specification 346 using several parameters which include minimum compressive

strength, air content, water-to-cement ratio, slump, unit weight, and minimum cementitious content. The FDOT database used to inventory each of the approved concrete mixtures documents aggregate sources and is a useful tool for the mixture selection process. Therefore, this research utilized the FDOT database of approved mixtures for the mixture design in the laboratory. Initial search parameters included mixes that were current, approved, and specified a desired gradation. The concrete mixes were accessed and filtered through an SQL server command, which discriminates mixes by the selected parameters as shown in Figure 3.1. The goal of the data query was to include as many mixes as possible, and over 1100 approved mixes were accessed and sorted using the SQL server. However, the determination of parameters to be queried was performed with the SQL database prior to investigation of the concrete mixes manually.

```
select distinct design_mix as Mix, class as Class, min_strength
  2  where a.dmkey = b.dmkey_ref
  3  and a.min_strength_units ='psi'
  4  and b.product_code ='C10'
  5  and b.product_name ='# 57 Stone'
  6  and a.class = any ('I PAVEMENT','II DECK','IV','V','VI')
  7  and a.dict_status ='CURRENT'
  8  and b.dict_status ='CURRENT'
  9  and a.mix_design_status  ='APPROVED';
```

Figure 3.1 Parameters used to filter FDOT approved mixes

Since coarse aggregate used in concrete is available in a variety of gradations, one of the first variables investigated was prevalence of the size and gradation of the coarse aggregate. Based on the initial data queries of Florida mixes and discussions with FDOT personnel, it was decided to use #57 stone for coarse aggregate in this research as this gradation is commonly used in FDOT approved concrete. Since the requirements per ASTM C39 specify aggregate size must be at least half the size of the diameter of the concrete specimen, it was decided to remove gradations containing aggregates larger than 2 inches as this research requires the use of four inch cylinders for specimen creation. Of all available gradations, #57 stone lies in the middle of the sieve size ranges as shown in Figure 3.2 (ASTM, 2004).

Size Number	Nominal Size	Amounts Finer than Each Laboratory Sieve, Mass Percent													
		4 in.	3 1/2 in.	3 in.	2 1/2 in.	2 in.	1 1/2 in.	1 in.	3/4 in.	1/2 in.	3/8 in.	No. 4	No. 8	No. 16	No. 50
1	3 1/2 to 1 1/2 in.	100	90 to 100	-	25 to 60	-	0 to 15	-	0 to 5	-	-	-	-	-	-
2	2 1/2 to 1 1/2 in.	-	-	100	90 to 100	35 to 70	0 to 15	-	0 to 5	-	-	-	-	-	-
3	2 to 1 in.	-	-	-	100	90 to 100	35 to 70	0 to 15	-	0 to 5	-	-	-	-	-
357	2 in. to No 4	-	-	-	100	95 to 100	-	35 to 70	-	10 to 30	-	0 to 5	-	-	-
4	1 1/2 to 3/4 in.	-	-	-	-	100	90 to 100	20 to 55	0 to 15	-	0 to 5	-	-	-	-
467	1 1/2 to No. 4	-	-	-	-	100	95 to 100	-	35 to 70	-	10 to 30	0 to 5	-	-	-
5	1 to 1/2 in.	-	-	-	-	-	100	90 to 100	20 to 55	0 to 10	0 to 5	-	-	-	-
56	1 to 3/8 in	-	-	-	-	-	100	90 to 100	40 to 85	10 to 40	0 to 15	0 to 5	-	-	-
57	1 in. to No. 4	-	-	-	-	-	100	95 to 100	-	25 to 60	-	0 to 10	0 to 5	-	-
6	3/4 to 3/8 in.	-	-	-	-	-	-	100	90 to 100	20 to 55	0 to 15	0 to 5	-	-	-
67	3/4 in. to No. 4	-	-	-	-	-	-	100	90 to 100	0	20 to 55	0 to 10	0 to 5	-	-
7	1/2 in. to No. 4	-	-	-	-	-	-	-	100	90 to 100	40 to 70	0 to 15	0 to 5	-	-
8	3/8 in. to No. 8	-	-	-	-	-	-	-	-	100	85 to 100	10 to 30	0 to 10	0 to 5	-
89	3/8 in to No. 16	-	-	-	-	-	-	-	-	100	90 to 100	20 to 55	5 to 30	0 to 10	0 to 5
9	No. 4 to No. 16	-	-	-	-	-	-	-	-	-	100	85 to 100	10 to 40	0 to 10	0 to 5

Figure 3.2 ASTM C33 gradation chart

The final selection of aggregates was based on aggregate properties such as durability, geologic background and frequency of use in FDOT mix designs. The availability of desirable gradations

as well as physical and chemical aggregate properties were primary factors with respect to the initial selection of aggregates. Facilitation of the selection process began with cross-comparing mixtures that utilized #57 stone with the current list of FDOT-approved aggregate sources. The frequency of use of #57 stone in Florida mixes was verified based on the database provided by FDOT and its inclusion in each mine source as provided by in Table 3.1. It is clear that #57 and #89 coarse aggregate are available from a variety of Florida mines regardless of geologic formation or geographic location. However, it was decided to use #57 gradation of coarse aggregate as the #89 gradation is less frequently used and has a smaller nominal size.

Table 3.1 Example of aggregate gradation with occurrences by mine

	Occurrences in FDOT mixes				
Mine #	87145	87339	934506	GA-178	AL-149
#89 Stone	57	45	96	34	18
#57 Stone	256	245	233	75	50

Portland cement concrete (PCC) is an engineered, heterogeneous material with a number of constitutive materials that are relatively expensive to transport, and is often locally sourced to minimize costs. Florida's mines have been producing aggregate for years and a number of mines are being depleted. In January of 2011, the Transportation Research Board (TRB) conducted a workshop entitled, "Aggregate Source Depletion and Future Supply" where the subject of finding future sustainable aggregates was of primary concern. Further studies have indicated that although the mining of aggregate declined during the economic recession of 2008-2011, net total demand has increased with an added emphasis of finding aggregates that provide durability for roadways (Meininger, et al. 2011). It is for this reason that aggregate selection for this study not only focused on FDOT approved aggregates that were most commonly used, but also less favorable aggregates that exhibited higher abrasion but may be required to become a more heavily sourced material once the supply of adequate aggregates is exhausted. The use of inferior or tiered aggregates, while not currently utilized, are anticipated to contribute a significant portion of the future supply due to the inevitable lack of sufficient coarse aggregate material in Florida (Bekoe, 2013). The incorporation of such aggregate in PCC will likely require a change in mixture design for each class of concrete.

A separate table was made listing Florida approved mines and the class of concrete mixtures that had been approved from these mines. While initially considered, it was decided not to include the use of unapproved (tiered) aggregates in this study. This facilitated the proper design of concrete mixtures by allowing approved mixes to be paired with aggregate sources. By doing so, selected aggregates would meet minimum standards of quality, durability, and gradation set by the FDOT. This eased an additional concern that once mix designs were finalized, tiered aggregates would not perform predictably, requiring modifications to critical mix design constraints like cement content or water-to-cement ratio and other mixture parameters. A summary table of each aggregate, and its use in concrete mixture class per FDOT specification 346 is shown in Figure 3.3.

Pit	I	II Pavement	IV	V	VI
GA553			X		
GA383			X		
GA178				X	
AL526	X	X	X		
AL519	X	X	X		
AL149	X	X	X	X	
93406	X	X	X	X	
87339	X	X	X	X	X
87145	X	X	X	X	X
87090	X	X	X	X	X
87089	X	X	X	X	X
87063	X	X	X	X	
87049	X	X	X		
38627	X	X	X	X	
38268	X	X	X	X	X
38228	X	X	X	X	X
12599		X	X		
12521	X	X	X	X	
12260	X	X	X	X	
12008	X	X	X	X	
10645	X	X	X	X	
8012	X	X	X		
8005		X	X		
3616	X	X	X	X	

Figure 3.3 Initial pit and mix type data integration

Each mine that utilizes #57 stone was queried and analyzed based on class of mix with class VI being the highest strength and class I, the lowest. The selection of aggregates then focused on three categories. First, common purpose aggregates from mines that could produce a majority of each mix class. Next, mines that were exclusive to higher strength mix designs as well as aggregates exclusive to lower strength designs. The lower strength classes indicate aggregate sources that could be potentially considered to be of inferior quality due to strength or durability. Aggregates used in multiple classes of concrete could be indicative of consistent quality, behavior, and availability. And aggregates that were exclusive to high strength classes may indicate high strength. This range of properties was a priority with respect to selecting aggregates. This would allow the analysis of many different aggregate effects in Florida concrete mixtures.

3.3 SELECTED AGGREGATES

3.3.1 Miami Oolite

Miami oolite is used in the majority of FDOT concrete mixes and is mined from one of the largest quarries in terms of production in the United States of America (Willet, 2009). Concrete produced with Miami oolite is stronger than concrete made with most other limestone from other mines in Florida (Williams & Tyner, 1949). The FDOT-approved mine from which this material was selected provides an abundant supply of limestone for concrete production in Florida. Boulders were sampled from the active mines, and the samples were cored from pit number 87090 in Miami. The mine sampled is named the F.E.C. Quarry.

3.3.2 Brooksville Limestone

Brooksville, FL aggregate, from pit number 08012, is considered part of the Ocala limestone formations by the USGS. Brooksville aggregate is a white, poorly to well indurated, poorly sorted, very fossiliferous limestone (Scott, 1991). This area produces a lower quality aggregate than oolite, and the mine has to blend rock from different limestone layers to acquire suitable material. The blending process happens before grading, and during the crushing process. Determining where limestone layers of suitable quality are located is governed primarily by specific gravity readings from sample cores. Subsequent to blending, the limestone can be crushed to specified gradations which provides an adequate and consistent blend of materials that are within the limits of FDOT specifications. Although there are typically several different sources of limestone present in the Brooksville formation, some of which are not acceptable for use on their own, the final product results in an acceptable product. Because of this, Brooksville mining typically produces aggregates of varying lithography. The marine formations in the limestone produced in Brooksville are from Eocene era, but literature also suggests that varying layers may constitute the makeup of mining strata depending on location (Hine, et. all, 1988). Brooksville aggregate is typically not used in high strength structural concrete mixes. Due to the presence of inadequate material within the final product, Brooksville aggregate was not found in FDOT mixes that required high strength, however it was present in class II deck, a structural mix. One physical aspect of the aggregate that relegates its use to lower strength is its comparatively lower resistance to abrasion. A test performed to qualify aggregates for FDOT use is the L.A. abrasion test, in which aggregates that exhibit high abrasion numbers (low durability) have lower compressive strength as presented in

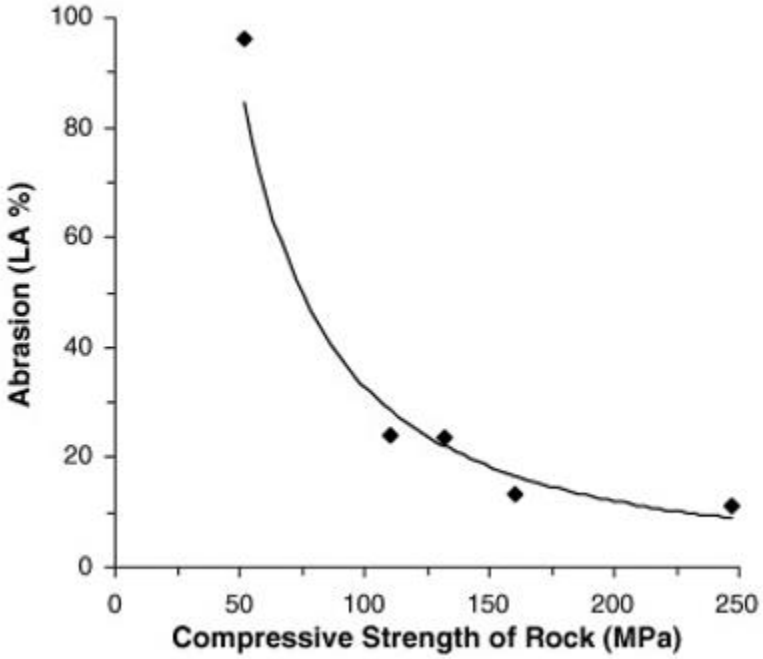

Figure 3.4 (Kılıç et al., 2008).

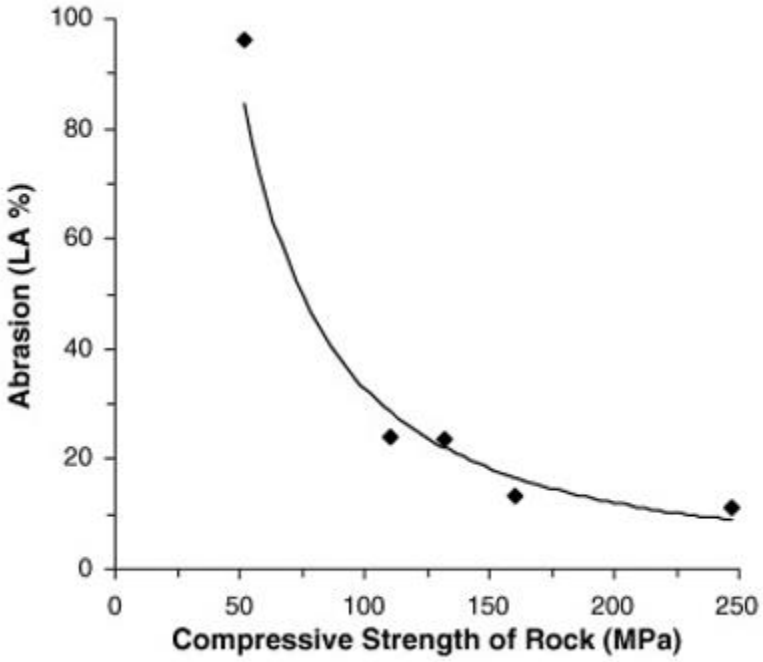

Figure 3.4 LA Abrasion relating to compressive strength (Kılıç et al., 2008).

3.3.3 Perry Limestone

For the third aggregate, a mine in Perry, FL with a pit number of 38228 was selected. Similar to Brooksville, this mine is situated in a geologic area that produces aggregates that vary in quality. However, unlike Brooksville limestone, Perry limestone is denser and has higher abrasion resistance. This aggregate is also unique due to its red coloration possibly attributed to ferric compounds deposited by algae or existing in the water at time of formation. The selection of this aggregate was predicated upon research showing comparable performance despite these unfavorable qualities. Final selection included the FDOT approved aggregate to conform to requirements for all aggregates to be of a similar minimum quality, but still variable in composition, performance, and location.

3.3.4 Calera Alabama Limestone

The fourth aggregate selected for comparison due to its strength and durability. It was sourced from Calera, Alabama, pit number AL-149. This limestone is known for its flint content and corresponding high durability. Not to be confused with Calera limestone from the California coast, this aggregate is made from Cambrian-Ordovician carbonate rocks which often give a bluish hue. This separates this limestone from Florida limestones, not by geographic region, but by another geologic formation period. This limestone showcases how limestone is a very general term that encompasses a large number of carbonate rocks which may have very different origins and properties. Its inclusion in the list also provides a limestone which may not suffer from high marine content or other deleterious materials present in Florida limestones. Calera limestone has low absorption, which may inhibit the formation of a dense, well-bonded (ITZ), affecting compressive strength and modulus of elasticity (Hussin & Poole, 2011).

3.3.5 Georgia Granite

Georgia granite was chosen to serve as a reference point for coarse aggregate in concrete with known strength and modulus properties; for reasons similar to those for Calera limestone. It has high strength, low porosity, and high durability, which as suggested for Calera limestone, may detrimentally affect ITZ development. In Florida, it is typically used only in high strength structural concrete. Granite is not mined in Florida and often has a higher cost with respect to local aggregate as a consequence of transportation-. The granite source was mine GA-178, located near Macon, Georgia.

4. MIX DESIGN SELECTION

4.1 BACKGROUND

This study was initiated to evaluate the suitability of different Florida aggregates for use in structural concrete. Rather than evaluate all classes of structural mix designs, two were chosen that represent the lowest and highest strength classes, Class II Deck and Class VI, respectively. Aggregates were selected that represented a range in quality of Florida limerock, along with high quality Calera limestone and granite. A primary goal of the research was to determine accurate values for the aggregate correction factors used for modulus prediction in design equations used by the FDOT Structures Design Office. Class F fly ash was the only SCM used in this study to minimize the compositional effects for the calculation of K_1 aggregate correction factors.

4.2 FDOT CLASSES OF CONCRETE

The Florida Department of Transportation (FDOT) specifies classes of concrete as shown in Table 4.1 (FDOT, 2015).

Table 4.1 FDOT Concrete Classes and Specifications Compiled from Standard Specifications for Road and Bridge Construction Section 346 (FDOT, 2015)

Class of Concrete	28-day Compressive Strength (psi)			Minimum Cementitious Content (lb/yd^3)	Maximum w/cm (lb/lb)*	Target Slump (in)
	Minimum	Over Design	With Over Design			
I	3,000	1,200	4,200	470	0.53	3
I (Pavement)	3,000	1,200	4,200	470	0.50	2
II	3,400	1,200	4,600	470	0.53	3
II (Bridge Deck)	4,500	1,200	5,700	611	0.44	3
III	5,000	1,200	6,200	611	0.44	3
III (Seal)	3,000	1,200	4,200	611	0.53	8
IV	5,500	1,400	6,900	658	0.41**	3
IV (Drilled Shaft)	4,000	1,200	5,200	658	0.41	8.5
V (Special)	6,000	1,400	7,400	752	0.37**	3
V	6,500	1,400	7,900	752	0.37**	3
VI	8,500	1,400	9,900	752	0.37**	3

*The calculation of the water to cementitious materials ratio (w/cm) is based on the total cementitious material including cement and any supplemental cementitious materials that are used in the mix.

**When the use of silica fume or metakaolin is required, the maximum water to cementitious material ratio will be 0.35. When the use of ultrafine fly ash is required, the maximum water to cementitious material ratio will be 0.30.

The Class II Bridge Deck and Class VI structural concrete mix categories were chosen to provide the maximum design strength range, 4500 psi and 8500 psi, respectively. Minimum cementitious content and maximum w/cm values are 611 lb and 0.44 for the Class II Bridge deck and 752 lb and 0.37 for the Class VI mix design.

4.2.1 Search Parameters

Mixes were procured from the FDOT database of approved mixtures using the LIMS database and the criteria used to search the database included the following:

- Mixes which were approved within the last 5 years,
- Utilized only one aggregate, a #57 gradation, and
- Contained aggregates from FDOT approved mines.

Class I Pavement, II, IV, V, and VI mix designs were queried and then compiled to list an average of properties. Recently approved mixes were selected for summary in order to associate the use of aggregate with current testing standards and applications, and to draw from mining resources which would most likely still be in production. The rationale for the use of the #57 gradation was discussed in section 3 in detail; however, in summary, its exclusive inclusion is to minimize as much variability as possible. Mixtures with differing gradations did not need to be considered.

4.2.2 Mixture Analysis

Each concrete class surveyed resulted in a number of mixes that met all criteria and were thus suitable for consideration. However, the number of mixtures available for each class ranged from 8 to 18. The comparison process considered each constituent material, its average quantity, and the ratios between these quantities. Of particular importance were the coarse-to-fine aggregate ratio and water-to-cementitious material ratio. Outlier mixes that were not considered included mixes that did not use similar admixtures, incorporated relatively high pozzolan contents, or contained other ingredients not suitable for this research. No additional cementitious replacements, such as slag or silica fume, were investigated; however, mixes containing each were queried as part of the selection process. The decision was made to reduce as many variables/ingredients as possible in order to focus on coarse aggregate interactions with typical portland cement concrete. Most FDOT-approved mix designs do not use slag or silica fume, making the proposed mix designs representative of most FDOT mixes.

Mix design selection involved the compilation of multiple FDOT mixes into datasets in an effort to determine the physical properties used to determine final mix selection. An example mix design for a class I pavement is displayed in Table 4.2. Proposed mixes for each class were selected by considering common attributes among these mixes. The preliminary proposed mixes are presented in Table 4.3.

Table 4.2 Typical FDOT approved concrete mixture designs for class I pavement

I Pavement								
Mine Number	**3616**	**3616**	**AL526**	**87089**	**87089**	**38627**	**38627**	**10645**
Mix Number	01-1114	01-1094	03-1827-01	05-1438-02	05-1495	02-1253-02	03-1626-03	353-117
Cement (lb)	400	204	405	400	200	406	423	850
Type	II	II	?	II MH	II	II	II	I
Slag (lb)		204			200			
Class F Fly Ash (lb)	115	102	103	105	100	102	119	
Silica Fume (lb)								
Name								
Metakaolin (lb)								
Source								
#57 Stone (lb)	1665	1670	1900	1725	1720	1756	1760	1600
Silica Sand (lb)	1395	1373	1324	1321	1325	1293	1362	1112
Air Entrainer (oz.)	3	3	1	3	2	5.1	1	3
Name	AEA92 S	AEA92 S	Darex AEA	Darex AEA	AEA92 S	AEA92 S	AEA92 S	Darex AEA
Type D Admixture (oz.)	25.75	40.8	25.4 ++ 7.6	24	45	20.3	51	21.3
Name	Eucon WR	Eucon WR WRDA 64 ++ Recover		WRDA 60	Eucon WR	Eucon WR	Eucon WR	WRDA
Type F Admixture (oz.)								51
Name								ADVA Cast 575
Type I Admixture (oz.)								
Name								
Type E Admixture (oz.)								448
Name								Daracce
Corr Inh Admixture (oz.)								
Name								
Water (weight)	250	254	254	254	250	248	271	274.9
Geological Type	Limestone	Limestone	Limestone	Limestone	Limestone	Limestone	Limestone	Limestone
W/C	0.485436893	0.498039216	0.5	0.502970297	0.5	0.488188976	0.5	0.353529412
w/cm max	0.502970297							
w/cm min	0.353529412							
w/cm avg	0.480281988							

Table 4.3 Proposed mix designs

Mix Designs

	Total Cementitous (lb)	W/CM	Coarse (lb)	Fine (lb)	Air Entrainment	Admixtures	Fly Ash Replacement
Type I	510	0.5	1730	1330	4%	Air Entrainer - AEA92 S Type D-Eucon WR	20%
Type II Deck	625	0.44	1740	1200	4%	Air Entrainer - AEA92 S Type D-Eucon WR	20%
Type IV	720	0.38	1720	1100	4%	Air Entrainer - AEA92 S Type D-Eucon WR Type F - Plastol 6200 EXT	20%
Type V	850	0.33	1700	1010	4%	Air Entrainer - AEA92 S Type D-Eucon WR Type F - Plastol 6200 EXT	20%
Type VI	940	0.3	1660	1000	4%	Air Entrainer - AEA92 S Type D-Eucon WR Type F - Gelnium 7500	20%

The incorporation of 20% fly ash replacement is standard in FDOT mixes; the incorporation of admixtures was suggested, but dosages were dependent on the individual mixes to ensure the plastic properties which were obtained throughout the mixing process remained consistent. Suggested dosages were incorporated as per manufacture and then experimentally verified with foot trial batches before the final mix design was selected. A testing matrix was developed to calculate the total volume of concrete that was to be made for testing purposes for all of the proposed mixes. This information is presented in 4.

4.2.3 Mix Class Selection

The testing for the laboratory portion of the research project required the concrete mixtures be created in the laboratory be approximately 17.5 cubic feet. Combined with the previously selected five aggregates used in Florida mixes and the five different classes of concrete mixes compiled, the amount of concrete and the associated time and cost to test these mixes expanded beyond the scope of this project. It was necessary to choose only two different classes of mixes which would best represent common uses for Florida concrete. One selection includes class II bridge deck pavements since these mixes do not require high strength and are commonly used for roadways, bridge decks, and slabs. The final selection was a class VI concrete, a high performance concrete that best matched previous research by the NCHRP into pre-stressing and high performance application where coarse aggregate was shown to have significant influence on concrete properties.

Table 4.4 Testing matrix used in calculating mix volumes and testing procedures

Mechanical Properties Aggregate Matrix - Core Blocks

Date: 10/3/2013	Cylinders and Blocks						Cylinders only		Total Number of Cylinders	Volume of Concrete for Cylinders	Total Volume of Concrete Cylinders
Test Method	ASTM C39	ASTM C469 *	ASTM C496	AASHTO TP-95	AASHTO TP-336	ASTM C78	ASTM C 157	ASTM C 157			
Common Test Name	Comp. Strength + E[1,2,3]	Modulus of Elasticity	Splitting Tension[1,2]	Surface Resistivity	Coeff. Thermal Exp.[1,2,4]	Beam Tension + E[1,2,3]	Shrinkage[1] (3"x3"x11")	Shrinkage[1]			
Sample Size	4"x 8" Cylinder	4"x 8" Cylinder	4"x 8" Cylinder	4"x8" Cylinder	4"x 8" Cylinder	4"x 4"x 12" Blocks	Concrete	Paste			
Mix Name	Number of Samples Per Test, PerTesting Time								70	(ft³)	(ft³)
Laboratory Mixes: Aggregate Type	3	3	3	3	2	3	3	3			7.33
1 day	☑ C39	☑ C469	☑ C496	-	☑ Tp-336	☑ C78	☐ C157	☐ C157-Paste	14	0.9733	
3 day	☑ C39	☑ C469	☑ C496	-	☑ Tp-336	☑ C78	☐ C157	☐ C157-Paste	14	0.9733	
7 day	☑ C39	☑ C469	☑ C496	-	☑ Tp-336	☑ C78	☐ C157	☐ C157-Paste	14	0.9733	
14 day	☑ C39	☑ C469	☑ C496	-	☑ Tp-336	☑ C78	☐ C157	☐ C157-Paste	14	0.9733	
28 day	☑ C39	☑ C469	☑ C496	☐ TP-95	☑ Tp-336	☑ C78	☐ C157	☐ C157-Paste	14	0.9733	
56 day	☑ C39	☑ C469	☑ C496	☐ TP-95	☑ Tp-336	☑ C78	☐ C157	☐ C157-Paste	14	0.9733	
91 day	☑ C39	☑ C469	☑ C496	☑ TP-95 (non destructive)	☑ Tp-336	☑ C78	☑ C157 (non destructive)	☑ C157-Paste (non destructive)	23	1.4942	
TOTAL CONCRETE (ft³)	23.70074										

4.3 FINAL MIX SELECTION AND PROCESS

With the final specifications in place, two final mixes were selected. One was a Class II bridge deck mix design with 625 lb of cementitious material and a water-to-cementitious material ratio of 0.46, and the other was a class VI with 920 lb of cement and a water-to-cementitious material ratio of 0.33. Trial batch testing was performed for each these two mixes and the weight of each component was adjusted to keep mix design volumes at 27 cubic ft per cubic yard, while maintain and cement and aggregate ratios. Batch sheets are provided by Table 4.5.

Table 4.5 Class II Deck and Class VI Mix Designs ($1yd^3$)

Component	Class II Deck	Class VI
Cementitious Content (lb)	625	920
w/cm	0.46	0.33
Cement (lb)	500	736
Class F Fly Ash (lb)	125	184
Water (lb)	285	298
GA-397 Fine Aggregate (lb)	1200	990
87-090 Coarse Aggregate (lb)	1615	1525
Air Entrainer (fl oz)	4.7	7.0
Type D Admixture (fl oz)	50.0	68.8
Type F Admixture (fl oz)	0.0	41.3
Design Air Content (vol%)	4.0	4.0

The Class II Deck mix design had a cementitious content of 625 lb (20% replacement by volume of cement with class F fly ash), a w/cm of 0.46, and a design air content of 4 volume percent (vol%). Note that due to a calculation error, the w/cm maximum of 0.44 was exceeded (0.46) for the Class II deck mixes. The Class VI mix design had a cementitious content of 920 lb (20% replacement by volume of cement with class F fly ash), a w/cm of 0.33, and a design air content of 4 vol%.

5. CEMENTITIOUS TESTING

5.1 ISOTHERMAL CALORIMETRY

Isothermal conduction calorimetry measures the heat evolved from hydrating cementitious materials, typically referred to as the heat of hydration. The information obtained by the measurement of the heat evolved from the cementitious material over time can provide insight into the relative reactivity or rate of hydration of the cementitious material.

5.1.1 Summary of Test Method (ASTM C1702)

The American Society of Testing and Materials (ASTM) has standardized the measurement of the heat of hydration of cementitious materials using isothermal conduction calorimetry (ASTM C1702, 2015). An isothermal heat conduction calorimeter consists of a constant-temperature heat sink to which two heat-flux sensors and sample holders are attached. One heat-flux sensor and sample holder contains the sample of interest (cementitious component). The other heat-flux sensor is composed of a reference cell containing a sample that evolves no heat. The heat of hydration released by the hydrating cementitious sample is passed across the sensor to the heat sink. The output measured by the calorimeter is the difference in heat flux (thermal power) between the sample cell and the reference cell. The heat flux gradient between the sample cell and the reference cell, stemming from the heat evolved from the cementitious sample, results in a very small temperature gradient, but this temperature difference is so small that for practical purposes, the sample is considered to be at a constant temperature (isothermal).

5.1.2 Equipment and Procedure

The University of Florida houses a TAM Air isothermal conduction calorimeter made by Thermometric AB, shown in Figure 5.1. The calorimeter has eight channels, which allow for the monitoring of eight individual specimens at a time with an operating temperature range of 5 °C to 60 °C.

Figure 5.1 Internal view of TAM Air isothermal conduction calorimeter

5.1.3 Mixing Procedure

The internal mixing procedure was used for isothermal conduction calorimetry testing in accordance with ASTM C1702 (ASTM C1702, 2015). In this method, dry cementitious material was weighed in a mixing vial and mixing water was drawn into syringes attached to a TA Instruments Admix Ampoule. A plastic stirrer was attached to the Admix Ampoule and it was mounted onto the mixing vial (see assembly in Figure 5.2). The assembly was placed inside the calorimeter and allowed to equilibrate to 23° C. Following the equilibrium phase (usually 2 to 3 hours), the mixing water was introduced to the cementitious material over a 30-second period. Then the material was mixed internally at a rate of approximately 120 rev/min for a period of 90 seconds. The heat evolved from the exothermic cementitious hydration reaction was measured for 7 days.

Figure 5.2 Mixing cell and ampoule used for internal mixing procedure

5.1.4 Isothermal Calorimetry Testing Methodology

Isothermal calorimetry was performed in accordance with ASTM C1702 on portland cement and portland cement-fly ash mixtures (20% fly ash replacement) corresponding to the concrete mix designs being investigated. Two figures are presented to characterize the heat properties of these cementitious materials. Figure 5.3 is the power or rate of change of heat generated over time by the cementitious materials, while Figure 5.4 represents the total heat generated over time of both cementitious mixtures. As exhibited by the figures, the pure cement had higher total heat generation and a higher rate of heat generation than the 20% fly ash replacement mixture. The reactivity of the cementitious system was slowed by incorporation of fly ash, which decreased heat evolution (Langan, Weng, & Ward, 2002).

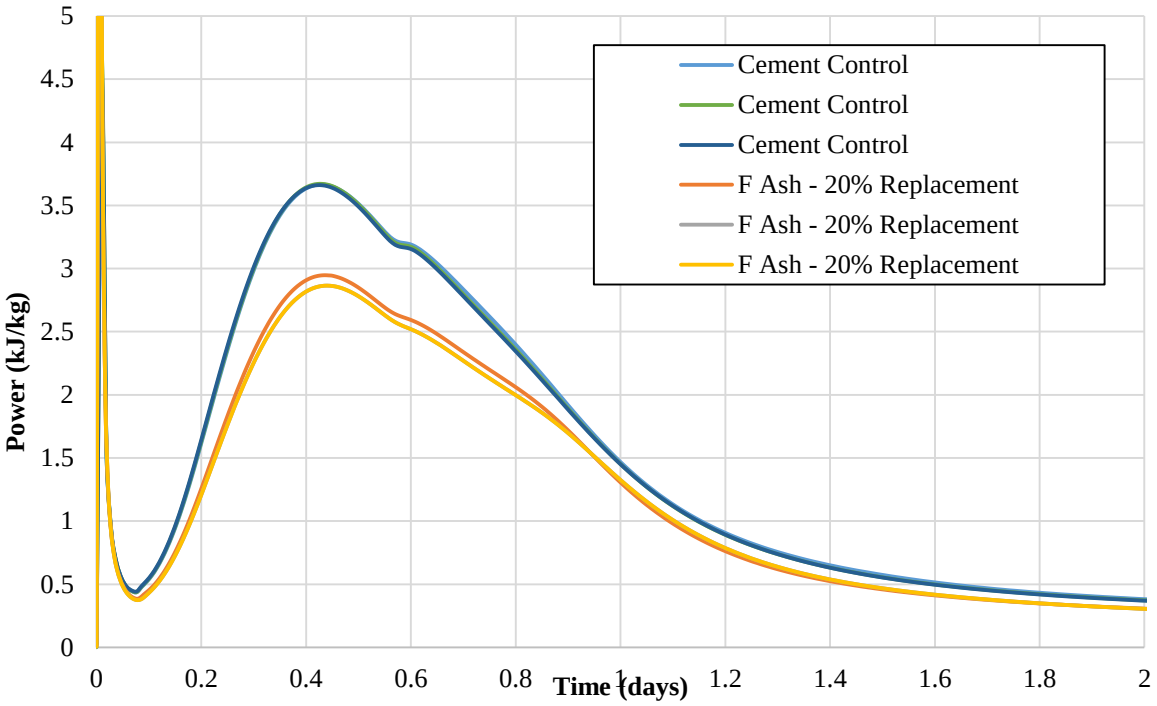

Figure 5.3 Power curve data of portland cement and 20% fly ash replacement

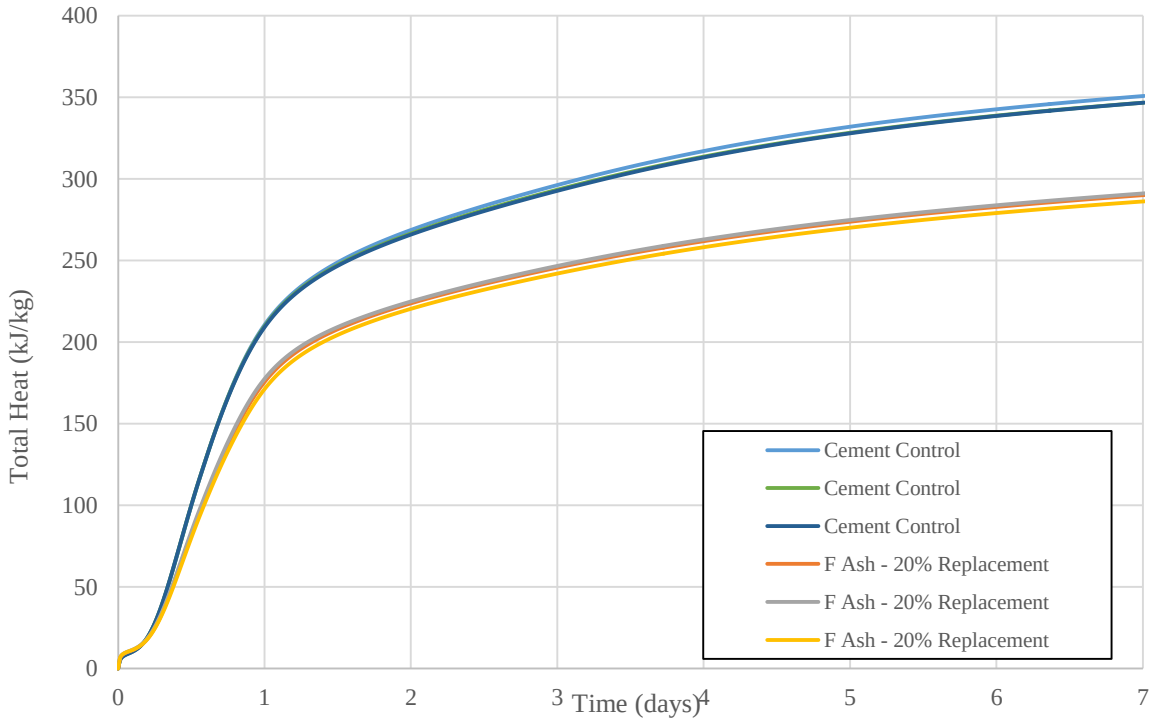

Figure 5.4 Isothermal heat evolution data of portland cement and 20% fly ash replacement

5.2 PARTICLE SIZE DISTRIBUTION

Particle size of materials used for cement replacement is an important characteristic because particle size is related to specific surface. Masses of small particles have larger surface area than the same mass of large particles, and specific surface is directly related to how much surface is available for hydration of the material. During the production of cement, clinker pellets and gypsum are ball-milled into a fine powder. The ultimate size of produced cement particles has a strong influence on the rate at which the cement will hydrate (Sarkar, 1990). The increased surface area (finer particles) contributes more available surface for chemical reaction to occur; increasing the rate of hydration and lowering reaction time (Bentz et al., 1999). This additional hydration contributes to a more completely hydrated and denser microstructure. ASTM C1070 Standard Test Method for Determining Particle Size Distribution of Alumina or Quartz by Laser Light Scattering, uses a machine that allows a representative powder sample to fall in air between two plates of glass as a laser beam is directed at the sample, scattering the light (ASTM C1070, 2014). Based on the light scattering, the size of particles can be determined. Plotting these values as a function of number of particles measured gives a particle size distribution. Figure 5.5 and Figure 5.6 characterize the particle size distribution and the cumulative particle size distribution of the cement used in this research. The mean particle size for the cement was measured to be 10µm. The laser scattering particle analyzer system used for this research was model number LA-950V2 manufactured by Horiba Instruments, Inc.

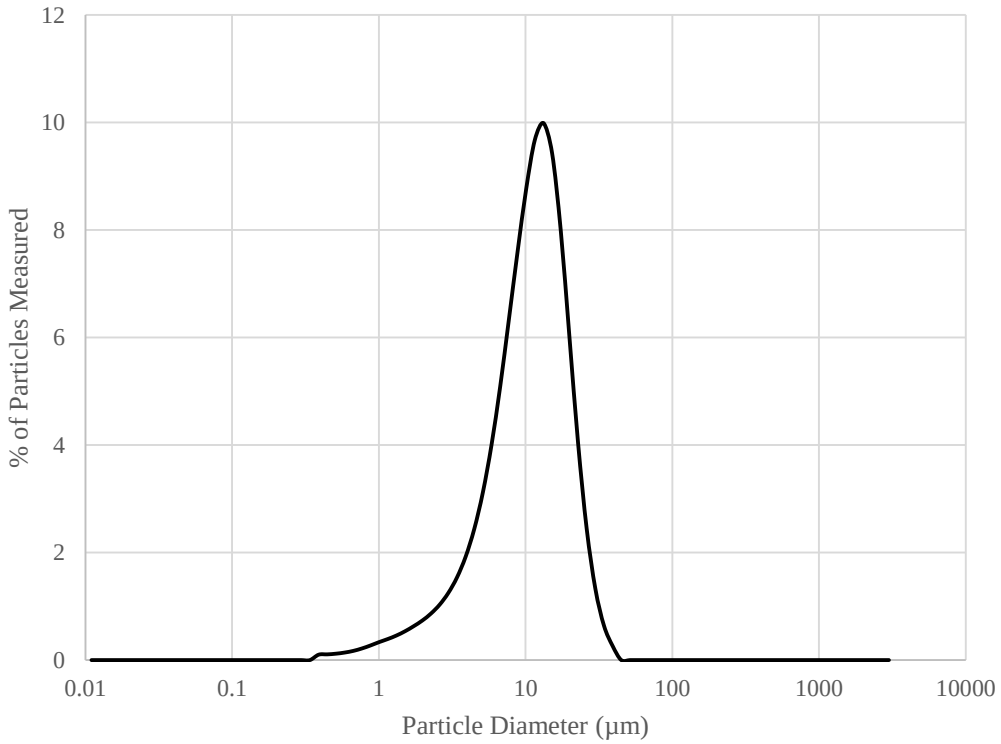

Figure 5.5 Cement particle size distribution

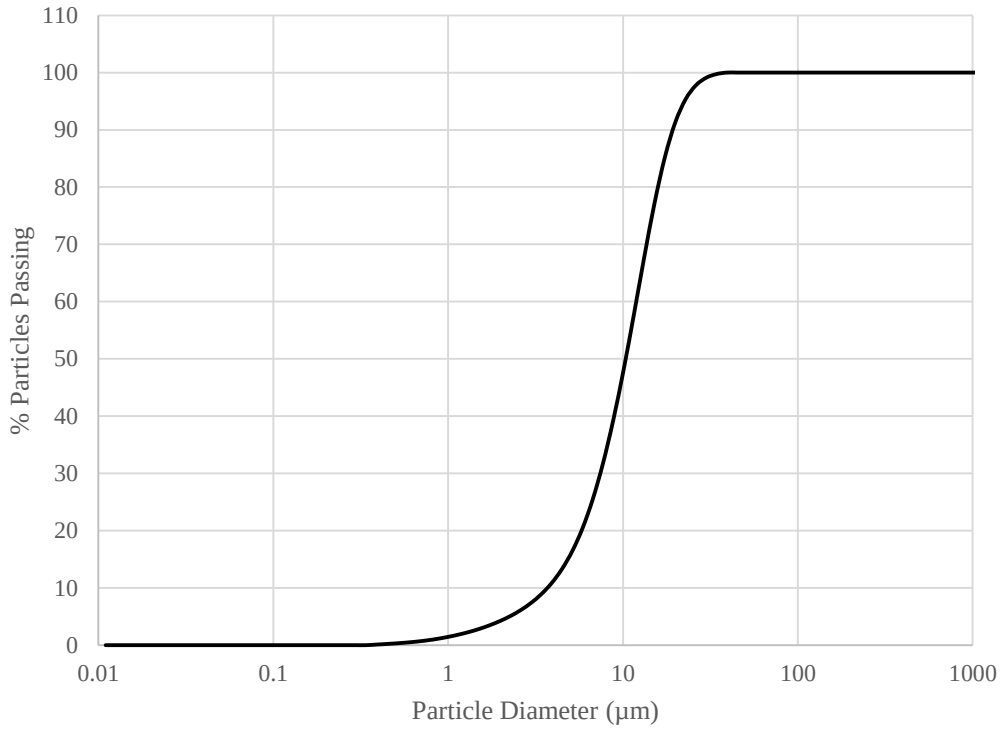

Figure 5.6 Cumulative particle size distribution

5.3 BLAINE FINENESS

The fineness of cements is most commonly determined by measuring the surface area of a cement sample using the Blaine air permeability test (ASTM C204, 2011). The general testing apparatus compares the time it takes a specific volume of air to pass through the standard sample to that of the test sample.

One of the main parameters to describe fineness is specific surface area. Due to biases from both sampling and the operator (amongst other possible factors listed in the specification), the cement was evaluated five times; the maximum and minimum fineness are presented in Table 5.1. "Although the test method may be, and has been, used for the determination of the measures of fineness of various other materials, it should be understood that, in general, relative rather than absolute fineness values are obtained," (ASTM C204, 2011). The average specific surface area of the cement using the Blaine fineness was measured to be 450.7m^2/kg. Note that the surface area increases as a function of the square of the particle diameter and as a function of particle surface roughness.

Table 5.1 Blaine fineness specific surface area

Average Specific Surface Area	443.9	m^2/kg
Maximum	450.7	m^2/kg
Minimum	437.0	m^2/kg

5.4 QUANTITATIVE X-RAY DIFFRACTION

Quantitative X-ray Diffraction is a laboratory method that involves subjecting a prepared powdered specimen to incident x-rays. As the x-rays interact with the crystallites present in the materials, the x-rays are diffracted. The change in angle (from the incident x-ray angle) is known as the Bragg angle (2θ). The 2θ change is related to the crystalline structure of the material being analyzed.

When measuring both the incident angle, Bragg angle, and intensity of light diffracted, a diffraction plot (or Bragg plot) can be constructed, as shown in Figure 5.7 X-ray diffraction pattern of cement sample Based on this plot, the diffraction pattern can be compared to the diffraction plot of known crystalline materials; when a mixture of crystalline materials is present (such as the different crystalline phases of cement), an analysis is done to "balance" the percentages of each material, this is known as a Rietveld analysis. The results of this Rietveld analysis for the portland cement used to create the concrete in this research is presented in Figure 5.7.

Table 5.2 X-ray diffraction of cement sample

Phase	Trial 1 %	Trial 2 %
C_3S	65.7	66
C_2S	14.2	13.8
C_4AF	12.4	12.5
C_3A Cubic	4.2	4
C_3A Orthorhombic	1.2	1.4
CaO (Free Lime)	0.2	0.2
Arcanite (K_2SO_4)	0.3	0.2
Gypsum	1	1.1

Two individual specimens were analyzed and the results are presented in Table 5.2. The results show that C_3S, the primary contributor to early-age strength development, constitutes approximately two-thirds of the mass of the cement sample. The remaining primary cement phases C_2S, C_3A, and C_4AF are present along with the typical minor phases (free lime, alkalis, and gypsum) found in cement (Balonis & Glasser, 2009).

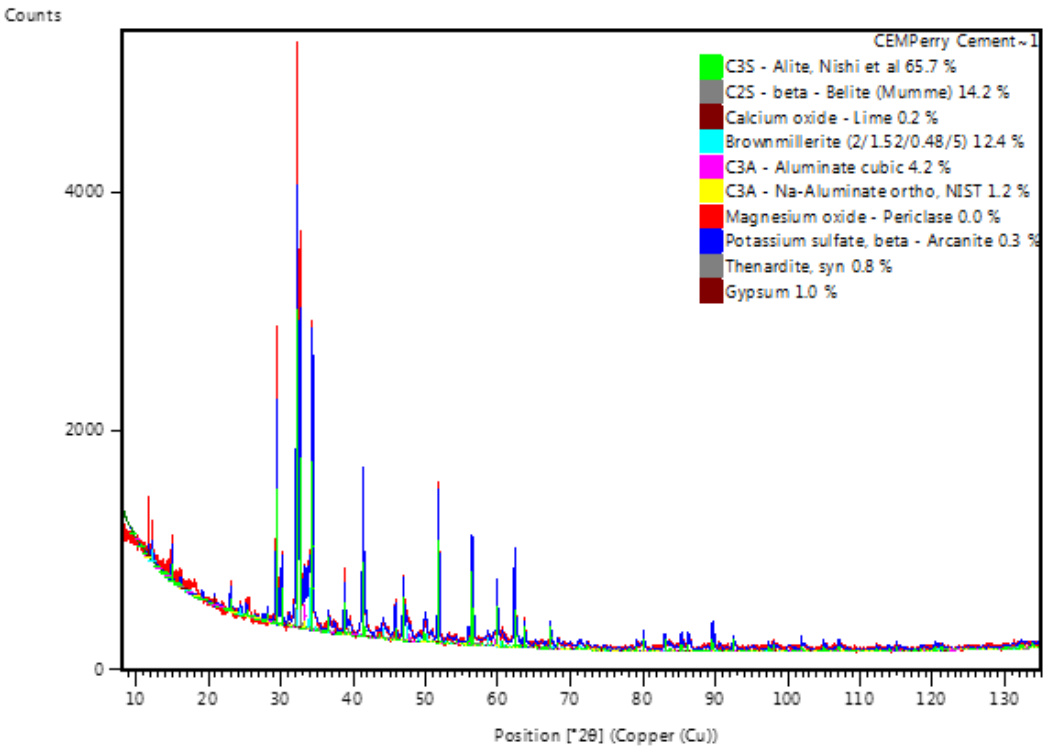

Figure 5.7 X-ray diffraction pattern of cement sample

6. CONCRETE MIXTURE AND SPECIMEN PREPARATION

6.1 BACKGROUND

This section describes the process of the concrete mixture and specimen preparation used for creating the test specimens analyzed in this study. This includes the trial mixes which determine final production mixture proportions, tests run during these mixes, and specimens prepared for later testing research. The Class II Deck and Class VI mix designs utilized for this project and are summarized in Table 6.1.

Table 6.1 Mixture summary used for trial batching

	Class II Deck	Class VI
Water/Cementitious	0.46	0.33
Cementitious Materials	625 lb/yd^3	920 lb/yd^3
Water	285 lb/yd^3	298 lb/yd^3
Fine Aggregate	1200 lb/yd^3	990 lb/yd^3
Coarse Aggregate	1595 lb/yd^3	1700 lb/yd^3
Air Entrainer	~ 5 oz/yd^3	~ 7 oz/yd^3
Water Reducing Admixture	0 to 60 oz/yd^3	0 to 70 oz/yd^3
Superplasticizer	-	0 to 50 oz/yd^3

6.1.1 Safety

Concrete mixing took place while using proper personal protection equipment. This included use of NIOSH approved 95 respirators, nitrile gloves, ear protection, safety-toed footwear, and ANSI Z87.1 approved eye protection.

6.1.2 Trial Mix Batching

Each production mix was preceded by trial batch mixes where plastic properties were targeted with the use of admixtures. Each trial batch was 2.0 cubic feet and used a 7-cubic foot rotary mixer. Trials mixes included all the materials used in production and were performed to the same specifications as the production mix. Materials included were coarse aggregate, fine aggregate, portland cement, class F fly ash, water, and three admixtures. These admixtures were an air entrainer, a Type D retarder and water reducer, and a Type F high range water reducer. Mixing, batching, and curing was conducted in general accordance with ASTM C192 Standard Practice for Making and Curing Concrete Test Specimens in the Laboratory. A total of three separate trial mixes were conducted before each production mix, necessitating the batching of a total of 6.0 cubic feet for each trial. This ensured that any laboratory errors in batching, mixing, and data collection would be apparent and gave the experimenters enough attempts to achieve the desired plastic properties. With two separate class mixtures for five different aggregates, a total of 30 different trial mixes were batched for a total of 60 cubic feet.

6.1.2.1 Coarse Aggregate

Aggregate was soaked for a minimum of 48 hours before each trial, as shown in Figure 6.1 and moisture samples were taken 24 hours before each trial. Batching took place 24 hours before each trial. Coarse aggregate was removed from soaking tanks and allowed to drain for 1 hour in ambient conditions. Coarse aggregate was then mixed together and quartered before batching took place (ASTM C702, 2011). Moisture samples were taken at this time and formed a representative sample from all locations of the batched aggregate. Moisture samples were weighed wet and then placed in an oven for 24 hours as shown in Figure 6.2 to allow a dry measurement prior trial batch production (ASTM C566, 2013). The coarse aggregate moisture content was used to make adjustments to the aggregate weight to compensate for differences from the saturated, surface-dry condition. Coarse aggregate, after proper batching, was stored in airtight containers to prevent evaporation or condensation.

Figure 6.1 Coarse aggregate soaking in tanks at FDOT State Materials Office

Figure 6.2 Moisture coarse aggregate sample placed in oven

6.1.2.2 Fine Aggregate

Fine aggregate was bagged and baked in the oven for 24 hours prior to batching to allow proper drying (ASTM C566, 2013). Fine aggregate was then measured for batching and stored in airtight containers to prevent contamination. The fine aggregate was added dry, so no weight adjustments were necessary.

6.1.2.3 Water

Water was properly batched and stored in airtight containers to prevent evaporation.

6.1.2.4 Cement and Fly Ash

Cement and fly ash were stored in a climate controlled area at the FDOT State Materials Office concrete testing laboratory. Cement was stored on a pallet that was plastic wrapped while fly ash was stored in drum containers with sealed lids. Both were batched and stored in airtight containers to reduce any contamination through hydration or deleterious materials as shown in Figure 6.3.

6.1.3 Trial Mix Procedures

Subsequent to batching, the trial mixing process were performed after proper adjustments were made with the moisture data. Mixes began by coating the mixer with a 'butter" that consisted of separate, pre-batched quantities representing 10% of the total trial. The mixer was then qualitatively inspected to verify proper coating. Once the mixer was properly coated, excess material was removed from the mixer and the trial batch commenced promptly.

Each material was then added in a specific order. In order to properly match mixing behavior between the 7-cubic foot mixer and the eventual production pan mixer, all materials and the order and times of addition to the mixer were recorded. Coarse aggregate was the first material to be added, followed by fly ash, a third of the volume of water, cement, fine aggregate, and the remainder of the water. Admixtures were added as required with the exception of air entrainment, which was always premixed with the first third of water. Fine aggregate was added last, which is not in exact accordance with ASTM C192 (ASTM C192, 2014).

The justification for this altered procedure was the result of workability concerns in the mixer caused by the strict adherence to water-to-cementitious material ratios between mixes. The cement is typically placed last in a mix, however the admixture interactions necessitated the addition earlier in the mix. Admixture effectiveness relies on the presence of cement and water and requires a certain amount of time until full effectiveness is achieved. By adding cement before fine aggregate, the cement and admixture was given time to interact to improve workability.

Figure 6.3 Trial mixes batched and ready for mixing

A standard mixing procedure was adopted, gathered from previous research including Mindess et al., 2003. The batch was mixed for 3 minutes, rested for 2 minutes, and then mixed for 2 additional minutes before plastic properties were taken. Once out of the mixer, the concrete was tested for unit weight (ASTM C143, 2014), slump (ASTM C143, 2014), air content (ASTM C173, 2014), and mix temperature (ASTM C1064, 2012). Once acceptable properties were obtained, admixture dosages were recorded and the final mix design was established.

6.1.4 Production Mix Batching

The batching and mixing of the production mixes followed the same steps as trial mixes in terms of preparation times, aggregate preparation, and order of addition of the materials, except for a few procedural changes due to the nature of a rotary pan mixer. Production mixes consisted of 17-cubic foot mixes and were mixed in a rotary pan mixer. The butter for this mix consisted of the same 10% values of a complete mix but excluded coarse aggregate.

6.1.4.1 Coarse Aggregate

Coarse aggregate was bagged and soaked in the same process as trial mixes but in larger quantity for production. After quartering and moisture samples were taken, coarse aggregate was batched using two large bins that could be lifted with a fork lift onto a suitable scale. Once properly weighed, coarse aggregate bins were wrapped in double layers of plastic and covered to prevent moisture loss.

6.1.4.2 Fine Aggregate

Fine aggregate was bagged, baked, and stored in the same process as trial mixes. Once all quantities of fine aggregate were batched, they were placed on one pallet to facilitate loading for production mixing.

6.1.4.3 Water

Water was batched and stored in the same process as in trial mixes. However, it was placed next to the pan mixer to allow easy access while mixing and was further organized in thirds to follow mixing procedures used in trials.

6.1.4.4 Cement and Fly Ash

Cement and fly ash were batched and stored using the same process as in trial mixes. Once all quantities of cement and fly ash were batched, they were placed on a pallet to allow proper loading for production mixing.

6.1.5 Production Mix Procedures

The pan mixer was first thoroughly coated with a 10% butter mixture of cement and fine aggregate paste by the use of an extended trowel as shown in Figure 6.4.

Figure 6.4 Butter mix being applied to the sides of pan mixer

The coarse aggregate was then hoisted by use of forklift to deposit into the mixer. When one bin of the coarse aggregate was emptied, half the fly ash was added as well. Fly ash was loaded onto the mixing platform by hand with the forklift lifting the pre-batched pallet. One third of the water was also added with the air entraining admixture premixed in. After this phase, portland cement was added as quickly as possible, again by hand with the use of a forklift. Another third of the water was also added while cement was being added. Water reducer was added along with this allotment of water. Finally, fine aggregate and the rest of the water along with plasticizer was added. Approximately 1/3 of the plasticizer was withheld until the other ingredients were properly mixed in case the mix behaved differently in the rotary pan mixer. Occasionally, slump tests were taken directly from the rotary pan mixer before the mix was deposited for placement. Slight adjustments were then made with the remaining admixture to ensure acceptable plastic properties.

After the materials were added, the same mixing procedure as used in the trial mixes was applied, 3 minutes of mixing, 2 of rest, and 2 of further mixing. Thoroughly mixed concrete was then deposited into two large containers, seen in Figure 6.5 under the rotary mixer.

Figure 6.5 Lancaster rotary pan mixer with bins underneath

6.2 SPECIMEN PREPARATION

6.2.1 Background

Specimens for each production mix included 66 cast cylinders, 15 flexure beam samples (contained in three 5-gang metal molds), and two slabs that were placed in a custom mold shown in Figure 6.6.

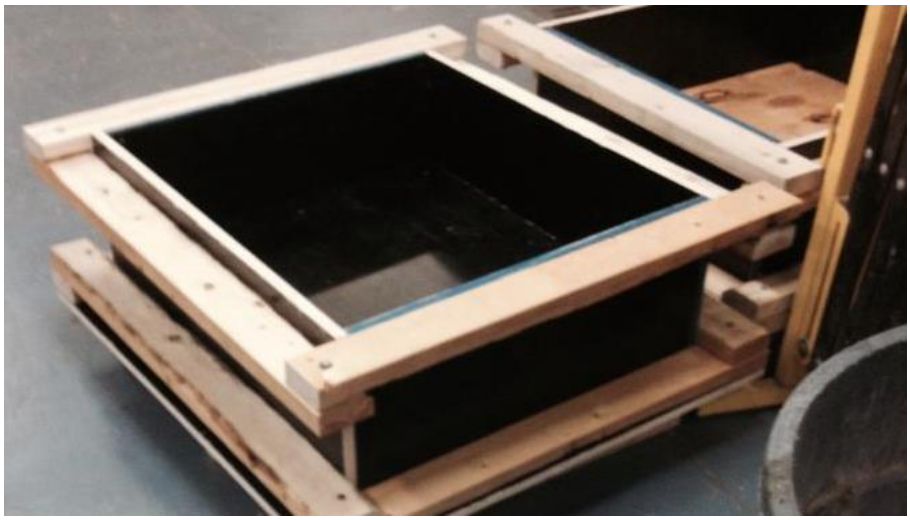

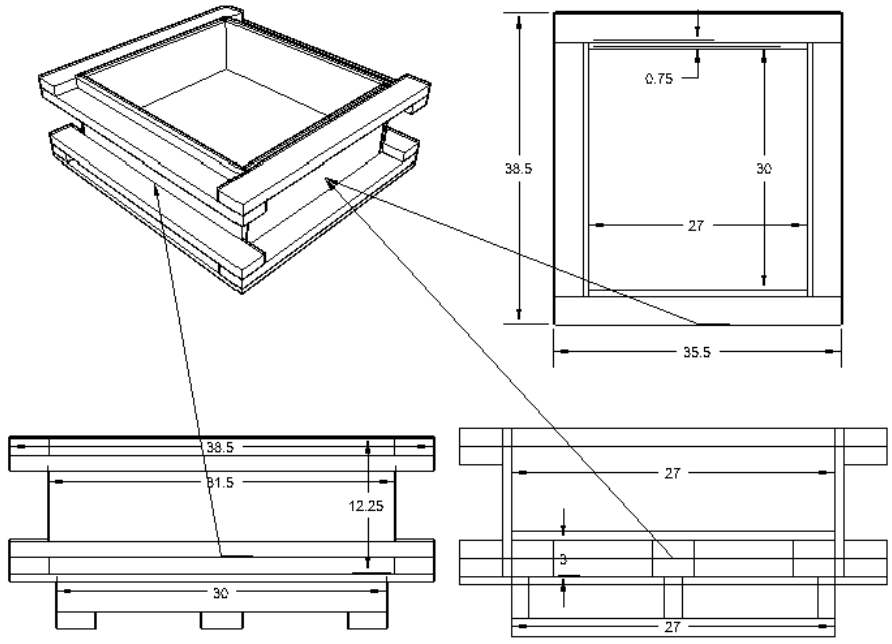

Figure 6.6 Slab mold with measurements in inches

Each mold was designed to allow the coring of thirty-three 4” by 8” specimens, for a total of 66 specimens between the two molds. The molds were designed to have a raised bottom so that a

forklift could be used to move them, allowing easier transport between the FDOT and University of Florida concrete materials laboratory.

6.2.2 Placement Procedure

All specimens were placed in two lifts and vibrated for 10 seconds on the first lift and 20 seconds on the second final lift. The total amount of specimens as well as volume of mixed concrete for the cast specimens is shown in Table 6.2.

Table 6.2 Production total mixture volume and specimens required for cast specimens only

	Cast Specimens Tested Per Day							
Test	3-day	7-day	14-day	28-day	56-day	91-day	Total Specimens	Total Volume (ft^3)
Compressive Strength	3	3	3	3	3	3	18	1.05
Splitting Tension	3	3	3	3	3	3	18	1.05
Modulus of Elasticity	3	3	3	3	3	3	18	1.05
Surface Resistivity	-	-	-	-	-	3	3	0.17
Thermal Expansion	-	-	2	2	-	2	6	0.35
						TOTAL	**63**	**3.67**
Flexure Beam	3	3	0	3	3	3	15	1.94
						TOTAL	**15**	**1.94**
				Totals for Cast Specimens			**78 specimens**	**5.61 ft^3**

6.2.2.1 Cast Cylinders

Cast cylinder specimens were placed in a frame that fit over a vibrating table shown in Figure 6.7. They were standard 4" x 8" cylinders with a lip to provide stability (ASTM C873, 2010). With aid of at least four additional experimenters, all specimens were placed at the same time. Before mixing, at least two workers were assigned to cylinders, one to plastic properties, and the remaining to flexure beam and slab molds.

Figure 6.7 Placement of concrete in cast specimens

6.2.2.2 Flexural Beam Specimens

Flexural beam specimens were 4” x 4” x 12” as per ASTM (ASTM C192, 2014). Flexural beam specimens were also vibrated on a vibrating table for proper consolidation. All techniques used in cast cylinder placement were used in flexural beam placement. Occasionally, stiffer or denser mixes required more vibrating time.

6.2.2.3 Slab Molds

Slab molds were placed in accordance with ASTM C192, which is essentially the same procedure as the smaller specimens, but on a larger scale. After the first lift, the slabs were vibrated using an internal vibrator. Vibration consisted of vibrating the fresh concrete in a matrix of 4 x 4 locations. This grid consisted of each corner, midpoint and quarter of a side extended along the mold. Vibration times varied depending on concrete plastic properties and was qualitatively determined to allow proper consolidation while not contributing to segregation. Vibration of the slab molds is shown in Figure 6.8. The size of the slab molds was calculated based on the number of specimens required and physical dimensions of the coring drill used at the University of Florida concrete materials laboratory.

Figure 6.8 Vibrating of slab molds

Thermocouples were inserted into the fresh slab concrete to monitor temperature rise due to the heat of hydration. An additional four cast cylinders were also monitored to compare slab temperature to cylinder temperature. Thermocouple placement is shown in Figure 6.9. Two thermocouples were centered in the middle and center of the slab. An additional thermocouple monitored the corner and the middle of the edge. Cast cylinder specimen thermocouples were placed in the very center of the cylinders. Temperature data was taken continuously for every minute during the first 24 hours of initial curing by method of a digital monitoring and recording device. Temperature data collected for each concrete mixture is presented in Appendix D.

Figure 6.9 Thermocouple placement

6.3 SPECIMEN STORAGE

After placement of all specimens was achieved, specimens were sealed with plastic to keep in moisture and allow initial curing to begin. After a 24-hour cure, specimens were removed from molds and stored in a moist curing room as shown in Figure 6.10 (water misters off), where constant 100% humidity and 23 degrees Celsius temperature was maintained until specimens were ready for testing.

Figure 6.10 Moist curing chamber at FDOT

6.4 SPECIMEN PREPARATION

Prior to testing, each specimen was prepared as per the relevant ASTM standard that applied to the testing procedure. Cylinders were ground as per ASTM C42. Grinding was accomplished at the FDOT facility so that a flat, planar surface was obtained. Cored specimens were cut and then ground to match cast specimens as shown in Figure 6.11 and Figure 6.12. Nominal cylinder dimensions were 4” x 8”.

Figure 6.11 Concrete saw

Figure 6.12 Grinding cylinders

Destructive tests performed on specimens included compressive strength, splitting tension, modulus of elasticity, and flexural strength. The cylindrical specimens used were prepared as stated above with beam specimens stored in the same moist cure room as cylinders. Non-destructive tests included rebound hammer, ultrasonic pulse velocity, and coefficient of thermal expansion. Only coefficient of thermal expansion required special specimen preparation. As per the AASHTO standard (AASHTO T 336, 2011) specimens were ground to 7" specimens and stored in a saturated lime bath solution at least 48 hours before testing began.

7. DESTRUCTIVE TESTING OF CONCRETE SPECIMENS

7.1 COMPRESSIVE STRENGTH

The main goal of this research was to study the effects of different coarse aggregate on the physical properties of portland cement concrete. Ultimately, the focus of the research was to evaluate the design equations, which incorporate the strength and modulus of elasticity and the correction factors used to evaluate structural adequacy of concrete as discussed in chapter 2. This chapter presents the data and discussion of compressive strength testing as they pertain to their incorporation into the design equations.

7.1.1 Class II Concrete

For Class II mixtures, concretes made with Miami oolite and Perry aggregates exhibited the highest strengths at all ages for both cast and cored specimens as shown in Figure 7.1 and Figure 7.2. With the cast specimens, the Calera and granite bearing mixtures had the next highest strengths, while Brooksville bearing concrete had the lowest ultimate strength. Cored specimens differed from cast with regards to the relative strengths of mixtures containing granite, Calera, and Brooksville aggregates, with Brooksville bearing cores having higher strengths at 91 days than those containing either granite or Calera aggregate. Cores made with Perry and oolite aggregates developed slightly higher 91-day strengths than their cast equivalents. No clear difference is apparent, however, between cast and cored specimens containing Brooksville, granite, or Calera aggregates.

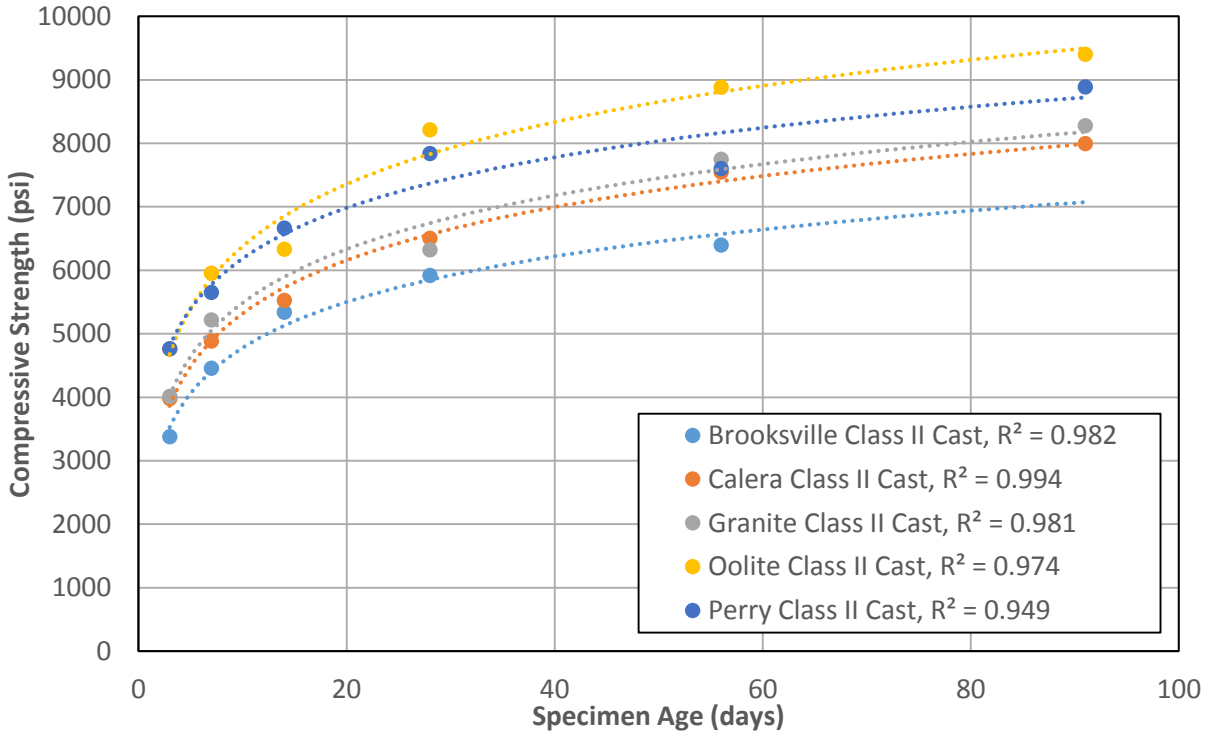

Figure 7.1 Compressive strength vs. time for class II cast concrete

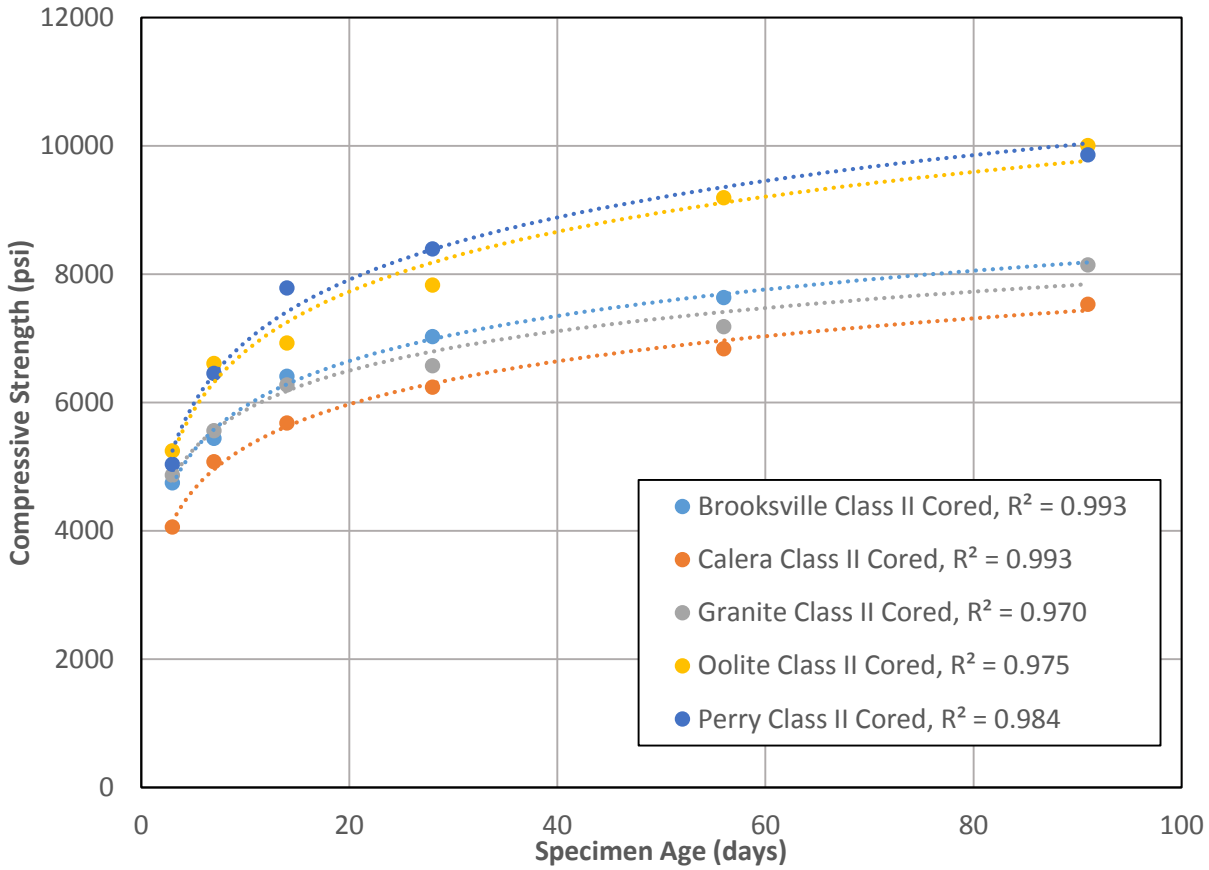

Figure 7.2 Compressive strength vs. time for class II cored concrete

7.1.2 Class VI Concrete

The compressive strength results for class VI mixtures used in this study exhibited generally higher strengths and more tightly distributed ultimate strengths than the class II mixtures (Figure 7.3 and Figure 7.4). Unlike the class II mixtures, compressive strength exhibited few clear dependencies on aggregate type. The differences between class VI cast and cored specimens are minimal.

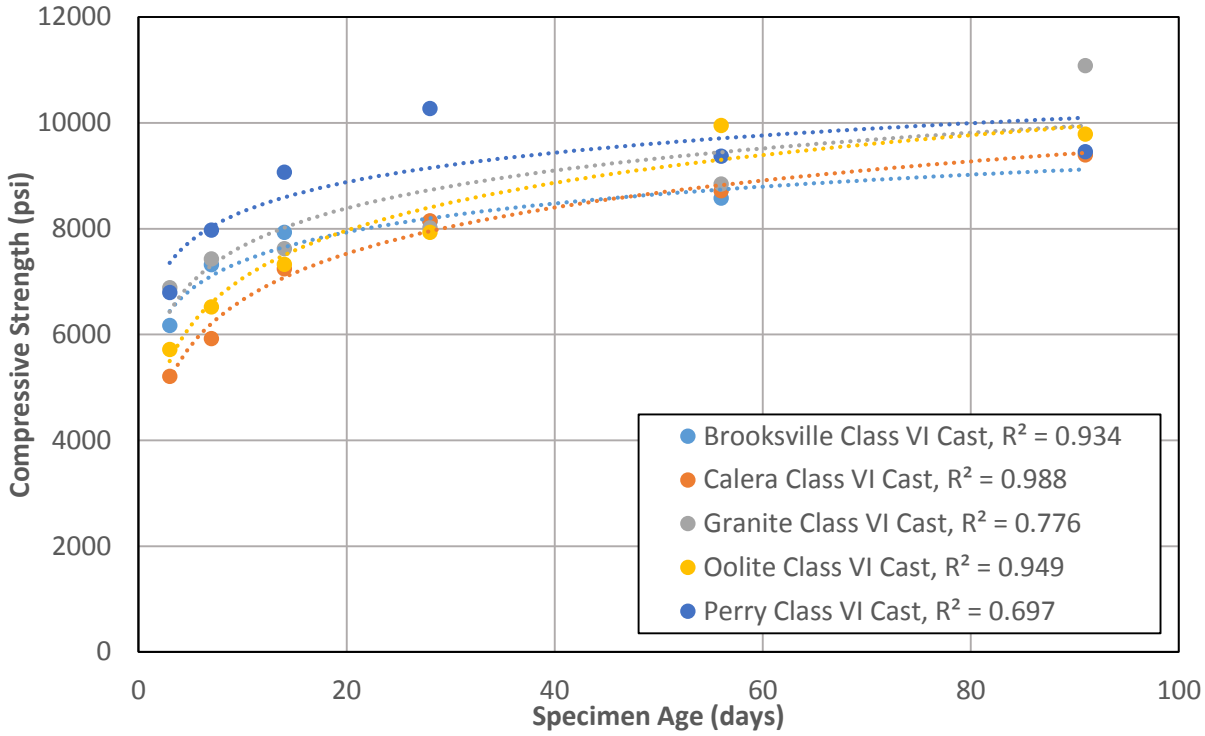

Figure 7.3 Compressive strength vs. time for class VI cast concrete

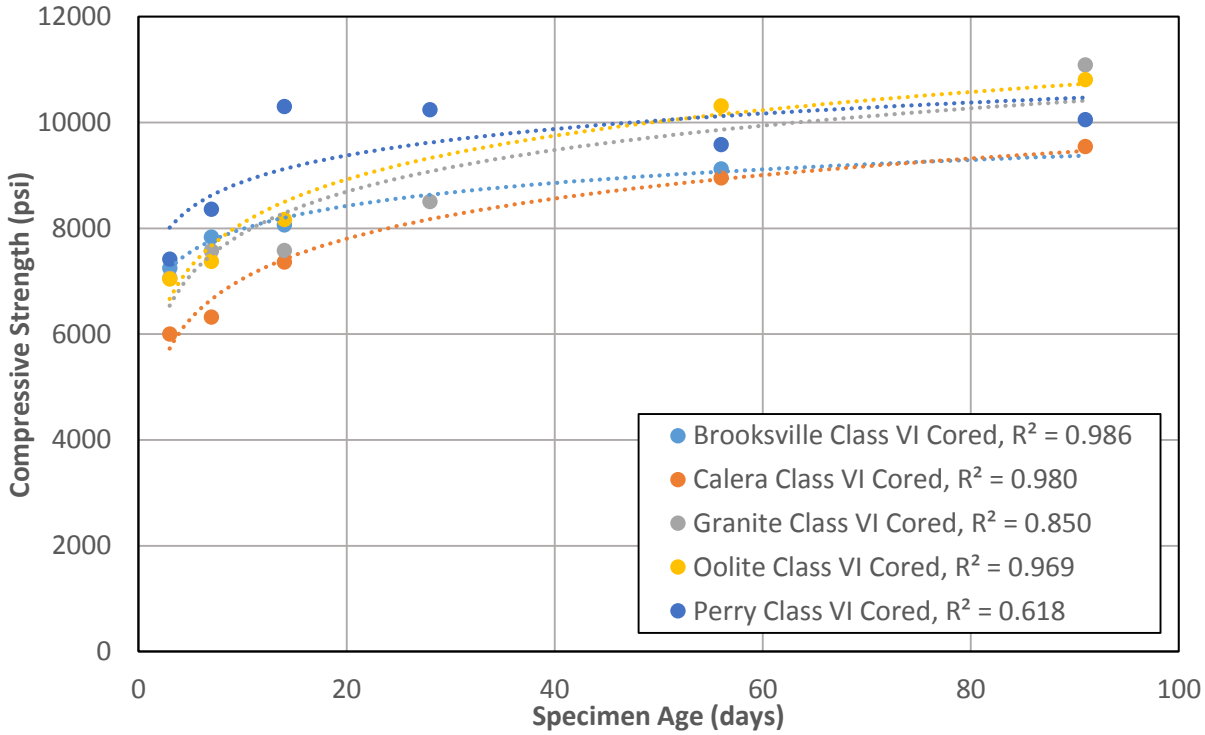

Figure 7.4 Compressive strength vs. time for class VI cored concrete

7.1.3 Compressive Failure Observations

During the compressive failure testing of the different concretes used in this study, it was clear that two different failure modes were present with respect to the formation of fracture planes around (intergranular) or through (transgranular) individual coarse aggregate particles. Visual inspection of failed specimens provided a clear indication that the relative predominance of these two failure modes was strongly dependent upon the origin of the aggregate present as well as the age of the specimen.

7.1.3.1 Brooksville Aggregate Concrete

Figure 7.5 and Figure 7.6 are typical of early-age specimens containing Brooksville coarse aggregate. Fracture planes were predominantly transgranular, with the few instances of intergranular failure (circled in red). At later ages the fracture planes were overwhelmingly transgranular. Figure 7.7 represents a typical 91-day specimen for Brooksville aggregate concretes; no intergranular failure was apparent in this particular specimen.

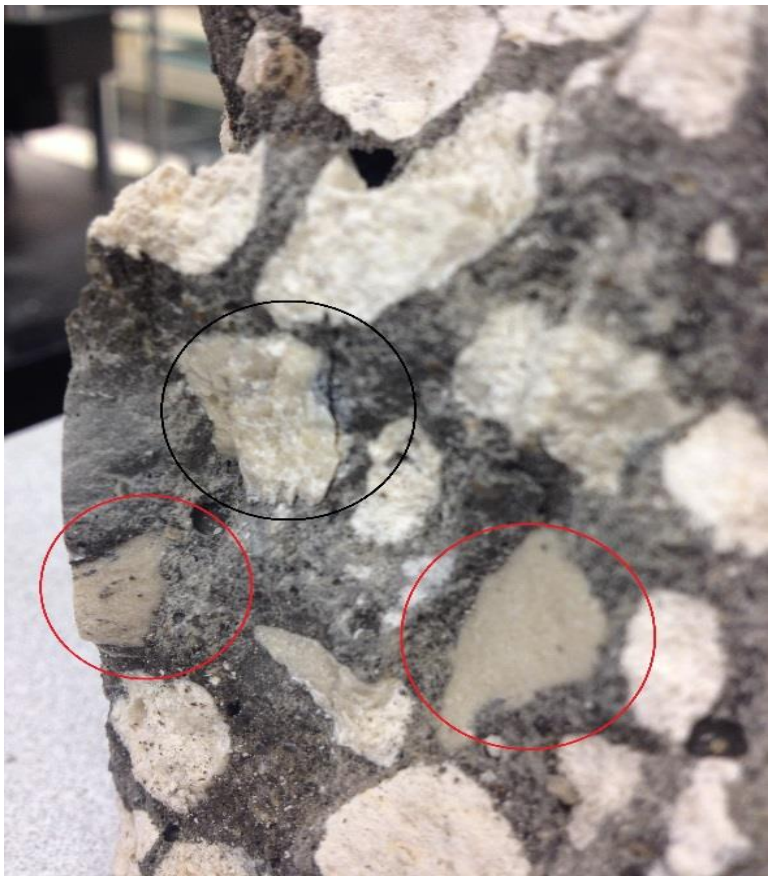

Figure 7.5 Class VI mixture with Brooksville aggregate, 3-day fracture plane

Figure 7.6 Class VI mixture with Brooksville aggregate, 7-day fracture plane

Figure 7.7 Class II mixture with Brooksville aggregate, 91-day fracture plane

7.1.3.2 Perry Aggregate Concrete

Figure 7.8 represents a typical early-age failure cone for specimens containing coarse aggregate from Perry Florida. Fracture planes at this age, unlike those of Brooksville aggregate bearing specimens, contain predominantly intergranular failures. The proportion of transgranular particle failures in specimen fracture planes increased with increasing age for concretes with Perry aggregate; Figure 7.9 shows a typical fracture plane for a 56-day specimen.

Figure 7.8 Class II mixture with Perry aggregate, 3-day failure cone

Figure 7.9 Class VI mixture with Perry aggregate, 56-day fracture plane

7.1.3.3 Granite Aggregate Concrete

Mixtures containing granite as the coarse aggregate exhibited fracture planes that were predominantly intergranular at all ages. Figure 7.10 and Figure 7.11 are representative of typical 3-day specimen failure. Some transgranular particle failure was present at all ages; Figure 7.12 shows a crack propagating through an aggregate particle, however, specimens containing granite coarse aggregate did not exhibit an obvious increase in transgranular particle fracture with increasing age (Figure 7.13), unlike those made with Brooksville and Perry aggregates.

Figure 7.10 Class II mixture with granite aggregate, 3-day failure cones

Figure 7.11 Class VI mixture with granite aggregate, 3-day failure cones

Figure 7.12 Class VI mixture with granite aggregate, 56-day fracture plane

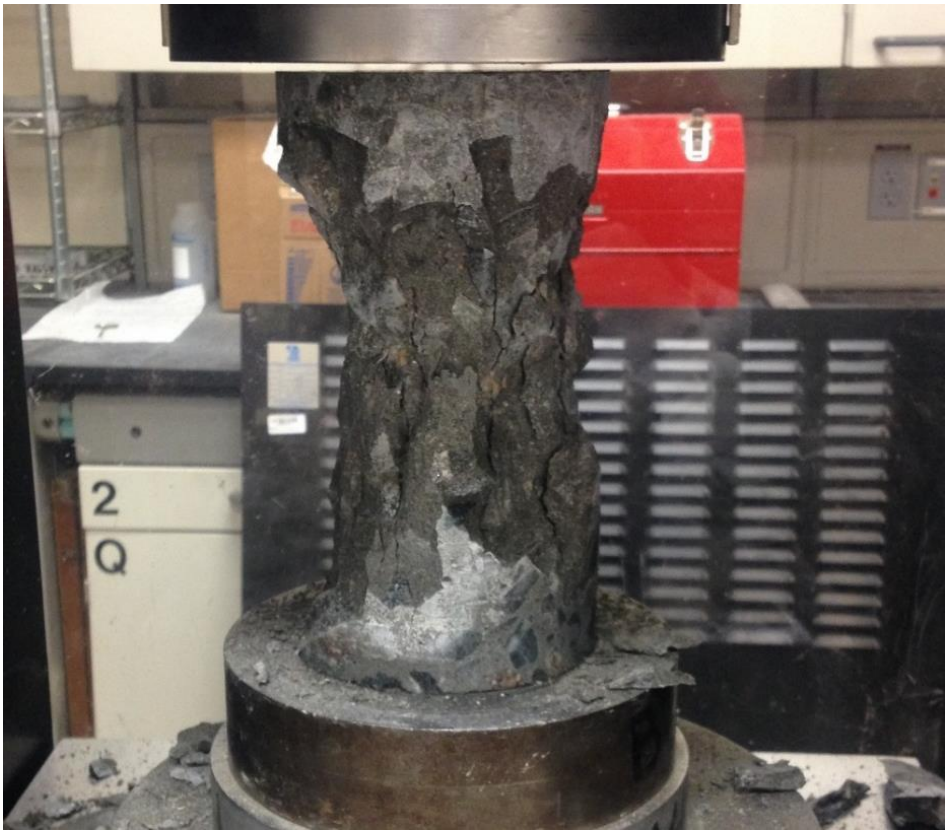

Figure 7.13 Class VI mixture with granite aggregate, 91-day cylinder failure

7.1.3.4 Calera Aggregate Concrete

Specimens containing Calera aggregate behaved similarly to those containing granite with regards to the formation of fracture planes. As with granite, the predominant mode was intergranular failure with very few instances of transgranular failure (Figure 7.14 and Figure 7.15). There was also no apparent increase in the relative proportions of these failures with respect to specimen age.

Figure 7.14 Class VI mixture with Calera aggregate, 14-day cylinder failure

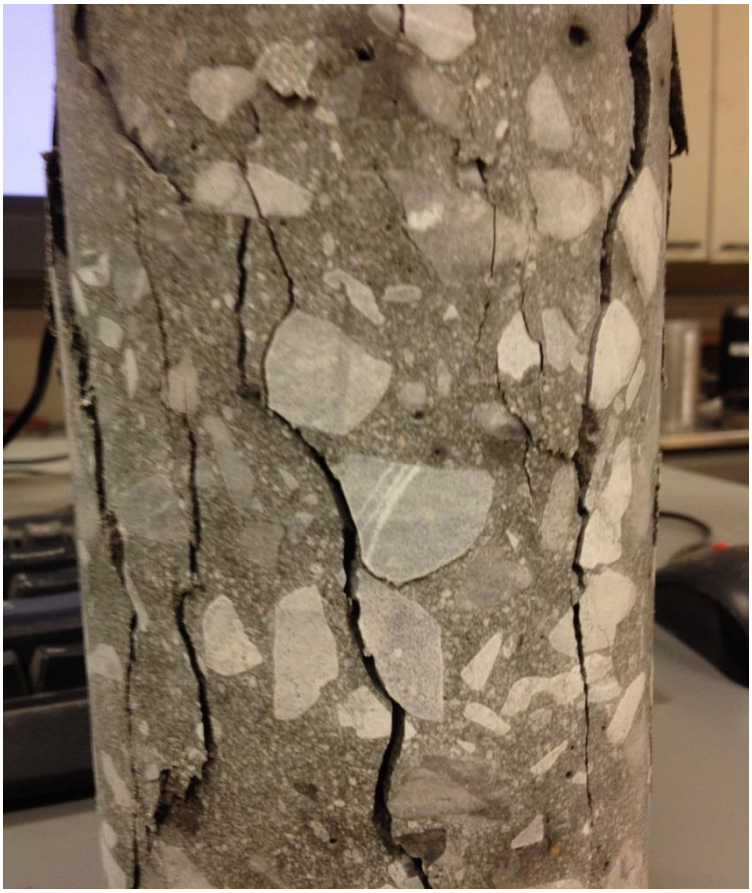

Figure 7.15 Class VI mixture with Calera aggregate, 14-day core failure

7.1.4 Discussion of Results

While class II mixtures examined in this study clearly indicated that Miami oolite and Perry aggregates produce the strongest concretes, the same trend was not exhibited in the compressive strength results for the class VI mixtures. The inconclusive nature of the class VI mixture results may potentially stem from several different factors. The water-to-cement ratio (w/cm) used for these mixtures was significantly lower (0.33 as opposed to 0.46) than that used for the class II concretes. The total cementitious content was also markedly higher than that of the class II concretes. Any effects of the different aggregates on the characteristics of the interfacial transition zone (ITZ) would likely be diminished by the lower w/cm (Noguchi and Nemati, 1995) of the class VI mixture design used in this study. The higher overall paste content may also diminish the contribution of the aggregate to the ultimate strength of the composite material.

Visual inspection of failed compressive testing specimens also revealed differences in the behavior of the different aggregates. Fracture planes formed in specimens containing Brooksville and Perry aggregates were mostly transgranular at later ages. This behavior is consistent with previously observed behavior for Florida limestones (Rich, 1980; Ferraro and Watts, 2013), and is likely indicative of both a denser ITZ and stronger paste-aggregate bond (Lo and Cui, 2004; Perry and Gillott, 1977; Wu et al., 2001).

7.2 MODULUS OF ELASTICITY

7.2.1 Class II Concrete

Modulus of elasticity testing on class II mixtures (Figure 7.16 and Figure 7.17) revealed a clear dependence upon the type of coarse aggregate used. Concrete containing Calera coarse aggregate attained the highest moduli at all ages, followed by mixtures made with Perry, oolite, and granite aggregates. Specimens made with Brooksville aggregate exhibited the lowest moduli; the 91-day modulus of Brooksville concrete was lower than the 3-day modulus attained by concrete containing Calera aggregate. The difference between cored and cast specimens was small, with the cored specimens attaining slightly higher 91-day moduli.

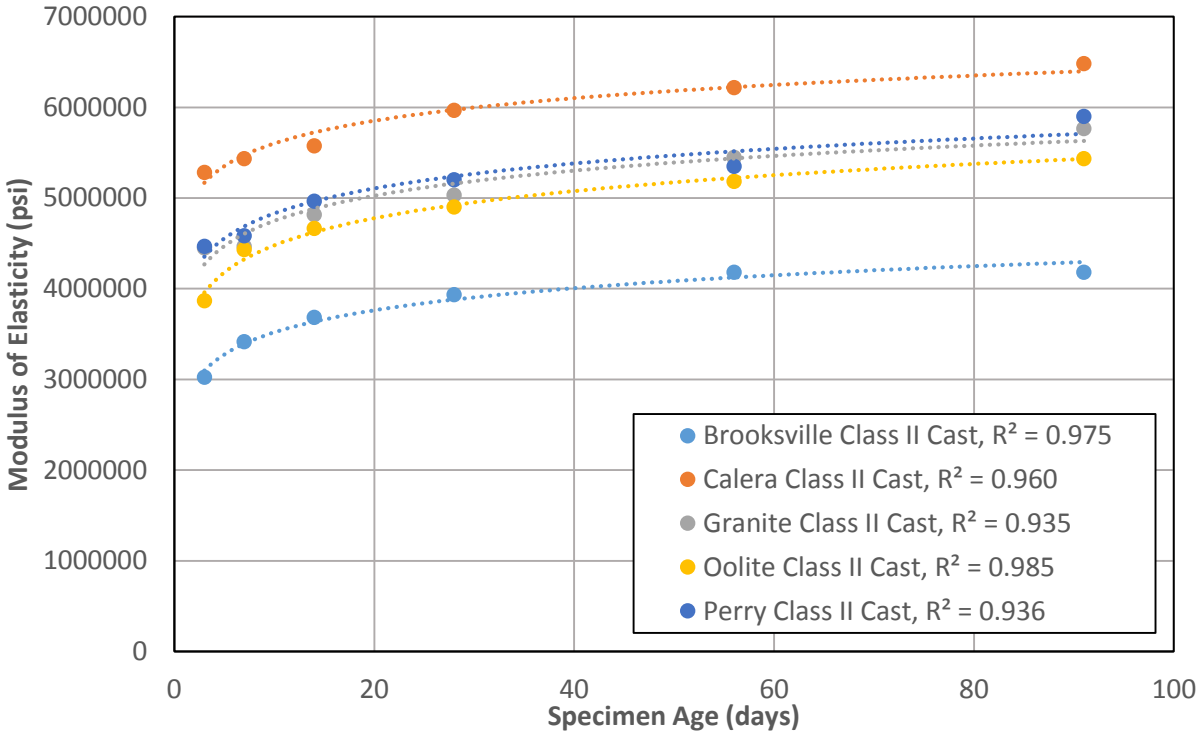

Figure 7.16 Modulus of elasticity vs. time for class II cast concrete

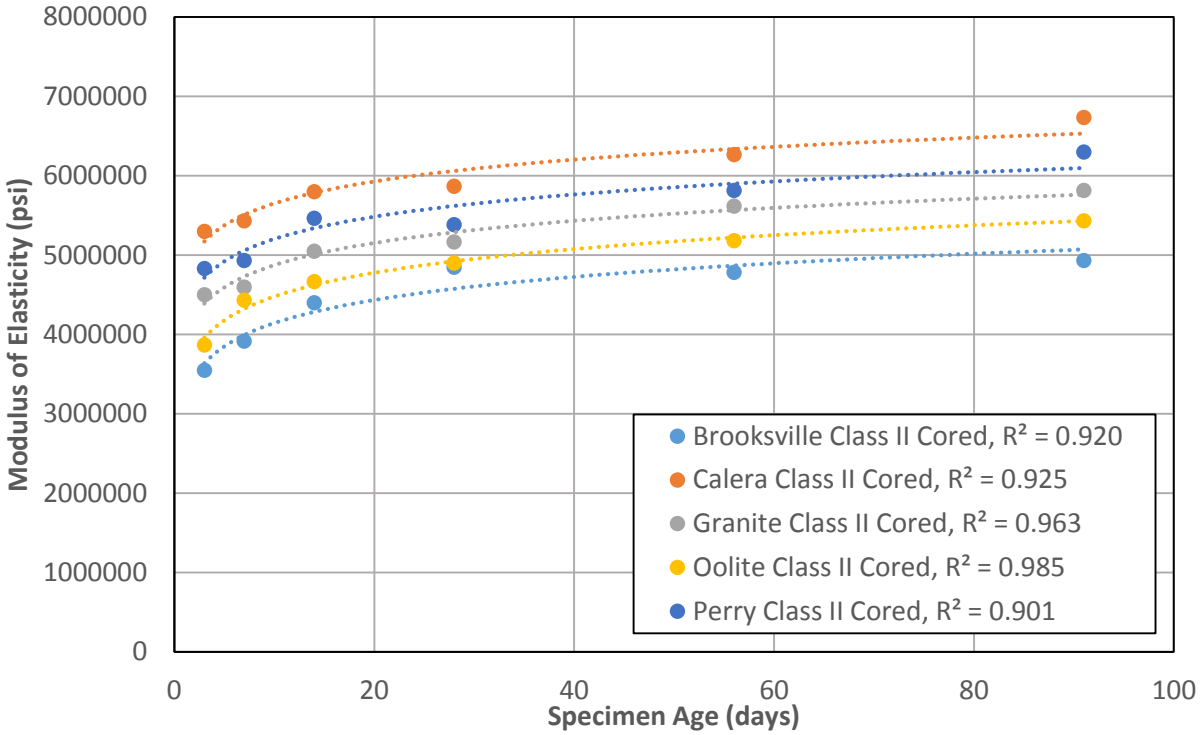

Figure 7.17 Modulus of elasticity vs. time for class II cored concrete

7.2.2 Class VI Concrete

The measured elastic moduli of class VI mixtures (Figure 7.18 and Figure 7.19) are comparable to those attained by the class II mixtures, with the highest moduli attained by mixtures containing Calera aggregate, followed by granite, Perry, oolite and Brooksville bearing mixtures respectively. The moduli of class VI mixtures were significantly larger than those attained by class II mixtures, specifically prior to 91 days of age; however, the ultimate moduli attained by the class VI mixtures were approximately the same as those of the class II mixtures. Similar to the class II mixtures, the increase in modulus associated with cored specimens was small.

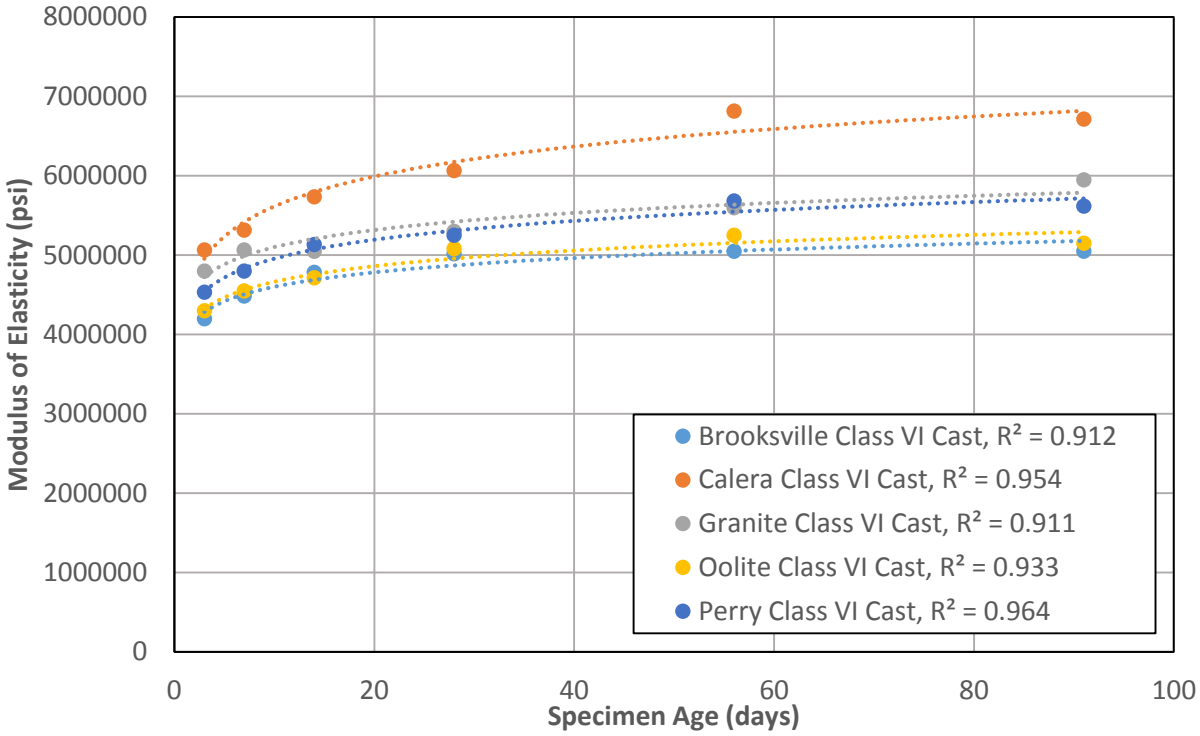

Figure 7.18 Modulus of elasticity vs. time for class VI cast concrete

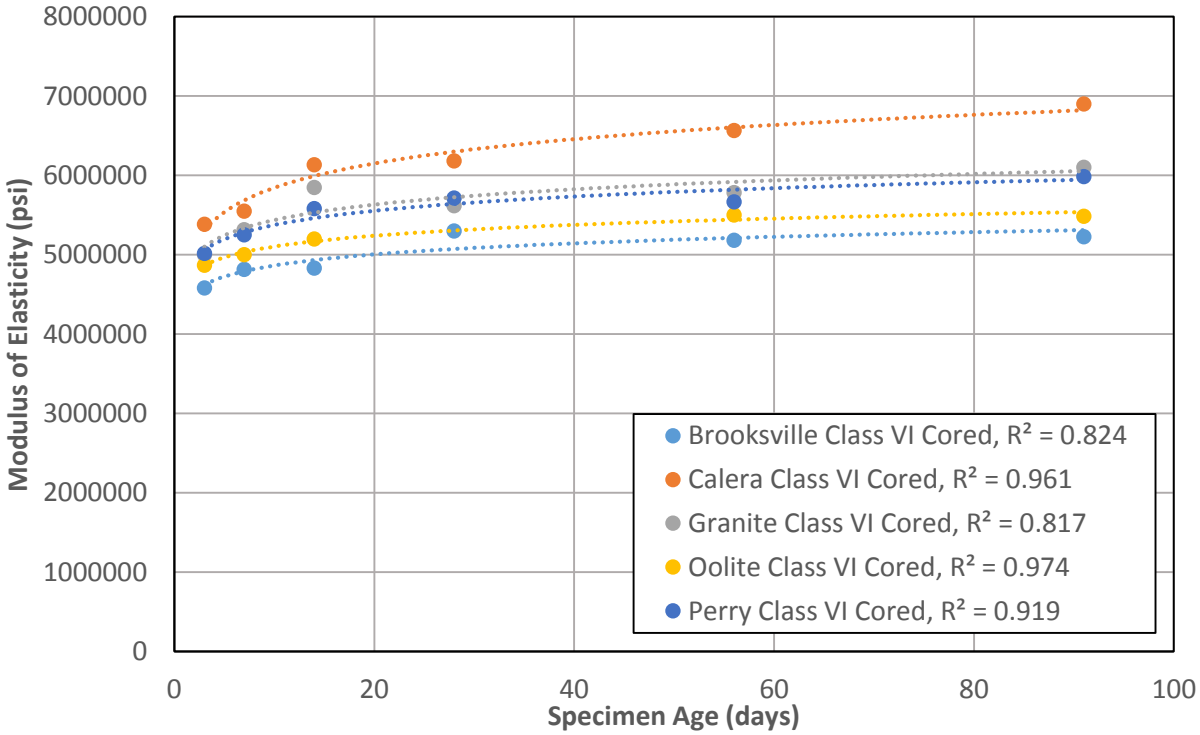

Figure 7.19 Modulus of elasticity vs. time for class VI cored concrete

7.2.3 Discussion of Results

The measurements of elastic modulus for all mixtures in this study showed that concretes produced with Calera aggregate resulted in the highest moduli. This contrasts with the compressive strength data, in which the highest strength was attained by mixtures containing Miami oolite. This is not unprecedented (Zhang et al., 2009), and can likely be explained by differences in the formation and properties of the ITZ (Akçaoğlu et al., 2004) as well as the relative stiffnesses of the aggregates themselves.

7.3 SPLITTING TENSILE STRENGTH

7.3.1 Class II Concrete

The results of tensile strength testing for class II mixtures (Figure 7.20 and Figure 7.21) exhibit similar behavior to the results of compressive strength testing, with concrete produced using oolite attaining the highest strengths, followed by mixtures containing Perry, granite and Calera aggregates, with concrete made with aggregate from Brooksville having the lowest strengths overall. Unlike the results of compressive strength testing, however, the mixtures containing Miami oolite did not have the highest strengths at all ages. The early-age strength of oolite-bearing concretes was comparable to that of the other mixtures. No difference in the tensile strength of cast and cored specimens was apparent for class II mixtures.

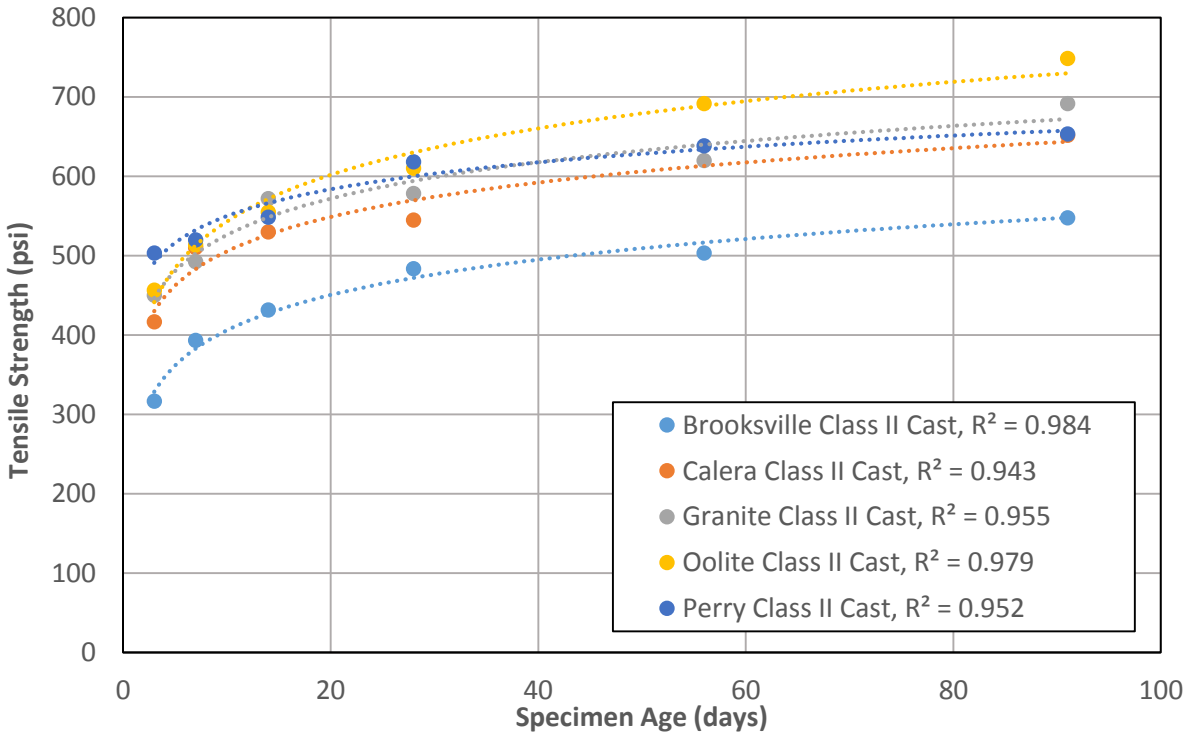

Figure 7.20 Tensile strength vs. time for class II cast concrete

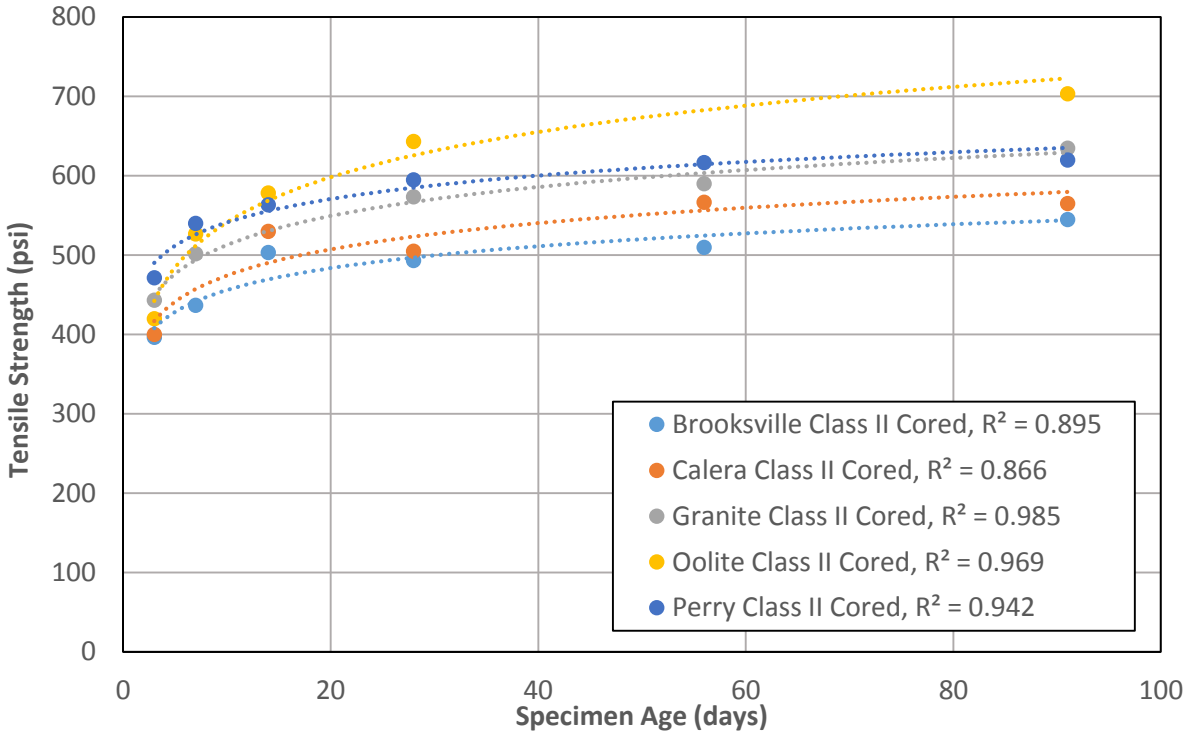

Figure 7.21 Tensile strength vs. time for class II cored concrete

7.3.2 Class VI Concrete

Class VI mixtures exhibited higher tensile strengths overall (Figure 7.22 and Figure 7.23) than the equivalent class II concretes, however few clear trends were apparent with regards to the relative strengths of mixtures containing different coarse aggregates. The only notable trend was the generally poor performance of mixtures containing Calera aggregate, particularly at early ages. As with the class II mixtures, there was no clear difference in tensile strength between the cast and cored specimens.

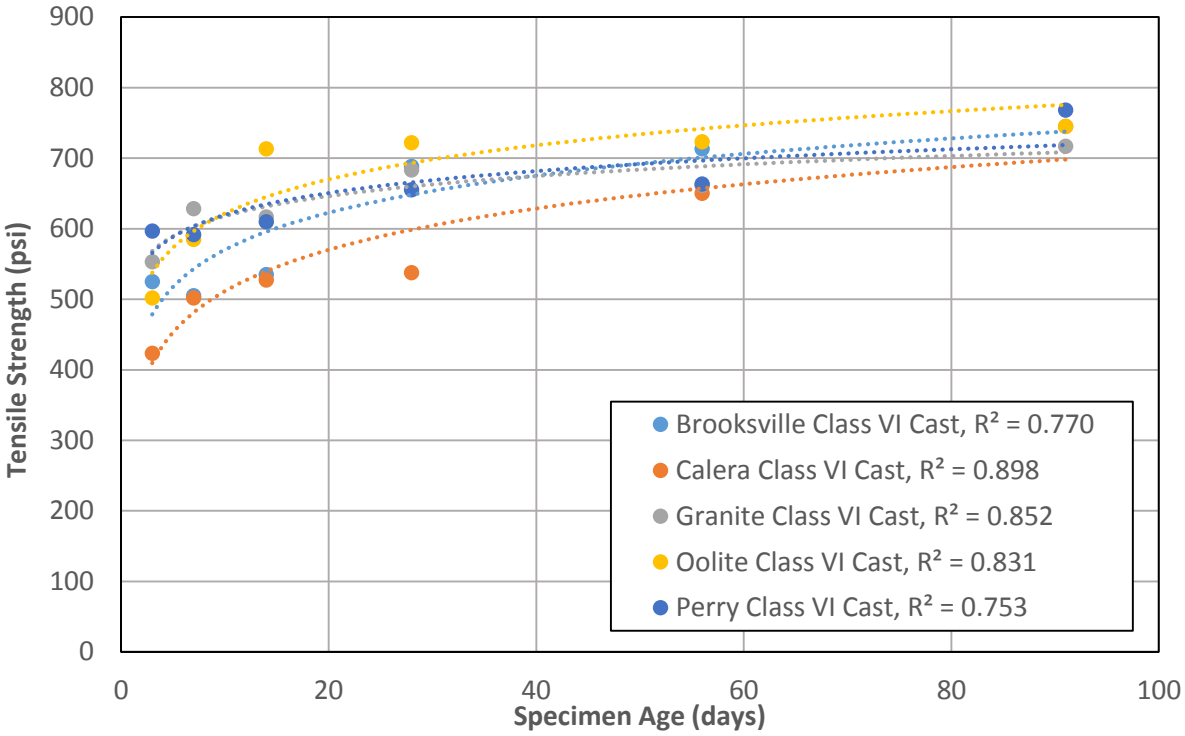

Figure 7.22 Tensile strength vs. time for class VI cast concrete

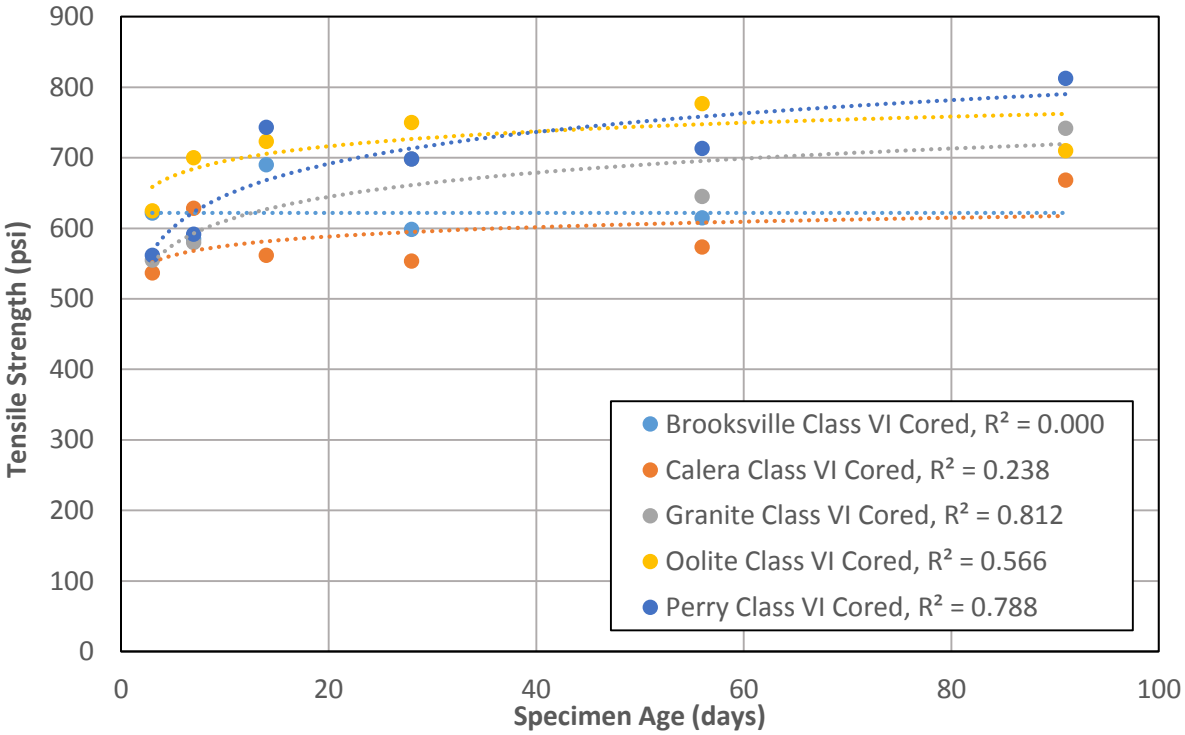

Figure 7.23 Tensile strength vs. time for class VI cored concrete

7.3.3 Discussion of Results

The results of tensile strength testing were similar to those for compression, in that the class II mixtures typically exhibited clearer trends with regards to the specific aggregates used. As with the compressive specimens, the class VI mixtures had both higher cementitious contents as well as lower w/cm, parameters which potentially diminish the overall contribution of the coarse aggregate to the properties of the bulk composite. The degree of variation for tensile specimens was larger than that of the compressive tests; however, this is consistent with known behavior of the splitting tensile strength test (Daniel, 2006).

7.4 FLEXURAL STRENGTH

7.4.1 Discussion of Results

The results for flexure testing for class II and class VI mixtures (Figure 7.24 and Figure 7.25) show few clear trends with regards to the different aggregates. The only clear trend common to both classes was the poor performance of mixtures containing Brooksville aggregate relative to the others. The class VI concretes did exhibit higher ultimate strengths overall than those of class II mixtures. The lack of clear distinguishing trends and generally high variability of the results for flexural strength are not inconsistent with expectations for that particular test method. Generally speaking "Flexural specimens are sensitive to small variations in molding, curing, and handling. The result is wider variations in test results than with testing for compressive strength." (Daniel, 2006).

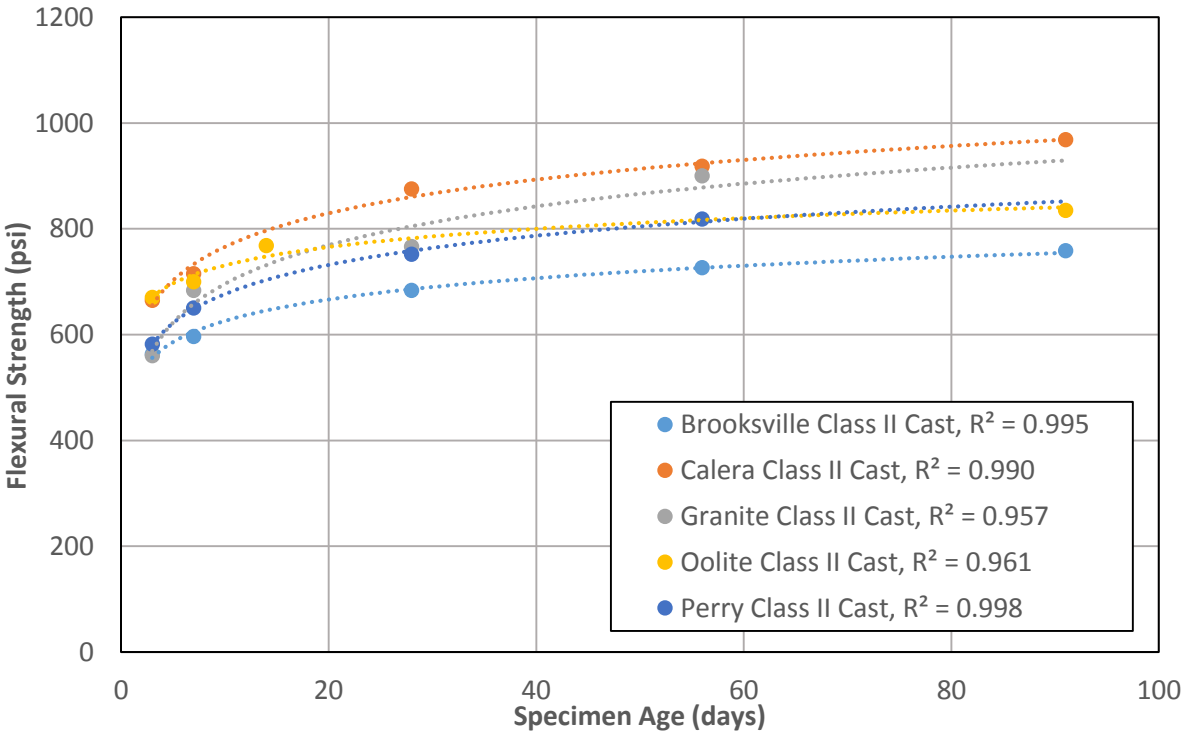

Figure 7.24 Flexural strength vs. time for class II cast concrete

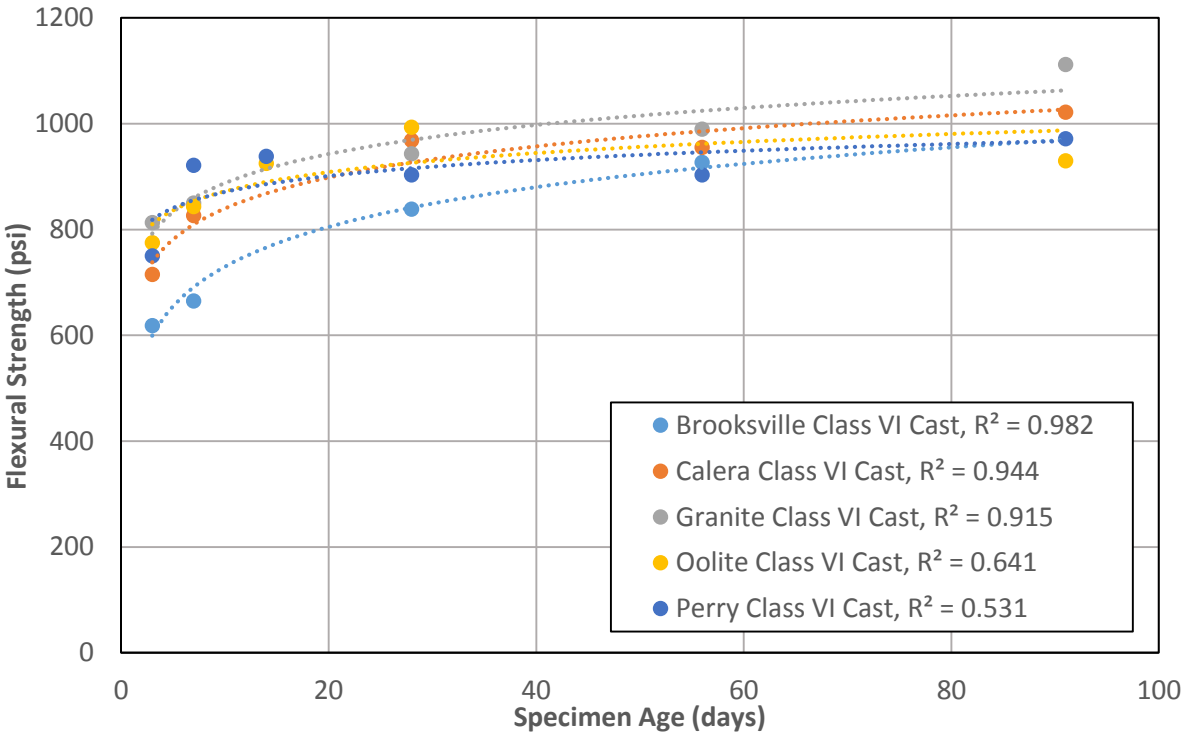

Figure 7.25 Flexural strength vs. time for class VI cast concrete

8. NON-DESTRUCTIVE TESTING OF CONCRETE SPECIMENS

8.1 BACKGROUND

Non-destructive testing of concrete is performed on concrete (and other materials) to allow the user to gather quantitative information on material specimens without damage. Although the majority of construction specifications require the use of destructive tests such as compressive strength testing for acceptance (FDOT 2015), the existence of adequate, repeatable, and accurate correlations between non-destructive tests and destructive tests would enable more extensive use of non-destructive tests. If compressive strength can be adequately modelled in a non-destructive test, reduction in the number of specimens might be possible, decreasing required time and labor and putting more emphasis on the quicker and easier non-destructive test methods. The added simplicity of obtaining physical measurements via non-destructive testing allows more specimens to be tested and statistical analysis more robust. However, there are still difficulties with correlating lab results, which require specimen preparation, with field observation.

8.2 REBOUND HAMMER

Rebound hammer testing is considered a "surface hardness method" which measures the relative compressive strength of concrete in-situ (Malhotra, 2003). Concrete testing procedures for each cylinder tested included ten readings taken on each "face" of the cylinder.

A modified version of ASTM C805, Standard Test Method for Rebound Number of Hardened Concrete was implemented in order to accommodate specimen size. Modifications of the standard include provisions for the smaller 4" x 8" cylinders and the locations and orientation of the concrete specimens (ASTM C805, 2013). A pattern was devised to optimally test the largest area of each specimen while maintaining space between locations to avoid interference between readings. This pattern was tested on both sides of each cylinder. A second modification involved properly securing each specimen in the testing machine. It was determined through experimentation that properly securing the specimen in compressive testing machines allowed an adequate confining stress that could also be monitored. Recording of the stress was deemed important as confining stress has been shown to increase rebound number. Testing for rebound number was conducted by placing specimens in two orientations: horizontal and vertical. The testing pattern and machine apparatus is shown in Figure 8.1 and Figure 8.2.

Rebound numbers were procured on all specimens that would undergo compressive and splitting tension destructive tests. Any damage obtained through the rebound hammer tests would be recorded on the data sheets for later tests, however this event was rare. The total number of readings per cylinder was 20, five for each side with two orientations. In another departure from the requirements of ASTM C805, results which fell outside of the average were incorporated into the analysis. Additionally, testing locations which rested on an exposed aggregate or a purely cement phase of the cored specimens were noted and recorded. Rebound number testing was performed on specimens prior to compressive and splitting tensile testing. In the extremely rare event in which damage was introduced to the cylinder as a result of rebound hammer testing, the damage was recorded on the data sheets.

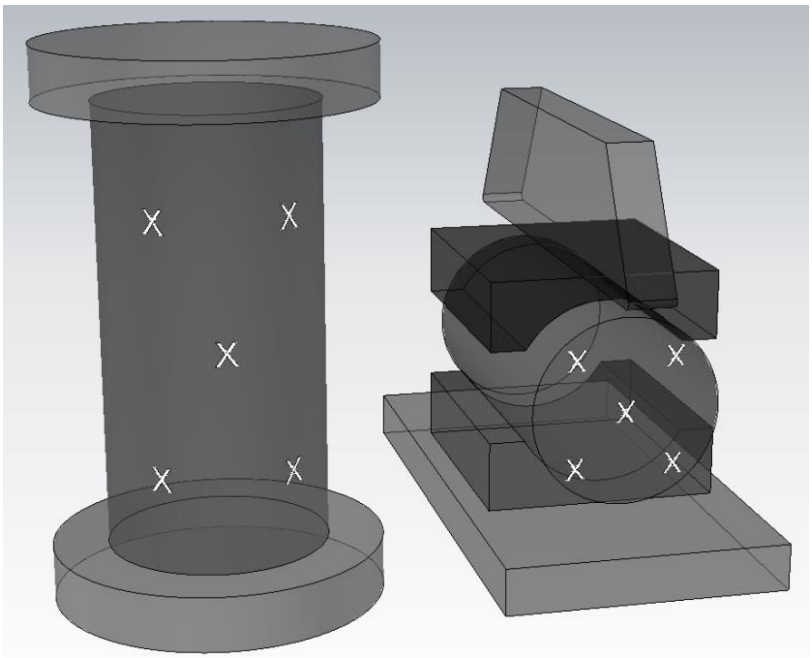

Figure 8.1 Proper confinement in rebound hammer testing apparatus, and markings of reading locations

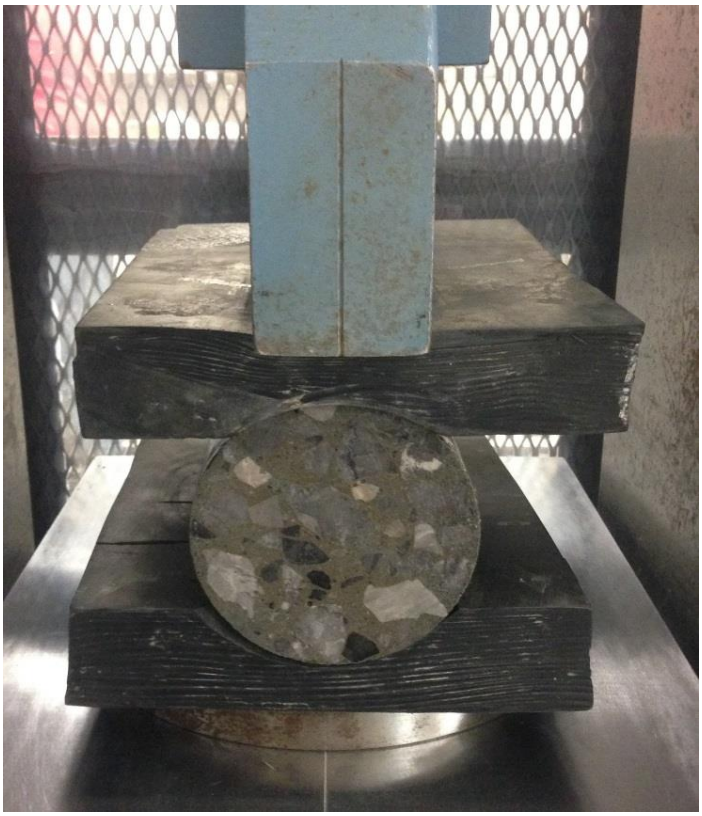

Figure 8.2 Specimen prepared for horizontal orientation for rebound numbers

8.2.1 Class II Concrete

Much like strength and modulus, rebound number increased over time for every aggregate as it is a function of the hardness of the concrete. Logarithmic trend lines illustrate an averaged reading and include R^2 values. Concrete with Miami oolite aggregate had the highest readings next to concrete with Perry limestone and Georgia granite aggregate for cast specimens as shown in Figure 8.3. Concrete with Brooksville limestone aggregate had the lowest rebound numbers for cast specimens, especially at the later ages. Cored specimens show more variability but similar trends as cast specimens as shown in Figure 8.4. Brooksville and Calera limestone concrete had the lowest values and did not show an increase in rebound hammer values over time. Overall, the gain in rebound hammer values was minimal over time for concrete made with most aggregates.

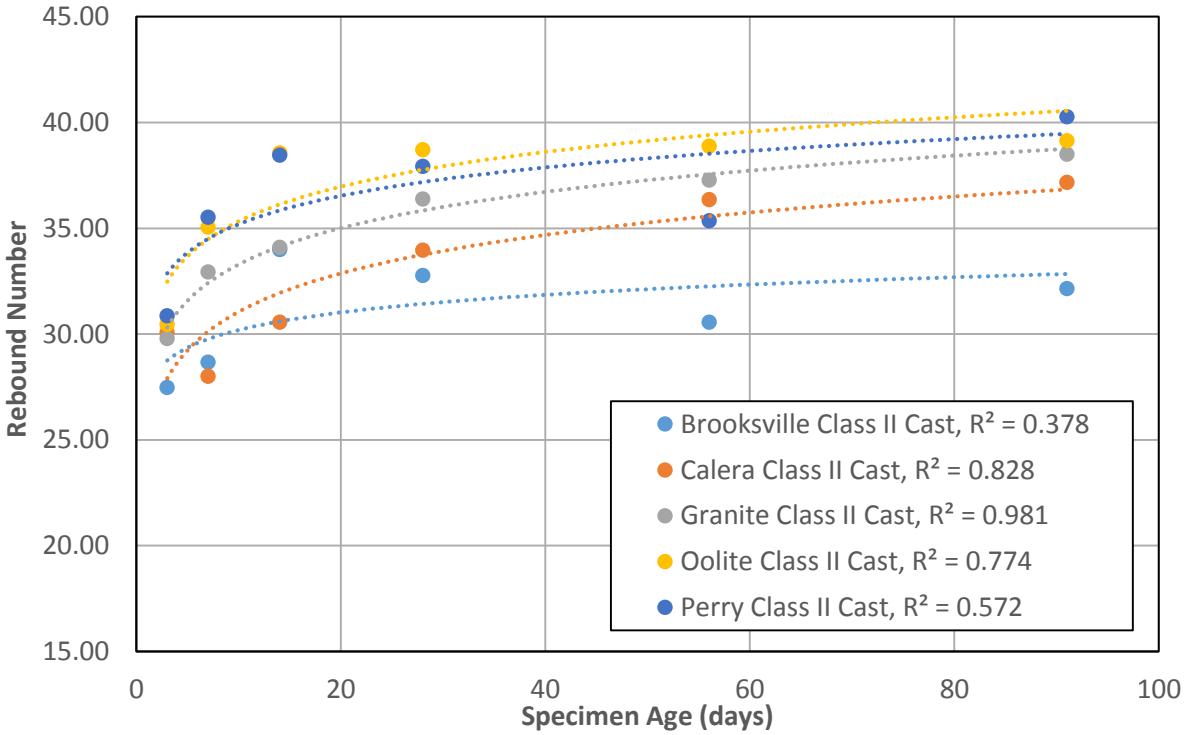

Figure 8.3 Rebound number vs. time for class II cast concrete

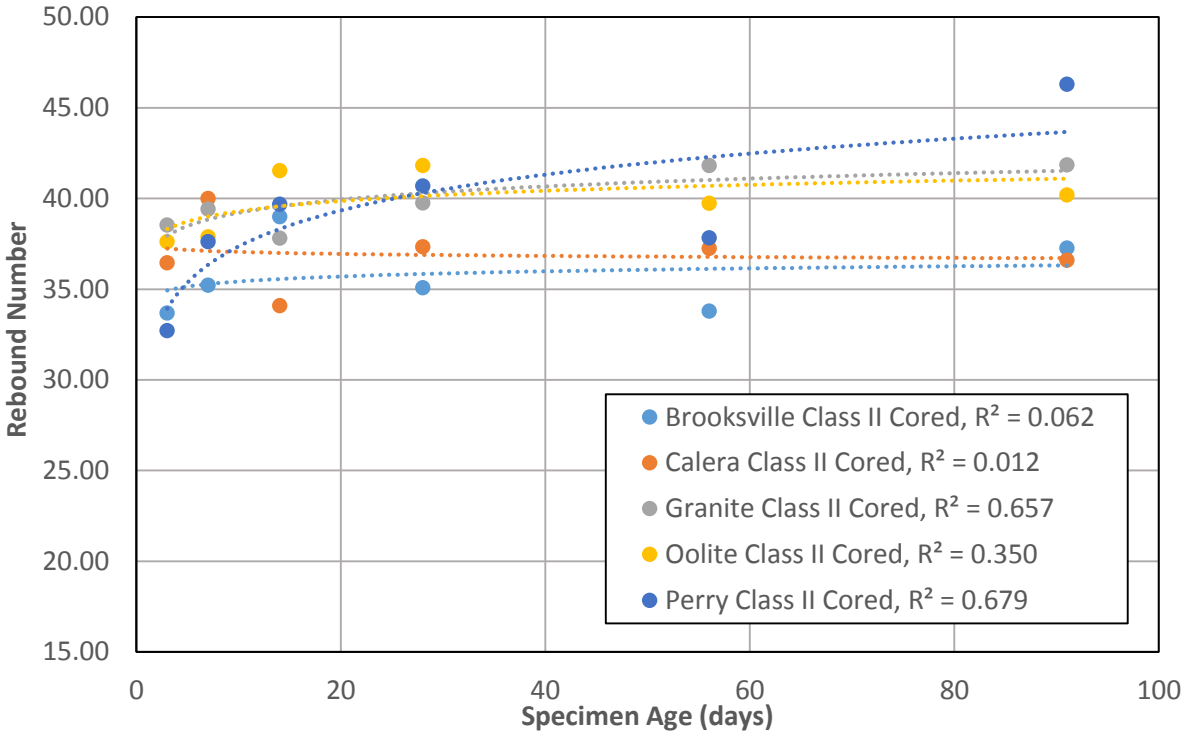

Figure 8.4 Rebound number vs. time for class II cored concrete

8.2.2 Class VI Concrete

Class VI mixtures provided higher rebound numbers than class II, but showed more variability than class II mixtures. For both class VI and II, cored specimens had more variable results than cast specimens. Figure 8.5 and Figure 8.6 illustrate the data for the class VI concrete specimens that were cast and cored, respectively.

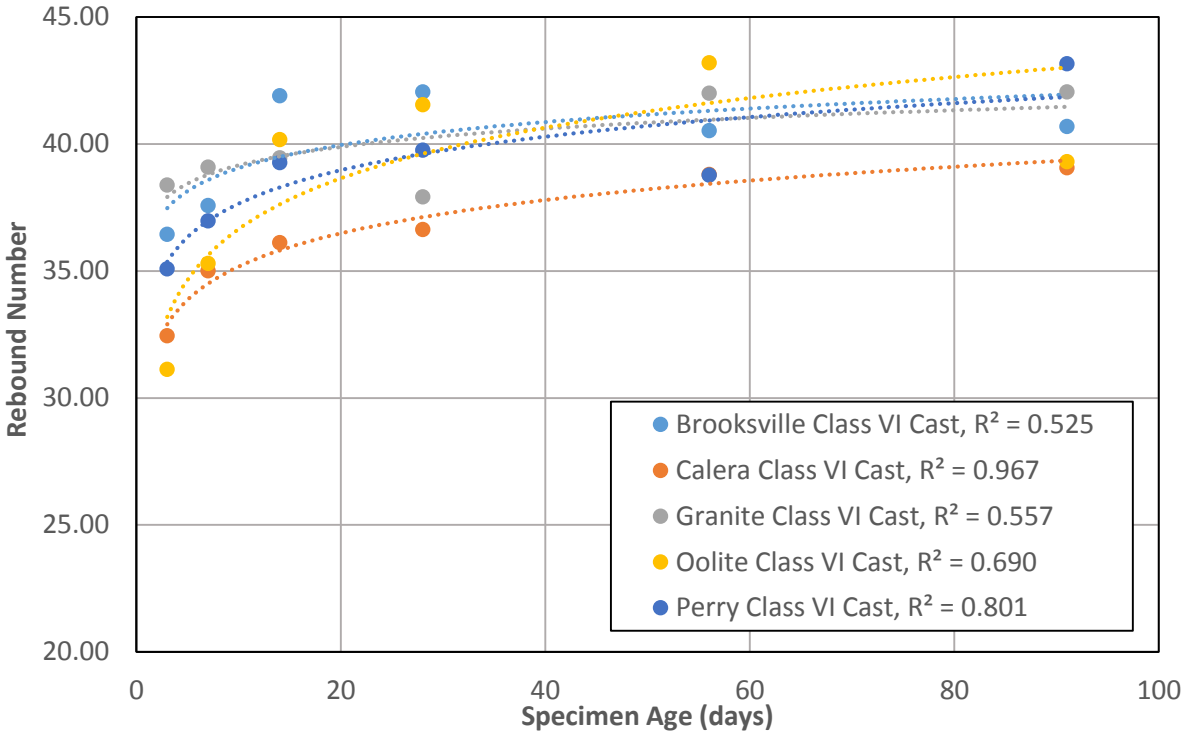

Figure 8.5 Rebound number vs. time for class VI cast concrete

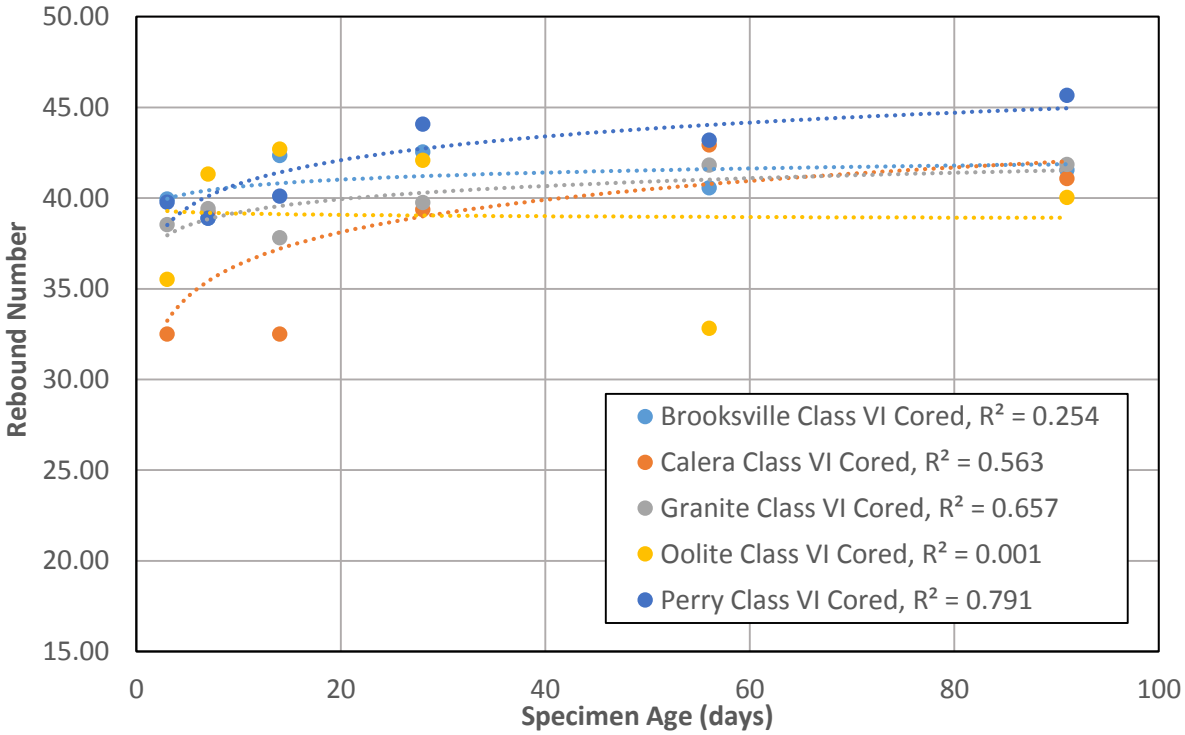

Figure 8.6 Rebound number vs. time for class VI cored concrete

8.2.3 Observations

General readings and hardened cement paste readings showed an increase in rebound hammer values over time, while aggregate-specific classifications do not. The rising trend shown in general readings and hardened cement readings paste showed a larger increase in class II mixtures than class VI mixtures. Cored specimens also had larger rebound number values than cast, which can be attributed to maturity of the larger slab from which the cored specimens are obtained. While both mixtures showed a poor fit on their trend lines, indicating high variability, cast specimens had better fitting trend lines than cored specimens.

Cast specimens, due to the nature of the casting method, were unable to have classifications of bearing surface difference in rebound hammer readings. Because of this, all cast readings were general averaged readings. These readings have similarities to compressive strength data with low compressive strength aggregates having similarly low rebound numbers. However, this trend is not always shared in cored readings.

Each measurement location classification represented a different lithological characteristic of the aggregates used. Light, dark, and glass classifications are basic descriptors that fit a general description of what aggregate was at the test locations on the samples. The fact that these numbers showed no increase in time, or correlation with other material tests, indicates that the aggregate itself does not change its rebound value over time.

8.3 PULSE VELOCITY

Ultrasonic pulse velocity per ASTM C 597 was conducted on each cylinder used for compressive and splitting tension destructive tests. These cylinders were measured for length and then their transit time using a pulse velocity machine was recorded as shown in Figure 8.7.With both length and time recorded, speed was calculated. Pulse velocity was recorded on the same data sheet as rebound numbers.

Figure 8.7 Pulse velocity recording transit time on cast specimen

Pulse velocity was conducted at each testing age before destructive tests were performed. Each data point represents the averaged total of six readings; three compressive and three tensile. The data is divided by class of concrete (class II and class VI) and then by type of specimen (cast and cored). Points and trend lines were colored to show the difference in coarse aggregate used for the concrete mixture. Ultrasonic pulse readings were taken in microseconds and, when combined with a distance reading, pulse velocity was calculated and is shown in km/s on the y-axis.

8.3.1 Class II Concrete

The pulse velocities for the class II cast and cored concrete specimens are illustrated in Figure 8.8 and Figure 8.9. Concrete made with Calera limestone aggregate had the highest pulse velocities for both cast and cored specimens. Concrete with Perry limestone and granite had the second and third highest readings while Miami oolite concrete was slightly lower. Brooksville limestone concrete clearly had the lowest pulse velocities for both cast and cored specimens by a good margin.

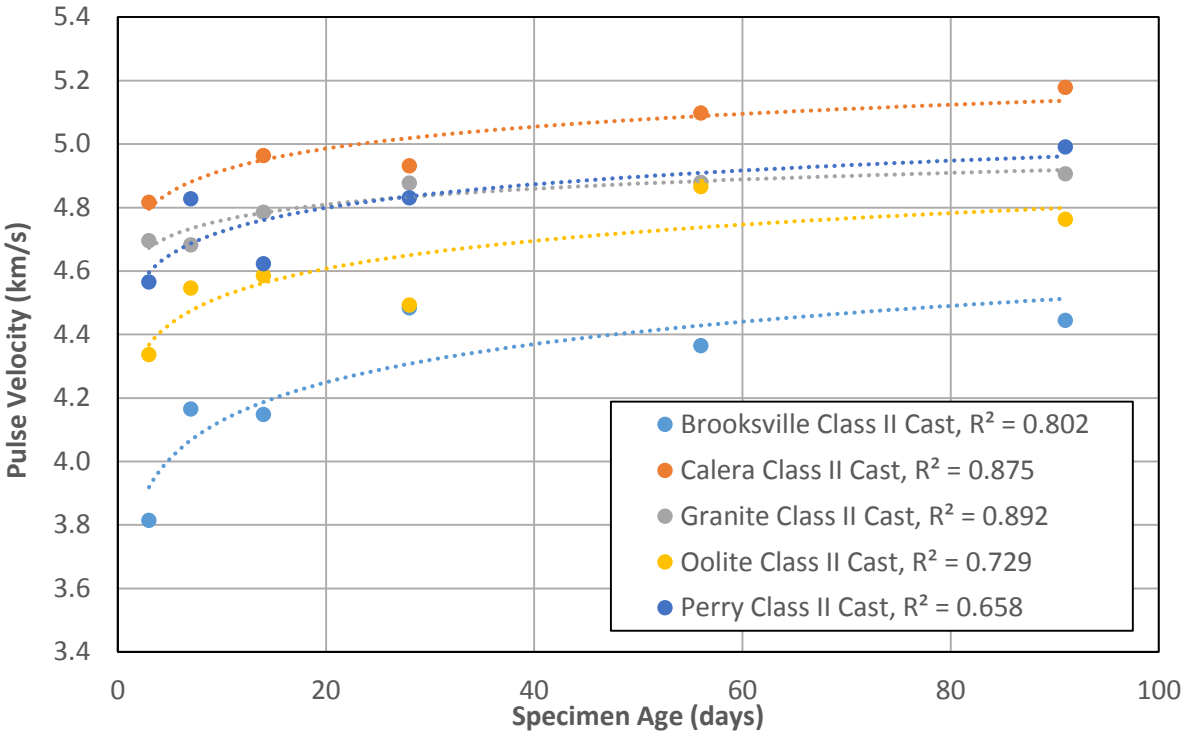

Figure 8.8 Pulse velocity vs. time for class II cast concrete

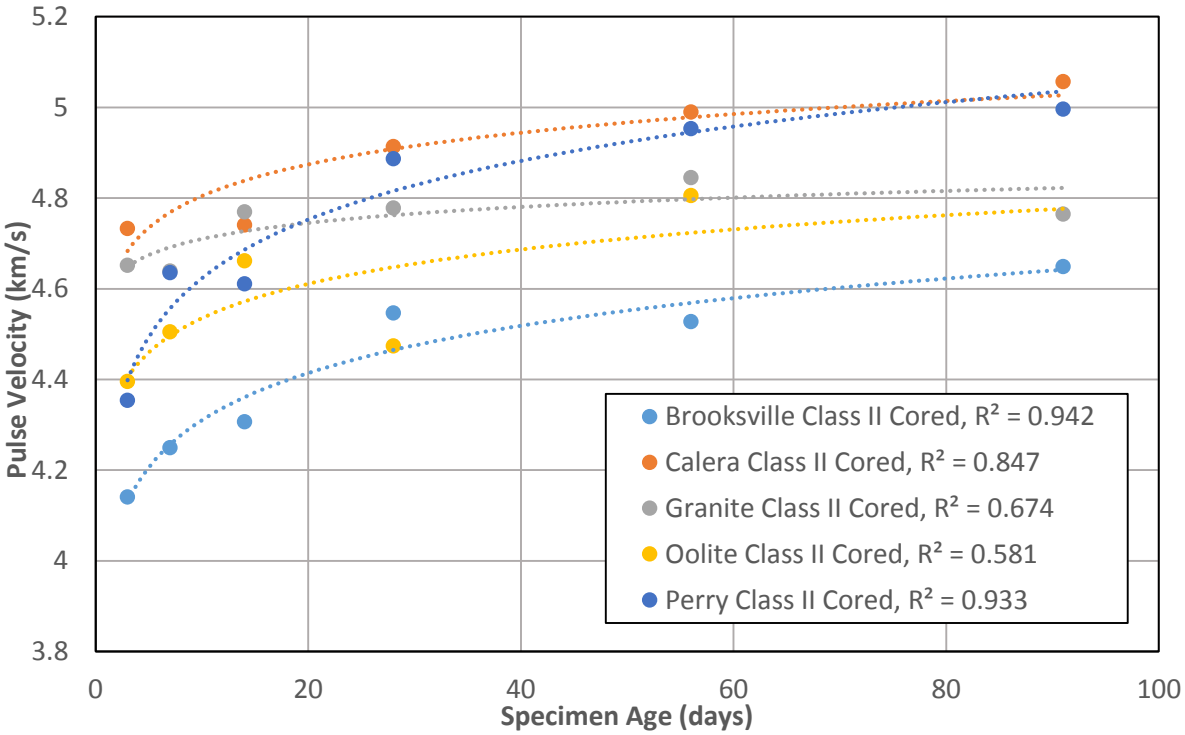

Figure 8.9 Pulse velocity vs. time for class II cored concrete

8.3.2 Class VI Concrete

Class VI concrete showed similar trends to class II concrete with respect to the different aggregate types as shown in Figure 8.10 and Figure 8.11. Calera limestone concrete again had the highest values, but there was less distinction between the lower trend lines. Concrete made with Miami oolite and Brooksville limestone had similar trend lines with the lowest velocities, but concrete with granite aggregate was also low. Class VI concrete had more variability in the data than class II concrete, following the same trend as with strength results.

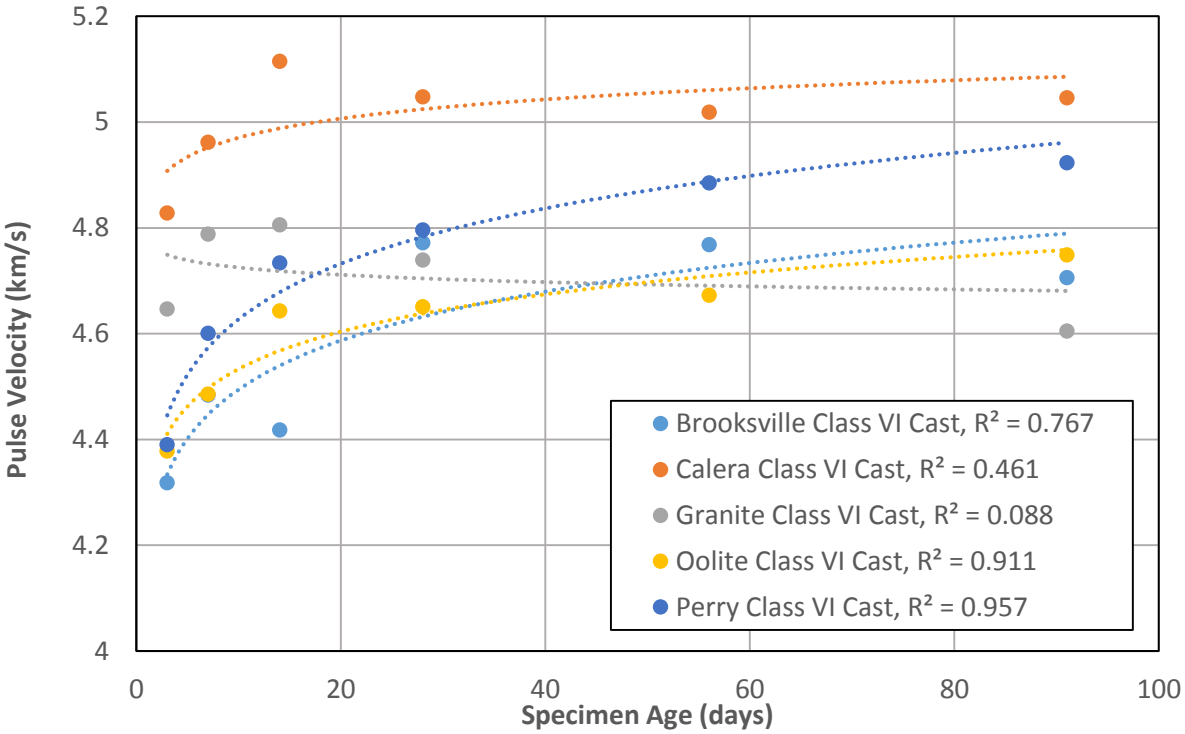

Figure 8.10 Pulse velocity vs. time for class VI cast concrete

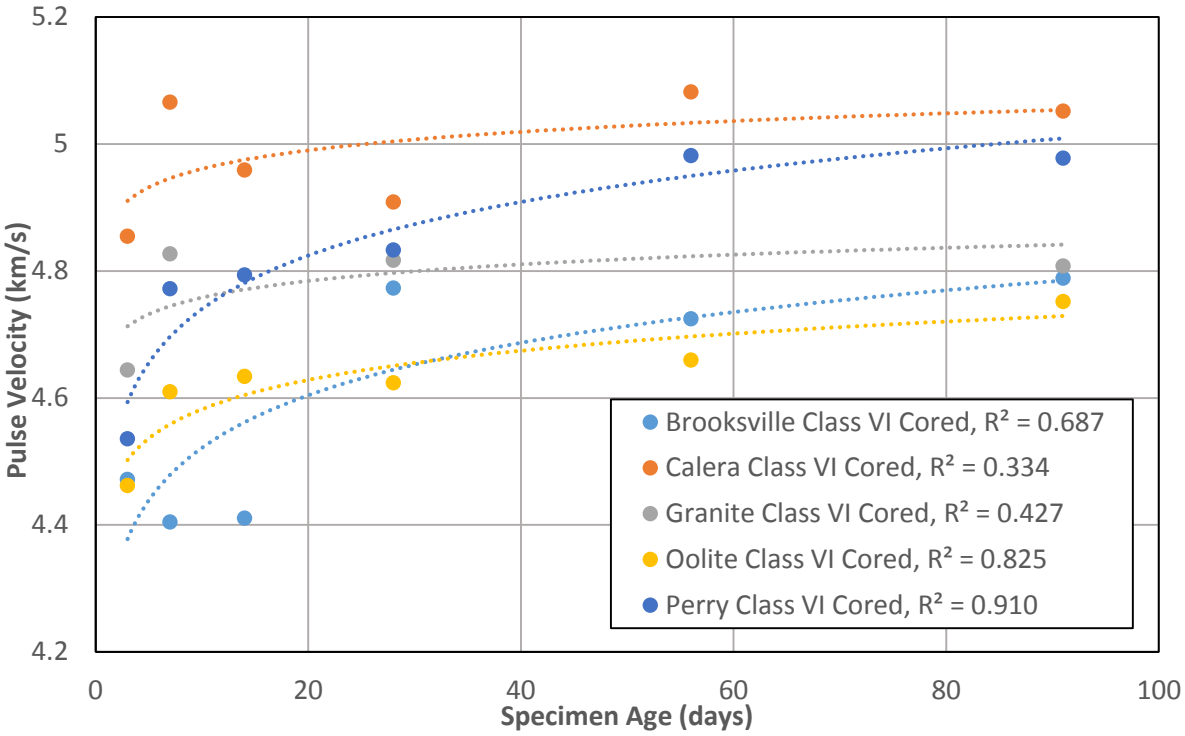

Figure 8.11 Pulse velocity vs. time for class VI cored concrete

8.3.3 Observations

Pulse velocity indirectly measures the density and dynamic modulus of elasticity of concrete through the translation of stress-waves through the matrix. While each concrete mixture had the same cement and aggregate proportion, the aggregate's chemical, physical and geological properties were variable. Pulse velocity results showed the established trend of denser aggregates producing faster velocities. Brooksville limestone was the only aggregate that displayed a definitive difference in pulse velocity, with class II deck mixtures having the slowest and class VI mixtures having the fastest velocities. Miami oolite, as well as Brooksville limestone, showed ultimate velocities of 4.8 km/s. The denser aggregates, Perry and Calera limestone and granite, had initial wave velocities around 4.5 km/s and ultimate velocities of approximately 5 km/s or higher.

Granite, the only non-limestone aggregate, also was the only aggregate that exhibited poor velocity gain over time, and poor-fitting data points. While each aggregate had a certain degree of variability, all limestones showed positive velocity gain over time. Brooksville limestone had the highest spread between initial pulse velocity and ultimate velocity, while granite had the lowest spread of approximately 0.2 km/s

8.4 COEFFICIENT OF THERMAL EXPANSION

Coefficient of thermal expansion testing was performed on each of the mixtures. Specimens were prepared for at least 48 hours before testing in a bath of lime-saturated water. Preparation

involved grinding cylinder heights to 7.0” and recording weights, both done at the FDOT. Replicates of two specimens were tested, a cast cylinder and a cored specimen for each mixture type, as well as a solid aggregate specimen (devoid of cement). Testing was conducted following AASHTO 336 and the results are presented in Figure 8.12, in millionths per °C (AASHTO T 336, 2011). When compared to the results provided by Davis 1930 and Tia et al. 2012, (Table 8.1), the general trends are within relatively good agreement. Limestone is typically reported to have of approximately 7 millionths per °C, where granite is reported to have a value of approximately 10 millionths per °C. The results indicate that the coefficient of thermal expansion for concrete with granite coarse aggregate was slightly higher than the published values in Table 8.1, which could be attributed to hygrothermal effects. Research has shown that hardened cement paste that is not fully saturated has a larger coefficient of thermal expansion than hardened cement paste that is fully saturated as presented in Figure 8.13 (Mindess, et al, 2003).

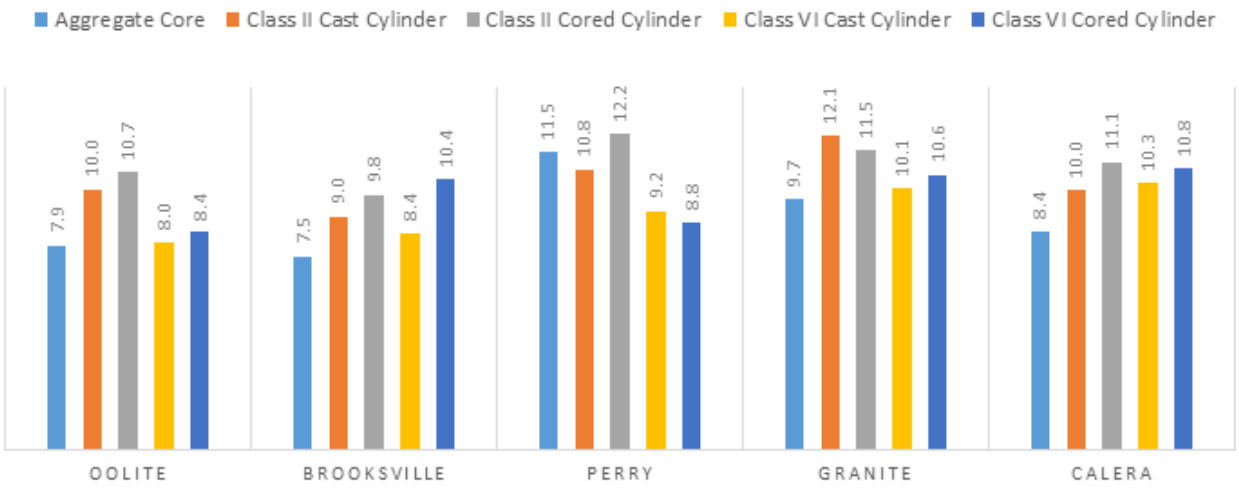

Figure 8.12 CTE of aggregates and cast and cored specimens

Table 8.1 Aggregate CTE (Davis, 1930)

Aggregate type (from one source)	Coefficient of expansion, millionths per °C	Coefficient of expansion, millionths per °F
Quartz	11.9	6.6
Sandstone	11.7	6.5
Gravel	10.8	6.0
Granite	9.5	5.3
Basalt	8.6	4.8
Limestone	6.8	3.8

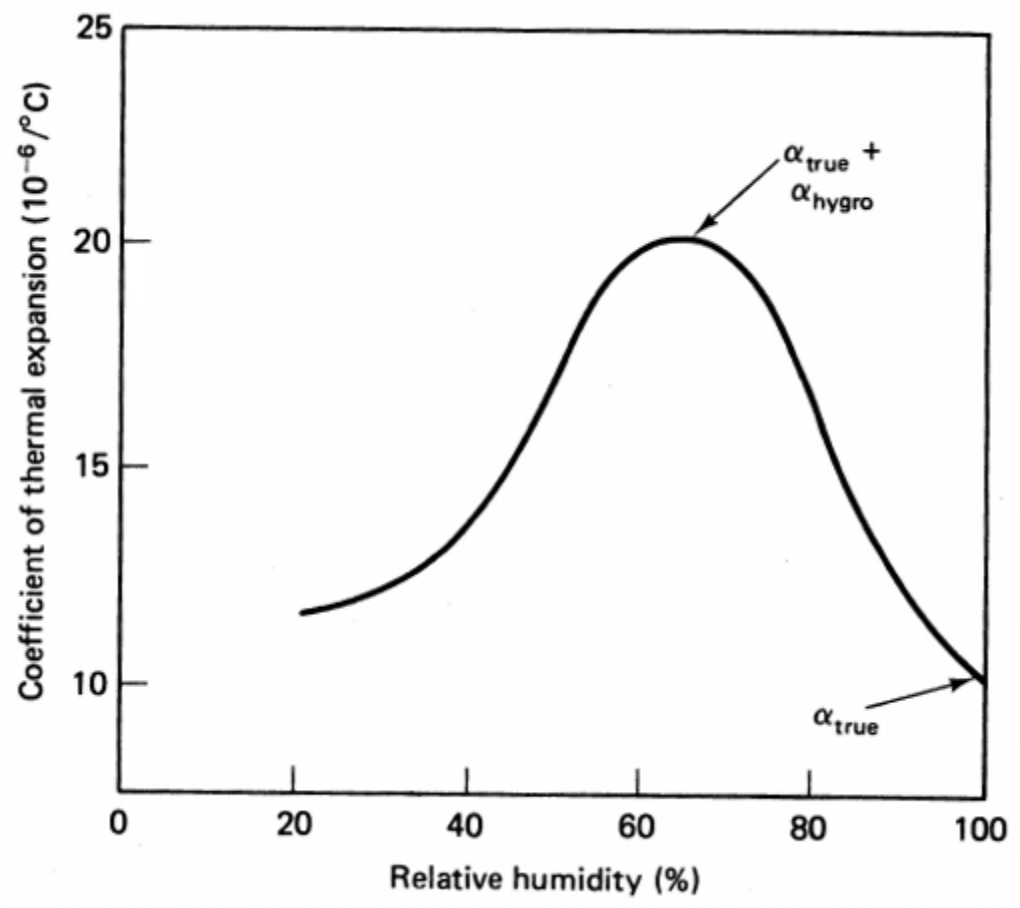

Figure 8.13 Variation of CTE with moisture content of cement paste (Mindess, et al, 2003)

9. COMPARATIVE RESULTS

The primary goal of this research was to determine the accuracy and adequacy of the predictive relationships between the compressive strength and modulus of elasticity of concrete incorporating different aggregates, especially those which are unique to the geology of Florida. This chapter focuses on the equations most commonly used for the design of concrete based on compressive strength. Ultimately, it was decided to utilize four different equations for strength and modulus of elasticity. Each of the equations use the compressive strength of concrete as the independent variable for the determination of modulus of elasticity. Some of these equations incorporate the unit weight of the concrete as a second independent variable.

The equations employed indicate that concrete mixtures of higher unit weight have higher predicted moduli of elasticity. However, none of the equations address the effects of mixture design, such as w/cm, cement content, or SCMs to establish the physical relationships. The equations used for analysis, as presented in this chapter, apply to concrete tested in this research. Equations for modulus of elasticity that incorporate different coarse aggregate types into the concrete mixture are developed. Accordingly, the chapter proposes revised "correction factors" labeled, K_1, based on the physical testing and results of this research.

9.1 MODULUS PREDICTION EQUATIONS

9.1.1 American Concrete Institute 318

The equations developed for prediction of the modulus of elasticity of concrete in ACI 318 are found in chapter 8, presented in equations 9-1 and 9-2 as follows (ACI 318, 2012):

$$E_c = 33 w_c^{\,1.5} \sqrt{f'c} \qquad \text{(9-1) – ACI 318}$$

$$E_c = 57000 \sqrt{f'c} \qquad \text{(9-2) – ACI 318}$$

Where:

E_c = Modulus of elasticity (psi)
w_c = the unit weight of concrete (psf)
f'_c = the compressive strength (psi)

Equation 9-1 is applied to lightweight or high strength concrete with a unit weight of 90 to 160 lb/ft^3. Equation 9-2 is acceptable for normal weight concrete with a density of 144 lb/ft^3 (Mindess et al., 2003) The research conducted by Tia et al 2005 and Ferraro and Watts confirmed the relative accuracy of equation for concrete, which incorporates Miami Oolite. This report will posit that correction based on just a difference in unit weight does not accurately predict concrete compressive strength and modulus due to aggregate interactions within the concrete.

9.1.2 American Association of State Highway and Transportation Officials 2013

The American Association of State Highway and Transportation Officials, (AASHTO) *LRFD Bridge Design Specifications* formula for predicting concrete material properties, specifically

modulus of elasticity, as presented in equation 9-3, or equation 5.4.2.4 per the LRFD specifications is dependent upon specified compressive strength, unit weight of concrete, and a variable, K_1, a "correction factor" for source of aggregate to be taken as 1.0 unless determined by physical test, and as approved by the authority of jurisdiction". (AASHTO, 2007) This equation is the ACI equation, with the addition of the aggregate correction term K_1, and was used in this manual up until June of 2014. The first inclusion of this factor was suggested by Tomosawa and Noguchi (1993). Ultimately, the correction factors are used in design specifications adopted by LRFD based on the Transportation Research Board's NCHRP report 496 (Tadros, 2003). K_1 represents an adjustment factor for coarse aggregate selection. Another factor, K_2, was also included, which represented a statistical representation of admixtures and is not considered in this report. The Equation used in this report is as follows:

$$E_c = 33{,}000\, K_1\, w_c{}^{1.5}\sqrt{f'c} \qquad \text{(9-3) AASHTO - 2013}$$

Where:

E_c = Modulus of elasticity (ksi)
w_c = the unit weight of concrete (ksf)
f'_c = the compressive strength (ksi)
K_1 = correction factor

9.1.3 American Association of State Highway and Transportation Officials 2014

The most recent publication of the LRFD manual has adopted a new equation for modulus prediction. The 2014 subcommittee on Bridges and Structures Annual Meeting (SCOB) implemented a new equation for use which is already being addressed in other publications such as the Florida Highway Administration. This Equation incorporates the same K_1 correction factor and is as follows:

$$E_c = 120{,}000\, K_1\, w_c{}^{2.0} f'c^{0.33} \qquad \text{(9-4) AASHTO - 2014}$$

Where:

E_c = Modulus of elasticity (ksi)
w_c = the unit weight of concrete (ksf)
f'_c = the compressive strength (ksi)
K_1 = correction factor

9.1.4 National Cooperative Highway Research Program Report 595

The last equation presented in this report (Equation 9-5) comes from the National Cooperative Highway Research Program (NCHRP) Report 595. (Rizkalla et al., 2007), which also makes proposed revisions to the LRFD manual. Equation 9-5 is a modification of Equation 9-4 in which the exponent of the unit weight is increased from 2.0 to 2.5, and the multiplier is increased from 120,000 to 310,000.

$$E_c = 310{,}000\, K_1\, w_c{}^{2.5} f'c^{0.33} \qquad \text{(9-5) NCHRP Report 595}$$

Where:

E_c = Modulus of elasticity (ksi)
w_c = the unit weight of concrete (ksf)
f'_c = the compressive strength (ksi)
K_1 = correction factor

9.2 MODULUS OF ELASTICITY PREDICTION RESULTS

Each aggregate presented in this research was evaluated using two different class mixes, II deck and VI. Cored samples, as well as traditionally cast cylindrical specimens, were tested. The summary of compressive strength testing, modulus of elasticity testing, as well as predicted results from each equation are presented in this section. Average compressive strength and measured average modulus of elasticity are presented alongside predicted values and the percentage differences. Correction factors, when present in the predictive equations, were taken at unity, as the act of regression line fitting would correct for and minimize error. Using these predicted modulus differences, correction factors are presented in the next section.

9.2.1 Miami Oolite

9.2.1.1 Class II Concrete Results

As exhibited in Table 9.1, each column labeled "Difference" represents the percent difference between predicted and measured values for each data point. Compressive strengths and elastic moduli were measured, and elastic moduli were calculated and compared with the measured values. All four equations are shown together with their average total difference. Negative differences represent under-prediction, as predicted modulus was lower than measured. Here, class II mixtures with cast specimens show an under-predicted modulus for each equation with the exception of ACI 318. Cored specimens are exhibited in Table 9.2.

Table 9.1 Miami oolite class II cast concrete predicted and measured results

Measured Values (psi)		Predictive Modulus Equations (psi) and Percentage Differences							
Compressive Strength	Modulus Measured	ACI 318	Difference	AASHTO 2013	Difference	AASHTO 2014	Difference	NCHRP	Difference
4,760	3,866,667	3,932,591	1.7%	3,849,309	-0.4%	4,044,630	4.6%	3,936,235	1.8%
5,953	4,433,333	4,397,878	-0.8%	4,304,744	-2.9%	4,354,430	-1.8%	4,237,733	-4.4%
6,333	4,666,667	4,536,073	-2.8%	4,440,011	-4.9%	4,444,261	-4.8%	4,325,157	-7.3%
7,133	4,900,000	4,814,059	-1.8%	4,712,110	-3.8%	4,622,195	-5.7%	4,498,322	-8.2%
8,880	5,183,333	5,371,329	3.6%	5,257,579	1.4%	4,968,722	-4.1%	4,835,562	-6.7%
9,403	5,433,333	5,527,242	1.7%	5,410,191	-0.4%	5,063,448	-6.8%	4,927,750	-9.3%
Average Difference			**0.3%**		**-1.8%**		**-3.1%**		**-5.7%**

Cored samples had higher measured compressive strengths and moduli. Average total percent differences were also higher when compared to cast specimens, with an approximate 2% difference in ACI 318 and AASHTO 2013 equations, and a 3% difference in AASHTO 2014 and

NCHRP. This difference also shows that cored specimens are under-predicted to a greater extent than cast specimens.

Table 9.2 Miami oolite class II cored concrete predicted and measured results

Measured Values (psi)		Predictive Modulus Equations (psi) and Percentage Differences							
Compressive Strength	Modulus Measured	ACI 318	Difference	AASHTO 2013	Difference	AASHTO 2014	Difference	NCHRP	Difference
5,246	4,216,667	4,128,473	-2.1%	4,041,043	-4.2%	4,176,493	-1.0%	4,064,565	-3.6%
6,610	4,783,333	4,634,213	-3.1%	4,536,073	-5.2%	4,507,492	-5.8%	4,386,692	-8.3%
6,926	4,916,667	4,743,692	-3.5%	4,643,234	-5.6%	4,577,493	-6.9%	4,454,818	-9.4%
7,833	5,300,000	5,044,746	-4.8%	4,937,913	-6.8%	4,767,215	-10.1%	4,639,455	-12.5%
9,193	5,400,000	5,465,173	1.2%	5,349,436	-0.9%	5,025,848	-6.9%	4,891,157	-9.4%
10,003	5,566,667	5,700,860	2.4%	5,580,132	0.2%	5,167,868	-7.2%	5,029,371	-9.7%
Average Difference			**-1.7%**		**-3.7%**		**-6.3%**		**-8.8%**

9.2.1.2 Class VI Concrete Results

Class VI mixtures are presented in Table 9.3 and Table 9.4. Class VI mixtures had higher compressive strengths and moduli compared to class II mixtures. While the equations may include a variable dependent on mixture unit weight, they do not take into account mixture type. Results for class VI cast specimens showed an over-prediction using the ACI equation (which does not utilize a unit weight variable) and an under-prediction for those equations that do incorporate unit weight as a parameter. Cored specimens exhibited higher compressive strengths and moduli. Average total differences were higher than all other classes and specimen types with the exception of ACI 318.

Table 9.3 Miami oolite class VI cast concrete predicted and measured results

Measured Values (psi)		Predictive Modulus Equations (psi) and Percentage Differences							
Compressive Strength	Modulus Measured	ACI 318	Difference	AASHTO 2013	Difference	AASHTO 2014	Difference	NCHRP	Difference
5,720	4,300,000	4,310,953	0.3%	3,975,882	-7.5%	3,969,636	-7.7%	3,787,375	-11.9%
6,523	4,550,000	4,603,615	1.2%	4,245,797	-6.7%	4,145,507	-8.9%	3,955,171	-13.1%
7,326	4,716,667	4,878,752	3.4%	4,499,549	-4.6%	4,307,409	-8.7%	4,109,639	-12.9%
7,933	5,083,333	5,076,846	-0.1%	4,682,246	-7.9%	4,422,057	-13.0%	4,219,024	-17.0%
9,950	5,250,000	5,685,738	8.3%	5,243,811	-0.1%	4,765,315	-9.2%	4,546,521	-13.4%
9,786	5,150,000	5,638,686	9.5%	5,200,416	1.0%	4,739,251	-8.0%	4,521,654	-12.2%
Average Difference			**3.8%**		**-4.3%**		**-9.2%**		**-13.4%**

Table 9.4 Miami oolite class VI cored concrete predicted and measured results

Measured Values (psi)		Predictive Modulus Equations (psi) and Percentage Differences							
Compressive Strength	Modulus Measured	ACI 318	Difference	AASHTO 2013	Difference	AASHTO 2014	Difference	NCHRP	Difference
7,040	4,866,667	4,782,573	-1.7%	4,410,845	-9.4%	4,251,175	-12.6%	4,055,987	-16.7%
7,376	5,000,000	4,895,372	-2.1%	4,514,877	-9.7%	4,317,088	-13.7%	4,118,874	-17.6%
8,170	5,200,000	5,152,124	-0.9%	4,751,673	-8.6%	4,465,224	-14.1%	4,260,209	-18.1%
7,870	5,050,000	5,056,647	0.1%	4,663,617	-7.7%	4,410,437	-12.7%	4,207,938	-16.7%
10,316	5,500,000	5,789,365	5.3%	5,339,384	-2.9%	4,822,461	-12.3%	4,601,044	-16.3%
10,813	5,483,333	5,927,184	8.1%	5,466,490	-0.3%	4,897,926	-10.7%	4,673,044	-14.8%
Average Difference			**1.5%**		**-6.4%**		**-12.7%**		**-16.7%**

9.2.2 Brooksville Limestone

9.2.2.1 Class II Concrete Results

Table 9.5 shows strength and modulus data for class II, cast concrete specimens containing Brooksville limestone coarse aggregate.

Table 9.5 Brooksville limestone class II cast concrete predicted and measured results

Measured Values (psi)		Predictive Modulus Equations (psi) and Percentage Differences							
Compressive Strength	Modulus Measured	ACI 318	Difference	AASHTO 2013	Difference	AASHTO 2014	Difference	NCHRP	Difference
3,380	3,516,667	3,313,856	-5.8%	3,048,222	-13.3%	3,325,239	-5.4%	3,169,772	-9.9%
4,456	3,416,667	3,804,940	11.4%	3,499,942	2.4%	3,642,774	6.6%	3,472,462	1.6%
5,336	3,683,333	4,163,736	13.0%	3,829,977	4.0%	3,865,997	5.0%	3,685,248	0.1%
5,916	3,933,333	4,384,190	11.5%	4,032,760	2.5%	3,999,905	1.7%	3,812,895	-3.1%
6,266	4,183,333	4,512,014	7.9%	4,150,338	-0.8%	4,076,497	-2.6%	3,885,907	-7.1%
5,703	4,183,333	4,304,542	2.9%	3,959,496	-5.4%	3,951,795	-5.5%	3,767,035	-10.0%
Average Difference			**6.8%**		**-1.8%**		**0.0%**		**-4.7%**

Usage of the ACI 318 equation resulted in an average over-prediction, while usage of the remaining equations produced a slight under-prediction. Use of the NCHRP equation produced the largest difference in prediction. The AASHTO 2014 equation produced an average total difference of 0%, however, individual data points had a wide range of percent difference.

Table 9.6 shows results for cored samples of the Class II Deck mix with Brooksville aggregate. Compressive strengths and elastic moduli were higher, similar to results for the Miami oolite. Unlike cast specimens, the prediction differences for cored samples followed along with Miami oolite. Elastic modulus predictions using the ACI 318 equation are overly optimistic, where all others showed a conservative under-prediction. The NCHRP equation had the largest percent

difference margin. Prediction difference also increased as compressive strength increased. This correlates to larger differences at later ages.

Table 9.6 Brooksville limestone class II cored concrete predicted and measured results

Measured Values (psi)		Predictive Modulus Equations (psi) and Percentage Differences							
Compressive Strength	Modulus Measured	ACI 318	Difference	AASHTO 2013	Difference	AASHTO 2014	Difference	NCHRP	Difference
4,750	3,550,000	3,928,458	10.7%	3,613,558	1.8%	3,720,396	4.8%	3,546,455	-0.1%
5,443	3,916,667	4,205,275	7.4%	3,868,187	-1.2%	3,891,410	-0.6%	3,709,473	-5.3%
6,410	4,400,000	4,563,565	3.7%	4,197,757	-4.6%	4,107,178	-6.7%	3,915,153	-11.0%
7,026	4,683,333	4,777,815	2.0%	4,394,832	-6.2%	4,233,446	-9.6%	4,035,518	-13.8%
7,636	4,783,333	4,980,905	4.1%	4,581,643	-4.2%	4,351,371	-9.0%	4,147,929	-13.3%
7,016	4,933,333	4,774,414	-3.2%	4,391,704	-11.0%	4,231,457	-14.2%	4,033,621	-18.2%
Average Difference			**4.1%**		**-4.2%**		**-5.9%**		**-10.3%**

9.2.2.2 Class VI Concrete Results

Results for Class VI mixtures are displayed in Table 9.7 for cast specimens and Table 9.8 for cored. Class VI initial compressive strengths were almost twice those of class II mixtures. The initial modulus increased from 3300 ksi to 4500 ksi, with a 4.3% over-prediction. The AASHTO 2013 equation was the most accurate, with only a 0.3% total difference. Both AASHTO 2014 and NCHRP equations had larger modulus differences as strength increased.

Cored specimens, shown in Table 9.8, had higher compressive strengths than cast counterparts. Modulus and compressive strength did not follow increasing trends expected and observed for other mixtures. However, results were similar, with those for the NCHRP equation were the most conservative and those for the ACI 318 equation showed small over-predictions.

Table 9.7 Brooksville limestone class VI cast concrete predicted and measured results

Measured Values (psi)		Predictive Modulus Equations (psi) and Percentage Differences							
Compressive Strength	Modulus Measured	ACI 318	Difference	AASHTO 2013	Difference	AASHTO 2014	Difference	NCHRP	Difference
6,170	4,200,000	4,477,317	6.6%	4,308,597	2.6%	4,307,393	2.6%	4,168,259	-0.8%
7,323	4,483,333	4,877,753	8.8%	4,693,943	4.7%	4,557,931	1.7%	4,410,705	-1.6%
7,933	4,783,333	5,076,846	6.1%	4,885,534	2.1%	4,679,880	-2.2%	4,528,715	-5.3%
8,136	5,016,667	5,141,392	2.5%	4,947,648	-1.4%	4,719,066	-5.9%	4,566,634	-9.0%
8,576	5,050,000	5,278,587	4.5%	5,079,672	0.6%	4,801,803	-4.9%	4,646,700	-8.0%
7,390	5,050,000	4,900,016	-3.0%	4,715,367	-6.6%	4,571,651	-9.5%	4,423,981	-12.4%
Average Difference			**4.3%**		**0.3%**		**-3.0%**		**-6.2%**

Table 9.8 Brooksville limestone class VI cored concrete predicted and measured results

Measured Values (psi)		Predictive Modulus Equations (psi) and Percentage Differences							
Compressive Strength	Modulus Measured	ACI 318	Difference	AASHTO 2013	Difference	AASHTO 2014	Difference	NCHRP	Difference
7,246	4,583,333	4,852,041	5.9%	4,669,200	1.9%	4,542,060	-0.9%	4,395,346	-4.1%
7,833	4,816,667	5,044,746	4.7%	4,854,644	0.8%	4,660,330	-3.2%	4,509,796	-6.4%
8,066	4,833,333	5,119,227	5.9%	4,926,318	1.9%	4,705,628	-2.6%	4,553,631	-5.8%
8,153	5,300,000	5,146,761	-2.9%	4,952,814	-6.6%	4,722,317	-10.9%	4,569,781	-13.8%
9,120	5,183,333	5,443,431	5.0%	5,238,304	1.1%	4,900,255	-5.5%	4,741,971	-8.5%
7,830	5,416,667	5,043,780	-6.9%	4,853,714	-10.4%	4,659,741	-14.0%	4,509,226	-16.8%
Average Difference			**2.0%**		**-1.9%**		**-6.2%**		**-9.2%**

9.2.3 Perry Limestone

9.2.3.1 Class II Concrete Results

Perry limestone was the densest Florida limestone aggregate, had higher unit weights and compressive strengths, as shown in Table 9.9.

Table 9.9 Perry limestone class II cast concrete predicted and measured results

Measured Values (psi)		Predictive Modulus Equations (psi) and Percentage Differences							
Compressive Strength	Modulus Measured	ACI 318	Difference	AASHTO 2013	Difference	AASHTO 2014	Difference	NCHRP	Difference
4,763	4,466,667	3,933,830	-11.9%	4,038,412	-9.6%	4,310,792	-3.5%	4,262,421	-4.6%
5,650	4,583,333	4,284,494	-6.5%	4,398,399	-4.0%	4,560,710	-0.5%	4,509,535	-1.6%
6,663	4,966,667	4,652,755	-6.3%	4,776,451	-3.8%	4,815,790	-3.0%	4,761,752	-4.1%
7,840	5,200,000	5,047,000	-2.9%	5,181,177	-0.4%	5,081,370	-2.3%	5,024,352	-3.4%
7,603	5,350,000	4,970,130	-7.1%	5,102,263	-4.6%	5,030,157	-6.0%	4,973,714	-7.0%
8,890	5,900,000	5,374,353	-8.9%	5,517,232	-6.5%	5,296,562	-10.2%	5,237,130	-11.2%
Average Difference			**-7.3%**		**-4.8%**		**-4.3%**		**-5.3%**

The ACI 318 equation severely under-predicted modulus at low (early) and high (late) strengths for Perry aggregate, the first aggregate to exhibit this behavior. The AASHTO 2013 and ACI 318 equation produced the largest under-predictions at early age.

Table 9.10 Perry limestone class II cored concrete predicted and measured results

Measured Values (psi)		Predictive Modulus Equations (psi) and Percentage Differences							
Compressive Strength	Modulus Measured	ACI 318	Difference	AASHTO 2013	Difference	AASHTO 2014	Difference	NCHRP	Difference
5,036	4,833,333	4,044,996	-16.3%	4,152,534	-14.1%	4,390,811	-9.2%	4,341,542	-10.2%
6,453	4,933,333	4,578,847	-7.2%	4,700,577	-4.7%	4,765,164	-3.4%	4,711,694	-4.5%
7,786	5,466,667	5,029,589	-8.0%	5,163,303	-5.5%	5,069,793	-7.3%	5,012,905	-8.3%
8,393	5,383,333	5,221,964	-3.0%	5,360,792	-0.4%	5,196,958	-3.5%	5,138,643	-4.5%
8,033	5,816,667	5,108,744	-12.2%	5,244,562	-9.8%	5,122,314	-11.9%	5,064,836	-12.9%
9,863	6,300,000	5,660,826	-10.1%	5,811,321	-7.8%	5,481,248	-13.0%	5,419,744	-14.0%
Average Difference			**-9.5%**		**-7.1%**		**-8.0%**		**-9.1%**

Cored samples exhibited severe under-prediction at early strengths as well as a spike in under-prediction at later-age strengths. Average total error was high with averages above 7% for all equations.

9.2.3.2 Class VI Concrete Results

Class VI mixtures suffered from erratic strength and modulus gain (Table 9.11).

Table 9.11 Perry limestone class VI cast concrete predicted and measured results

Measured Values (psi)		Predictive Modulus Equations (psi) and Percentage Differences							
Compressive Strength	Modulus Measured	ACI 318	Difference	AASHTO 2013	Difference	AASHTO 2014	Difference	NCHRP	Difference
6,796	4,533,333	4,698,962	3.7%	4,603,341	1.5%	4,554,089	0.5%	4,433,290	-2.2%
7,976	4,316,667	5,090,587	17.9%	4,986,996	15.5%	4,801,169	11.2%	4,673,816	8.3%
9,070	5,133,333	5,428,488	5.7%	5,318,022	3.6%	5,009,200	-2.4%	4,876,329	-5.0%
10,270	5,250,000	5,776,443	10.0%	5,658,896	7.8%	5,218,866	-0.6%	5,080,434	-3.2%
9,370	5,683,333	5,517,535	-2.9%	5,405,256	-4.9%	5,063,281	-10.9%	4,928,975	-13.3%
9,453	5,616,667	5,541,918	-1.3%	5,429,143	-3.3%	5,078,038	-9.6%	4,943,341	-12.0%
Average Difference			**5.5%**		**3.4%**		**-2.0%**		**-4.6%**

Measured modulus was lower for these class VI cast specimens than class II cast specimens shown in Table 9.9. The high compressive strength and low modulus, when combined with observations of poor cohesion in the ITZ, may be a result of differential stress and non-uniform stresses exacerbated by the higher amount of cementitious materials in class VI mixtures.

Table 9.12 Perry limestone class VI cored concrete predicted and measured results

Measured Values (psi)		Predictive Modulus Equations (psi) and Percentage Differences							
Compressive Strength	Modulus Measured	ACI 318	Difference	AASHTO 2013	Difference	AASHTO 2014	Difference	NCHRP	Difference
7,420	5,016,667	4,909,952	-2.1%	4,810,037	-4.1%	4,688,039	-6.6%	4,563,687	-9.0%
8,360	5,250,000	5,211,688	-0.7%	5,105,633	-2.7%	4,876,250	-7.1%	4,746,906	-9.6%
10,303	5,583,333	5,785,716	3.6%	5,667,980	1.5%	5,224,394	-6.4%	5,085,815	-8.9%
10,240	5,716,667	5,768,000	0.9%	5,650,624	-1.2%	5,213,831	-8.8%	5,075,532	-11.2%
9,583	5,666,667	5,579,895	-1.5%	5,466,347	-3.5%	5,100,978	-10.0%	4,965,672	-12.4%
10,056	5,983,333	5,715,943	-4.5%	5,599,627	-6.4%	5,182,726	-13.4%	5,045,252	-15.7%
Average Difference			**-0.7%**		**-2.7%**		**-8.7%**		**-11.1%**

Compressive strength was high for the cored cylinders, but did not follow the normal strength gain shown in the porous Florida limestones.

9.2.4 Georgia Granite

Granite, the only igneous aggregate, has low permeability and high density. Concrete mixtures utilizing granite exhibited intergranular failure at all ages and strengths.

9.2.4.1 Class II Concrete Results

Data for class II cast specimens are shown in Table 9.13. These samples had lower initial compressive strengths than the majority of the samples with limestone aggregate and decent strength gain over time. Measured elastic modulus was higher than predicted for each equation. ACI 318 and AASHTO 2013 equations both under-predicted early strength by over 18%. While later-age prediction was more accurate, all equations exhibited a 10% or greater under-prediction at ultimate strength. Elastic modulus and compressive strength both exhibited continual gains over time. Similar behavior is shown in Table 9.14, with the cast specimens.

Table 9.13 Georgia granite class II cast concrete predicted and measured results

Measured Values (psi)		Predictive Modulus Equations (psi) and Percentage Differences							
Compressive Strength	Modulus Measured	ACI 318	Difference	AASHTO 2013	Difference	AASHTO 2014	Difference	NCHRP	Difference
4,013	4,450,000	3,610,853	-18.9%	3,616,134	-18.7%	3,941,432	-11.4%	3,865,151	-13.1%
5,220	4,666,667	4,118,229	-11.8%	4,124,252	-11.6%	4,298,733	-7.9%	4,215,537	-9.7%
5,340	4,816,667	4,165,296	-13.5%	4,171,388	-13.4%	4,331,096	-10.1%	4,247,274	-11.8%
6,323	5,033,333	4,532,490	-10.0%	4,539,118	-9.8%	4,579,456	-9.0%	4,490,827	-10.8%
7,746	5,450,000	5,016,653	-8.0%	5,023,989	-7.8%	4,896,714	-10.2%	4,801,945	-11.9%
8,276	5,766,667	5,185,439	-10.1%	5,193,022	-9.9%	5,004,837	-13.2%	4,907,976	-14.9%
Average Difference			**-12.0%**		**-11.9%**		**-10.3%**		**-12.0%**

Table 9.14 Georgia granite class II cored concrete predicted and measured results

Measured Values (psi)		Predictive Modulus Equations (psi) and Percentage Differences							
Compressive Strength	Modulus Measured	ACI 318	Difference	AASHTO 2013	Difference	AASHTO 2014	Difference	NCHRP	Difference
4,870	4,500,000	3,977,771	-11.6%	3,983,588	-11.5%	4,201,397	-6.6%	4,120,085	-8.4%
5,563	4,750,000	4,251,379	-10.5%	4,257,596	-10.4%	4,389,966	-7.6%	4,305,005	-9.4%
6,276	5,050,000	4,515,613	-10.6%	4,522,217	-10.5%	4,568,194	-9.5%	4,479,783	-11.3%
6,573	5,166,667	4,621,225	-10.6%	4,627,983	-10.4%	4,638,432	-10.2%	4,548,662	-12.0%
7,183	5,616,667	4,830,902	-14.0%	4,837,966	-13.9%	4,776,284	-15.0%	4,683,846	-16.6%
8,143	5,816,667	5,143,604	-11.6%	5,151,125	-11.4%	4,978,151	-14.4%	4,881,806	-16.1%
Average Difference			**-11.5%**		**-11.3%**		**-10.6%**		**-12.3%**

Compressive strength and modulus values did not increase as much for granite. Prediction differences were very similar and did not provide an adequate fit for any equation.

9.2.4.2 Class VI Concrete Results

Class VI mixtures continued to gain significant strength over time as well as being substantially higher (approximately 50% increase) as seen in Table 9.15.

Table 9.15 Georgia granite class VI cast concrete predicted and measured results

Measured Values (psi)		Predictive Modulus Equations (psi) and Percentage Differences							
Compressive Strength	Modulus Measured	ACI 318	Difference	AASHTO 2013	Difference	AASHTO 2014	Difference	NCHRP	Difference
6,886	4,800,000	4,729,974	-1.5%	4,761,567	-0.8%	4,742,933	-1.2%	4,659,202	-2.9%
7,430	5,066,667	4,913,259	-3.0%	4,946,076	-2.4%	4,863,446	-4.0%	4,777,588	-5.7%
7,623	4,900,000	4,976,663	1.6%	5,009,903	2.2%	4,904,778	0.1%	4,818,191	-1.7%
8,013	5,300,000	5,102,381	-3.7%	5,136,460	-3.1%	4,986,206	-5.9%	4,898,181	-7.6%
8,846	5,600,000	5,361,036	-4.3%	5,396,844	-3.6%	5,151,626	-8.0%	5,060,680	-9.6%
11,080	5,950,000	5,999,916	0.8%	6,039,991	1.5%	5,549,016	-6.7%	5,451,055	-8.4%
Average Difference			**-1.7%**		**-1.0%**		**-4.3%**		**-6.0%**

With higher strengths but similar moduli, the predicted moduli were closer in value to the measured modulus. In Table 9.16, cored samples showed a slight increase in compressive strength and modulus.

Table 9.16 Georgia granite class VI cored concrete predicted and measured results

Measured Values (psi)		Predictive Modulus Equations (psi) and Percentage Differences							
Compressive Strength	Modulus Measured	ACI 318	Difference	AASHTO 2013	Difference	AASHTO 2014	Difference	NCHRP	Difference
7,060	5,000,000	4,789,362	-4.2%	4,821,351	-3.6%	4,782,152	-4.4%	4,697,729	-6.0%
7,576	5,316,667	4,961,297	-6.7%	4,994,435	-6.1%	4,894,778	-7.9%	4,808,367	-9.6%
7,580	6,000,000	4,962,607	-17.3%	4,995,753	-16.7%	4,895,631	-18.4%	4,809,205	-19.8%
8,503	5,616,667	5,256,073	-6.4%	5,291,179	-5.8%	5,084,832	-9.5%	4,995,066	-11.1%
8,893	5,783,333	5,375,259	-7.1%	5,411,162	-6.4%	5,160,642	-10.8%	5,069,538	-12.3%
11,086	6,103,333	6,001,540	-1.7%	6,041,626	-1.0%	5,550,007	-9.1%	5,452,029	-10.7%
Average Difference			**-7.2%**		**-6.6%**		**-10.0%**		**-11.6%**

9.2.5 Calera Limestone

Calera limestone was the densest sedimentary aggregate tested in this research. This limestone was unique in its low permeability and high density, resembling granite.

9.2.5.1 Class II Concrete Results

Similar to granite, concrete containing Calera aggregate had low compressive strengths, but with the highest moduli of any mixture previously tested, as seen in Table 9.17. The concrete exhibited a low early-age strength of about 4000 psi with a modulus of about 5300 ksi.

Table 9.17 Calera limestone class II cast concrete predicted and measured results

Measured Values (psi)		Predictive Modulus Equations (psi) and Percentage Differences							
Compressive Strength	Modulus Measured	ACI 318	Difference	AASHTO 2013	Difference	AASHTO 2014	Difference	NCHRP	Difference
3,976	5,283,333	3,594,169	-32.0%	3,633,199	-31.2%	3,978,639	-24.7%	3,913,803	-25.9%
4,886	5,433,333	3,984,300	-26.7%	4,027,566	-25.9%	4,258,649	-21.6%	4,189,251	-22.9%
5,526	5,450,000	4,237,217	-22.3%	4,283,230	-21.4%	4,435,196	-18.6%	4,362,920	-19.9%
6,503	5,966,667	4,596,552	-23.0%	4,646,467	-22.1%	4,679,989	-21.6%	4,603,724	-22.8%
7,546	6,216,667	4,951,465	-20.4%	5,005,234	-19.5%	4,915,456	-20.9%	4,835,354	-22.2%
7,996	6,483,333	5,096,965	-21.4%	5,152,314	-20.5%	5,010,318	-22.7%	4,928,670	-24.0%
Average Difference			**-24.3%**		**-23.4%**		**-21.7%**		**-23.0%**

The consequence of this behavior was the largest under-prediction found for the concrete studied, with average total differences approaching 25%. The ACI 218 and AASHTO 2013 equations severely under-predicted early strength with percent differences above 30%. Cored samples had marginal increases in compressive strength and modulus as seen in Table 9.18.

Table 9.18 Calera limestone class II cored concrete predicted and measured results

Measured Values (psi)		Predictive Modulus Equations (psi) and Percentage Differences							
Compressive Strength	Modulus Measured	ACI 318	Difference	AASHTO 2013	Difference	AASHTO 2014	Difference	NCHRP	Difference
4,060	5,300,000	3,631,937	-31.5%	3,671,377	-30.7%	4,006,184	-24.4%	3,940,899	-25.6%
5,080	5,433,333	4,062,629	-25.2%	4,106,746	-24.4%	4,313,723	-20.6%	4,243,427	-21.9%
5,680	5,966,667	4,295,853	-28.0%	4,342,503	-27.2%	4,475,610	-25.0%	4,402,675	-26.2%
6,240	5,866,667	4,502,644	-23.3%	4,551,539	-22.4%	4,616,663	-21.3%	4,541,430	-22.6%
6,690	6,266,667	4,662,172	-25.6%	4,712,800	-24.8%	4,723,978	-24.6%	4,646,996	-25.8%
7,533	6,733,333	4,947,198	-26.5%	5,000,920	-25.7%	4,912,660	-27.0%	4,832,603	-28.2%
Average Difference			**-26.7%**		**-25.9%**		**-23.8%**		**-25.1%**

9.2.5.2 Class VI Concrete Results

With increased cement content and coarse-to-fine ratio, class VI mixtures had higher compressive strength than class II. Exhibited in Table 9.19, the differences averaged above 15%, less than class II mixtures. This was due to the elastic modulus equations dependence on compressive strength, which increased compared to measured modulus.

Table 9.19 Calera limestone class VI cast concrete predicted and measured results

Measured Values (psi)		Predictive Modulus Equations (psi) and Percentage Differences							
Compressive Strength	Modulus Measured	ACI 318	Difference	AASHTO 2013	Difference	AASHTO 2014	Difference	NCHRP	Difference
5,210	5,066,667	4,114,283	-18.8%	4,202,058	-17.1%	4,410,049	-13.0%	4,353,116	-14.1%
5,923	5,316,667	4,386,783	-17.5%	4,480,372	-15.7%	4,600,719	-13.5%	4,541,325	-14.6%
7,243	5,733,333	4,851,036	-15.4%	4,954,530	-13.6%	4,916,545	-14.2%	4,853,074	-15.4%
8,146	6,066,667	5,144,551	-15.2%	5,254,307	-13.4%	5,110,914	-15.8%	5,044,934	-16.8%
8,716	6,816,667	5,321,498	-21.9%	5,435,029	-20.3%	5,226,268	-23.3%	5,158,798	-24.3%
9,396	6,716,667	5,525,184	-17.7%	5,643,061	-16.0%	5,357,450	-20.2%	5,288,287	-21.3%
Average Difference			**-17.8%**		**-16.0%**		**-16.7%**		**-17.7%**

Results for the cored samples shown in Table 9.20 are very similar to those for cast samples, mirroring what was observed for class II mixtures: that specimen type (cast or cored) did not significantly impact modulus prediction for Calera limestone concrete mixtures.

Table 9.20 Calera limestone class VI cored concrete predicted and measured results

Measured Values (psi)		Predictive Modulus Equations (psi) and Percentage Differences							
Compressive Strength	Modulus Measured	ACI 318	Difference	AASHTO 2013	Difference	AASHTO 2014	Difference	NCHRP	Difference
6,003	5,383,333	4,416,309	-18.0%	4,510,528	-16.2%	4,621,133	-14.2%	4,561,476	-15.3%
6,320	5,550,000	4,531,415	-18.4%	4,628,090	-16.6%	4,700,279	-15.3%	4,639,599	-16.4%
7,653	6,133,333	4,986,446	-18.7%	5,092,829	-17.0%	5,006,698	-18.4%	4,942,063	-19.4%
8,566	6,183,333	5,275,508	-14.7%	5,388,058	-12.9%	5,196,414	-16.0%	5,129,329	-17.0%
8,953	6,566,667	5,393,362	-17.9%	5,508,426	-16.1%	5,272,743	-19.7%	5,204,673	-20.7%
9,546	6,900,000	5,569,112	-19.3%	5,687,926	-17.6%	5,385,525	-21.9%	5,315,999	-23.0%
Average Difference			**-17.8%**		**-16.1%**		**-17.6%**		**-18.6%**

9.3 CORRECTION FACTORS

Analysis of the design equations entailed fitting measured data with predicted data. Non-linear regression methods were used to calculate correction factors for each aggregate as well as concrete class. The analysis involved two concrete classes, five different aggregates, and four different design equations. The correction factor for these design equations is based on aggregate type. Due to the difference in prediction error between cast and cored specimens, correction factors were calculated for both specimen types. Data for cast specimens are shown in Table 9.21 and data for cored specimens are given in Table 9.22.

Table 9.21 Correction factors for class II and VI cast specimens

Cast – Aggregate	Class II	Class VI	Equation
Oolite	1.00	0.96	ACI 318
Oolite	1.01	1.00	AASHTO - 2013
Oolite	1.04	1.10	AASHTO - 2014
Oolite	1.07	1.16	NCHRP
Brooksville	0.93	0.96	ACI 318
Brooksville	1.01	1.00	AASHTO - 2013
Brooksville	1.00	1.04	AASHTO - 2014
Brooksville	1.05	1.07	NCHRP
Perry	1.08	0.95	ACI 318
Perry	1.05	0.97	AASHTO - 2013
Perry	1.05	1.03	AASHTO - 2014
Perry	1.06	1.06	NCHRP
Granite	1.12	1.02	ACI 318
Granite	1.12	1.01	AASHTO - 2013
Granite	1.11	1.05	AASHTO - 2014
Granite	1.13	1.07	NCHRP
Calera	1.31	1.22	ACI 318
Calera	1.30	1.19	AASHTO - 2013
Calera	1.28	1.21	AASHTO - 2014
Calera	1.30	1.22	NCHRP

The equation used is displayed in the right column with aggregate type in the left column. Class II and class VI mixtures are shown next to each other for easy comparison. Some general observations can be made for both the cast and cored specimens:

1. In almost all cases, the elastic modulus equations under-predicted, having aggregate correction factors greater than 1.0.
2. For Brooksville and oolite aggregates, the correction factors for Class II Deck mixes were about the same or slightly lower than those for Class VI mixes, indicating that the equations were more slightly more accurate for the lower strength Class II Deck mixes.
3. For Perry, granite, and Calera aggregates, the correction factors for Class II Deck mixes were higher than those for Class VI mixes, indicating that the equations were more accurate for the higher strength Class VI mixes.
4. For the Florida limestone aggregates, the tendency of the equations to under-predict increased in the order of ACI 318, AASHTO-2013, AASHTO-2014, and NCHRP.
5. For both concrete classes with granite and Calera aggregates, the predictions from all equations were similar.
6. Cored specimens had slightly higher correction factors than the cast specimens.

Table 9.22 Correction factors for class II and VI cored specimens

Cored – Aggregate	Class II	Class VI	Equation
Oolite	1.01	0.98	ACI 318
Oolite	1.05	1.02	AASHTO - 2013
Oolite	1.07	1.14	AASHTO - 2014
Oolite	1.10	1.20	NCHRP
Brooksville	0.97	0.98	ACI 318
Brooksville	1.05	1.02	AASHTO - 2013
Brooksville	1.07	1.07	AASHTO - 2014
Brooksville	1.13	1.10	NCHRP
Perry	1.10	1.01	ACI 318
Perry	1.07	1.03	AASHTO - 2013
Perry	1.09	1.10	AASHTO - 2014
Perry	1.10	1.13	NCHRP
Granite	1.13	1.10	ACI 318
Granite	1.13	1.09	AASHTO - 2013
Granite	1.12	1.12	AASHTO - 2014
Granite	1.15	1.14	NCHRP
Calera	1.36	1.22	ACI 318
Calera	1.35	1.19	AASHTO - 2013
Calera	1.32	1.22	AASHTO - 2014
Calera	1.34	1.23	NCHRP

Based on these results, the use of an aggregate correction factor of 0.9 for Florida limestones is excessively conservative. The average aggregate correction values (combining cast and cored specimen values) are given in Table 9.23, along with the average standard deviation values.

Table 9.23 Average aggregate correction factors

Aggregate	Correction Factor	
	Average	Standard Deviation
Miami Oolite	1.06	0.07
Brooksville	1.03	0.05
Perry	1.06	0.05
Granite	1.10	0.04
Calera	1.27	0.06

10.SUMMARY AND RECOMMENDATIONS

Fracture behavior varied greatly between concretes with different aggregate. Modulus prediction based on compressive strength can be improved by using an aggregate correction factor, K_1. Miami oolite, had the highest compressive strength and most predictable relationships between compressive, splitting tensile, and modulus of elasticity strengths.

It was found that although Florida aggregates are less dense, more porous, and lower in strength than granite and Calera limestone aggregates, their strength performance is comparable due to better paste-aggregate bonding. This better bonding is likely due to the rougher surface and higher porosity providing more surface area for bonding, and possibly an internal curing effect from water contained in the aggregate. It is thought that these effects lead to a denser and stronger interfacial transition zone, resulting in better strengths. The effect of better bonding can be observed from the transgranular fracture that occurs during strength testing. This is compared to the typical intergranular fracture observed for concretes containing granite.

Cast specimens do not cure in the same manner as specimens cored from slabs with respect to concrete hydration and strength development. Early-age curing of cast specimens occurs essentially at room temperature, whereas cored specimens come from slabs that experience higher temperatures at early ages due to mass heating effects. However, this difference did not significantly affect the concrete properties, and aggregate correction factors for cast specimens were very similar to those for cored specimens.

Based on these results of this study, the use of an aggregate correction factor of 0.9 for Florida limestones is excessively conservative. It is recommended that current specifications be revised to incorporate the average aggregate corrections values found in this study:

Aggregate	Correction Factor
Miami Oolite	1.00
Brooksville	0.97
Perry	1.01
Granite	1.06
Calera	1.21

REFERENCES

AASHTO LRFD Bridge Design Specifications, American Association of State Highway Transportation Officials, Washington, DC, 2011

AASHTO T 336-11, Coefficient of Thermal Expansion of Hydraulic Cement Concrete, American Association of State Highway Transportation Officials, Washington, DC, 2011

ACI Committee 318: "Building Code Requirements for Structural Concrete (ACI 318- 11) and Commentary", American Concrete Institute, Farmington Hills, MI, 2011

American Concrete Institute Committee 363, Report on High-Strength Concrete, Farmington Hills, MI, 2010

Aïtcin, P.-C., High performance concrete. Taylor & Francis, 2011

Akçaoğlu, T., Tokyay, M., Çelik, T., "Effect of coarse aggregate size and matrix quality on ITZ and failure behavior of concrete under uniaxial compression". Cement and Concrete Composites. 26, 633–638, 2004

ASTM C33, Standard Specification for Concrete Aggregates. ASTM International West Conshohocken, PA., 2004

ASTM C39, Standard Test Method for Compressive Strength of Cylindrical Concrete Specimens. ASTM International West Conshohocken, PA., 2014

ASTM C143, Standard Test Method for Slump of Hydraulic-Cement Concrete. ASTM International West Conshohocken, PA., 2014

ASTM C173, Standard Test Method for Air Content of Freshly Mixed Concrete by the Volumetric Method. ASTM International West Conshohocken, PA., 2014

ASTM C192, Standard Practice for Making and Curing Concrete Test Specimens in the Laboratory. ASTM International West Conshohocken, PA., 2014

ASTM C204, Standard Test Methods for Fineness of Hydraulic Cement by Air-Permeability Apparatus Active Standard ASTM C204 West Conshohocken, PA., 2011

ASTM C469, Standard Test Method for Static Modulus of Elasticity and Poisson's Ratio of Concrete in Compression. ASTM International West Conshohocken, PA. 2014

ASTM C566, Test Method for Total Evaporable Moisture Content of Aggregate by Drying. ASTM International West Conshohocken, PA, 2013

ASTM C702, *Practice for Reducing Samples of Aggregate to Testing Size*. ASTM International West Conshohocken, PA., 2011

ASTM C805, Standard Test Method for Rebound Number of Hardened Concrete. ASTM International West Conshohocken, PA. 2011

ASTM C1064, Standard Test Method for Temperature of Freshly Mixed Hydraulic-Cement Concrete. ASTM International West Conshohocken, PA., 2014

ASTM C1070, Standard Test Method for Determining Particle Size Distribution of Alumina or Quartz by Laser Light Scattering. ASTM International West Conshohocken, PA., 2014

ASTM C1702, Standard Test Method for Measurement of Heat of Hydration of Hydraulic Cementitious Materials Using Isothermal Conduction Calorimetry. ASTM International West Conshohocken, PA., 2015

Balonis, M., & Glasser, F. P. "The density of cement phases", Cement and Concrete Research, 39(9), 733–739, 2009

Beer, F., Johnston, J., E. Russell, DeWolf, J., Mazurek, D., Mechanics of Materials, 6 edition. McGraw-Hill New York, 2014

Bekoe, P. *Concrete containing marginal aggregates: Mechanical and application in concrete pavement*. University of Florida, 2013

Bentz, D. P., Garboczi, E. J., Haecker, C. J., & Jensen, O. M. "Effects of cement particle size distribution on performance properties of Portland cement-based materials". Cement and Concrete Research, 29(10), 1663–1671, 1999

Boynton, R.S., Chemistry and technology of lime and limestone, 2d ed. ed. Wiley, New York, 1980

Brameshuber, W., Raupach, M., Schröder, P., & Dauberschmidt, C., Non-destructive determination of the water content in the concrete cover using the multiring electrode. International Symposium (NDT-CE 2003) Non-Destructive Testing in Civil Engineering, 2009

CEB-FIP Model Code 1990 (CEB-FIP MC90), 1993.

Chen, H.H., Su, R.K.L., Tension softening curves of plain concrete. Constr. Build. Mater. 44, 440–451., 2013

Daniel, D. Gene, Significance of Tests and Properties of Concrete and Concrete-Making Materials, STP 169D. ASTM International, West Conshohocken, PA, 2006

Davis, R. E., "A summary of the results of Investigations having to do with volumetric changes in cements, mortars, and concretes due to causes other than stress" Proceedings of the American Concrete Institute, 1930

De Larrard, F., Concrete mixture proportioning: a scientific approach. CRC Press, 1999

Elices, M., & Rocco, C. G., "Effect of aggregate size on the fracture and mechanical properties of a simple concrete" Engineering Fracture Mechanics, 75(13), 3839–3851, 2008

FDOT, Florida Department of Transpiration, Standard Specifications for Road and Bridge Construction Section 346, 2015

FDOT, Florida Department of Transpiration, Structures Design Guidelines, 2015a

Ferraris, C.F., Measurement of the rheological properties of high performance concrete: state of the art report. J. Res.-Natl. Inst. Stand. Technol. 104, 461–478, 1999

Ferraro, C.C., Determination of test methods for the prediction of the behavior of mass concrete, University of Florida, PhD Dissertation, 2009

Gaswirth, S.B., Budd, D.A., Crawford, B.R., "Textural and stratigraphic controls on fractured dolomite in a carbonate aquifer system, Ocala limestone, west-central Florida", Sediment. Geology 184, 241–254, 2006

Haranki, B., Strength, modulus of elasticity, creep and shrinkage of concrete used in Florida. University of Florida, M.E. Thesis, 2009.

Hassannejad, M., Berenjian, J., javadTaheri Amiri, M., n.d. The investigation on the effect of the aggregate type in the modulus of elasticity and tensile strength in high strength concrete.

Hine, A. C., Belknap, D. F., Hutton, J. G., Osking, E. B., & Evans, M. W., Recent geological history and modern sedimentary processes along an incipient, low-energy, epicontinental-sea coastline: northwest Florida. Journal of Sedimentary Research, 58(4) 1988

Hoffmeister, J.E., Stockman, K.W., Multer, H.G., Miami Limestone of Florida and its recent Bahamian counterpart. Geol. Soc. Am. Bull. 78, 175–190, 1967

Hussin, A., Poole, C., Petrography evidence of the interfacial transition zone (ITZ) in the normal strength concrete containing granitic and limestone aggregates. Constr. Build. Mater. 25, 2298–2303, 2011

Ioannides, A.M., Mills, J.C., Effect Of Larger Sized Coarse Aggregates On Mechanical Properties Of Portland Cement Concrete Pavements And Structures. University of Cincinnati, 2006

Iravani, S., "Mechanical properties of high-performance concrete" ACI Materials Journal, 93, 1996

Kesler, C.E., "Strength" Significance of Tests and Properties of Concrete and Concrete-Making Materials, ASTM STP-169, pp. 144-159, 1966

Kessler, R. J., Powers, R. G., Vivas, E., Paredes, M. A., & Virmani, Y. P., "Surface resistivity as an indicator of concrete chloride penetration resistance", Concrete Bridge Conference, St. Louis, Missouri, 2008

Kılıç, A., Atiş, C. D., Teymen, A., Karahan, O., Özcan, F., Bilim, C., & Özdemir, M., "The influence of aggregate type on the strength and abrasion resistance of high strength concrete" Cement and Concrete Composites, 30(4), 290–296, 2008

Langan, B. W., Weng, K., & Ward, M. A., Effect of silica fume and fly ash on heat of hydration of Portland cement. Cement and Concrete Research, 32(7), 1045–1051, 2002

Lo, T.Y., Cui, H.Z., "Effect of porous lightweight aggregate on strength of concrete" Mater. Lett. 58, 916–919, 2004

Lothenbach, B., Le Saout, G., Gallucci, E., & Scrivener, K., Influence of limestone on the hydration of Portland cements. Cement and Concrete Research, *38*(6), 848–860, 2008.

Malhotra V.M., "Surface Hardness Methods", Malhotra, V. M., & Carino, N. J. Handbook on Nondestructive Testing of Concrete Second Edition, CRC press, 2003

Maliva, R.G., Missimer, T.M., Clayton, E.A., Dickson, J.A.D., "Diagenesis and porosity preservation in Eocene microporous limestones, South Florida", USA. Sedimentary Geology 217, 85–94, 2009

Maso, J. C., "Influence of the Interfacial Transition Zone on Composite Mechanical Properties". pp. 114-129 in Interfacial Transition Zone in Concrete, Rilem Report 11, E & FN Spon, London, UK, 1996

Meininger, R. C., Stokowski, S. J., & Langer, B., "Wherefore Art Thou Aggregate Resources for Highways", Public Roads, 75(2), 34–41, 2011

Miller, J. A., Hydrogeologic framework of the Floridian aquifer system in Florida and parts of Georgia, Alabama and South Carolina: United States Geological Survey Professional Paper 1403-B, 91 p, 1986

Mindess, S., Young, J. F., & Darwin, D., Concrete, Prentice Hall, 2002

Myers, J.J., Carrasquillo, R.L., Production and quality control of high performance concrete in Texas bridge structures, Texas DOT, Austin, TX, 1998

Neville, A.M., Properties of concrete. J. Wiley, 1996

NCHRP 496, Report of Prestress Losses in Pretensioned High Strength Concrete Bridge Girders, Transportation Research Board, Washington, D.C., 2002

Noguchi, T., Nemati, K.M., "Relationship between compressive strength and modulus of elasticity of high strength concrete" Journal of Structural and Construction Engineering 474, 1–10, 1995

Oates, J.A.H., Lime and limestone: chemistry and technology, production and uses. Wiley-VCH, Weinheim ; New York, 1998

Perry, C., Gillott, J.E., "The influence of mortar-aggregate bond strength on the behaviour of concrete in uniaxial compression", Cement and Concrete. Research. 7, 553–564, 1977

Popovics, S. Analysis of the Concrete Strength Versus Ultrasonic Pulse Velocity Relationship. Materials Evaluation, 59(2), 2001

Rich, D.W.,Porosity in Oolitic Limestones, University of Illinois at Urbana-Champaign, PhD Dissertation, 1980

Richardson, J.M., Long term deformations of concrete made with Florida aggregates, University of Florida, PhD Dissertation, 1985

Rizkalla, S., Mirmiran, A., Zia, P., Russell, H., Mast, R.,NCHRP Report 595 "Application of the LRFD Bridge Design Specification to High-Strength Structural Concrete: Flexure and Compression Provisions", Transportation Research Board Washington DC, 2007

Ross, C.A., Jerome, D.M., Tedesco, J.W., & Hughes, M.L., "Moisture and Stain Rate Effects on Concrete Strength" ACI Materials Journal, 93, 293-300, 1996

Rubinsky, I. A., "Heat of hydration in concrete" Magazine of Concrete Research, 6(17), 79–92, 1954

Sarkar, S. L. "Effect of Blaine fineness reversal on strength and hydration of cement", Cement and Concrete Research, 20(3), 398–406, 1990

Scott, Thomas M. P.G. #99, Text to Accompany the Geologic Map of Florida, Open-file Report 80, Florida Geological Survey, 2001.

Scrivener, K.L., Crumbie, A.K., Laugesen, P., "The Interfacial Transition Zone (ITZ) Between Cement Paste and Aggregate in Concrete", Interface Science, 12, 411–442, 2004

Sellards, E.H., Geology of Florida., Journal of Geology, 27, 286–302, 1919

Stock, A.F., Hannantt, D.J., Williams, R.I.T.," The effect of aggregate concentration upon the strength and modulus of elasticity of concrete" Magazine of Concrete Research, 31, 225–234, 1979

Tadros, M.K., "Prestress losses in pretensioned high-strength concrete bridge girders" Transportation Research Board, Washington, DC, 2003

Tia, M., Bekoe, P., & Chen, Y., "Development of Tiered Aggregate Specifications for FDOT Use" Florida Department of Transportation, Tallahassee, FL, FDOT-BDK-977-29, 2012

Tia, M., Liu, Y., Brown, D., "Modulus of elasticity, creep and shrinkage of concrete", Florida Department of Transportation, Tallahassee, FL,FDOT-BC-354, 2005

Tia, M., Liu, Y., Haranki, B, Su, Y,,M., "Modulus of Elasticity Creep and Shrinkage of Concrete Used in Florida, Part I - Creep Study" Florida Department of Transportation, Tallahassee, FL, FDOT BD545-67, 2009

Tia, M., Verdugo, D., & Kwon, O., "Evaluation of Long-Life Concrete Pavement Practices for Use in Florida" Florida Department of Transportation, Tallahassee, FL, FDOT BDK75 977-48, 2012

Tyner, M., "The Effect of Moisture on the Thermal Conductivity of Limerock Concrete" Journal of the American Concrete Institute, 18, 9-18, 1946

Willet, J., The Nation's Top 25 Producers, Aggregates Manager, (web citation) Retrieved from http://www.aggman.com/the-nation%E2%80%99s-top-25-producers-2, 2009, last accessed October, 2015

Williams, C. D., & Tyner, M., "Report on Limerock Research, 1941-1948" Florida Engineering and Industrial Experiment Station, College of Engineering, University of Florida, 1949

Wittmann, F.H.,Interaction of Hardened Cement Paste and Water, Journal of the American Ceramic Society 56 (8), 409-415, 1973

Wu, K.-R., Chen, B., Yao, W., Zhang, D.,"Effect of coarse aggregate type on mechanical properties of high-performance concrete", Cement and Concrete Research, 31, 1421–142, 2001

Yaman, I.O., Hearn, N., Aktan, H.M., "Active and Non-active Porosity in Concrete Part I: Experimental Evidence". Materials and Structures, 35, 102–109, 2009

Yazdani, N., McKinnie, B., Haroon, S., "Aggregate-Based Modulus of Elasticity for Florida Concrete" Transportation Research Rerecord., TRB, 1914, 15–23, 2005

Yazdani, N. McKinnie B.,2004, Time Dependent Compressive Strength and Modulus of Elasticity of Florida Concrete, Florida Department of Transportation, Tallahassee, FL, BD-221, 2004

APPENDIX A. LABORATORY AND INSTRUMENT DESIGN

A.1 BACKGROUND

Equipment has been procured and has been installed at the University of Florida campus civil engineering materials testing laboratory (Weil Hall). The coefficient of thermal expansion (CTE) was determined using a thermal bath depicted in Figure A.1. The CTE experiments were conducted in accordance with AASHTO T336.

Figure A.1 Thermal Bath used for AASHTO T336.

The process of completing the construction of the apparatus, its testing procedures, and its instructional documents also were a part of this task and have all been completed. At the time of this writing, testing is ready to begin using the new UF machine.

A.2 INTRODUCTION

CTE 9 is a software application developed in National Instruments® LabVIEW™ 2013 to perform coefficient of thermal expansion (CTE) of concrete testing in accordance with AASHTO T336. The software is capable of controlling a PolyScience® or VWR® water bath over RS232 serial interface, and reading temperature and displacement data over a Measurement Computing® USB data acquisition (DAQ) device. The software includes provisions for configuration, calibration, and sampling of two linearly variable differential transformers (LVDTs) and four thermistor elements as presented in Figure A.2. The software also provides for internal calculation of a frame correction factor for each of two CTE testing frames using either a single point correction factor or a sample height dependent linear correction equation. These features allow CTE 9 to perform concrete CTE testing following AASHTO T336, Modified AASHTO T336 using a fixed frame and multi-point correction factor, as well as a fully customizable user-defined test procedure.

Figure A.2 CTE bath system at the FDOT State Materials Office

Proper use of CTE 9 requires correct configuration of the PolyScience® or VWR® water bath using the built-in interface as well as proper configuration of the Measurement Computing® DAQ using the manufacturer's InstaCal™ software. The procedures discussed herein, more advanced configuration and troubleshooting may require consultation of the relevant equipment manual as supplied by the manufacturer.

The accurate measurement of the CTE value of concrete requires extremely precise measuring equipment due to the scale of the value; typically the CTE of Portland cement concrete is taken to be between 7 and 13 millionths of strain (or in/in) per degree Celsius. A typical specimen used in these systems will expand approximately 0.003 inches over its 7-inch length during its thermal cycle. Because the equipment used in this testing requires a high degree of precision and accuracy, it is very dependent on proper maintenance and care. The purpose of this document is not intended to replace, but merely to supplement proper training in the testing of CTE on these systems. Any technician intending to use a CTE bath system should be instructed in its use by an experienced operator and should not rely solely on this manual to operate the system. Care should be taken to ensure that no unauthorized persons are allowed to operate or tamper with the systems and that all components are protected from accidental damage or destruction. No operator should attempt to modify or repair any component of the hardware or software of the system without proper consultation by an expert on the CTE bath systems.

A.3 HARDWARE COMPONENTS

A.3.1 Overview

The following hardware components constitute the CTE bath system. The system pictured here belongs to the FDOT State Materials Office; other systems may vary.

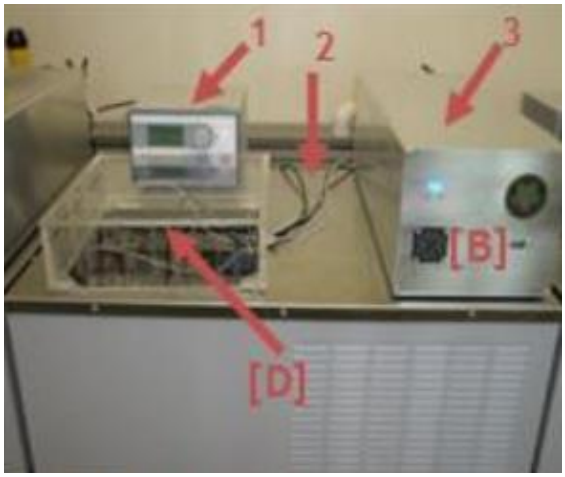

Figure A.3 CTE Bath System

As shown in Figure A.3, the CTE Bath System is composed of 5 different systems denoted 1, 2, 3 B & D:

1. Bath control and pump housing
2. PolyScience® (newer) or VWR® (older) circulating programmable water bath
3. Electronics enclosure

B. Computer Front Panel

D. Super Invar Frame Assembly as shown in Figure 4.

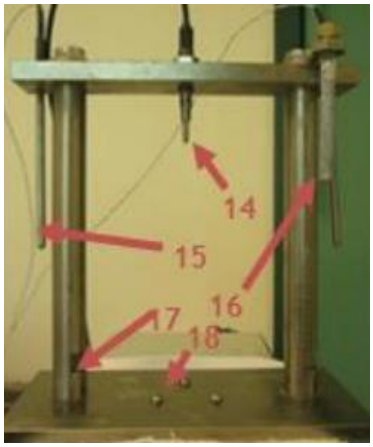

Figure A.4 INVAR Frame Assembly

The CTE bath systems are designed to test portland cement concrete in temperature-controlled water. The thermal transfer properties of water allow for a more stable thermal environment for the concrete than if it were to be tested in temperature-controlled air. The water baths, whether they are the older VWR® models or the newer PolyScience® models, have integral refrigeration and heating systems connected to a control box and pump housing. The control box receives temperature set points from the computer and controls the operation of the heater and the refrigerator to hold the water in the 13-liter reservoir to within 0.005°C of the set point. The computer communicates with the water bath controller via RS232 serial cable.

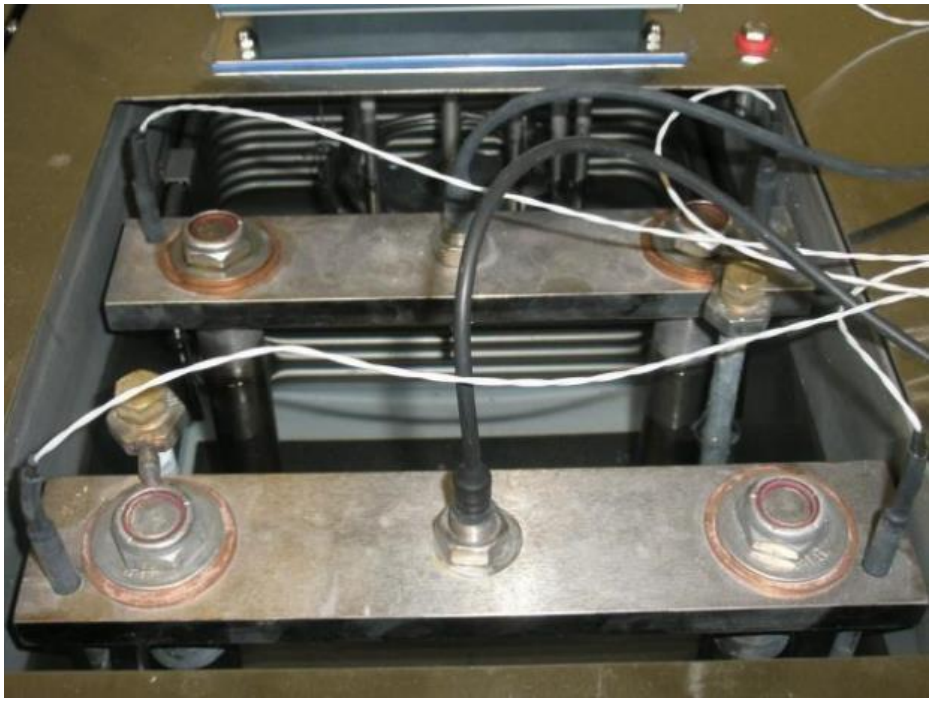

Figure A.5 Water bath reservoir with INVAR frames in place (FDOT system)

Inside the reservoir shown in Figure A.5, there is a lining of 0.125" thick PTFE sheet surrounded by 0.5" PTFE angle trim to prevent the sliding of the frames from damaging the walls and bottom of the stainless steel reservoir. Two INVAR frames sit atop this liner and hold one specimen each while testing. The frames are separated from the coils of the refrigerator at the rear of the tank by a 0.25" thick stainless plate that sits behind the rear frame on the PTFE liner (FDOT system only). This plate also serves to hold the liner in place when the INVAR frames are removed. The reservoir is closed by an acrylic lid that insulates the tank and protects the instruments and specimens during testing. For more information on the water baths, consult the technical manual provided by PolyScience®.

A.3.2 Specimen Frames

The INVAR specimen frames are designed to hold a specially prepared concrete cylinder or core during testing. To measure the CTE value, each frame also carries two thermistors to measure the temperature of the water bath and one LVDT transducer to measure the displacement of the cylinder or core at its center with respect to the base plate of the frame.

The frames consist of a base plate, two threaded INVAR rods, and a top plate. The FDOT system has nickel plated INVAR rods and plates as presented in Figure A.6, while the UF system has fully threaded heat treated INVAR rods and 316 stainless steel plates. The rods thread into the base plate, and the top plate is held in place by 316 stainless nuts. The UF system is height adjustable while the FDOT system is fixed height. The zinc anode is attached to one of the brass or copper washers and helps prevent corrosion of the INVAR frames. The anode must be cleaned regularly and replaced periodically as it decays.

Figure A.6 INVAR specimen frame (FDOT system)

The INVAR components of the FDOT system are all plated in nickel to help retard corrosion. This nickel coating is, however, very thin and easily scratched. This is why the soft copper washers are used to separate the plated INVAR from the hard stainless washers. Care must be taken when moving, disassembling, or assembling the frames or when placing or removing specimens so as to avoid scratching the nickel finish. Non-marring tools should be used at all times when working on the frames. Refer to the System Operation section for more details on safely placing specimens.

A.4 SELF-CONTAINED COMPUTER AND DATA ACQUISITION

A.4.1 Overview

All the electronic components necessary to interface with the thermistors, LVDTs, and bath controllers for each water bath system are contained within a 6.5” X 8” X 18” long aluminum enclosure along with a miniature PC called a digital engine. This enclosure should NEVER be opened unless absolutely necessary and only then by an expert on the CTE bath system. Opening the enclosure without intimate knowledge of it can result in the damage or destruction of the delicate instruments inside.

The enclosures contain two shelves connected by standoffs. All the electronics of the system are mounted to the shelves and connected to their various ports, plugs, and jacks on the front and rear panels of the enclosure as shown in Figure A.7. A USB powered fan is mounted to the front

panel of the enclosure in order cool CTE 9 User's power supply and digital engine. Air is drawn in from the front of the panel and exhausted out of the rear. For this reason, the enclosure should be placed with plenty of air space front and rear and the foam filters should be cleaned periodically to prevent overheating. Refer to the Equipment Care section for more information.

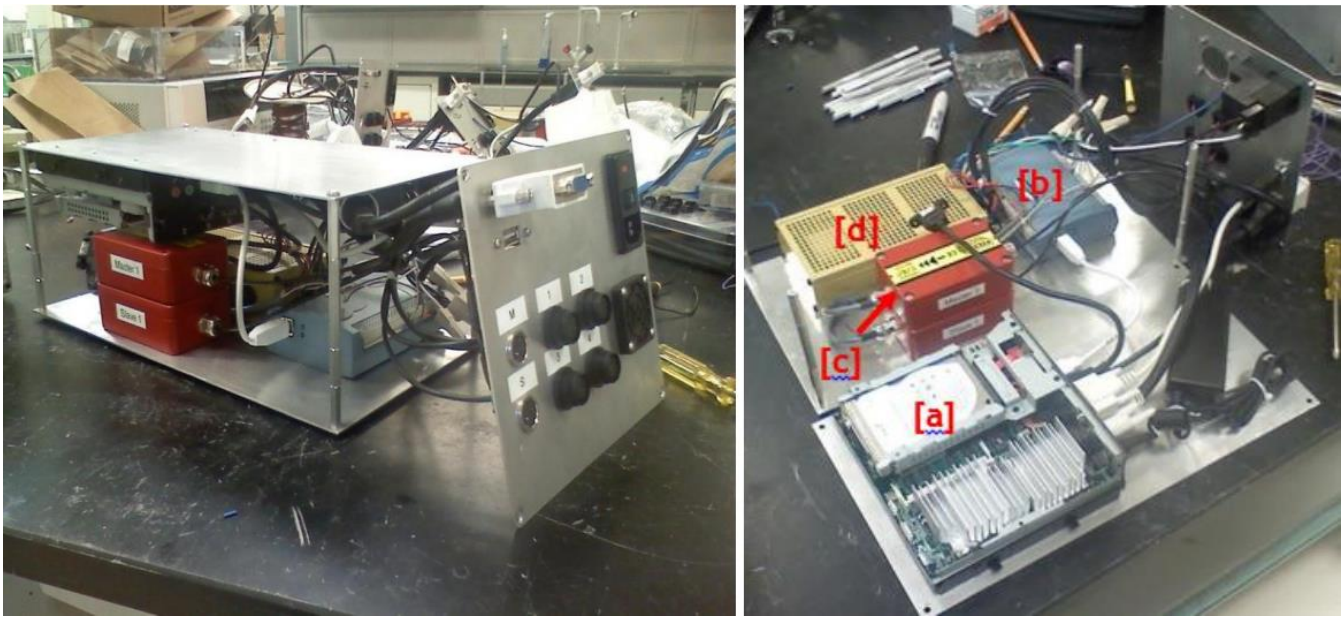

Figure A.7 Electronics enclosure internal components

A.4.2 Digital Engine (AOpen® DE2700)

As pictured as [a] in Figure A.7, the digital engine is the 'brain' of the CTE water bath system. It operates the LabVIEW™ programs that give commands to the water bath and collect data from the LVDTs and thermistors. The digital engine is simply a compact PC and runs Windows™ like a desktop machine. It interfaces with the data acquisition system via USB, powers the auxiliary fan via USB, and is connected directly to the RS232 jack, DVI jack, USB ports, power button, and power plug on the enclosure. Though the digital engine has a pair of Ethernet ports, these are inside the enclosure because connecting the system to a network is strongly discouraged. Since the system is powered on continuously for long periods of time, loads such as network connections should be eliminated where possible. Data should be retrieved from the digital engine via the front USB port and a USB flash drive. See the Data Retrieval section for more information

A.4.3 DAQ (Measurement Computing® USB-TEMP-AI)

As pictured as [b] in Figure A.7, this 24-bit USB data acquisition system (DAQ) receives signals from the two LVDTs and four thermistors on each system and interprets them for the digital engine. It connects to the digital engine via USB and is powered by the USB 5 VDC power source. Because this particular DAQ is far more sensitive than more common DAQs and because it uses a 24-bit protocol, the DAQ must 'warm-up' for thirty minutes prior to calibration or operation. Note that the DAQ is only powered when the digital engine is on.

A.4.4 Signal Conditioners (RDP Electrosense™ S7AC Transducer Amplifier) (FDOT system only)

As pictured as [c] in Figure A.7, signal conditioners operate LVDTs and convert their signals into a form a DAQ can use, in this case a +/-10 VDC signal. LVDTs require an AC excitation to produce a DC signal voltage, and the signal conditioners create this excitation using an internal oscillator. One signal conditioner is configured as a master oscillator and has its connector marked with an 'M', while the other is a slave and marked with an 'S'.

The master oscillator produces an excitation and also drives the excitation in the slave so that their AC signals are in-phase. This is so that the two AC signals will not interfere with each other where the wires are close together. The signal conditioners connect the DAQ to the DIN connectors, and thereby the LVDTs, and require an external DC power supply.

The UF CTE system does not require external signal conditioners as this function is performed within the LVDTs themselves. The LVDTs are provided a clean 12 VDC excitation from the power supply and a +/-10 VDC signal is returned through the DIN connectors.

A.4.5 Power Supply (Acopian® TN6T Linear Regulated Power Supply)

As pictured as [d] in Figure A.7, the power supply is used to operate the LVDTs and their respective signal conditioners. It produces an ultra-clean 24 VDC voltage that is used to drive the signal conditioner oscillators and/or excite the LVDTs. It is a high efficiency, fanless, noiseless system that requires almost no maintenance. Its output voltage is manually adjusted via a screw on the front face. This was done at assembly and should not need to be done again over the life of the system unless erroneous voltages are encountered.

A.5 INITIAL SETUP

A.5.1 Hardware Installation

Begin setup of the CTE system by choosing a suitable location for the bath and electronics enclosure. Use a strong, stable, level, waterproof countertop with ample space nearby for specimen placement. A nearby water source is preferred as the bath will have to be periodically refilled with clean tap water and regularly cleaned. Avoid using hard (well) water when possible as this will lead to mineral deposits that will require more frequent cleaning of the bath.
Place the bath system on the chosen countertop and level as necessary. Place the PTFE liners and spacer plate in the reservoir if desired. Assemble the INVAR frames with caution to avoid scratching the nickel plating if applicable. For the fixed height frames, tighten the INVAR rods and stainless locknuts to moderate torque. For the adjustable height frames, tighten the threaded rods into the base plate but leave the nuts on the upper plate hand-tight only as they will be adjusted later. After checking the zinc anodes to ensure they are clean and still have substantial remaining material, install them in the small brass pipe nuts attached to the frame washers.

Coat the threads of the LVDTs with a thin layer of high quality, multi-temperature, hydrophobic grease to prevent corrosion and seizing of the threads. DOW-Corning® high vacuum grease works well for this purpose. With the LVDT cable free (FDOT system) or disconnected (UF system) to avoid twisting, thread the LVDT into its hole on each INVAR frame. Do not tighten the lock nut as the LVDTs will be adjusted later.

Carefully place the frames in the water bath reservoir. Place a suitable calibration standard in Frame 1 (the rear frame) making sure to keep the LVDT plunger raised so as not to bend or scratch its delicate armature. Place the four thermistors in an evenly spaced manner on the two frames. For the FDOT system, holes are provided in the INVAR frames to receive a plastic shroud which will hold the thermistor element. For the UF system, plastic ties may be used to hold the thermistor elements in the desired locations on the frames.

Fill the reservoir with clean, fresh tap water at a level just above the top plate of the INVAR frames. Reinstall the LVDT cables if they were removed (UF system). Manually power the bath on and set the temperature to 20.00℃ using the rotary knob control. Place the acrylic lid on the reservoir while carefully passing the thermistor and LVDT cables through the provided slot in the lid. Take care not to scratch the jacket of the thermistor elements as water ingress will destroy the element.

Place the electronics enclosure on the water bath top. Connect the serial port to the bath controller, the thermistor elements to their respective connectors, and the LVDTs to their respective connectors. Note that Frame 1, the rearward frame, is sometimes referred to as "Master" or "M" while Frame 2 may be called "Slave"/"S." Connect a monitor to the DVI port using an adapter if necessary. Connect a keyboard/mouse combo such as a small multimedia keyboard with trackpad to the rear USB port. You are now ready to begin software installation.

A.5.2 Software Installation

The provided CTE 9 media will install CTE 9 by Five-P Consulting, InstaCal™ by Measurement Computing®, and all necessary drivers and runtime software by National Instruments®. Connect an external DVD drive to the front USB panel of the CTE electronics enclosure or copy the contents of the DVD onto a USB flash drive to allow the digital engine to access the contents. Run "setup.exe" and follow the prompts in the installation package to install the software onto the computer.

The installer package will create a number of directories on the computer. The two main programs you will need to use are InstaCal™ which can be found under Start > Programs > Measurement Computing and CTE 9 under Start > Programs > Five-P Consulting.

A.5.3 DAQ Setup using InstaCal™

Attempting to run CTE 9 before configuring the DAQ device in InstaCal™ will result in an error popup on program launch and a DAQ configuration error within the program runtime. InstaCal™ is used to write a board configuration to the DAQ and to provide CTE 9 with a library

of functions to call during the execution of a test. This setup process will only have to be performed once unless a hardware or software fault overwrites the configuration.
To setup the DAQ board, open InstaCal™. If connectivity is established and Windows® recognizes the device, a popup will show the connected DAQ device (USB-TEMP-AI) and allow its selection. If this does not occur, shut down the computer using the Windows® shutdown function and power off the electronics enclosure using the switch on the power entry module. Wait a few moments, power the system back on, and retry. Select the "USB-TEMP-AI" and set it as "Board #0" as depicted in Figure A.8.

Figure A.8 InstaCal™ interface

Setup the analog channels by navigating to "Calibrate > A/D". The voltage channels (LVDT) should be set such that channels 0 and 1 are enabled and reading -10 to 10 VDC. The temperature channels should be set to two-wire thermistors on channels 0-3 with the Steinhart-Hart Coefficients provided by the manufacturer or determined using the following equation.

$$\frac{1}{T} = A + B\ln(R) + C(\ln(R))^3$$

Equation 1. Steinhart-Hart Equation. Online solvers exist to solve this equation from three data points.

Once the analog channels have been properly configured, confirm operation by clicking the "AnalogTest" icon on the InstaCal™ toolbar. Navigate to the voltage input and temperature test tabs and confirm the incoming data is reasonable and moving appropriately when the instruments are shifted manually as presented in Figure A.9.

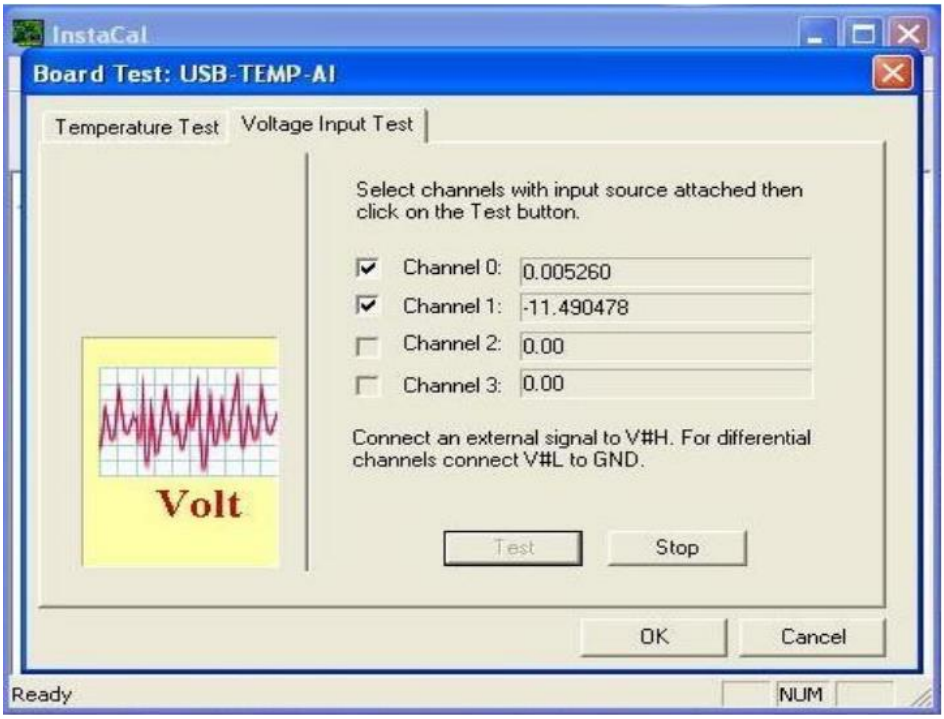

Figure A.9 Board test panel

A.5.4 CTE 9 Program Setup

After initially configuring the DAQ using InstaCal™, close InstaCal™ and start CTE 9. A brief start-up procedure will complete and you will be prompted for a user name. Choose an existing name if applicable or enter your own. New user names are saved in the CTE 9 configuration file automatically. Once the program starts, the main screen will appear. At this point, the indicator in the upper left will likely show "SYSTEM ERROR" indicating a critical fault state is preventing a test from being conducted. The error list will provide details of the error source(s), but most likely the first error will be a configuration error. To correct this, navigate to the System Configuration panel as shown in Figure A.10

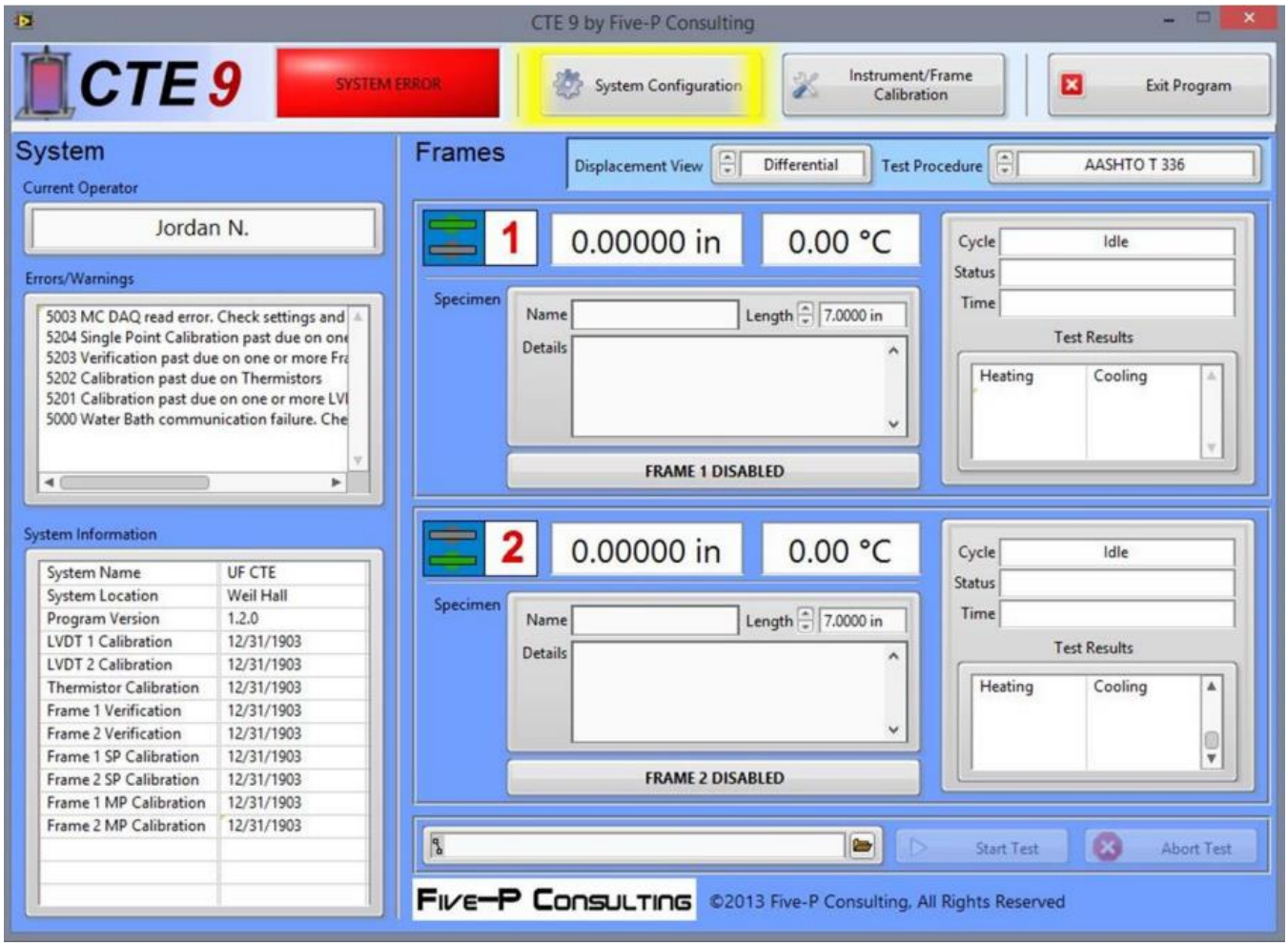

Figure A.10 CTE 9 main panel with system configuration button highlighted

In the system configuration window, you will assign a name and location for this particular CTE bath system that will be included in the header of the report files generated by the software. CTE 9 measures and records the time since the last instrument and frame calibrations and can alert you when calibration is due following the settings in the “Calibration Warnings” menu. CTE 9 is also tolerant of thermistor faults and will provide indications of a bad thermistor element while removing it from the calculation for the average bath temperature up to the abort condition specified in “Thermistor Fault Tolerance”. If the number of failed thermistor elements exceeds the abort condition during a test, the test will be aborted.

Use the “Bath Port Settings” and “DAQ Settings” menus to configure CTE 9 to communicate with the water bath and DAQ. These settings must match the settings of the devices themselves and the default values are shown in Figure A.11. Refer to the documentation for the bath and DAQ if you suspect these settings have been altered.

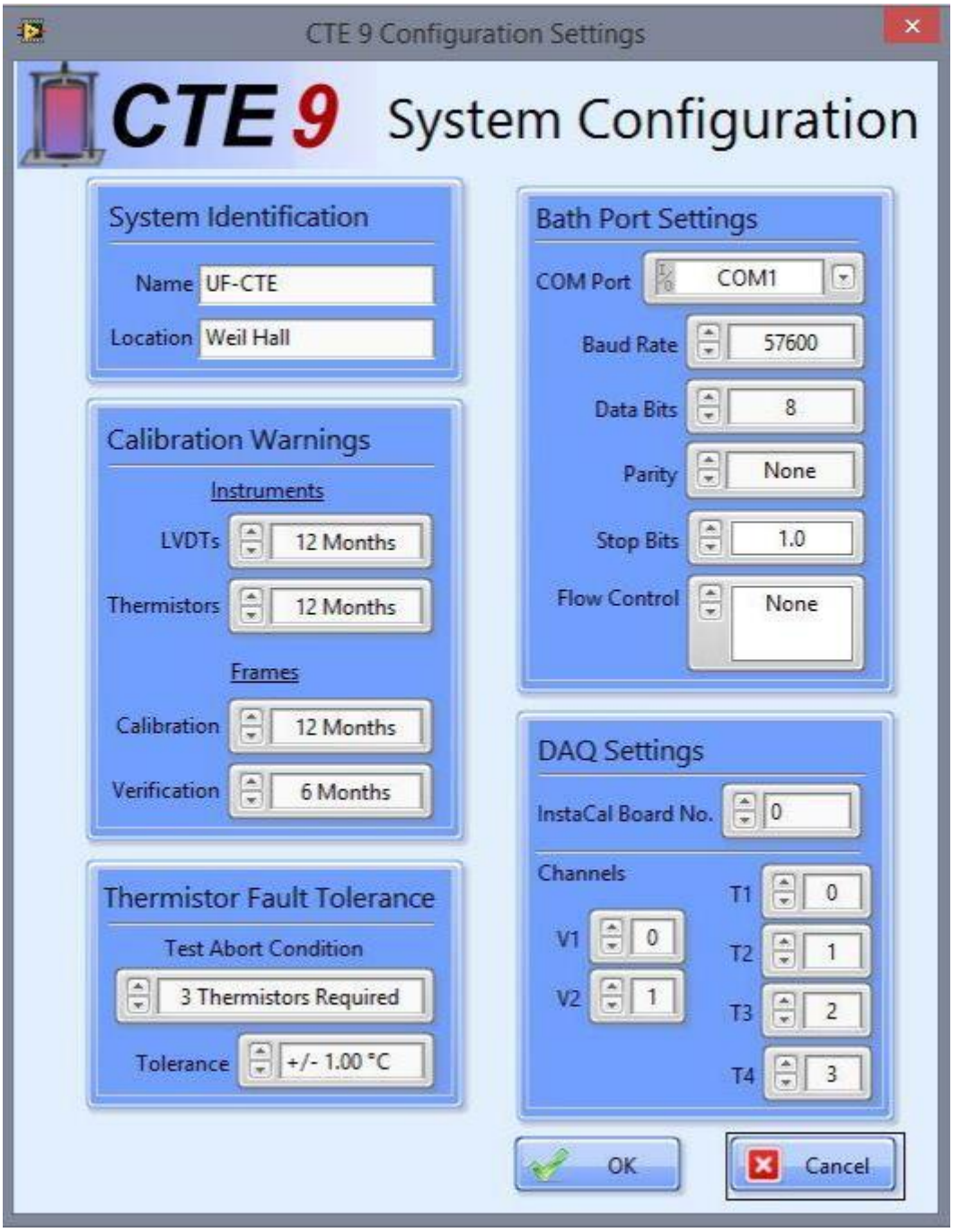

Figure A.11 System Configuration panel with default values for Bath Port and DAQ

After changing the System Configuration settings, you will be prompted to restart the program. During the start-up sequence, CTE 9 will command the water bath to power on, go to 20.00℃, and lock out the front control panel from manual interference. If these steps occur, you will readily know that the Bath Port Settings are correct. If there has been a communication error, the Errors/Warnings list will alert you to its possible cause(s).

At this time, CTE 9 is ready to accept instrument and frame calibrations and begin testing specimens.

A.6 CALIBRATION

A.6.1 Overview

Because proper calibration is such an integral part of successful CTE testing, CTE 9 includes a number of useful toolkits to make the calibration process as user-friendly and accurate as possible. In general, it is wise to calibrate the instruments and frames annually and perform frame verification every 3 months. To open the instrument calibration, frame verification, and frame calibration toolkits, select Instrument/Frame Calibration.

The Summary tab is the default display of the Instrument and Frame Calibration panel. This panel displays all the current calibration factors as CTE 9 will use them to calculate displacements, temperatures, and CTE values. The panel allows the user to export a summary of current calibration factors as a tab-delimited (*.txt) file. This file is essentially the header portion of a CTE raw or CTE report file.

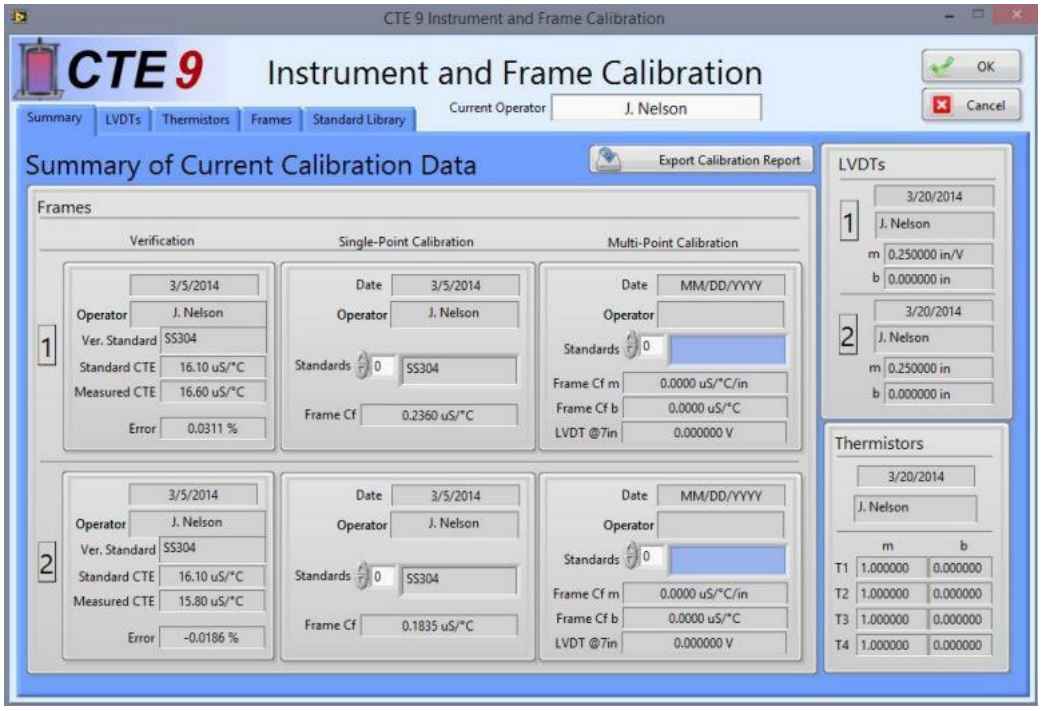

Figure A.12 Instrument/Frame Calibration panel Summary tab

A.6.2 LVDT Calibration

To calibrate the LVDTs using CTE 9, first mount the LVDT to be calibrated in stable calibration device with a precision micrometer head or space for placement of length calibration blocks. Follow good practice for LVDT calibration including environmental temperature control, proper range and data point resolution selection, and appropriate delay to allow the instrument to reach

steady-state values. Navigate to the LVDT tab in the Instrument and Frame Calibration Panel presented in Figure A.12.

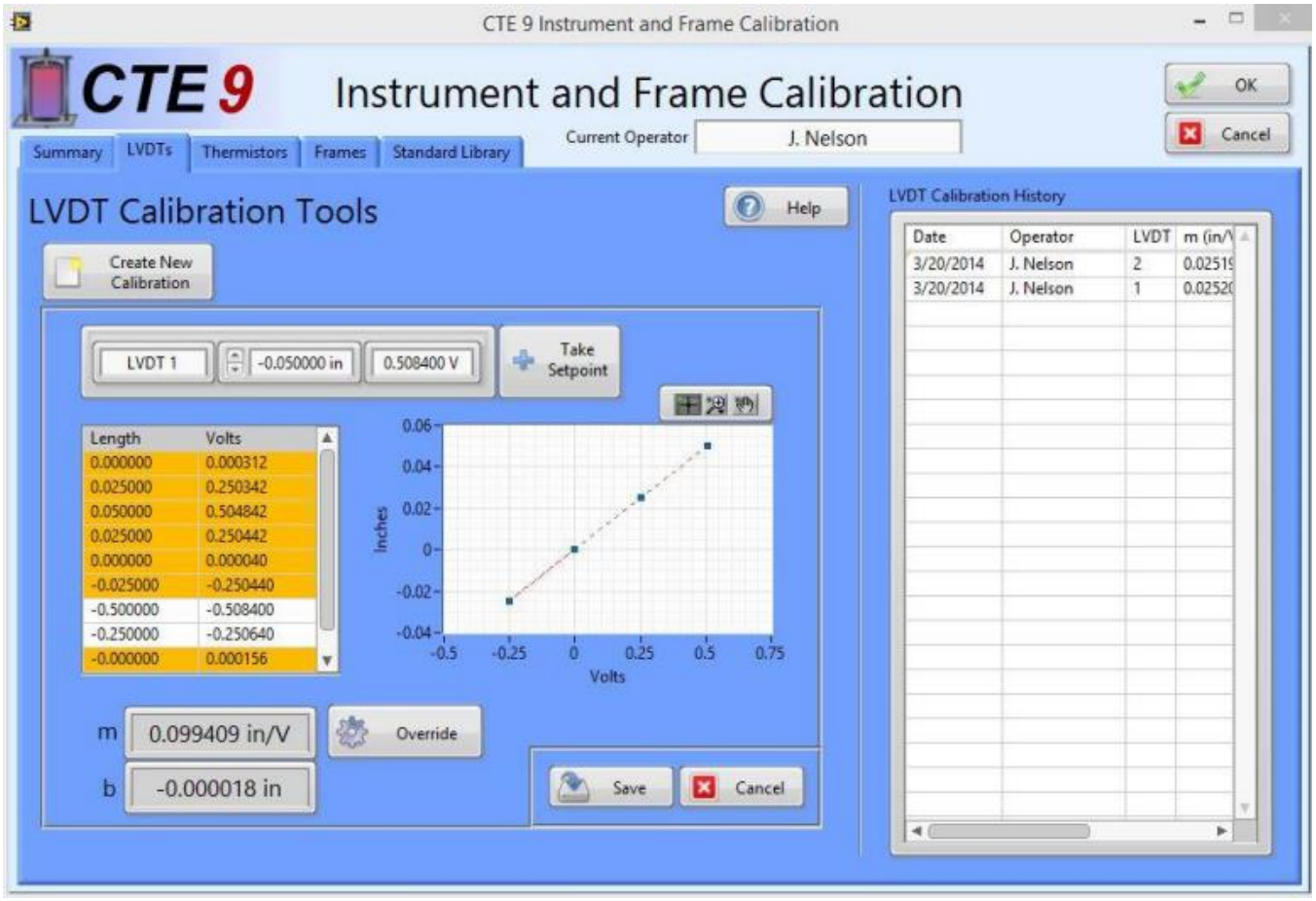

Figure A.13 LVDT calibration toolkit

The LVDT calibration panel contains an area for recording and selecting setpoints which is presented in Figure A.13, controls to override the calculated value, save, and cancel the calibration, and a list describing the local LVDT calibration history. To calibrate an LVDT, choose "Create New Calibration". Choose "LVDT 1" or "LVDT2". Enter the reading in inches on the calibration gauge or blocks and allow the voltage to come to steady state. Select "Take Setpoint" to store the data point. If erroneous values are saved by mistake, you may simply skip them when you select the data points used to calculate the LVDT calibration factor (m) and offset (b). Ctrl-click or Shift-click to select multiple data points and display a scatter plot indicating the data points you have chosen and the calculated calibration equation. You may choose Override if you wish to enter your own calibration data without using this toolkit. Choose Save to store the new calibration factor and update the Summary tab.

IMPORTANT: to save the LVDT calibration factor permanently with the system, you must close the Instrument and Frame Calibration panel with the "OK" button. Canceling the panel will erase any changes made in your current session of the Instrument and Frame Calibration panel.

A.6.3 Thermistor Calibration

A.6.3.1 Manual Calibration

While not usually necessary, you may calibrate the thermistor channels by navigating to the "Thermistor" tab of the "Instrument and Frame Calibration" panel provided by Figure A.14. This step is usually performed to adjust the thermistor values to match that of the water bath, as in the event the average temperature of the thermistors differs significantly from the temperature of the water bath CTE 9 will not be able to discern whether or not the bath has reached a steady state temperature. One method for manual calibration of the thermistors is therefore to use the CTE water bath itself as the calibration bath. Ideally, both systems would be calibrated to a single NIST-traceable temperature bath, but since the temperature variation in the CTE of concrete test is relatively large and we are interested only in the overall temperature change, a minor amount of error is acceptable.

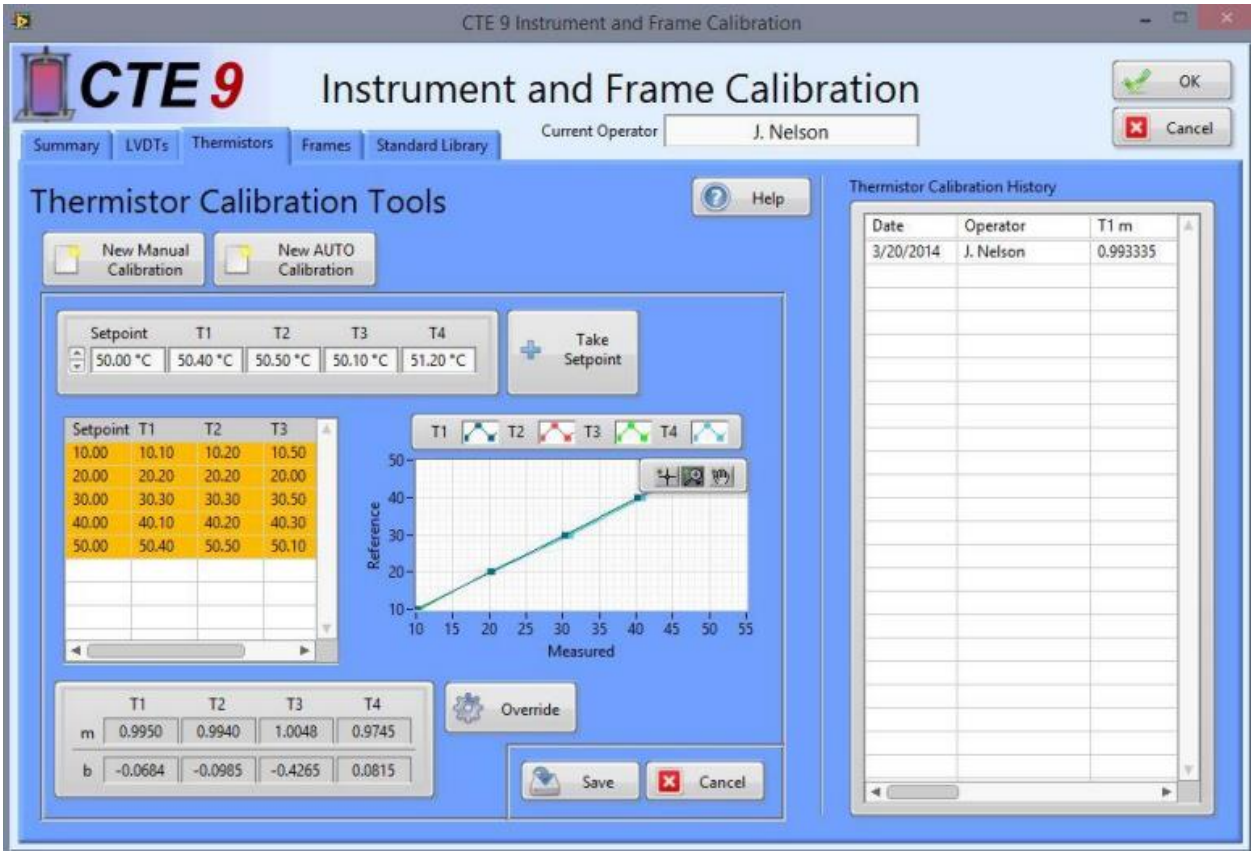

Figure A.14 Thermistor calibration toolkit

Calibrate the thermistors following a similar procedure as the LVDTs. Use a temperature bath to create a temperature setpoint, allow the thermistor elements to reach steady state, take a data point, and repeat the procedure over an appropriate range and number of data points. Select the data points from the list using "Ctrl-click or Shift-click" and calculate the calibration data, or

choose Override to enter your own. Choose “Save” to update the thermistor calibration history and current value on the summary tab.

A.6.3.2 Auto Calibration

This function is not available at the time of the release of version 1.2.0 of CTE 9, however once it is released it will support the automated assignment and collection of temperature data points using a serial controlled reference bath or the CTE water bath itself.

IMPORTANT: to save the thermistor calibration factors permanently with the system, you must close the Instrument and Frame Calibration panel with the OK button. Canceling the panel will erase any changes made in your current session of the Instrument and Frame Calibration panel.

A.7 FRAME CALIBRATION

A.7.1 Running a Standard

Running a calibration or verification standard is the first step to frame calibration or verification. Selecting the “Run a Standard” option under the Frame calibration toolkit will bring up the panel shown in Figure A.15.

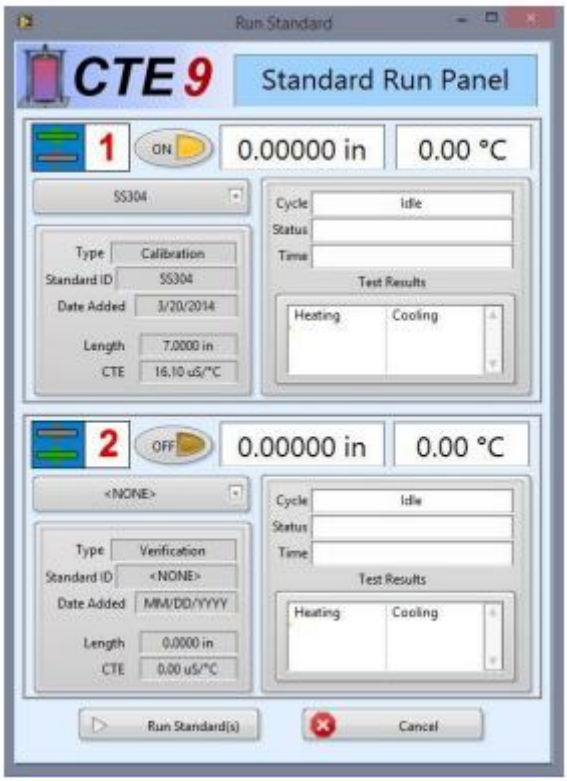

Figure A.15 Standard Run Panel

Place the calibration standard(s) in the frame(s) to be used following the same procedure used for test specimens. If you follow AASHTO T336 or any other procedure requiring the LVDT to be zeroed before testing, adjust the LVDT to bring the displacement indicator to zero before running the standard(s). Select the calibration or verification standard using the menu under the frame label. In general, verification specimens should be unique from calibration specimens and not used to serve the other's function. Refer to current state of the practice (AASHTO T336 or successors) for more information. Use the "ON/OFF" control to enable or disable each of the frames and choose "Run Standard(s)" to proceed. Standard run CTE report files are saved to the default CTE 9 file directory and overwritten automatically. Successful or failed completion of the sample run will be conveyed to the operator in a popup window once the run is complete.

A.7.2 Verification

Verification is the process of using a known standard specimen to check the proper function of the CTE bath system. Its CTE should be well known and documented, similar to the material being tested (concrete) but different than the calibration standard(s). Titanium is a good choice for a verification standard.

Impose a frame verification by navigation to Verification under the" Frame Calibration" panel as presented in Figure A.16. Select "New Verification" for the frame you which to impose verification on. Select a single standard run of a verification standard to automatically calculate new values for the verification data. Select "OK" to save the new verification. Verification history is not saved in the CTE 9 data base as verification data is calculated directly from standard run data.

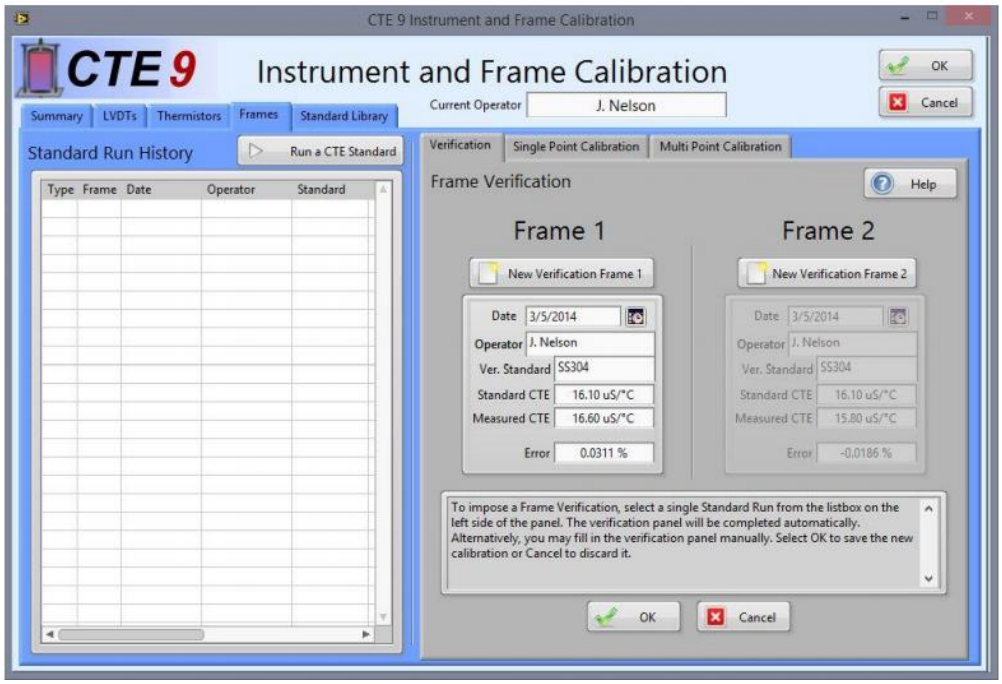

Figure A.16 Frame verification toolkit

A.7.3 Single-Point Calibration

A single-point calibration is for a CTE system which follows AASHTO T336, specifically the section requiring the LVDT to be zeroed on the specimen before each test which is performed per the menu provide in Figure A.17. Choose the "Single Point Calibration" toolkit and New SP Cal for the desired frame. You may "Ctrl-click" or "Shift-click" multiple standard runs to obtain an average Frame Cf, but note this is not the same as a "Multi-Point Calibration" correction factor and assumes no length dependency on the results of the CTE test.

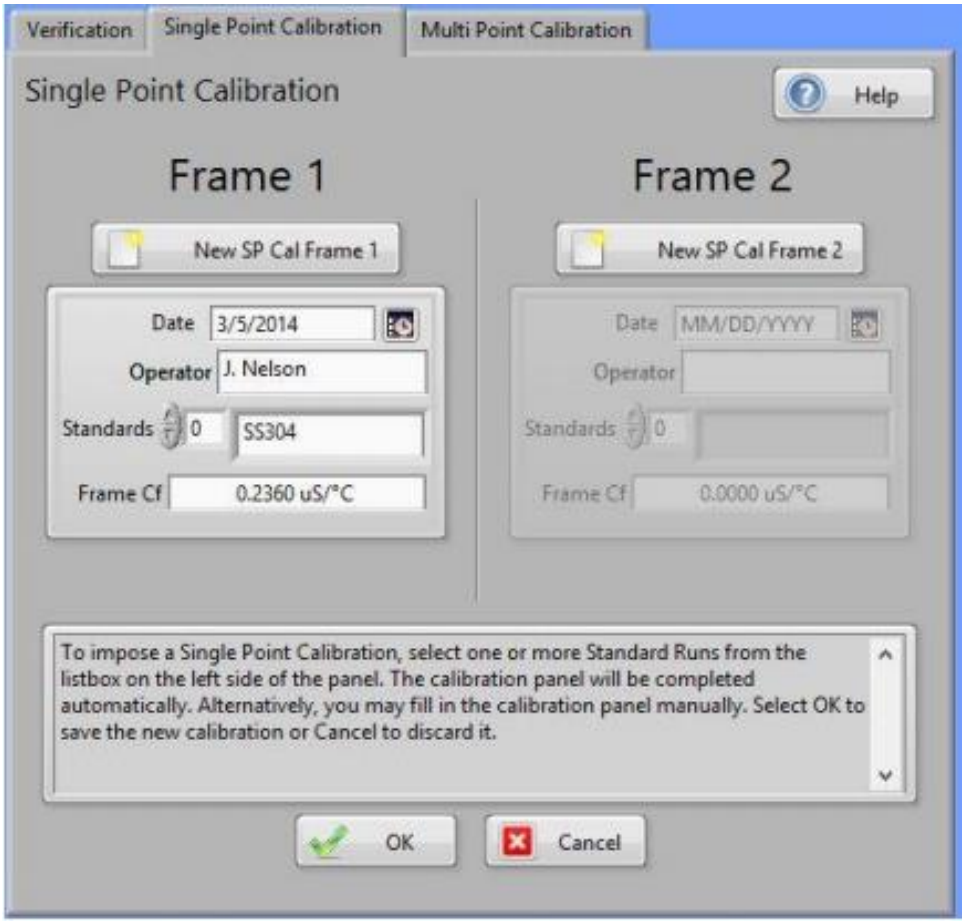

Figure A.17 Single Point Calibration toolkit

A.7.4 Multi-Point Calibration

Multi-Point Calibration is for fixed-frame CTE bath systems that use a specimen length-dependent frame correction equation, specifically those that follow AASHTO T336 SMO-MOD. Select multiple standard runs of calibration specimens of differing nominal length to generate a linear equation for the frame correction factor as defined by the nominal specimen length. During a CTE test with a multi-point frame correction factor, the frame correction factor will be calculated using the specimen length determined from the pretest equilibration (if enabled) or from the user provided specimen length (if equilibration is disabled).

A.8 STANDARD LIBRARY

The CTE Standard Library provided in Figure A.18 contains the vital details of all calibration and verification standards associated with the CTE bath system. Standards can be associated disassociated with the local system by adding or deleting them from this database. To add a new standard, choose “New” and enter the relevant details. Delete standards by selecting them in the list and choosing Delete.

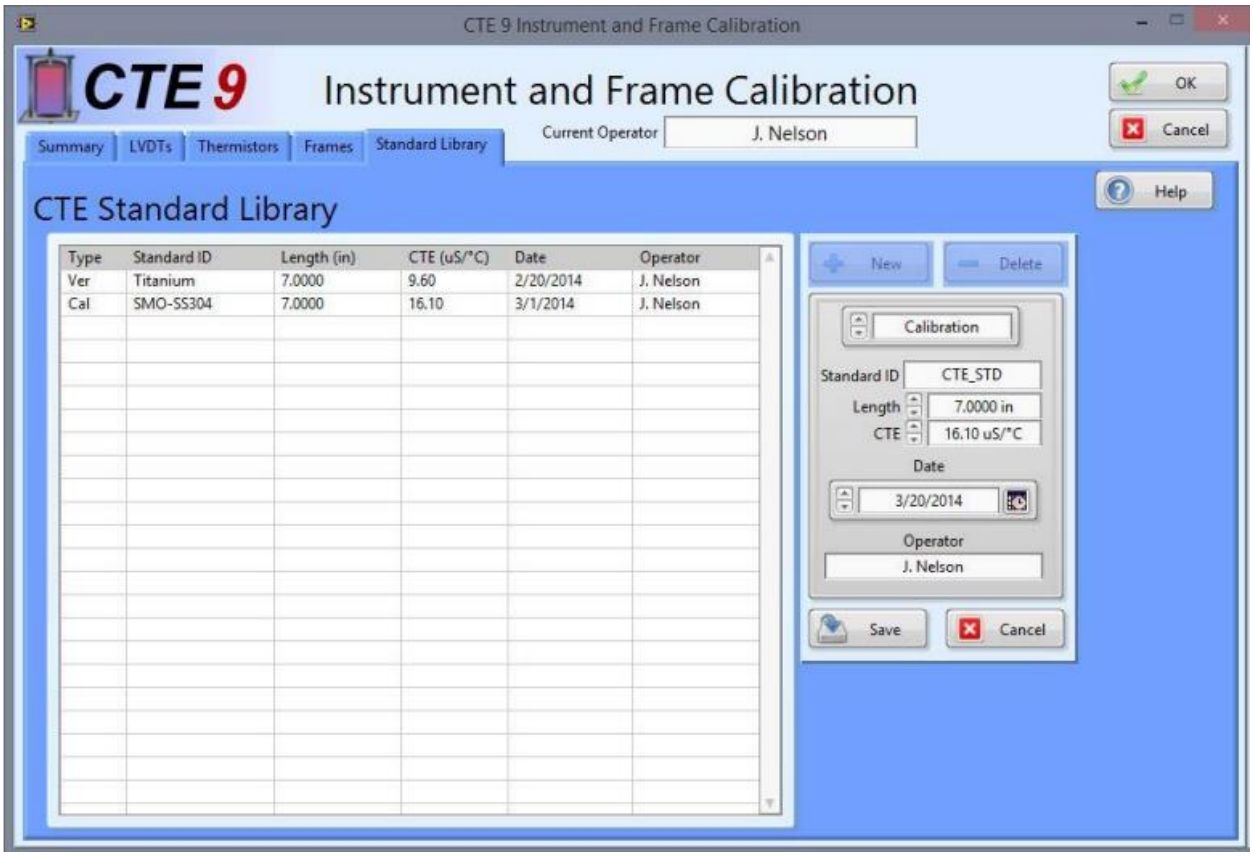

Figure A.18 CTE Standard Library

IMPORTANT: to save the updated Standard Library permanently with the system, you must close the Instrument and Frame Calibration panel with the OK button. Canceling the panel will erase any changes made in your current session of the Instrument and Frame Calibration panel.

A.9 PERFORMING A TEST

A.9.1 Specimen Conditioning

A good specimen for CTE testing possesses characteristics that both maximize the accuracy of the test results and minimize potential hazards for the CTE bath system itself. Specimens should be chemically stable, clean, well saturated, cut and/or ground to 7.00”, and have smooth surfaces free of indentations and protrusions in contact with the frame supports and LVDTs. It is not

advisable to test concrete at early ages in this system as the temperature fluctuations used in the test may adversely affect the ongoing hydration reaction.

Once a proper specimen is selected, grind the surfaces to a smooth finish while maintaining a 7.00" nominal length. Saturate the specimen in lime water until significant mass change is no longer observed. Clean the outer surface of the specimen before placing it in the water bath reservoir as the addition of free lime or other debris may damage the water bath.

A.9.2 Specimen Placement

Place the specimen in the desired frame by carefully lowering it into the reservoir and placing it on the ball supports while keeping the LVDT armature raised and protected with your free hand. Do not allow the specimen to drag against the LVDT armature. Some sliding on the ball supports is permissible as they are relatively hard steel and will not readily wear. Ensure the reservoir does not overflow while placing specimens. Refill the reservoir so that the water level slightly covers the top plate of the INVAR frames after placing the specimen(s).

Ensure the LVDT is centered on the specimen and the specimen is stable on the ball supports. If the INVAR frame uses a moving LVDT or top plate and you are testing using a single point correction factor, adjust the LVDT height until the height display on CTE 9 reads "0" (differential) or "7" (absolute). This step has a major impact on the accuracy of the test and must be performed before each test.

A.9.3 Program Operation

After specimen placement, ensure the system reads ready and that no warnings that may adversely impact the test exist in the session as shown in Figure A.19. Select a procedure using the menu at the top of the panel Complete the specimen details including name, specimen length, and any pertinent details. Enable or disable frames as required. Choose a file path for the CTE report tab delimited (*.txt) file and select "Start Test".

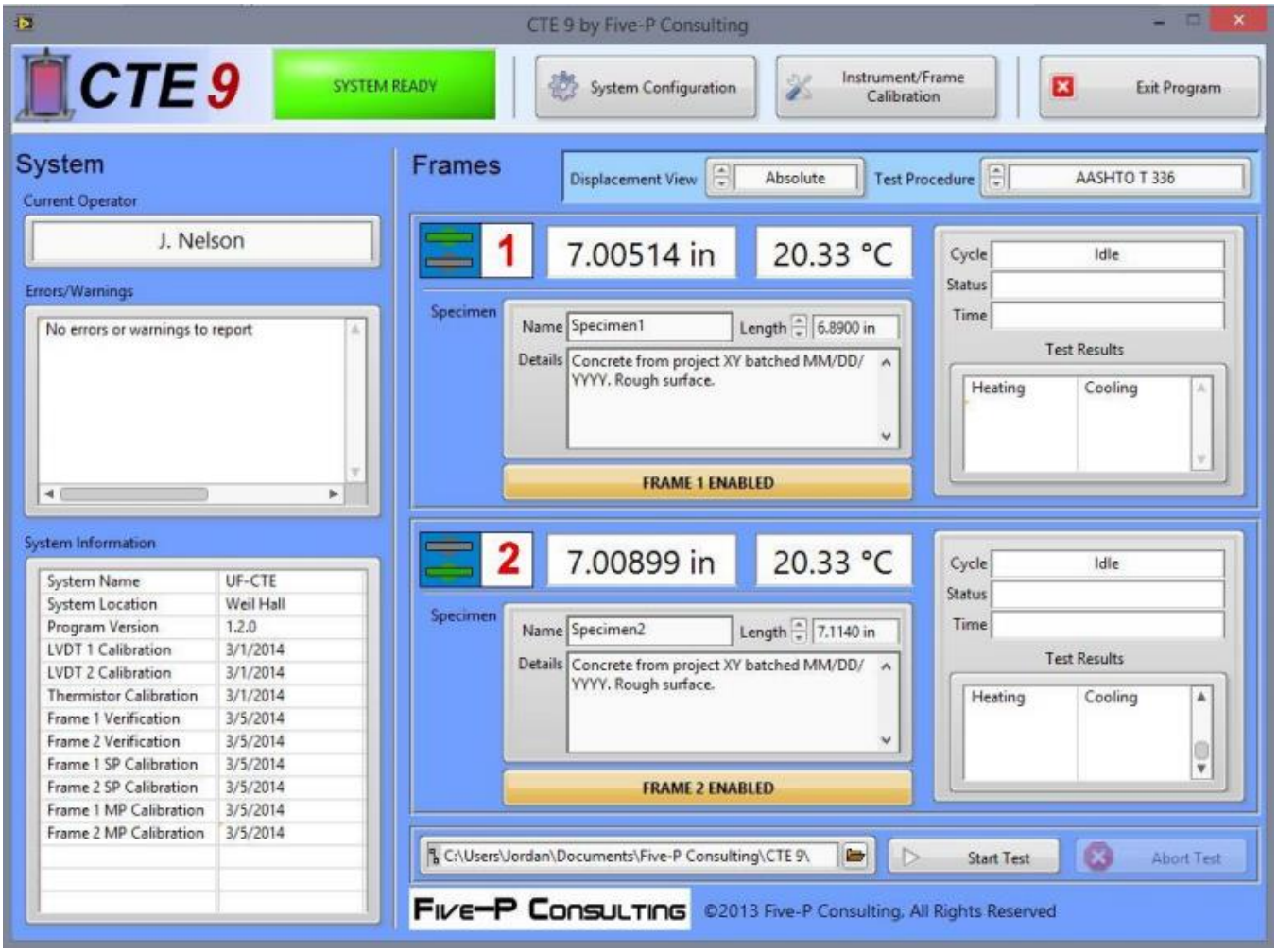

Figure A.19 CTE 9 ready to begin a test following AASHTO T336

If "Custom Setpoints" was chosen for the procedure, the panel shown in Figure A.20 will appear. The last custom procedure will be entered by default. The custom procedure can be named and the temperatures for the high, low, and equilibration setpoints may be chosen. Sample Equilibration defines a beginning and ending setpoint equal to the equilibration temperature and is optional. Test End Condition allows selection of "Run All Cycles" in which the setting under "Max Cycles" will define the test duration, or an end condition based on a tolerance between successive calculations of CTE as shown in Figure A.20. In the latter choice, the value of "Max Cycles" will define an upper limit of cycles to run before the test is aborted.

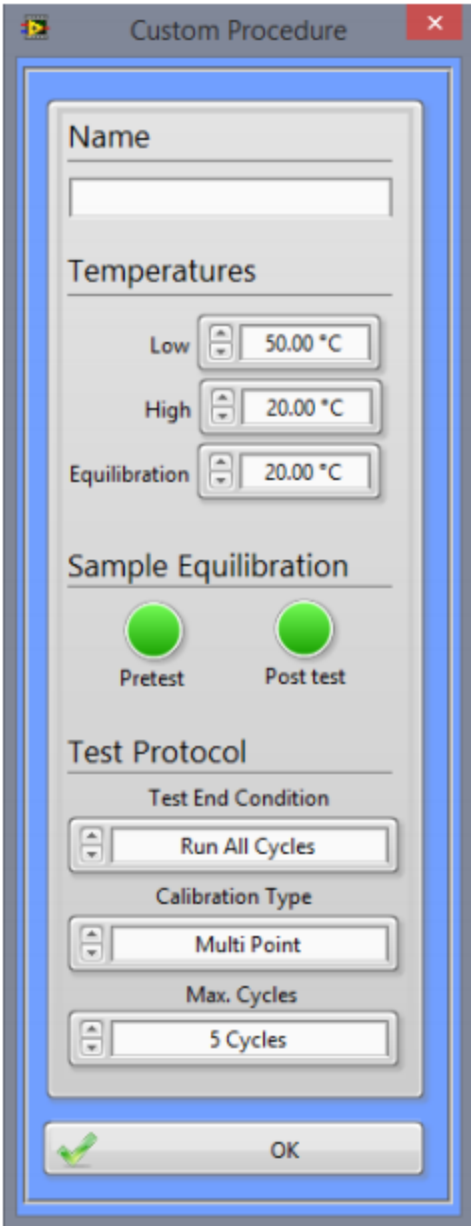

Figure A.20 Custom Procedure popup

During the test, certain controls will be unavailable to the operator. The test feedback displays next to each specimen entry panel will inform the operator of the current cycle, current task, and the time at each cycle as well as the overall test duration. The CTE value calculated at each setpoint is displayed for nominal information on the results for the specimen. After the test completes successfully or is aborted, the operator will be notified with a dialog box. The report file may then be retrieved from the directory specified before the test was started.

A.10 WORKING WITH DATA FILES

All CTE 9 data files are tab-delimited (*.txt) files that open readily in Microsoft® Excel™. The raw data file (User Documents\Five-P Consulting\CTE9_RawDataTemp.txt) is a temporary file

containing minute-by-minute data of the instrument values collected during a test. It contains a long history of the previous test and can be used to diagnose issues with a test run including erroneous data points or unexpected faults.

The raw data file has a standard header and a long data table of instrument values. The CTE report file consists of a standard header, a data table of each recorded setpoint including equilibration setpoints if used, the time of termination of the test run and its condition, and a list of any extant warnings or errors.

All pertinent raw data, calibration values, and calculated data for a test is included on the CTE report file and may be used to verify or adjust test results as needed. If CTE testing is done on a production level scale, it is advisable to make an Excel™ template that will automatically format these report files in a finalized format.

	A	B	C	D	E	F
1	***CTE 9 Data File***					
2	File Version 1.0.0					
3	©2013 Five-P Consulting					
4						
5	File Type:	CTE Report File				
6	File Created:	3/7/2014				
7	Operator:					
8						
9	CTE System Name:	UF-CTE				
10	System Location:	Weil Hall				
11						
12	LVDT Calibration					
13		M (in/V)	B (in)	Date	Operator	
14	LVDT 1	0.025203	-0.000041	3/5/2014	Jordan N.	
15	LVDT 2	0.025196	-0.000038	3/5/2014	Jordan N.	
16						
17	Thermistor Calibration					
18		M (°C/°C)	B (°C)	Date	Operator	
19	T1	1	0	3/3/2014	Jordan N.	
20	T2	1	0	3/3/2014	Jordan N.	
21	T3	1	0	3/3/2014	Jordan N.	
22	T4	1	0	3/3/2014	Jordan N.	
23						
24	Frame Verification					
25		Error (%)	Date	Operator		
26	Frame 1	0	12/31/1903			
27	Frame 2	0	12/31/1903			
28						
29	Single Point Calibration					
30		Cf (uS/°C)	Date	Operator		
31	Frame 1	0.1662	3/7/2014	Jordan N.		
32	Frame 2	0.1662	12/31/1903			
33						
34	Multi Point Calibration					
35		Cf M (uS/°C/in)	Cf B (uS/°C)	VDC @ 7.00000 i	Date	Operator
36	Frame 1	0	0	0	12/31/1903	

Figure A.21 CTE 9 report file opened in Excel™ displaying header information

A.11 MAINTENANCE

A.11.1 Water Bath

The water baths are generally low maintenance devices. The pump, heater, and refrigerator are self-contained and permanently lubricated. If any of these components begin to show signs of wear or damage, consult the bath manual or call the manufacturer. Otherwise, follow these procedures at every 6 months or as needed to ensure long bath life.

- Remove the frames, stainless plate, and PTFE liner from the reservoir. Wipe them off with a damp rag and mild detergent. NEVER use bleach
- Open the petcock on the back of the reservoir and allow the water to drain completely. Use wedges to tilt the bath back if necessary.
- Wipe out the interior of the reservoir with mild detergent and flush with clean water
- Check the heater coil for excessive debris and calcium build up. Clean if necessary
- Check the insulated rubber hose on the back of the pump housing for cracks, wear, or blockage. Replace if necessary
- Carefully slide the water bath forward until it slightly hangs over the counter. Rotate the plastic retaining clip under the front of the bath and remove the air filter. Rinse the filter and allow to air dry completely before reinstalling
- Replace the liner, plate, and frames. Close the petcock and refill the bath with clean water
- Wipe the exterior of the bath with a mild detergent

A.11.2 Instruments

Every 6 months, or if unusual data is encountered, it is advisable to check the thermistors and LVDTs for proper function and accuracy. If an LVDT or thermistor appears significantly damaged or consistently gives false data, it needs to be returned to the manufacturer and/or replaced.

- Remove each thermistor and check the cable, connector, and thermistor body for cracks, unusual wear, or other damage.
- Check the thermistor connections for a firm, solid contact with the jack panel
- Check each LVDT cable, connector, and body for damage or wear
- Wipe the LVDT body with mild detergent
- Check the threads on the LVDT body for excessive rust or damage
- Check the LVDT plunger for damage or corrosion by pushing it in and allowing it to extend under spring pressure several times. If it takes excessive force to move the plunger, contact the manufacturer
- Visually check the air filters on the computer enclosures for excessive blockage. If the filters appear clogged, remove the panel(s) and clean or replace the foam filters

A.12 TROUBLESHOOTING

Many common issues the CTE system might encounter are handled by the error module within CTE 9. Descriptions of the error and the error code will be provided in the error and warning display as well as at the end of the CTE report file. Common issues outside of the scope of the software will be presented here.

Water bath will not turn on

- Try to turn the bath on manually
  - Bath turns on…
    - Check serial connectivity between bath and electronics enclosure
    - Make sure serial cable is not a null modem (crossover) cable
    - Check Bath Port Settings in CTE 9
  - Bath does not turn on…
    - Check power to bath
    - Refer to bath manual for troubleshooting or contact manufacturer

Computer enclosure will not turn on

- Check the main switch on the back of the enclosure
- Check the power supply to the enclosure
- Unplug the enclosure, pry open the plastic face of the power entry connector with a small screwdriver, pull out the red fuse holder, and check the internal bus fuse
- Allow the unit to sit unplugged for 10 minutes, plug in and retry

Keyboard and/or mouse does not work

- Ensure all human interface devices are connected to a USB port on the enclosure
- Hard restart (hold the blue power button) the system
- Check to see if the fan is running. If it is not, USB power has been terminated by Windows. This is most likely due to an internal fault. Contact Five-P Consulting.

Bath does not heat/cool

- Check to see if the setpoint on the bath matches that on CTE 9
  - Setpoints match…
    - Heating or cooling system fault. Contact the bath manufacturer.
  - Setpoints do not match…
    - Serial communication fault, check serial port settings. If problem persists contact Five-P Consulting

Bath temperature does not match thermistor temperature

- For temperature differences of a degree or less, this is normal
- Check thermistor calibration and placement in bath
- Check for defective thermistors or defective bath temperature probe

Erroneous data encountered

- Check calibration of instruments
- Inspect instruments for damage
- Recalibrate erroneous instruments

APPENDIX B. DESTRUCTIVE TESTING DATA

B.1 COMPRESSIVE STRENGTH

B.1.1 Class II Concrete

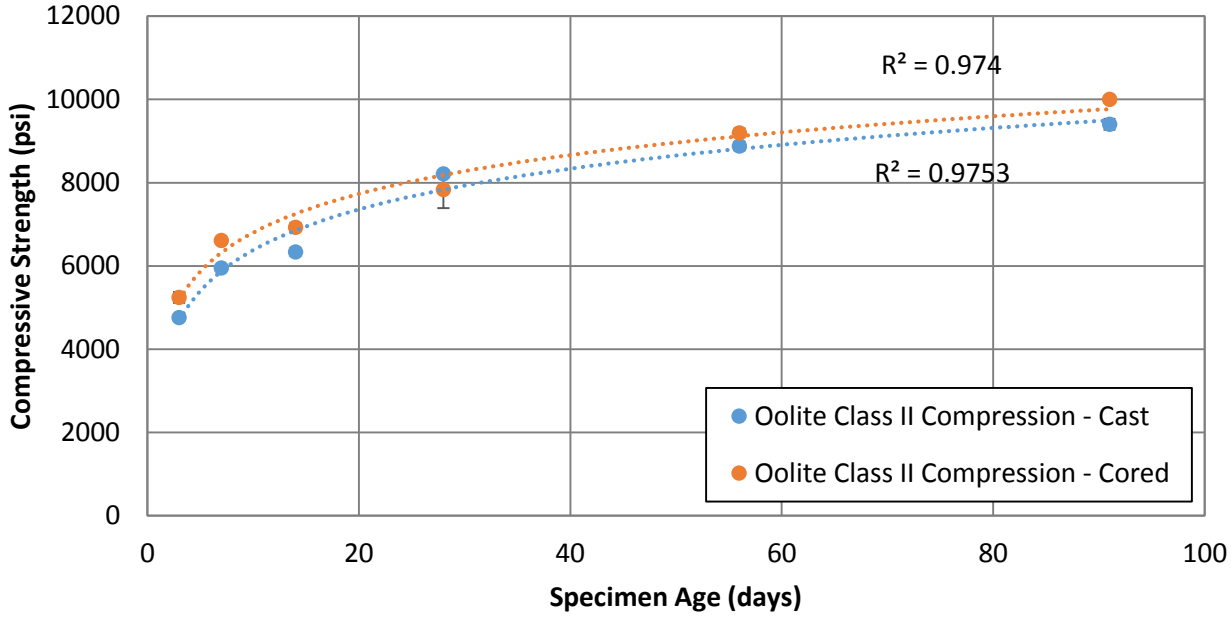

Figure B.1 Compressive strength vs. time for class II Miami oolite concrete

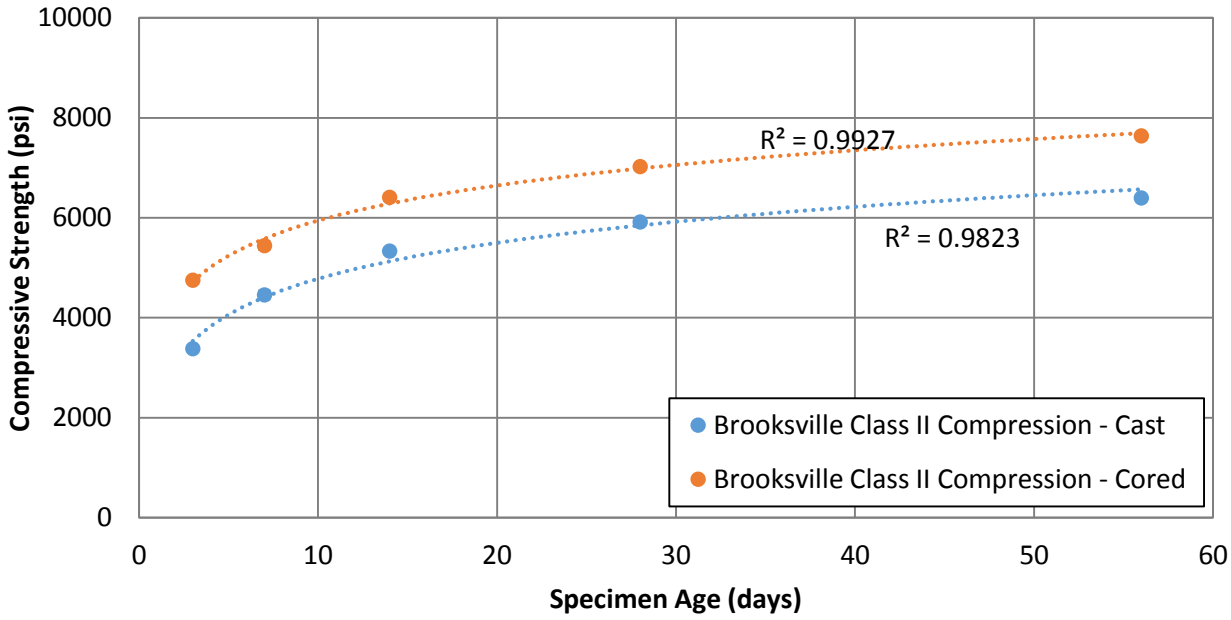

Figure B.2 Compressive strength vs. time for class II Brooksville limestone concrete

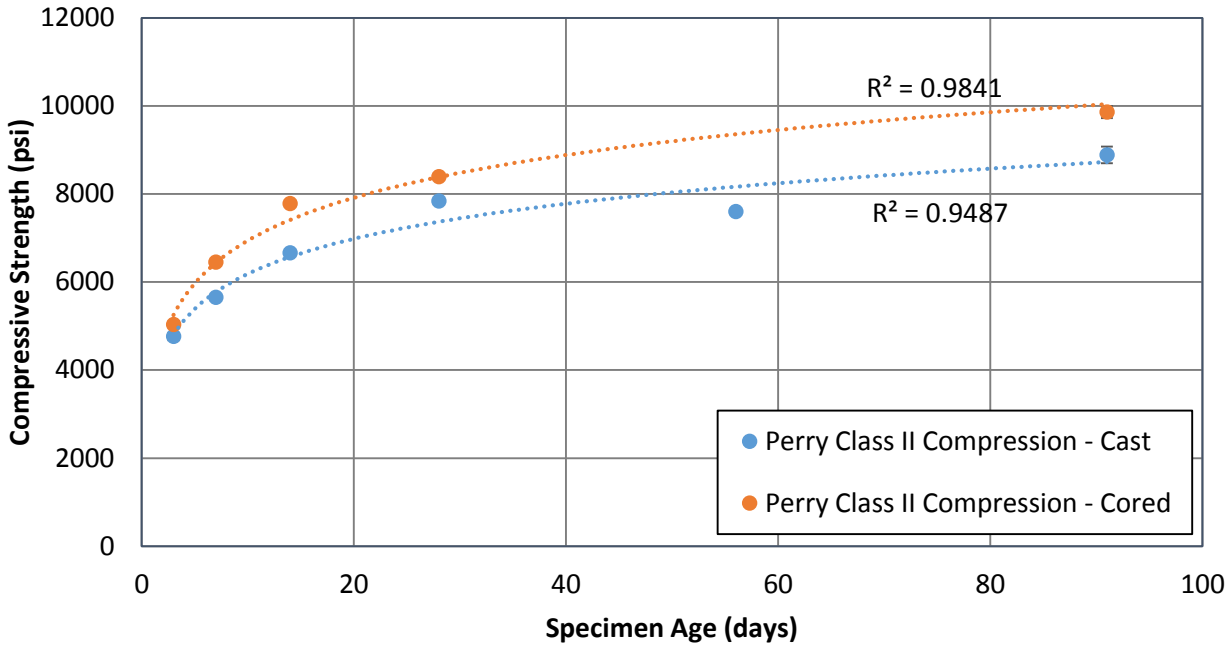

Figure B.3 Compressive strength vs. time for class II Perry limestone concrete

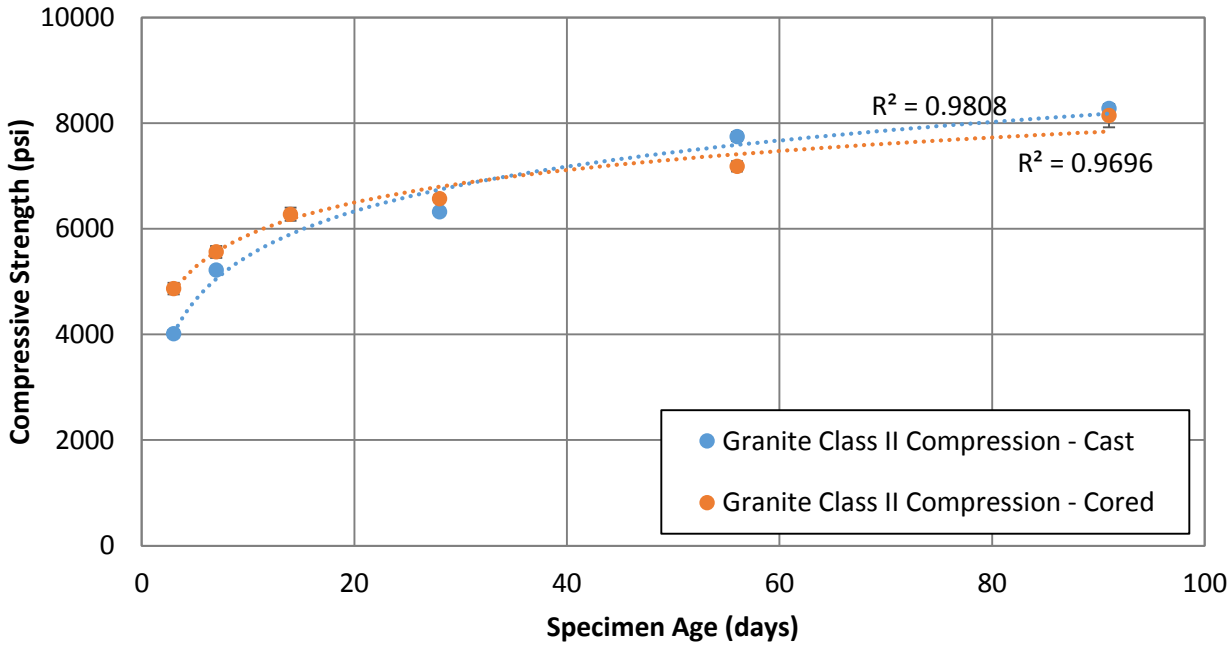

Figure B.4 Compressive strength vs. time for class II Georgia granite concrete

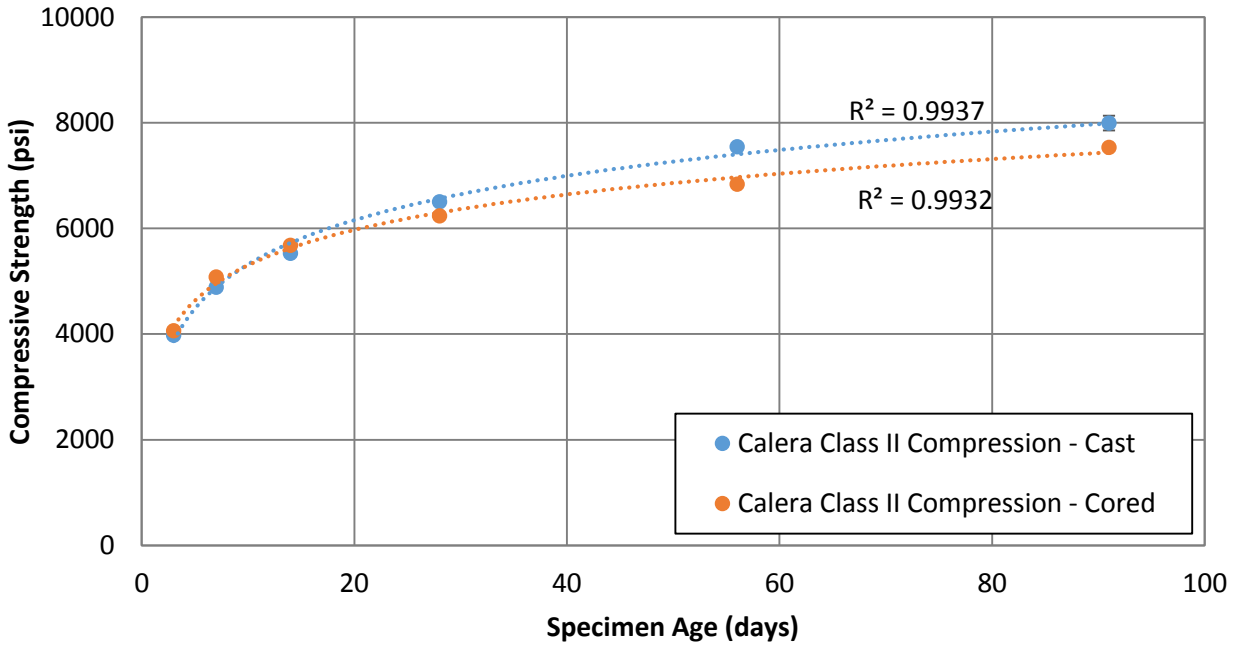

Figure B.5 Compressive strength vs. time for class II Calera limestone concrete

B.1.2 Class VI Concrete

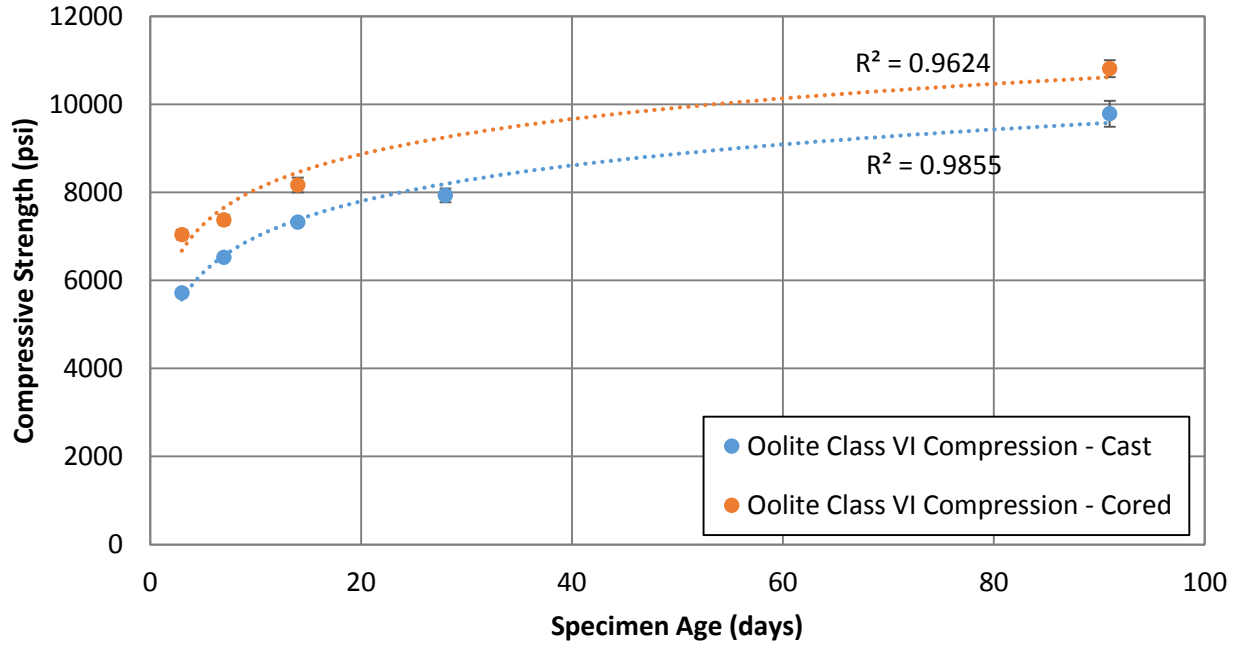

Figure B.6 Compressive strength vs. time for class VI Miami oolite concrete

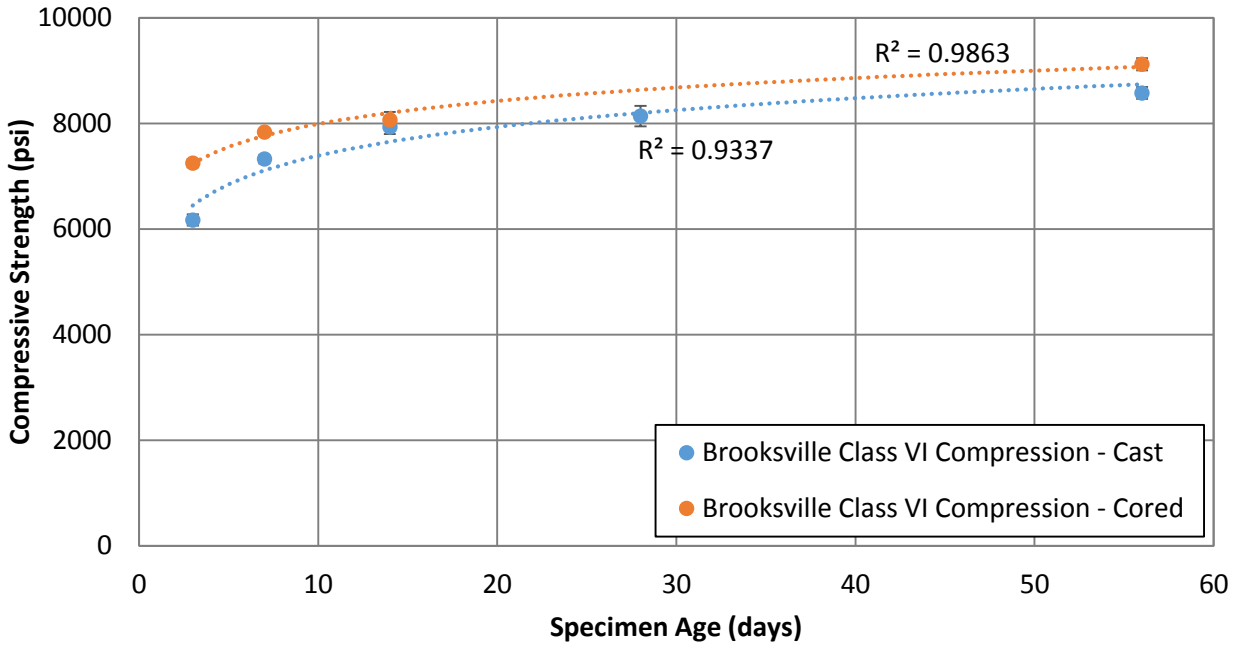

Figure B.7 Compressive strength vs. time for class VI Brooksville limestone concrete

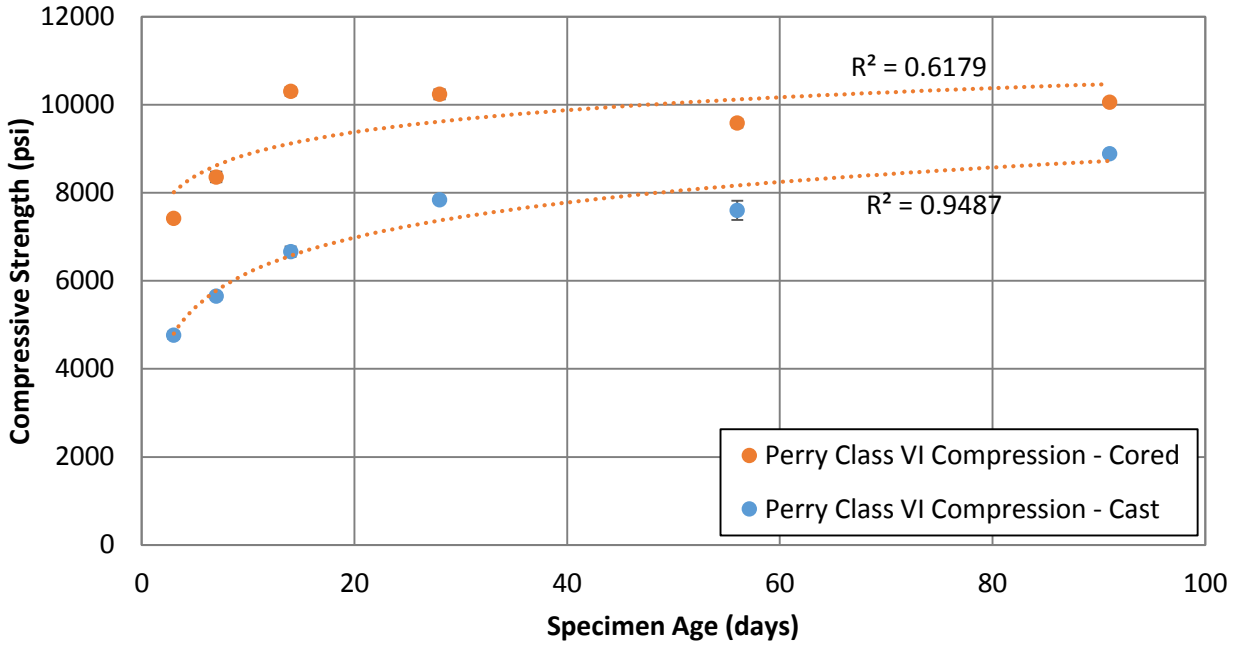

Figure B.8 Compressive strength vs. time for class VI Perry limestone concrete

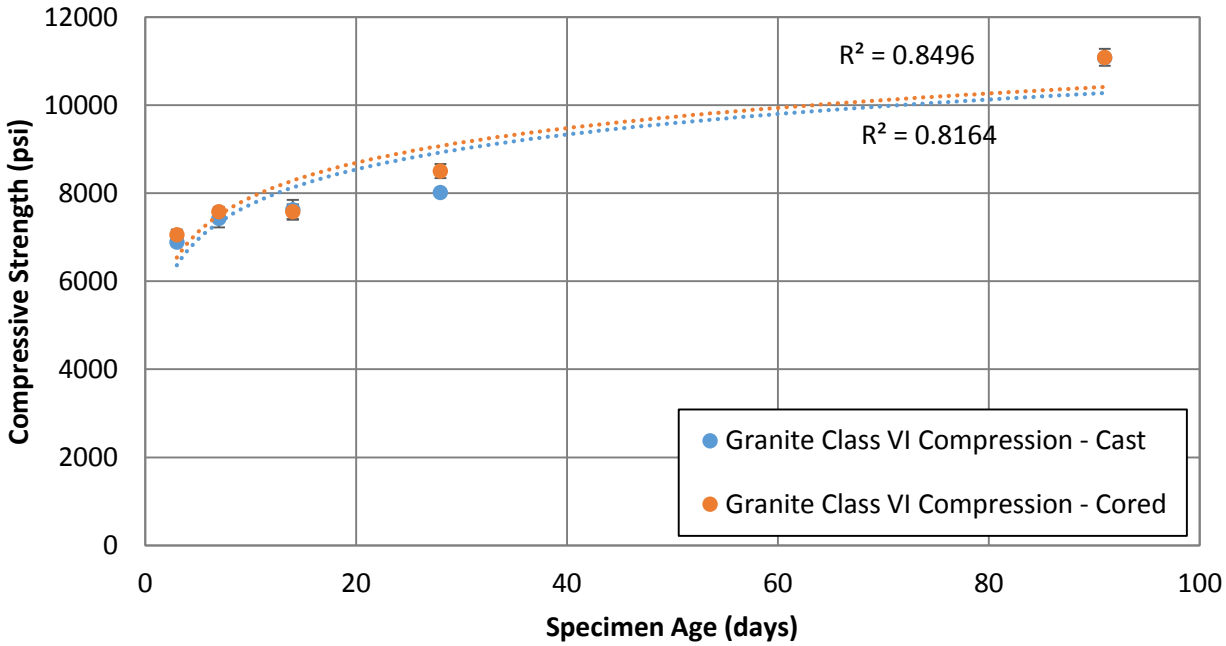

Figure B.9 Compressive strength vs. time for class VI Georgia granite concrete

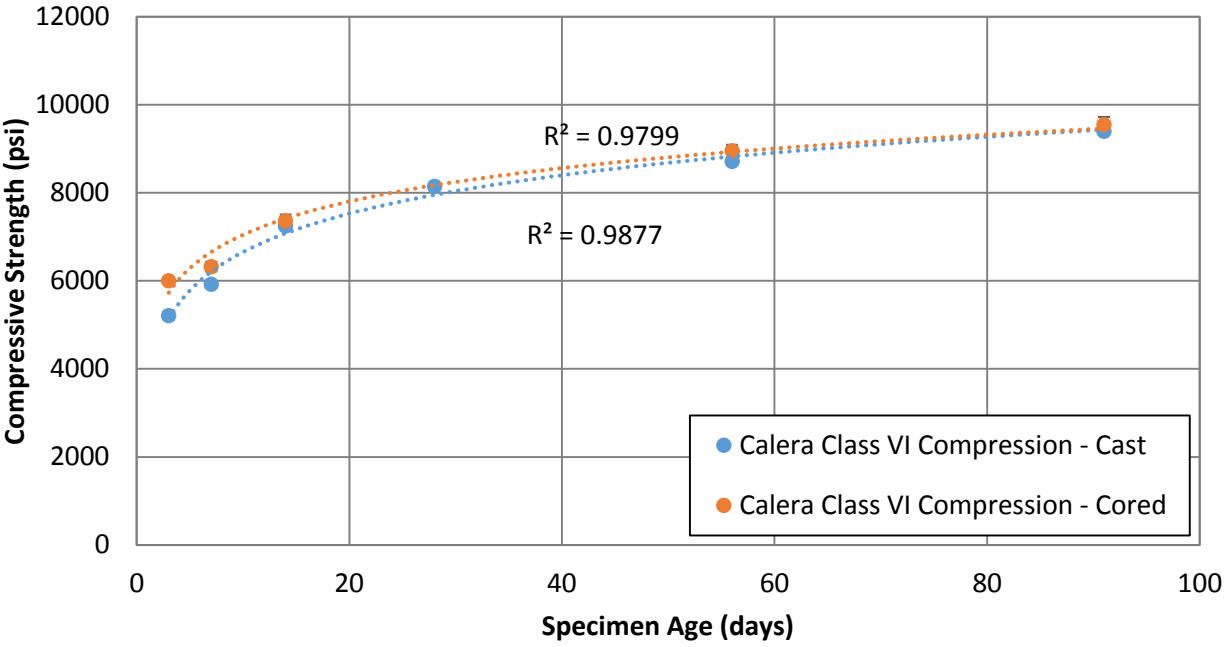

Figure B.10 Compressive strength vs. time for class VI Calera limestone concrete

B.2 MODULUS OF ELASTICITY

B.2.1 Class II Concrete

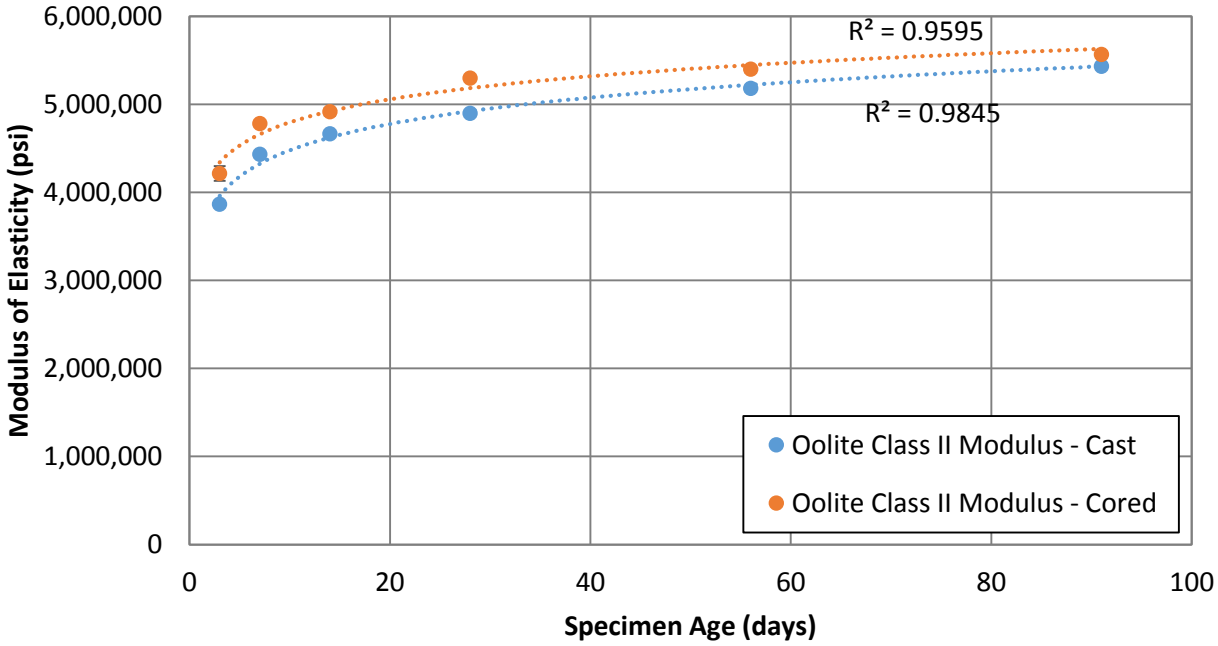

Figure B.11 Modulus of elasticity vs. time for class II Miami oolite concrete

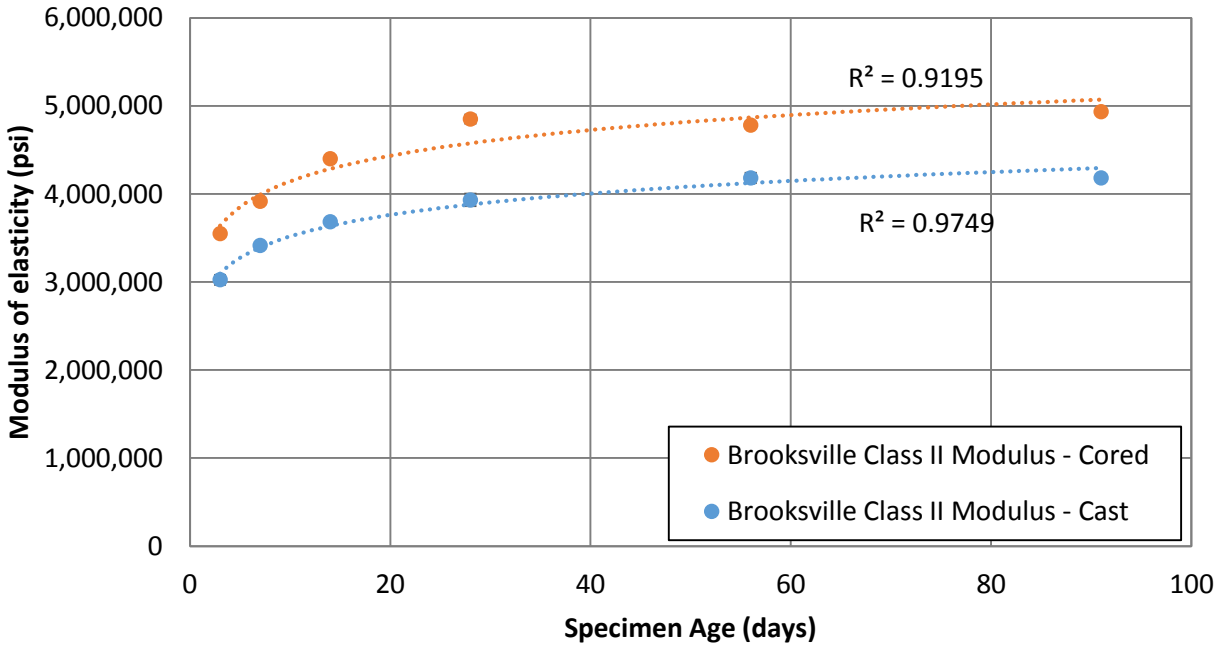

Figure B.12 Modulus of elasticity vs. time for class II Brooksville limestone concrete

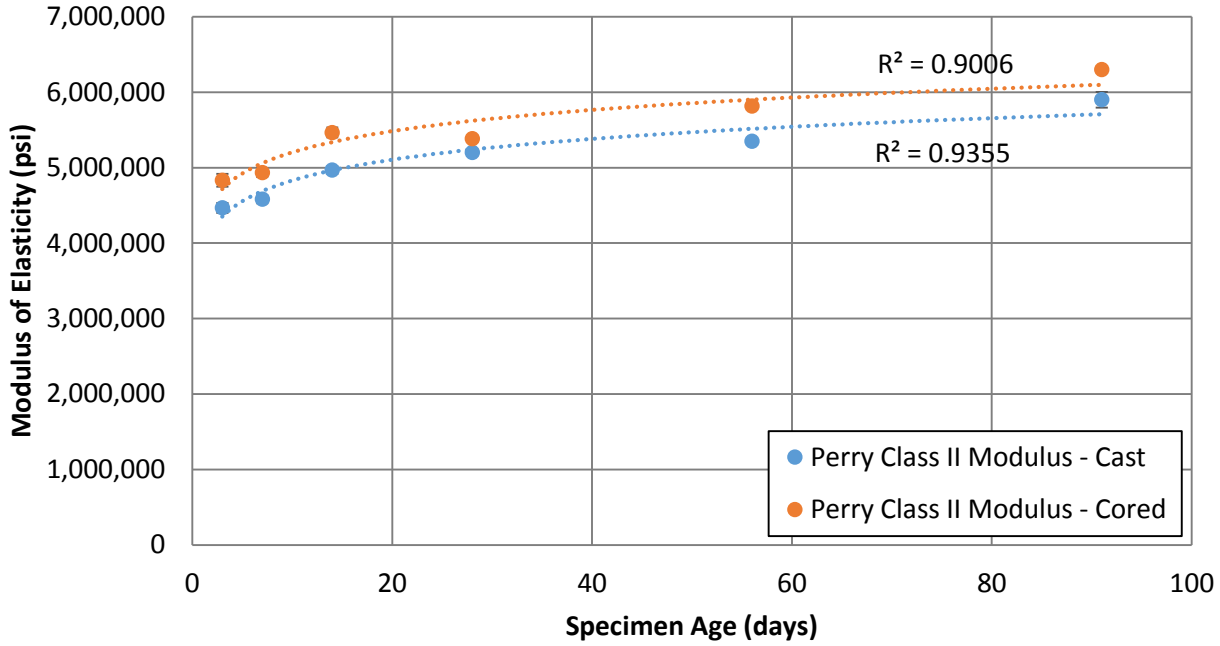

Figure B.13 Modulus of elasticity vs. time for class II Perry limestone concrete

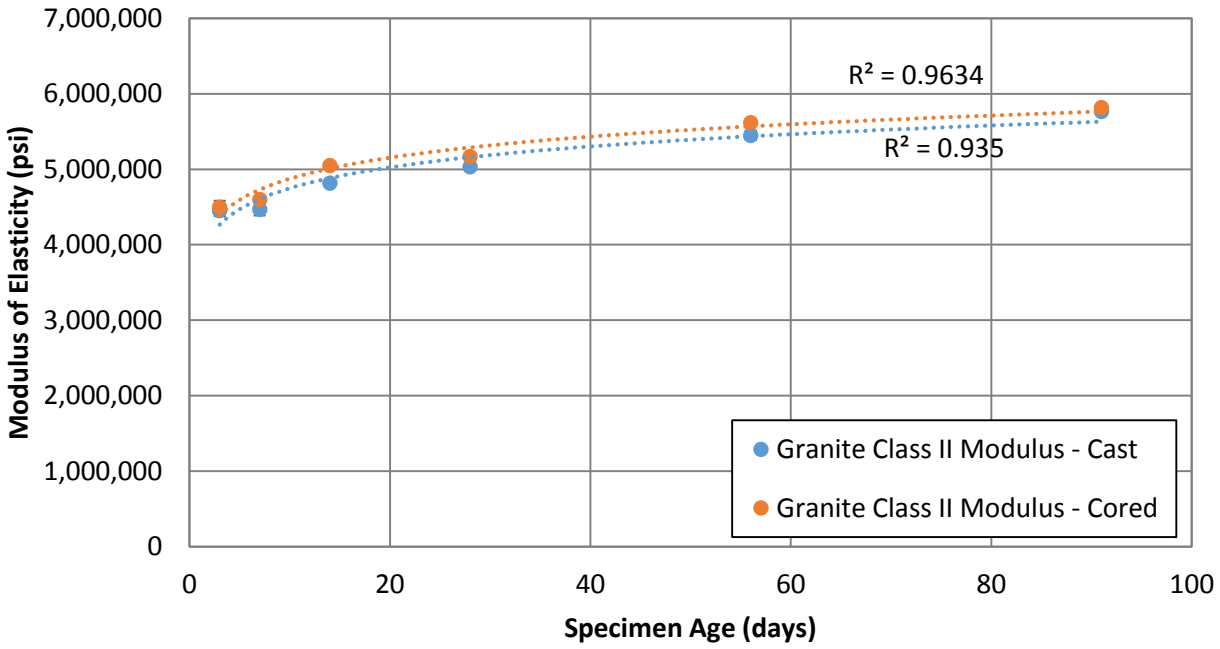

Figure B.14 Modulus of elasticity vs. time for class II Georgia granite concrete

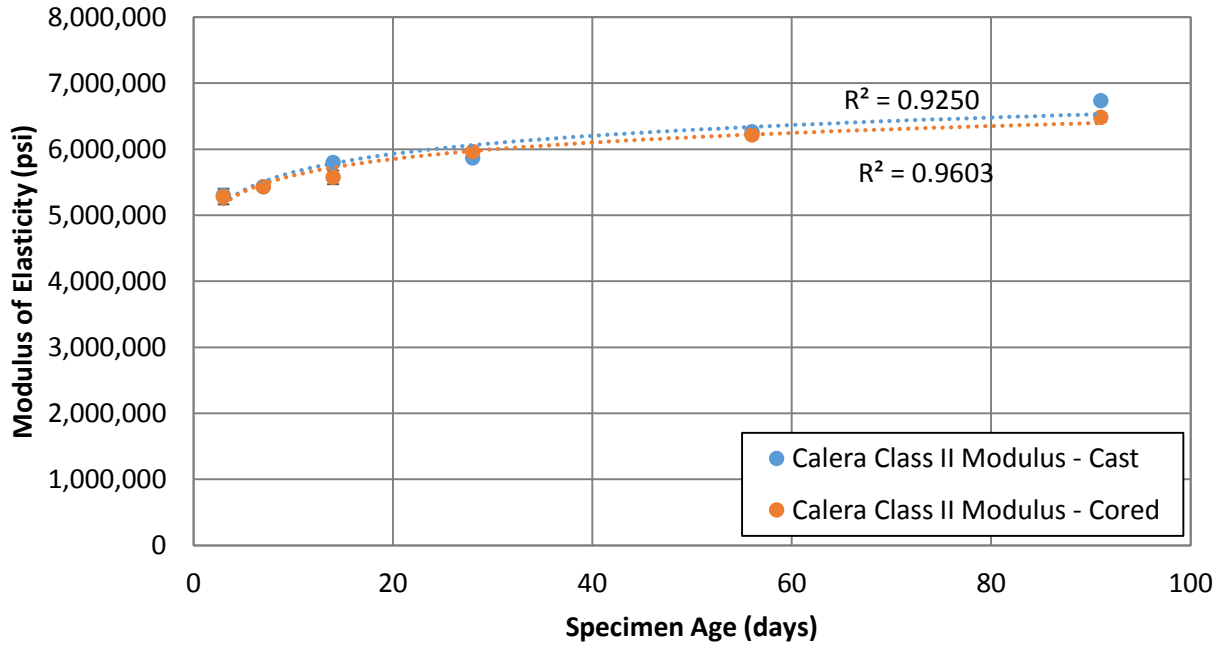

Figure B.15 Modulus of elasticity vs. time for class II Calera limestone concrete

B.2.2 Class VI Concrete

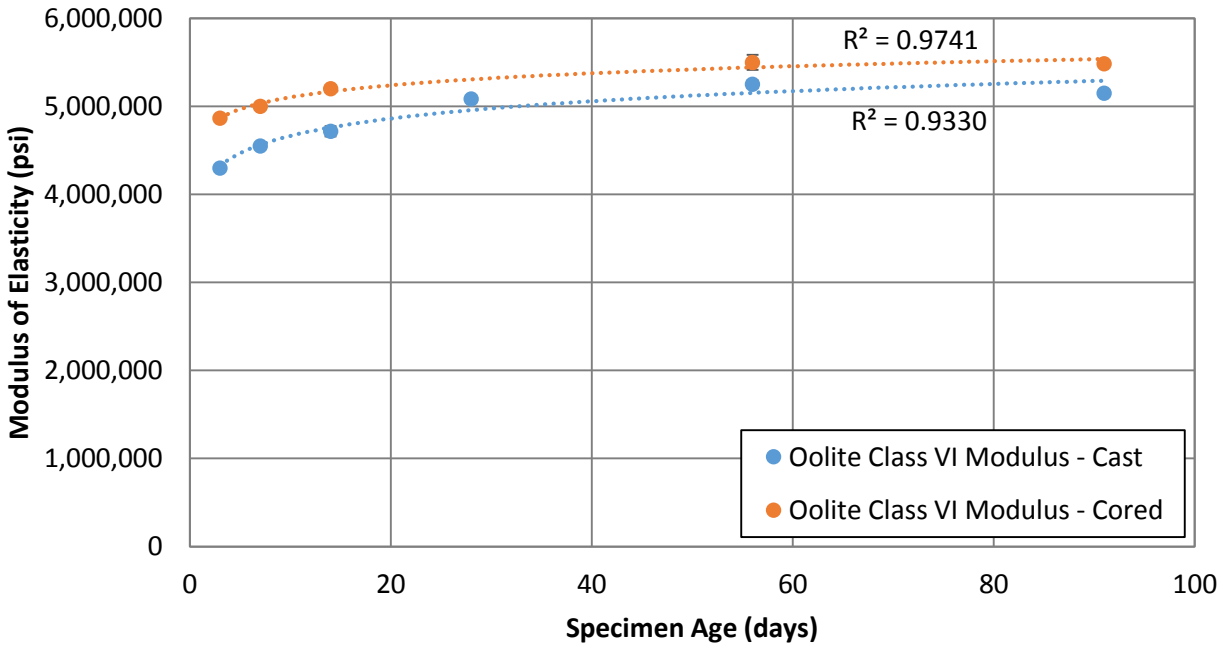

Figure B.16 Modulus of elasticity vs. time for class VI Miami oolite concrete

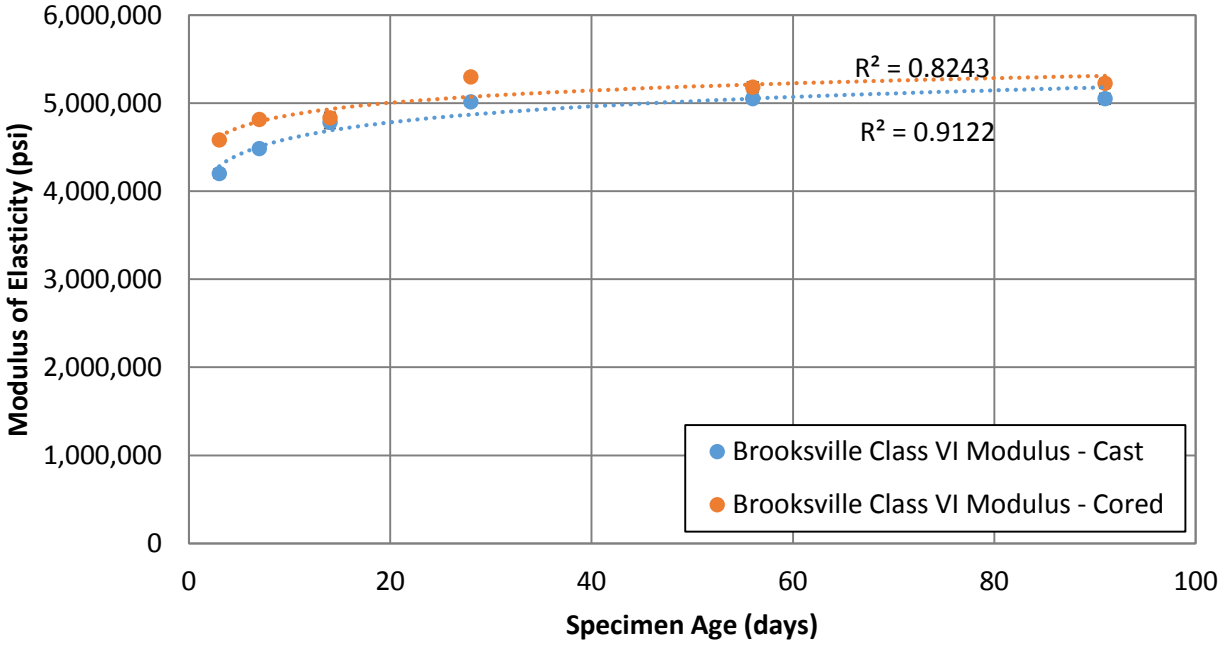

Figure B.17 Modulus of elasticity vs. time for class VI Brooksville limestone concrete

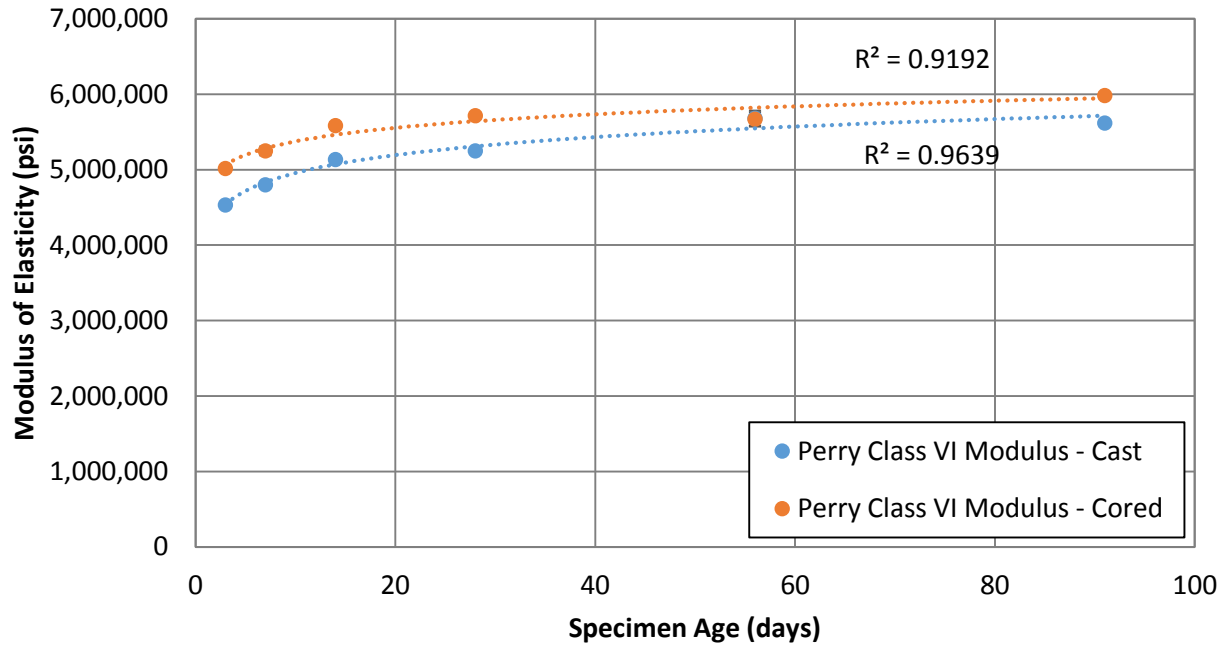

Figure B.18 Modulus of elasticity vs. time for class VI Perry limestone concrete

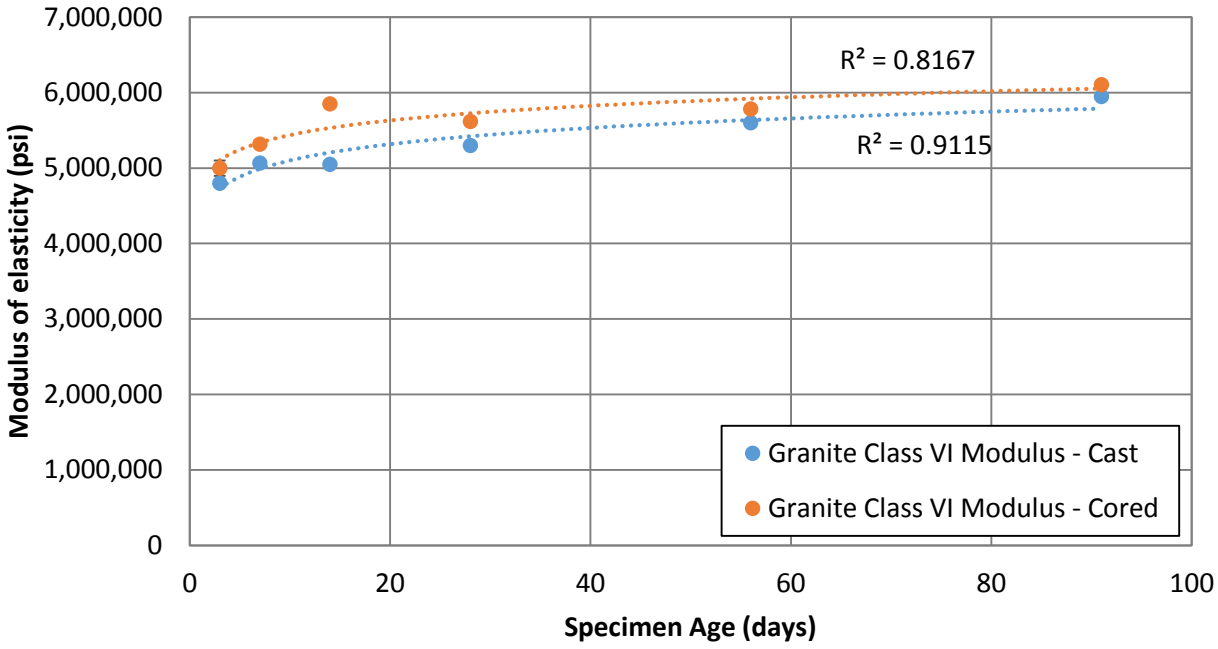

Figure B.19 Modulus of elasticity vs. time for class VI Georgia granite concrete

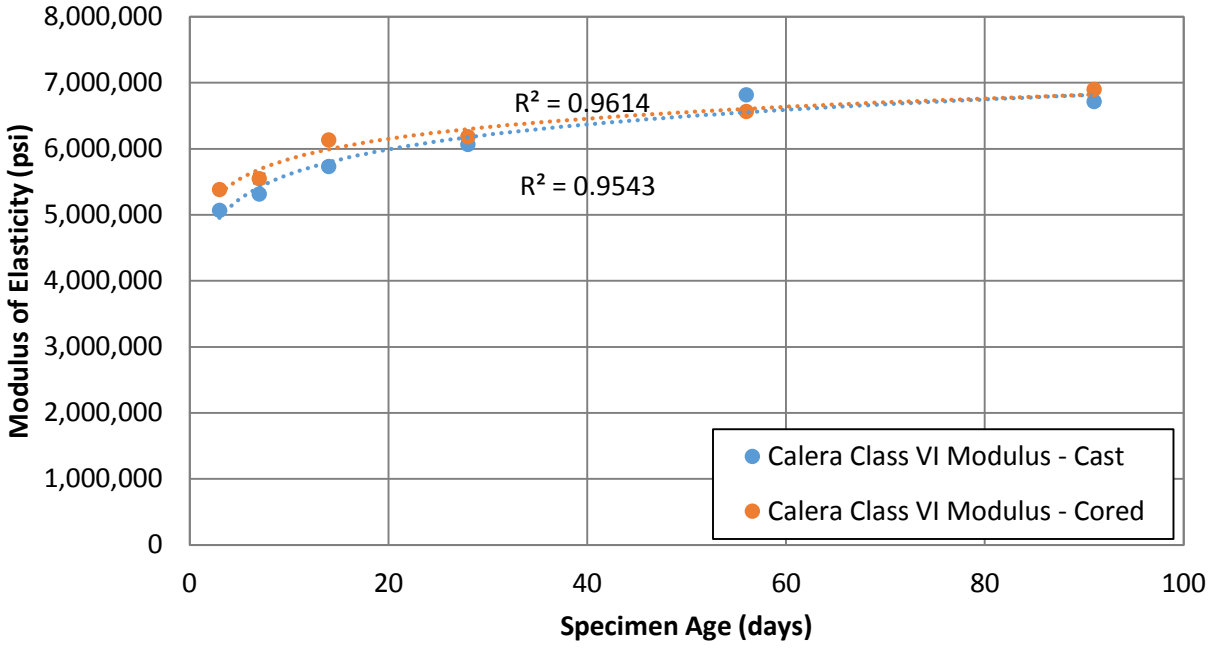

Figure B.20 Modulus of elasticity vs. time for class VI Calera limestone concrete

B.3 SPLITTING TENSILE STRENGTH

B.3.1 Class II Concrete

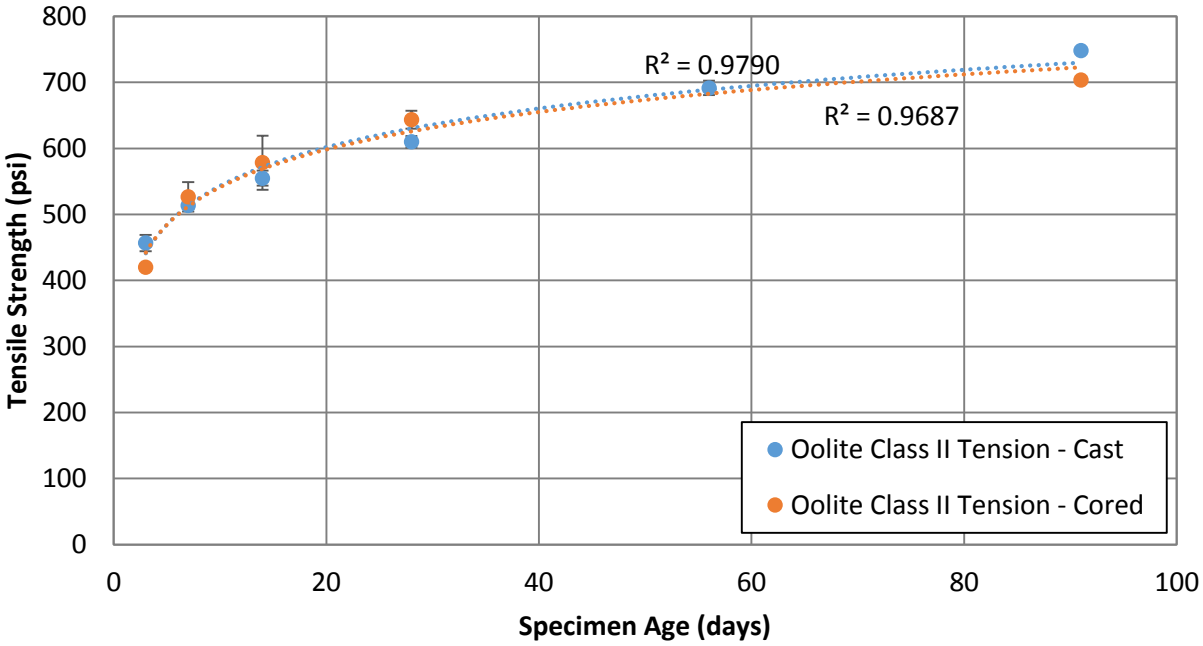

Figure B.21 Splitting tensile strength vs. time for class II Miami oolite concrete

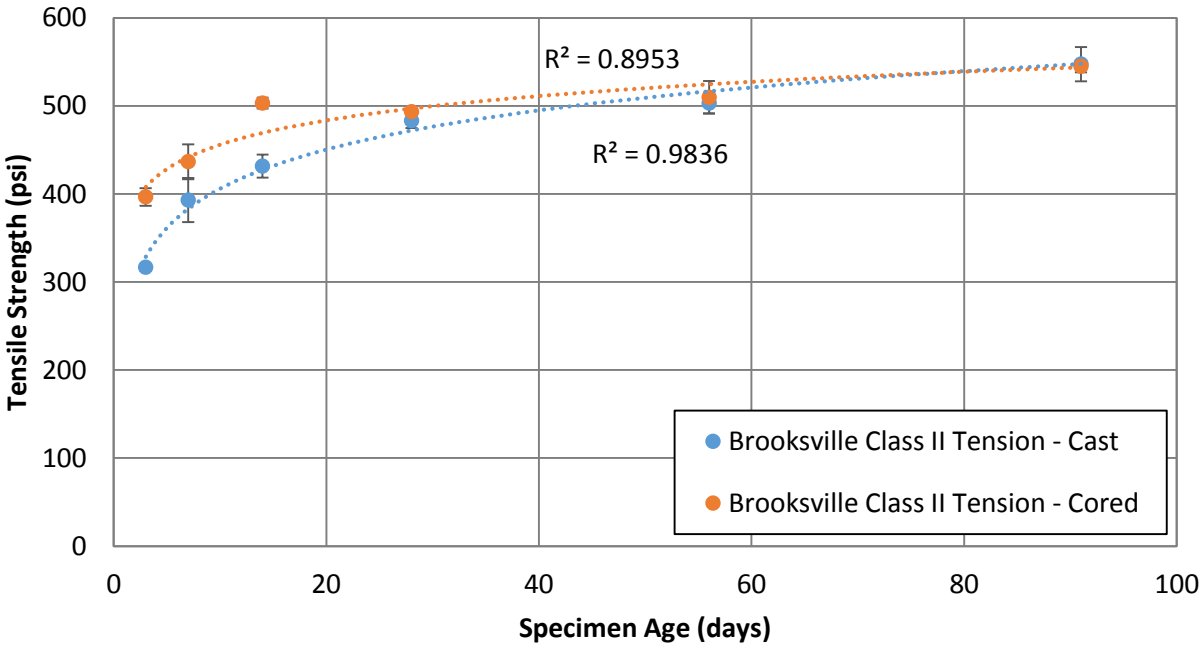

Figure B.22 Splitting tensile strength vs. time for class II Brooksville limestone concrete

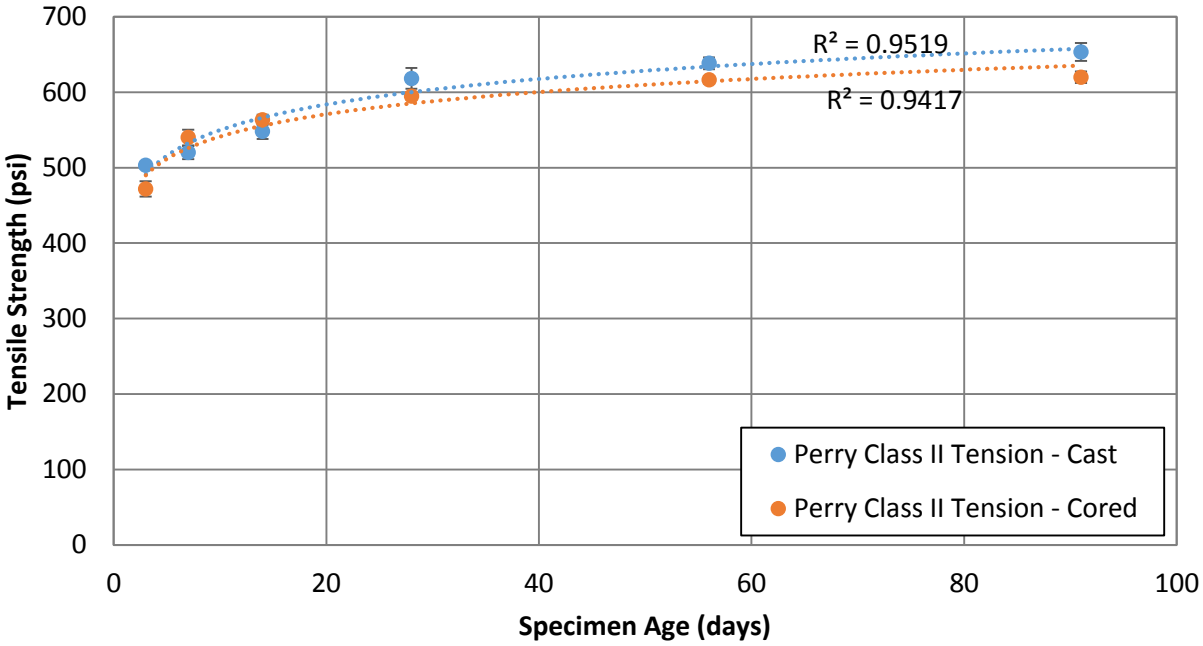

Figure B.23 Splitting tensile strength vs. time for class II Perry limestone concrete

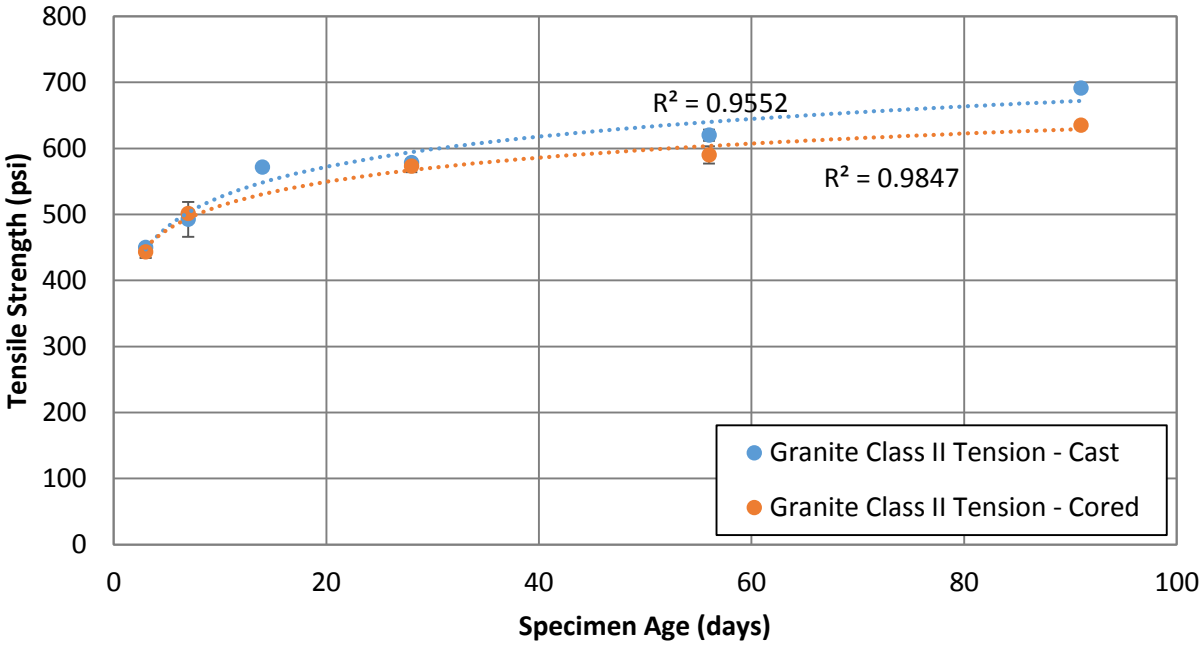

Figure B.24 Splitting tensile strength vs. time for class II Georgia granite concrete

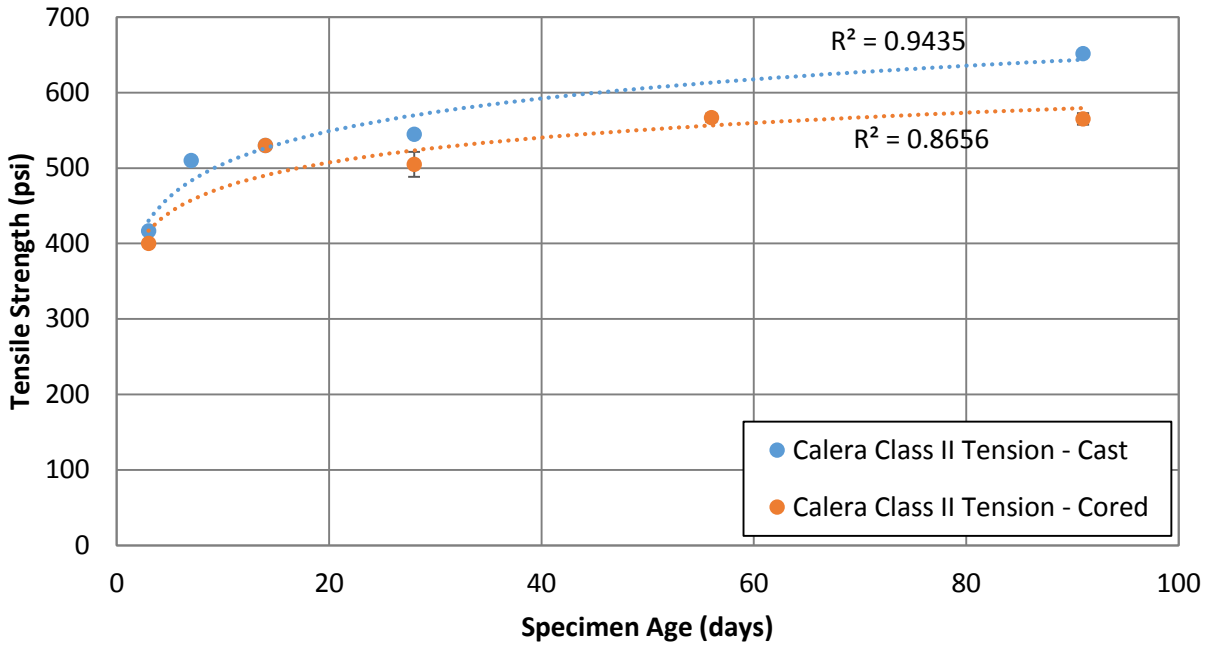

Figure B.25 Splitting tensile strength vs. time for class II Calera limestone concrete

B.3.2 Class VI Concrete

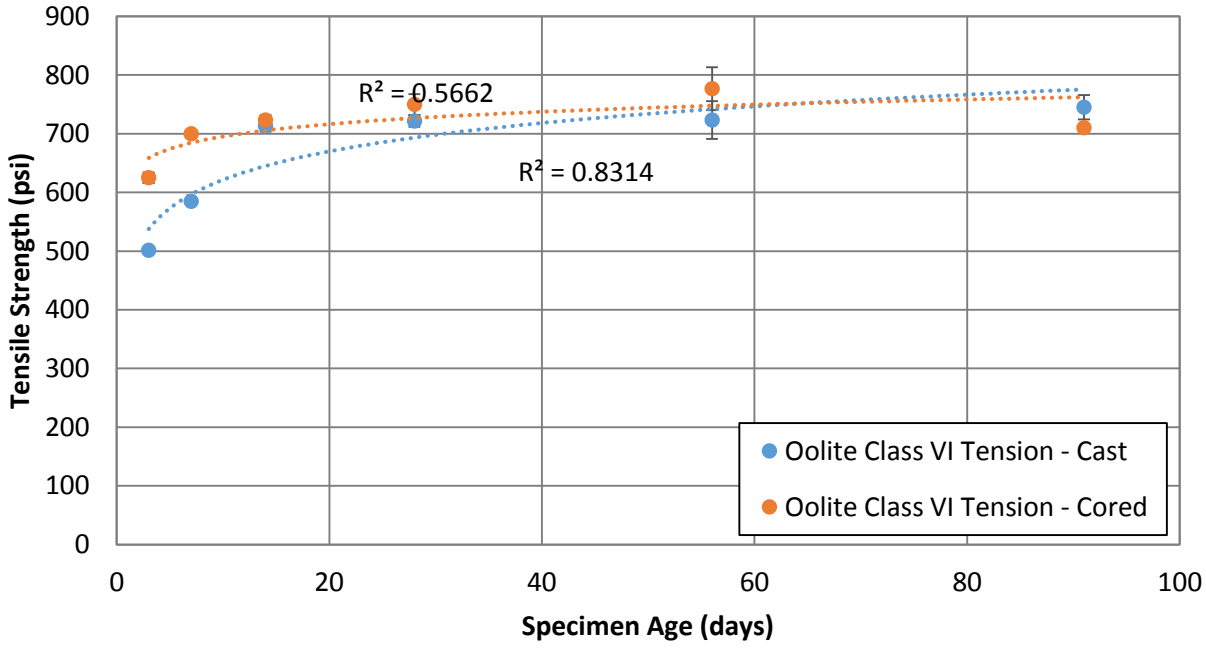

Figure B.26 Splitting tensile strength vs. time for class VI Miami oolite concrete

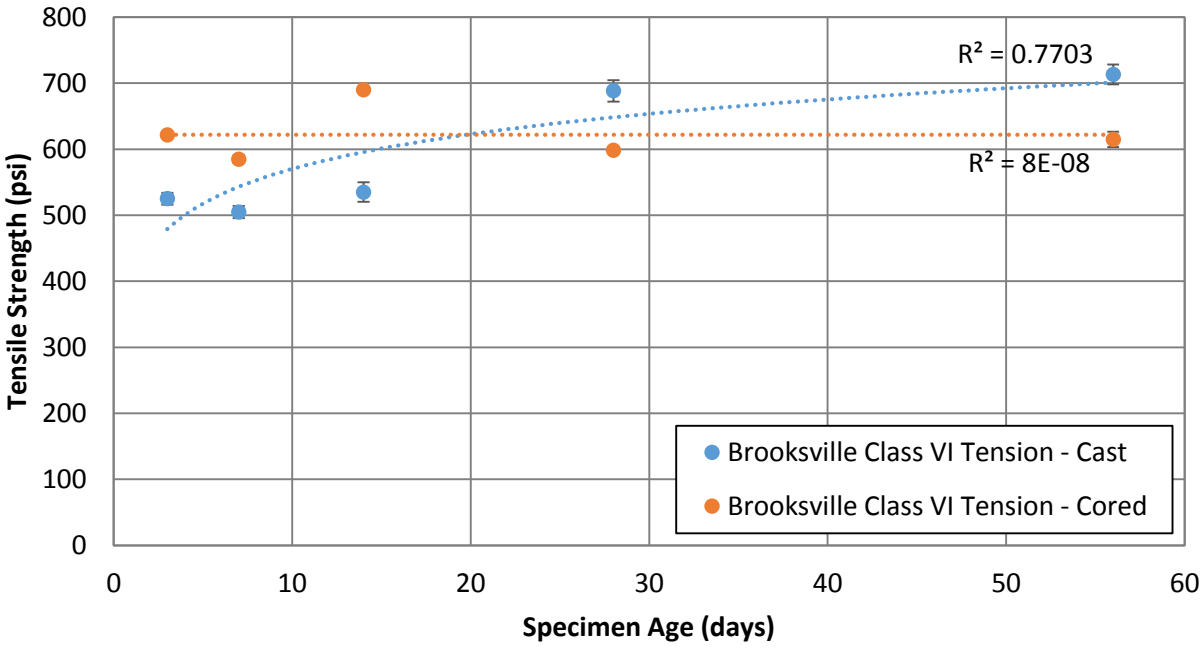

Figure B.27 Splitting tensile strength vs. time for class VI Brooksville limestone concrete

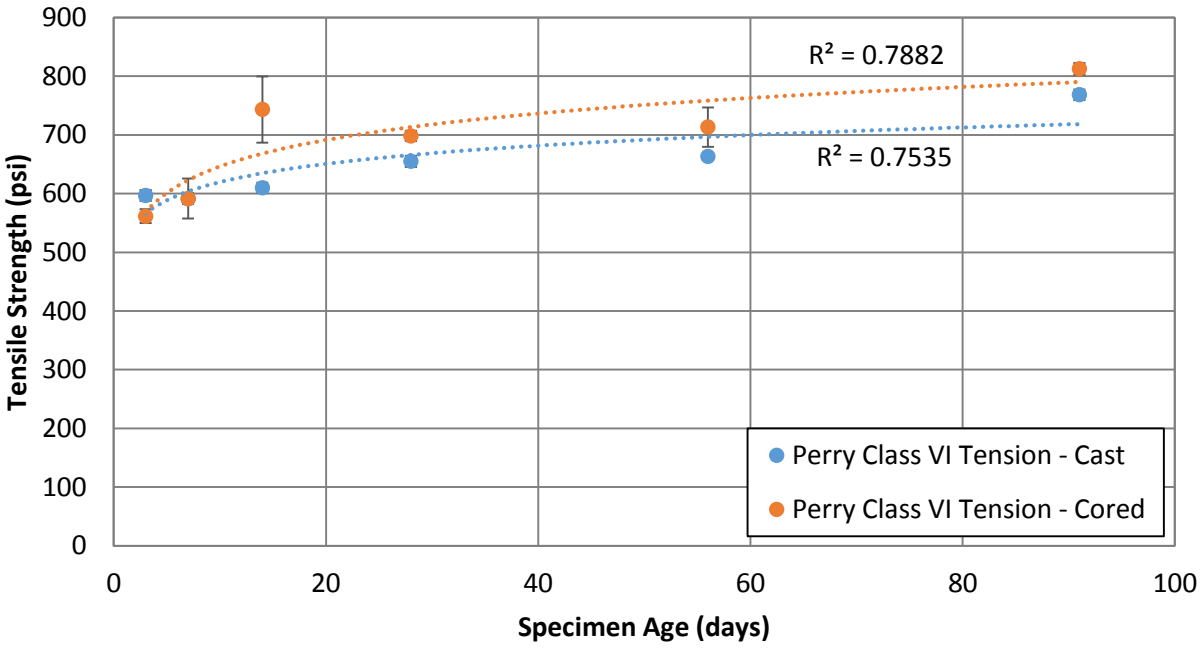

Figure B.28 Splitting tensile strength vs. time for class VI Perry limestone concrete

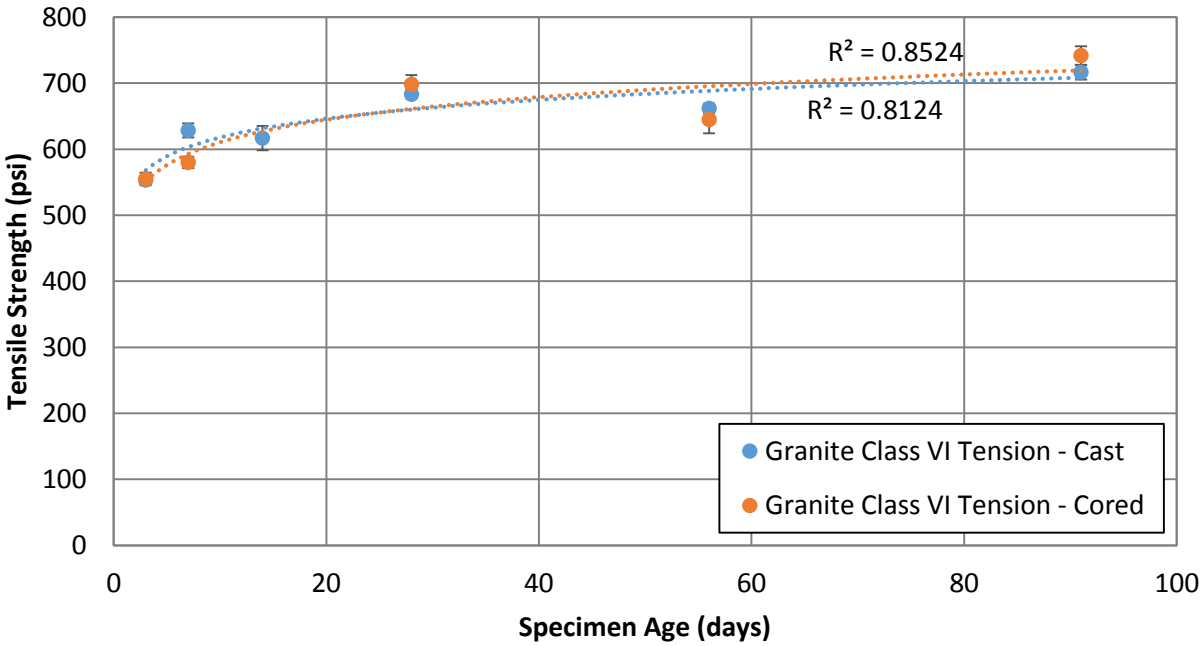

Figure B.29 Splitting tensile strength vs. time for class VI Georgia granite concrete

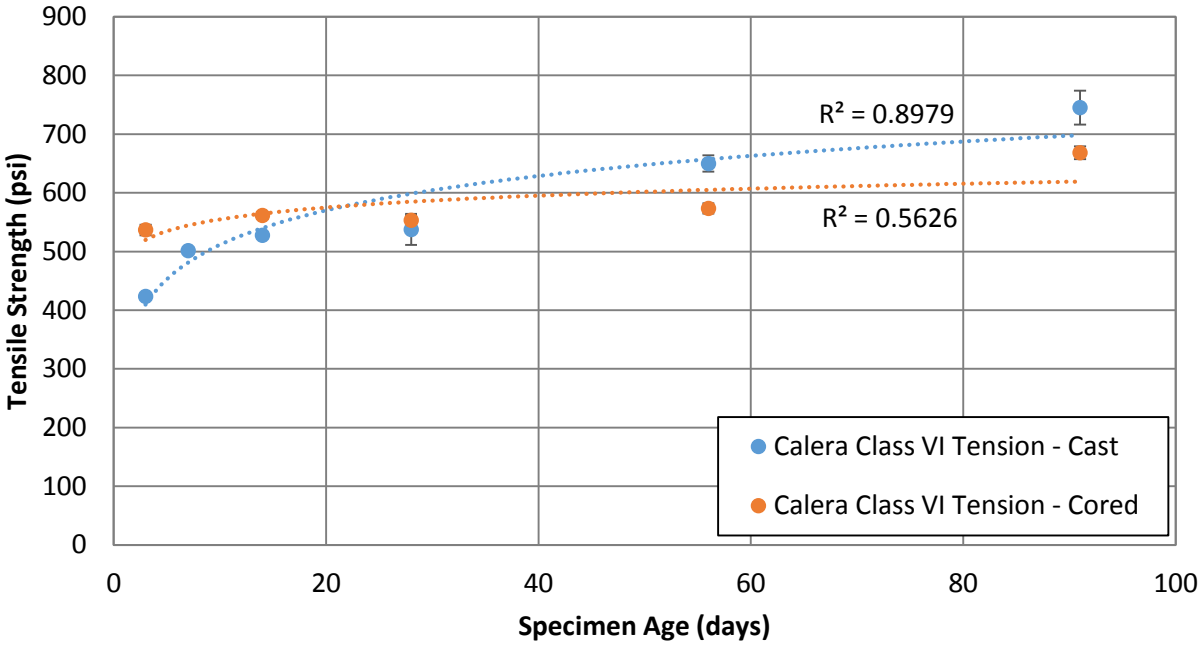

Figure B.30 Splitting tensile strength vs. time for class VI Calera limestone concrete

B.4 FLEXURAL STRENGTH

B.4.1 Class II Concrete

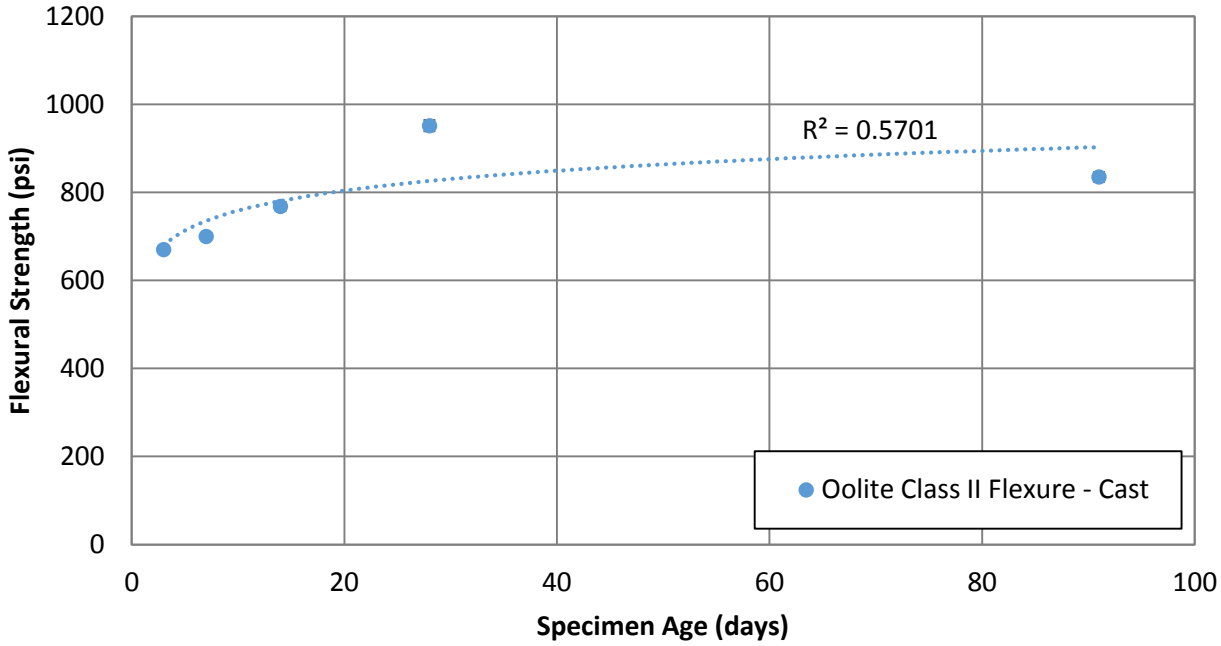

Figure B.31 Flexural strength vs. time for class II Miami oolite concrete

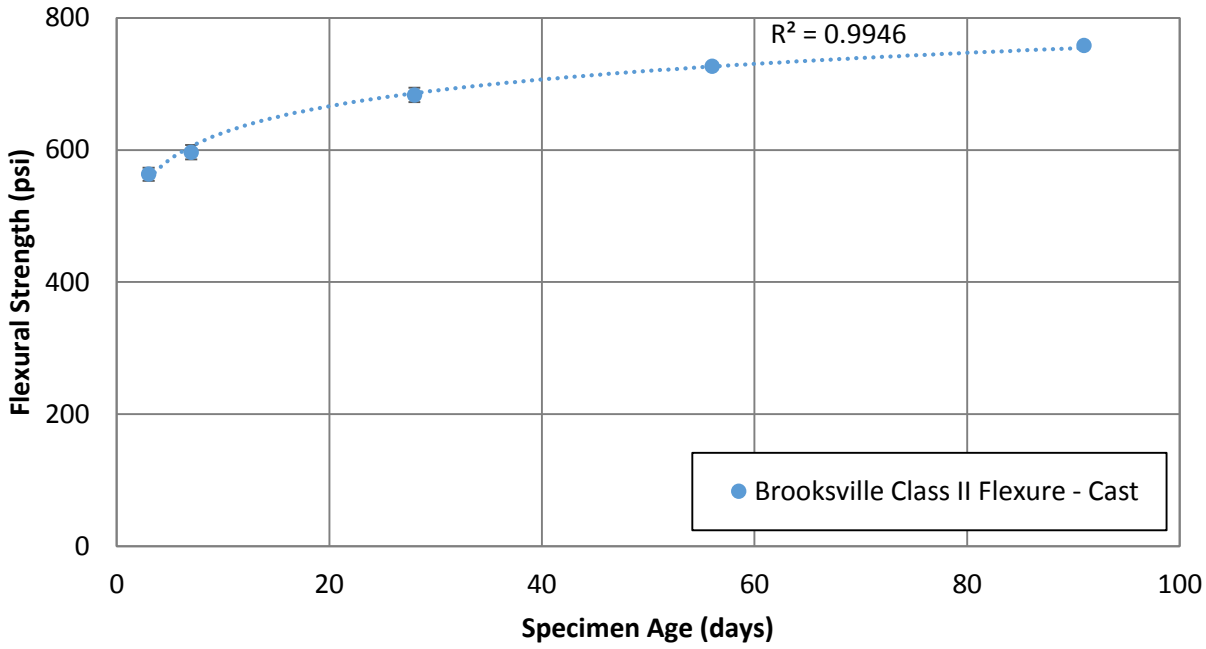

Figure B.32 Flexural strength vs. time for class II Brooksville limestone concrete

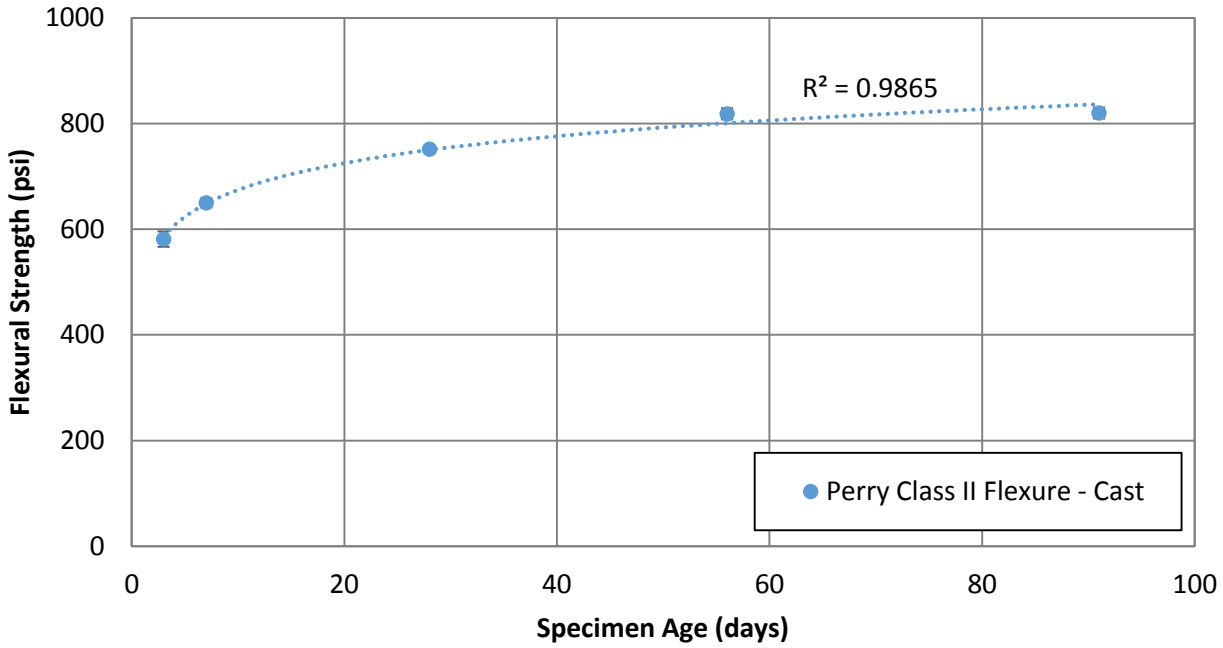

Figure B.33 Flexural strength vs. time for class II Perry limestone concrete

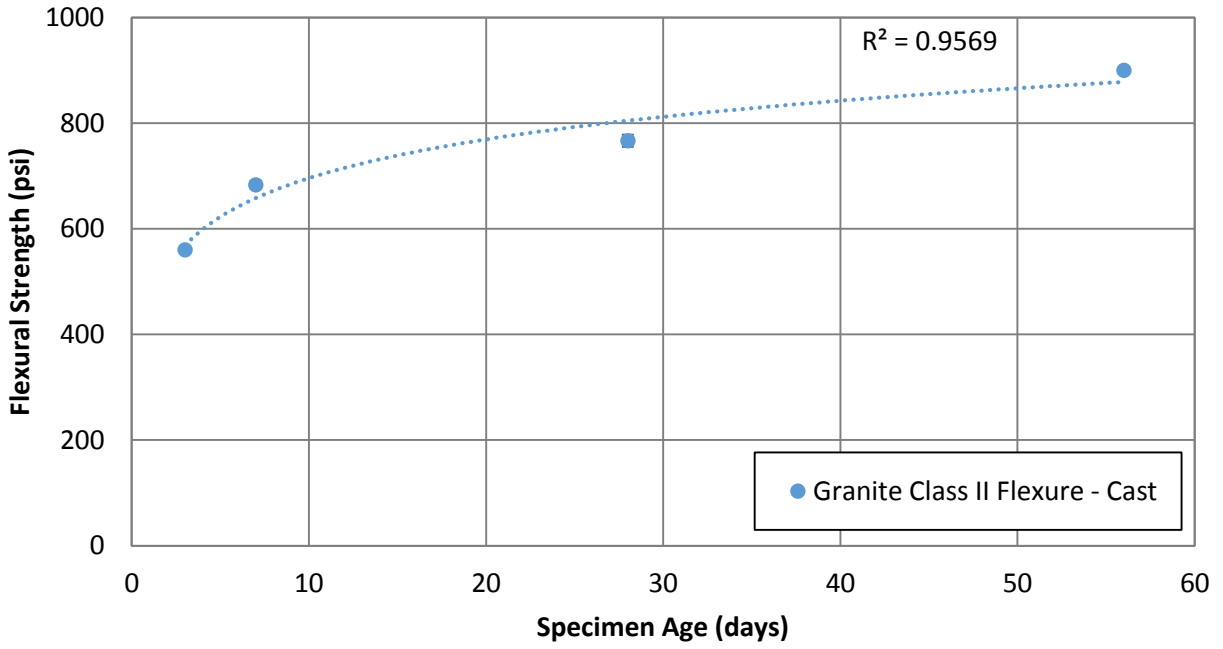

Figure B.34 Flexural strength vs. time for class II Georgia granite concrete

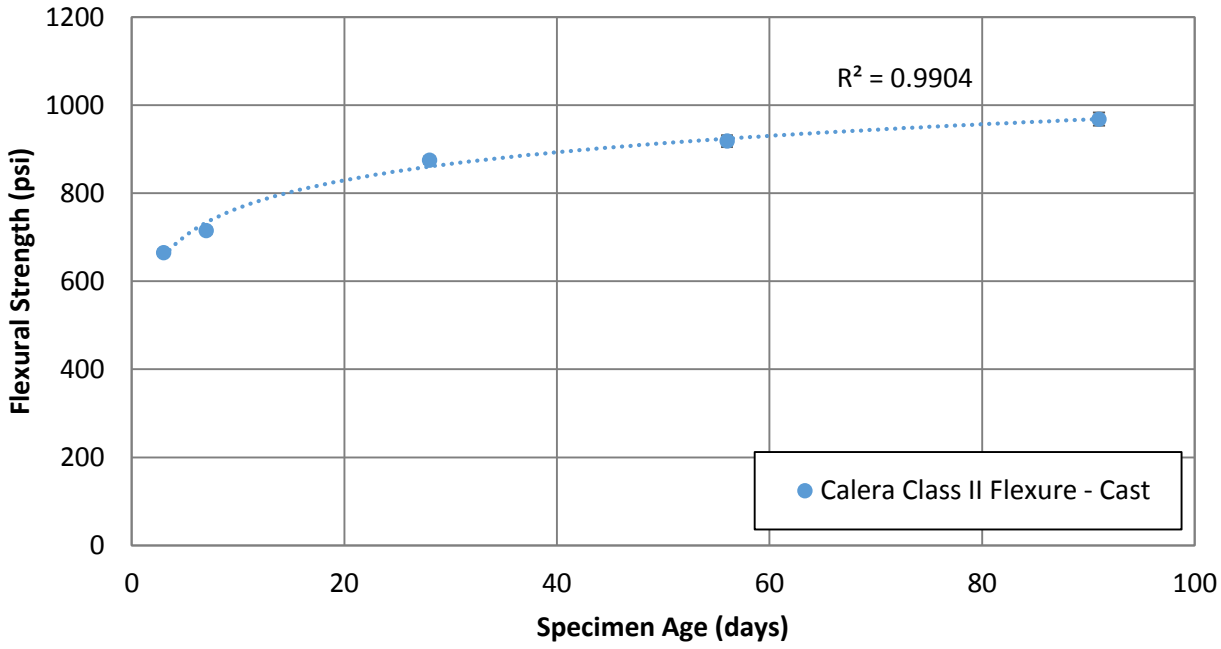

Figure B.35 Flexural strength vs. time for class II Calera limestone concrete

B.4.2 Class VI Concrete

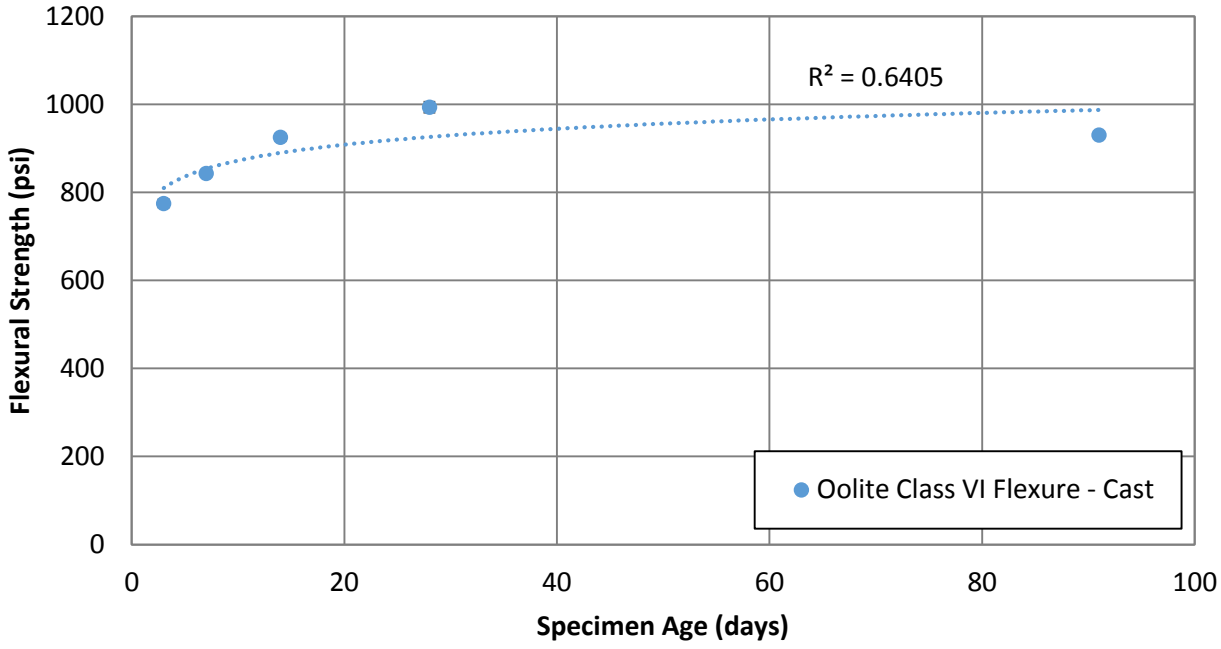

Figure B.36 Flexural strength vs. time for class VI Miami oolite concrete

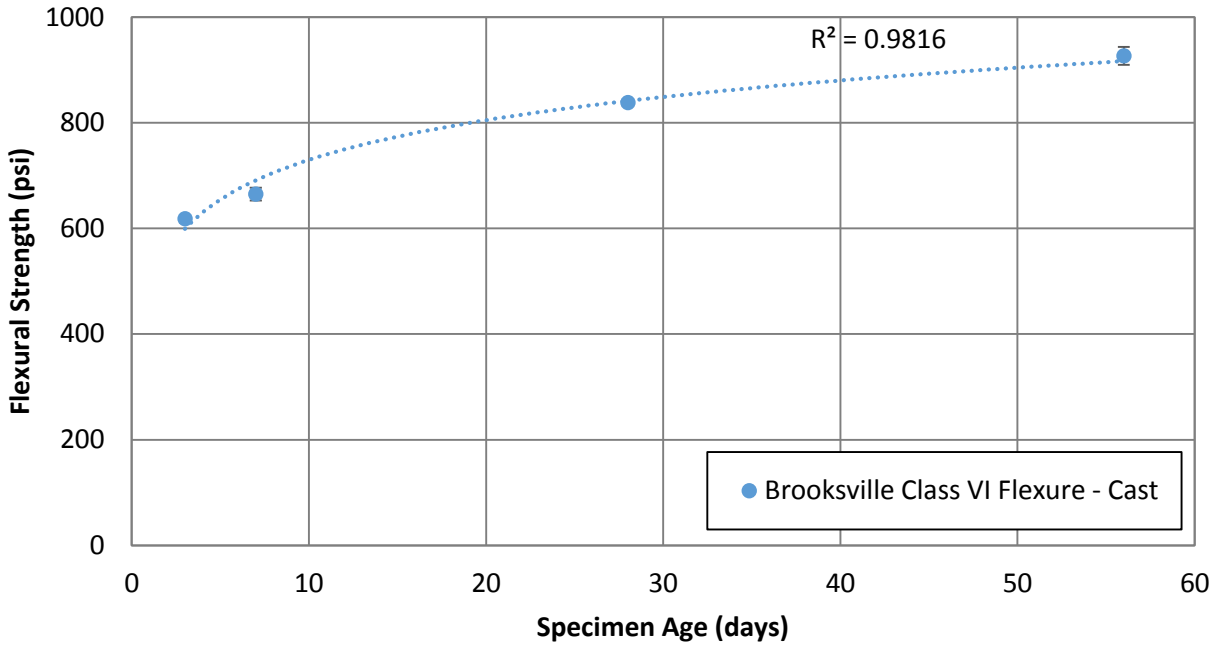

Figure B.37 Flexural strength vs. time for class VI Brooksville limestone concrete

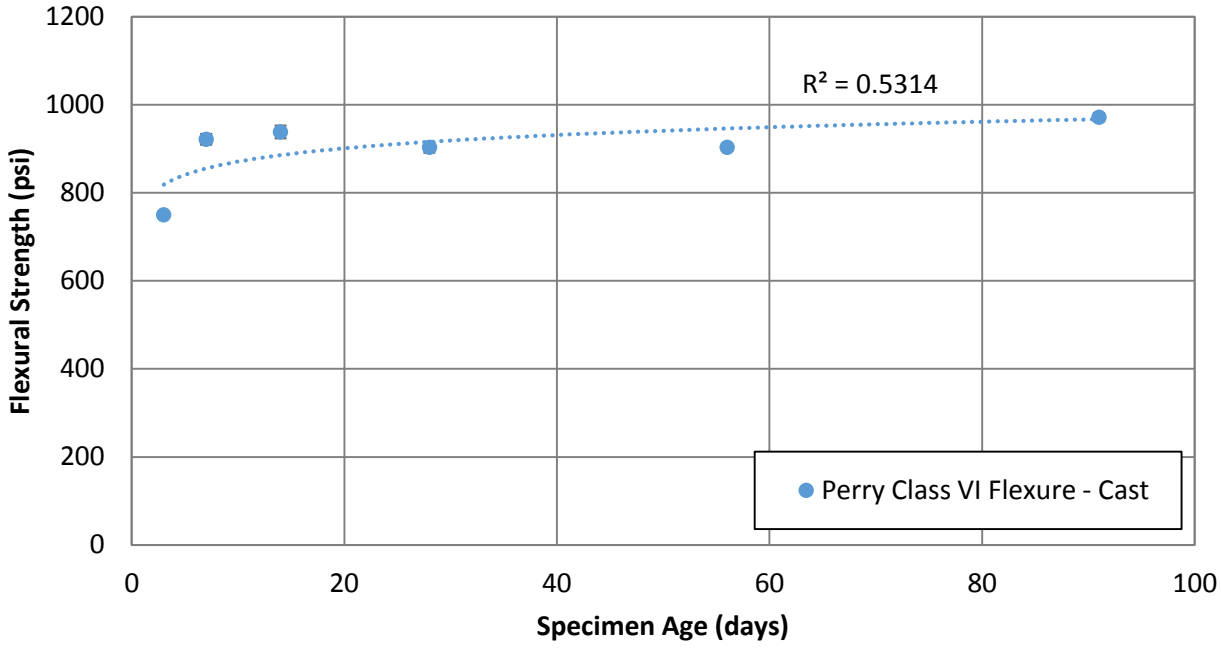

Figure B.38 Flexural strength vs. time for class VI Perry limestone concrete

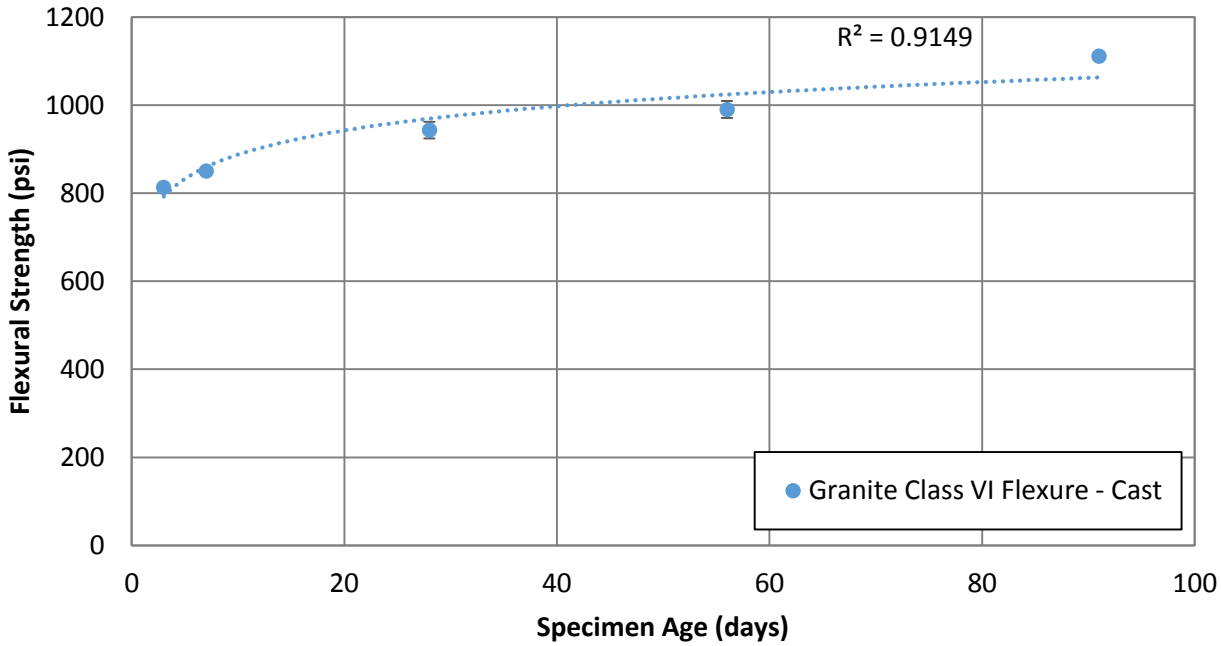

Figure B.39 Flexural strength vs. time for class VI Georgia granite concrete

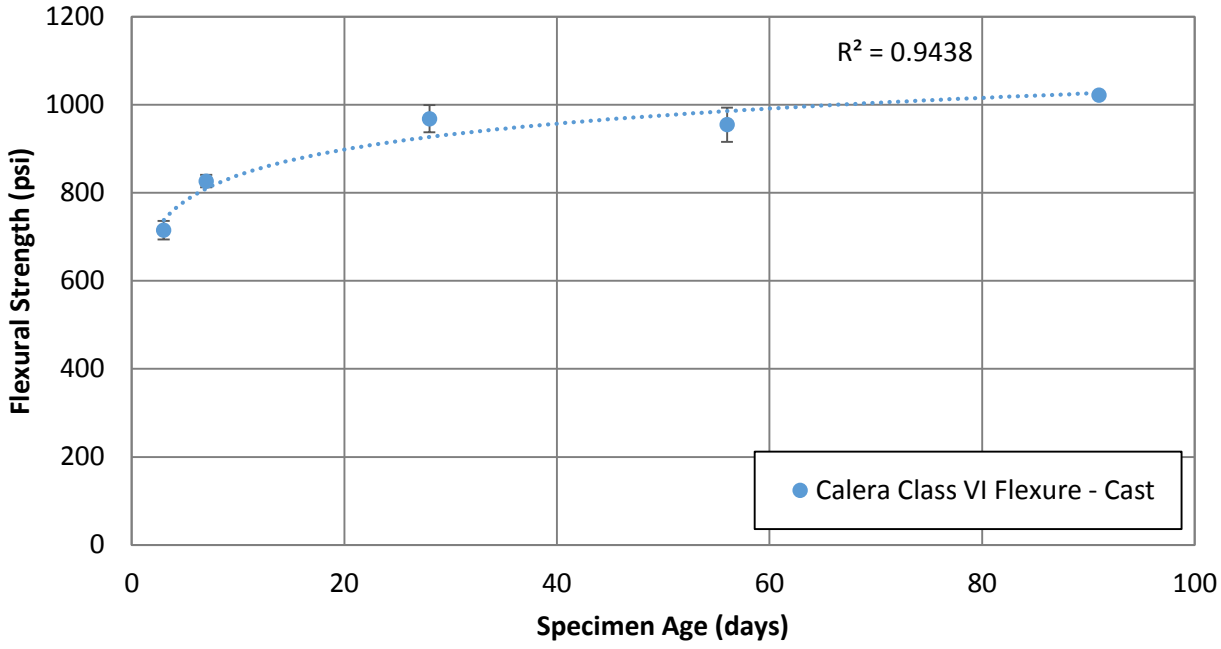

Figure B.40 Flexural strength vs. time for class VI Calera limestone concrete

APPENDIX C. TENSILE STRENGTH PREDICTION

Presentation of both compressive strength and splitting tensile strength has already been accomplished, however comparing the two quantities may help characterize concrete performance or showcase specific concrete behavior related to aggregates used. Additionally, ACI-318 has predictive equations that can be used to estimate splitting tensile strength based on compressive strength. This relationship is plotted in the charts below in red, starting with Figure C.1.

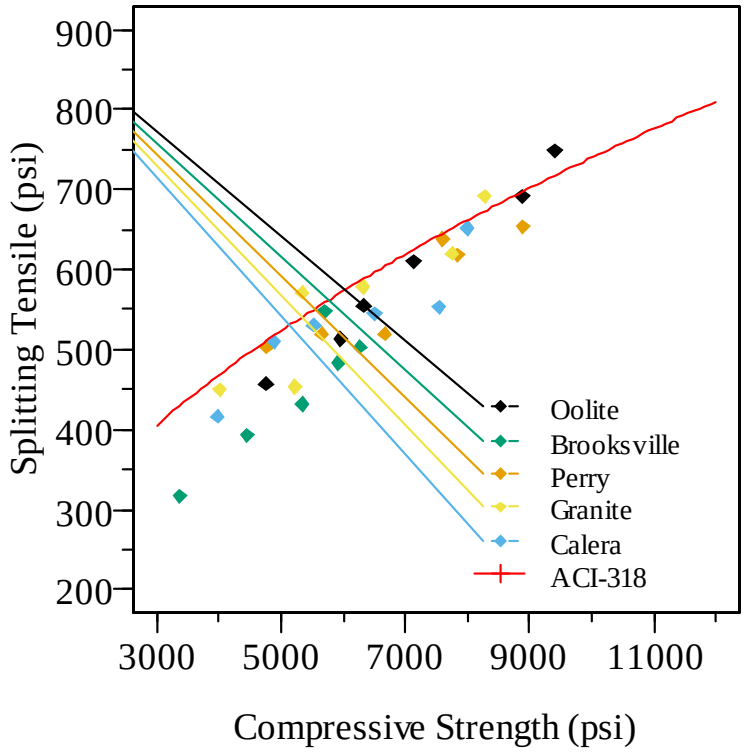

Figure C.1 Compressive strength vs. splitting tensile strength for class II cast specimens

This figure shows cast specimens composed with the class II mixture design. Aggregate type is identified by color with no best fit lines due to the close proximity of points. As a group, the majority of the mixes perform below ACI prediction. This relationship is more loosely correlated for class VI specimens as can be seen in Figure C.2.

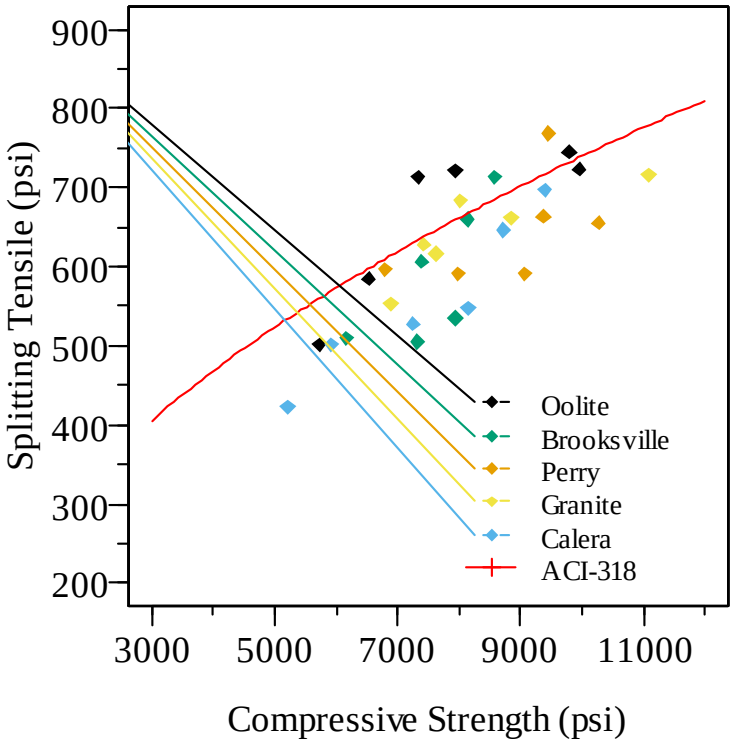

Figure C.2 Compressive strength vs. splitting tensile strength for class VI cast specimens

Class VI mixtures exhibit a higher degree of spread and deviation from the ACI prediction curve. Data points are more intermixed when compared to class II mixtures. Difference between classes is also present in cored specimens, despites their trend line variability. As exhibited in Figure C.3 and Figure C.4, the ACI equation mostly over estimates the tensile to compressive strength relationship. Miami oolite, granite, and Perry limestone occupy the upper and left side of each figure showing they exhibit high splitting tensile strength and compressive strength.

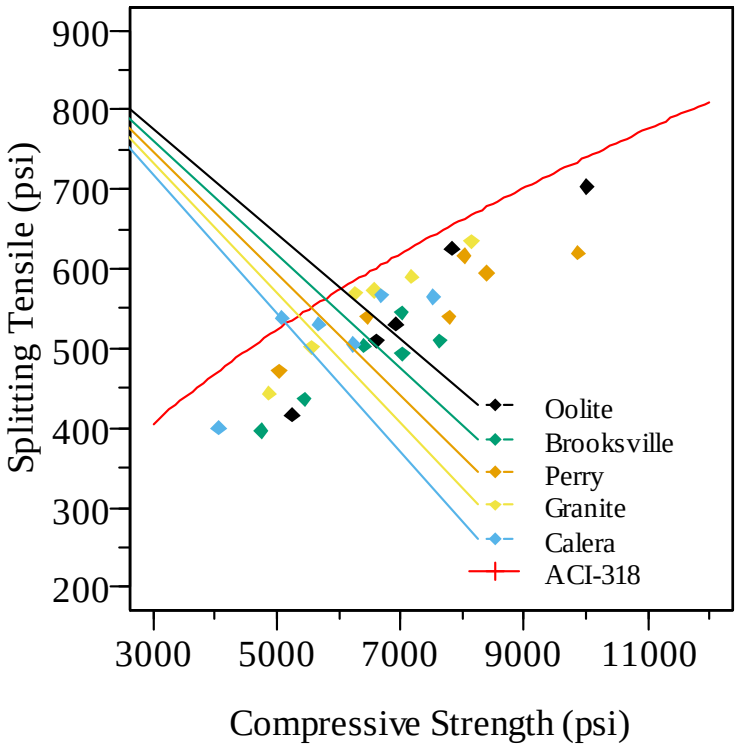

Figure C.3 Compressive strength vs. splitting tensile strength for class II cored specimens

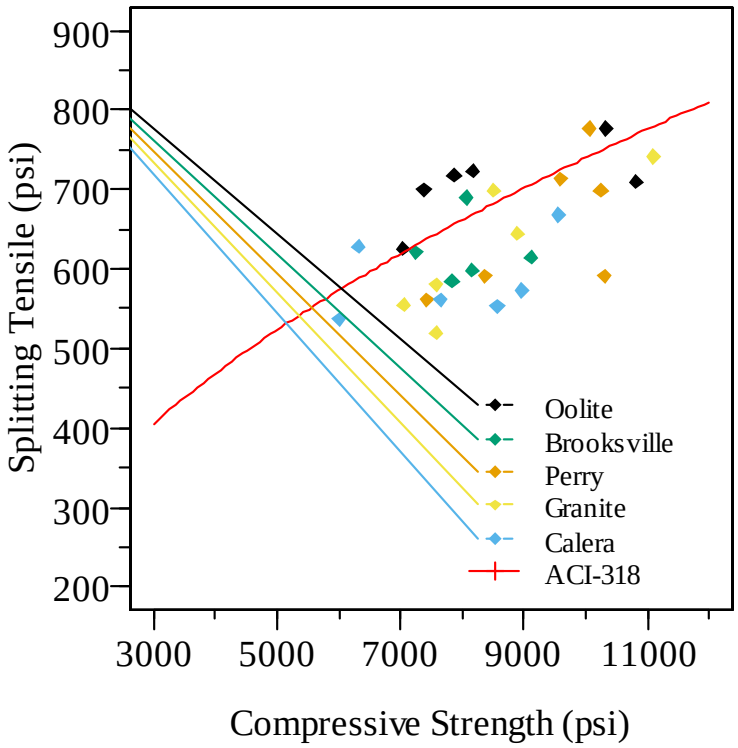

Figure C.4 Compressive strength vs. splitting tensile strength for class VI cored specimens

APPENDIX D. SETTING TEMPERATURE DATA

Temperature was taken immediately after placement of concrete into the slab forms. Temperature data was deemed significant because the strength of a given concrete mixture can be seen as a function of its age and temperature data (Malhorta & Carino, 2004). The age history can be expressed with the concept of maturity. Maturity depends on the temperature of a specimen and how long that temperature during the specified time interval. Concrete that may have experienced higher temperature for shorter periods could have equal maturity to concrete than experienced lower temperatures for longer periods of time. While there are well known strength-maturity relationships, this research conducted tests at equal ages, making consideration into during only temperatures of primary importance.

The use of up to eight temperature probes in various locations were used for temperature data acquisition. The presentation of data follows a color coded method to ease comprehension and to successfully illustrate temperature data. In Figure D.1, a representation of the slab depicts location of temperature probes where heat data was obtained.

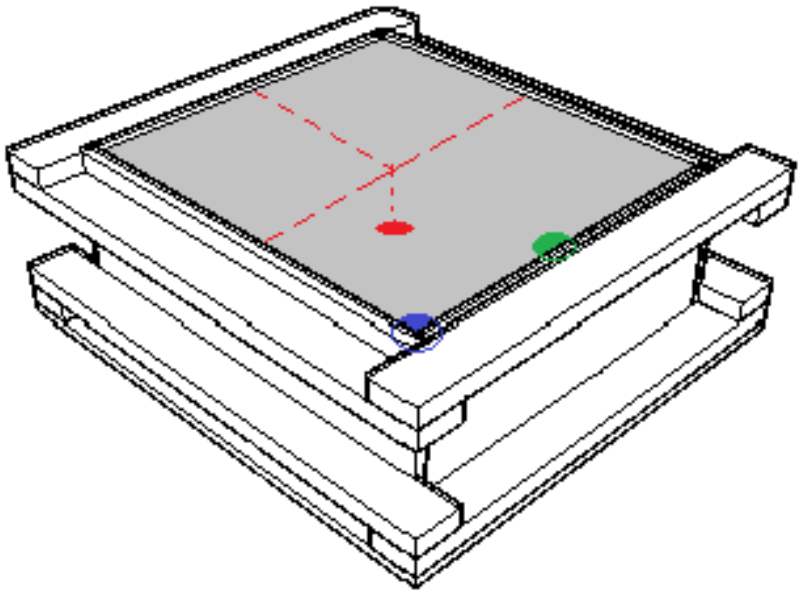

Figure D.1 Placement of temperature probes in slab

The color red depicts where the hottest temperatures could be expected, the center of the slab in all axis's. Here, heat transfer to the surrounding environment is not directly possible allowing the hydration of cement to contribute the most heat over time. The color green depicts the location at which two dimensions can contribute to heat loss, the upper edge. Here, heat from hydration dissipates through the top and vertical side. The blue color represents the location where heat transfer can occur in three dimensions, the corner. Heat transfer along the corner should have the highest loss as it can be radiated from all sides and into the surrounding environment. Not shown in the figure is the temperature probe position of individual cast cylinders. The temperature probe for cast specimens was located at the center of each cylinder.

Temperature data for class II and class VI Brooksville limestone concrete is shown in Figure D.2. Figure D.2 shows two sets of temperature curves for class II and class VI mixtures. The colors represent thermocouple placement while the relative position identifies the class II from the class VI mixture. Class II mixture had a maximum temperature of approximately 105 degrees at 12 hours, while the class VI mixture has a maximum of 140 degrees at around the same time. Brooksville aggregate did not have separate cast cylinder data as shown in granite mixtures in Figure D.3.

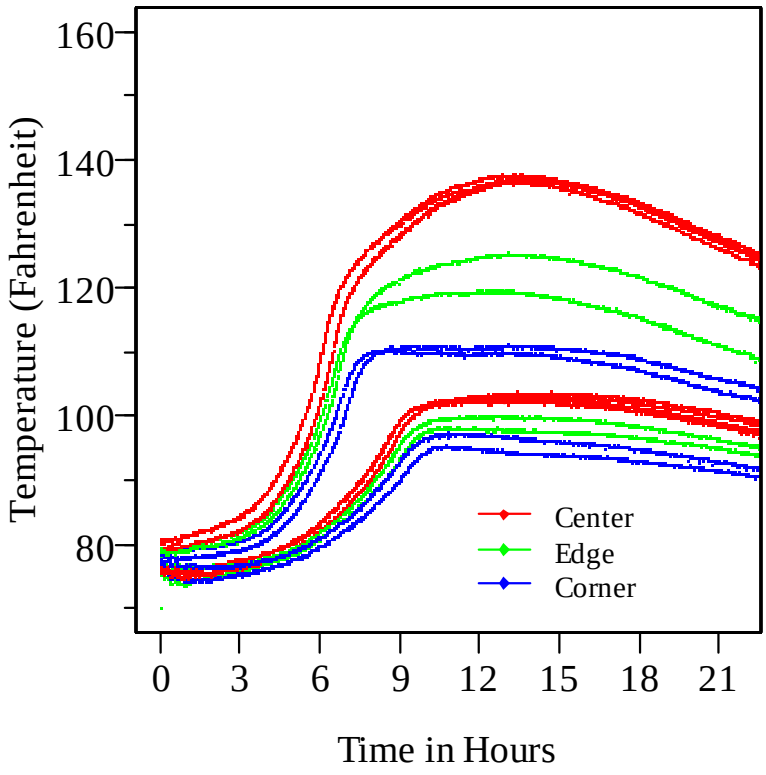

Figure D.2 Brooksville concrete mixtures temperature data

Granite mixtures include data for cast cylinders as shown as the lowest two curves in brown and yellow (Figure D.3). Class VI mixtures experienced the highest temperatures and are shown in darker red, green, and blue. Class II mixture experience a similar spread of temperature but at lower absolute temperatures compared to class VI. Maximum temperatures experienced are lower than Brooksville mixtures, most likely due to the lack of admixtures required for the denser aggregates. This behavior is also visible in Figure D.4, with Calera limestone mixtures. Granite experiences less heat increase between class II and class VI mixtures. The maximum temperature reached by the class VI mixture is approximately 135 degrees.

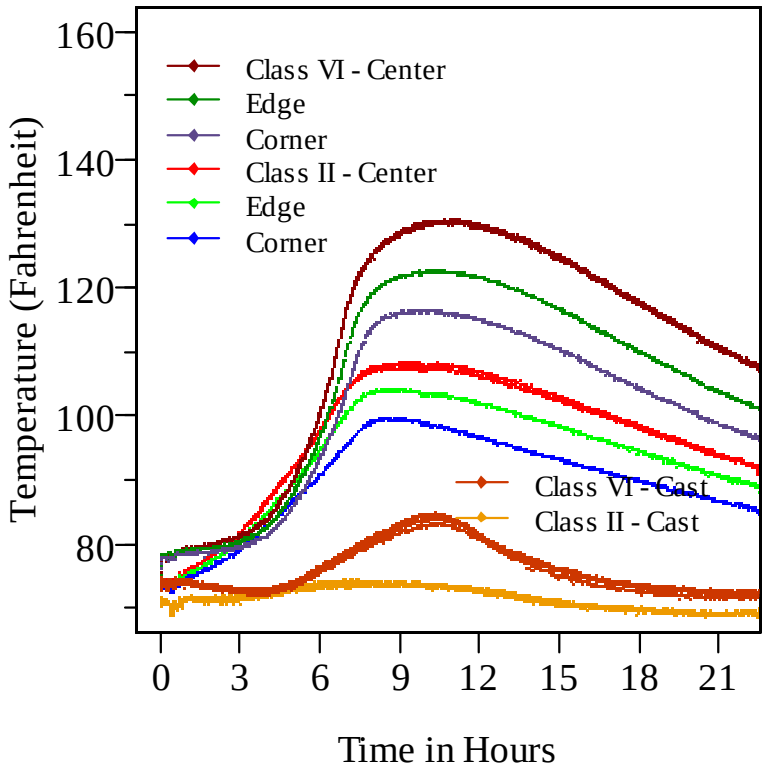

Figure D.3 Granite concrete mixtures temperature data

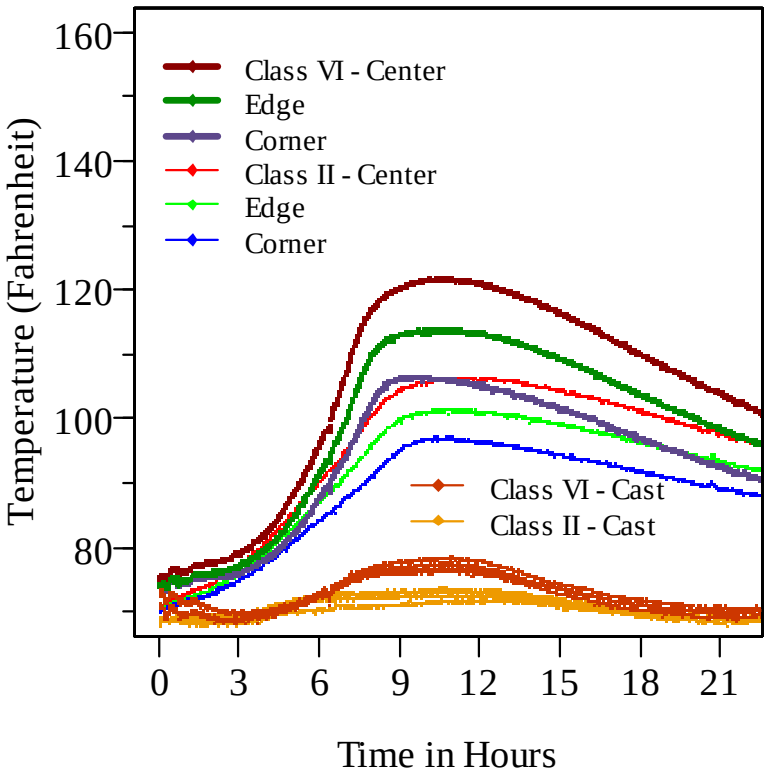

Figure D.4 Calera concrete mixtures temperature data

Plots exhibiting the difference in peaks and temperature change between the hottest averages of each class are shown in Figure D.5. The hottest temperatures were reached in the center position of each slab.

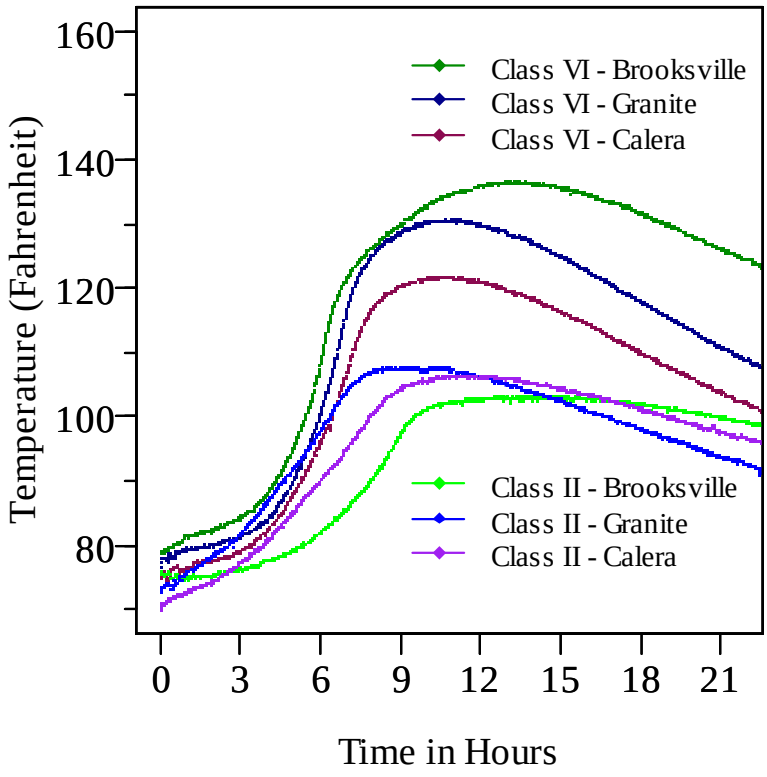

Figure D.5 Maximum temperatures in Brooksville, granite, and Calera concrete mixtures

As shown in Figure D.5, the Brooksville class VI mixture has the highest maximum temperature but also reaches its maximum at approximately 12-13 hours of data readings. This retardation of hydration and subsequent delayed increase in temperature is most likely caused by the higher percentage of superplasticizer and water-reducing admixtures needed in the Brooksville mixtures. Delayed hydration can be one effect of mineral admixtures (Siler, Kratky, & Belie, 2012). The increase in temperature can be attributed to the increase in cement content in class VI mixes. The increase in heat for Brooksville mixtures can be explained by the effect of the higher dosages of polycarboxylate superplasticizers needed for acceptable rheological properties. This mineral admixtures delay hydration as can be seen by the later maximum peak temperatures as well as cause renewed C_3A hydration and increasing heat evolution (Kumar, Singh, & Singh, 2012).

The inclusion of cast cylinder heat data highlights the issue of accurate portrayal of concrete behavior between application and lab tests. Typical construction approximates slab placement, where heat generation by larger volumes of concrete is significant. Cast cylinders do not represent typical construction as they have higher surface area to volume ratios and can dissipate heat much quicker, and have less total mass to retain heat.